Effects of Polymers on Carbamazepine cocrystals phase transformation and release profiles

PhD Thesis

Shi Qiu

This thesis is submitted in partial fulfilment of the requirements of De Montfort University for the award of Doctor of Philosophy

August 2015

Faculty of Health and Life Sciences

De Montfort University

Leicester

CONTENTS

DECLARATION

I declare that the word described in this thesis is original work undertaken by myself for the Doctor of Philosophy degree, at the Pharmacy School, Faculty of Health and Life Sciences, De Montfort University, Leicester, United Kingdom.

No part of the material described in this thesis has been submitted for the award of any other degree or qualification in this or any other university or college of advanced education.

Shi Qiu

ABSTRACT

The aim of this study is to investigate the effects of coformers and polymers on the phase transformation and release profiles of cocrystals. Pharmaceutical cocrystals of Carbamazepine (CBZ) (namely 1:1 carbamazepine-nicotinamide (CBZ-NIC), 1:1 carbamazepine-saccharin (CBZ-SAC) and 1:1 carbamazepine-cinnamic acid (CBZ-CIN) cocrystals, were synthesized. A Quality by Design (QbD) approach was used to construct the formulation.

Dissolution and solubility were studied using UV imaging and High Performance Liquid Chromatography (HPLC). The polymorphic transitions of cocrystals and crystalline properties were examined using Differential Scanning Calorimetry (DSC), X-Ray Powder Diffraction (XRPD), Raman spectroscopy (Raman) and Scanning Electron Microscopy (SEM). JMP 11 software was used to design the formulation.

It has been found that Hydroxupropyl methylcellulose (HPMC) cannot inhibit the transformation of CBZ-NIC cocrystals to Carbamazepine Dihydrate (CBZ DH) in solution or in the gel layer of the matrix, as opposed to its ability to inhibit CBZ Form III (CBZ III) phase transition to CBZ DH.

The selection of different coformers of SAC and CIN can affect the stability of CBZ in solution, resulting in significant differences in the apparent solubility of CBZ. The dissolution advantage of the CBZ-SAC cocrystal can only be shown for 20 minutes during dissolution because of the conversion to its dihydrate form (CBZ DH). In contrast, the improved CBZ dissolution rate of the CBZ-CIN cocrystal can be realised in both solution and formulation because of its stability.

The polymer of Hypromellose Acetate Succinate (HPMCAS) seemed to best augment the extent of CBZ-SAC and CBZ-CIN cocrystal supersaturation in solution. At 2 mg/ml of HPMCAS concentration, the apparent CBZ solubility of CBZ-SAC and CBZ-CIN cocrystals can increase the solubility of CBZ III in pH 6.8 phosphate buffer solutions (PBS) by 3.0 and 2.7 times respectively. All pre-dissolved polymers in pH 6.8 PBS can increase the dissolution rates of CBZ cocrystals. In the presence of a 2 mg/ml HPMCAS in pH 6.8 PBS, the cocrystals of CBZ-NIC and CBZ-CIN can dissolve by about 80% within five minutes in comparison with 10% of CBZ III in the same dissolution period. Finally, CBZ-NIC cocrystal formulation was designed using the QbD principle. The potential risk factors were determined by fish-bone risk assessment in the initial design, after which Box-Behnken design was used to optimize and evaluate the main interaction effects on formulation quality. The results indicate that in the Design Space (DS), CBZ sustained release

tablets meeting the required Quality Target Product Profile (QTPP) were produced. The tablets' dissolution performance could also be predicted using the established mathematical model.

ACKNOWLEDGEMENTS

First I would like to express my sincere appreciation to my supervisors Dr Mingzhong Li and Dr Walkiria Schlindwein for their continuous support and guidance throughout my PhD studies. Your profound knowledge, creativeness, enthusiasm, patience, encouragement give me great help to do my PhD research.

I am very grateful to all technicians in the faculty of Health and Life Sciences who provide me technical support and equipment support for my experiments.

I would like to thank my PhD colleagues in my lab Ning Qiao, Huolong Liu and Yan Lu, for years of friendship, accompany and productive working environment.

More specifically, I wish to express my sincere gratitude to De Montfort University who gives me scholarship to pursue my PhD study.

Finally, I wish to thank my beloved parents, my dearest husband for their endless love, care and encouraging me to fulfil my dream.

LIST OF FIGURES

LIST OF TABLES

ABBREVIATIONS

API	Active Pharmaceutical Ingredient
BCS	Biopharmaceutics Classification System
CBZ	Carbamazepine
CBZ III	Carbamazepine form III
CBZ I	Carbamazepine form I
CBZ IV	Carbamazepine form IV
CBZ DH	Carbamazepine Dihydrate
CBZ-NIC cocrystal	1: 1 Carbamazepine – Nicotinamide cocrystal
CBZ-SAC cocrystal	1:1 Carbamazepine –Saccharin cocrystal
CBZ-CIN cocrystal	1:1 Carbamazepine –Cinnamic acid cocrystal
CIN	Cinnamic acid
CQA	Critical Quality Attributes
CSD	Cambridge Structural Database
DSC	Differential Scanner Calorimetry
DoE	Design of Experiment
DS	Design Space
FTIR	Fourier Transform Infrared Spectroscopy
GI	Gastric Intestinal
GRAS	Generally Recognized As Safe

HPLC	High Performance Liquid Chromatography
HPMC	Hydroxypropyl Methylcellulose
HPMCAS	Hypromellose Acetate Succinate
HPMCP	Hypromellose Phthalate
HSPM	Hot Stage Polarised Microscopy
IDR	Intrinsic Dissolution Rate
IR	Infrared spectroscopy
IND	Indomethacin
IND-SAC cocrystal	Indomethacin-Saccharin cocrystal
MCC	Microscrystalline cellulose
NIC	Nicotinamide
NMR	Nuclear Magnetic Resonance
PAT	Process Analytical Technology
PEG	Polyethylene Glycol
PVP	Polyvinvlpyrrolidone
QbD	Quality by Design
QbT	Quality by Testing
QTPP	Quality Target Product Profile
RC	Reaction Cocrystallisation
RH	Relative Humidity

RSM	Response Surface Methodology
SEM	Scanning Electron Microscope
SDG	Solvent Drop Grinding
SDS	Sodium Dodecyl Sulphate
SLS	Sodium Lauryl Sulphate
SMPT	Solution Mediate Phase Transformation
SSNMR	Solid State Nuclear Magnetic Resonance Spectroscopy
TGA	Thermal Gravimetric Analysis
TPDs	Ternary Phase Diagrams
XRD	X-Ray Diffraction
XRPD	X-Ray Powder Diffraction

Chapter 1 Introduction

1.1 Research background

In the pharmaceutical industry, it is poor biopharmaceutical properties (low biopharmaceutical solubility, dissolution rate and intestinal permeability) rather than toxicity or lack of efficacy that are the main reasons why less than 1% of active pharmaceutical compounds eventually get into the marketplace [1, 2]. Enhancing the solubility and dissolution rates of poorly water soluble compounds has been one of the key challenges to the successful development of new medicines in the pharmaceutical industry. Although many methods including prodrug, solid dispersion, micronisation and salt formation have been developed to answer this purpose, pharmaceutical cocrystals have been recognised as an alternative approach with the enormous potential to provide new and stable structures of active pharmaceutical ingredients (APIs) [1, 3]. Apart from offering potential improvements in solubility, dissolution rate, bioavailability and physical stability, pharmaceutical cocrystals frequently enhance other essential properties of APIs such as hygroscopicity, chemical stability, compressibility and flowability [4]. These behaviours have been rationalised by the crystal structure of the cocrystal *vs.* the parent drug [5]. Different coformers can form different packing styles and hydrogen bonds with an API, conferring significantly different physicochemical properties and *in vivo* behaviours on the resultant cocrystals [6, 7].

Although pharmaceutical cocrystals can offer the advantages of higher dissolution rates and greater apparent solubility to improve the bioavailability of drugs with poor water solubility, a key limitation of this approach is that a stable form of the drug can be recrystallized during the dissolution of the cocrystals, resulting in the loss of the improved drug properties. For example, in the previous study of the Mingzhong's lab, they investigated the dissolution and phase transformation behaviour of the CBZ-NIC cocrystal using the *in situ* technique of the UV imaging system and Raman spectroscopy, demonstrating that the enhancement of the apparent solubility and dissolution rate has been significantly reduced due to its conversion to CBZ DH [8]. In order to inhibit the form conversion of the cocrystals in aqueous media, the effects of various coformers and polymers on the phase transformation and release profiles of cocrystals in aqueous media and tablets were studied. Most research work on coformer selection is currently focused on the possibility of cocrystal formation between APIs and coformers. Only a small amount of work has been carried out to identify a coformer to form a cocrystal with the desired properties, and there has been even less research into polymers that inhibit crystallization during cocrystal dissolution [9].

1.2 Research aim and objectives

The Biopharmaceutics Classfication System (BCS) has been introduced as a scientific framework for classifying drug substances according to their aqueous solubility and intestinal permeability [9]. CBZ is classified as a Class II drug, with the properties of low water solubility and high permeability. This class of drug is currently estimated to account for about 30% of both commercial and developmental drugs [10]. The aim of this study is to investigate the influence of coformers and polymers on the phase transformation and release profile of CBZ cocrystals in solution and tablets. The QbD approach was used to develop a formulation that ensures the quality, safety and efficacy of the tablets. The specific objectives of this research can be summarised as follows:

Objective 1: A brief review of strategies to overcome poor water solubility is presented. The definition of pharmaceutical cocrystal is introduced together with the relevant basic theory, as well as recent progress in the field. The formulation of tablets designed by QbD is introduced.

Objective 2: Three pharmaceutical cocrystals, CBZ-NIC, CBZ-SAC and CBZ-CIN, were prepared using solvent evaporation and cooling crystallisation methods. Various techniques were used to characterize the prepared CBZ cocrystals.

Objective 3: The effect of coformers and polymers on the phase transformation and release profiles of CBZ cocrystals is investigated. The mechanism of the phase transformation of pharmaceutical cocrystals in aqueous media for the selection of lead cocrystals to ensure the success of product development is explored in order to acquire an understanding of the process.

Objective 4: QbD principles and tools were used to design the CBZ-NIC cocrystal tablets. DOE was used to optimize and evaluate the main interaction effects on the quality of formulation. Mathematical models are established to predict the dissolution performance of the tablet.

1.3 Thesis structure

This thesis is organized into nine chapters:

Chapter 1 briefly describes the research background, research aim, objectives and structure of Shi's PhD research.

Chapter 2 reviews the mechanisms used to overcome poor water solubility. One of these, the pharmaceutical cocrystal, is defined and detailed, the relevant basic theories are presented and

recent progress is outlined. The drug delivery system of tablets is introduced, together with some definitions and the principles of QbD. Finally, CBZ, including CBZ cocrystals and CBZ formulation, is summarized.

Chapter 3 introduces all the materials and methods used in this study. The principles underlying the analytical techniques used are given in this chapter. Operation and methods developments are described in detail, as are the preparation of dissolution media and the various test samples.

Chapter 4 characterises all CBZ samples used in this study. The characterization results of the various forms of CBZ samples, which include CBZ III and CBZ DH, three cocrystals of CBZ, which include CBZ-NIC cocrystal, as well as the CBZ-SAC and CBZ-CIN cocrystals, are presented, together with the molecular structures of the CBZ-NIC, CBZ-SAC and CBZ-CIN cocrystals.

Chapter 5 covers the influence of HPMC on the phase transformation and release profiles of the CBZ-NIC cocrystal in solution and in sustained release matrix tablets. The examination by DSC, XRPD, Raman spectroscopy and scanning electron microscopy of polymorphic transitions of the CBZ-NIC cocrystal and its crystalline properties is described, as well as the investigation by UV-imaging of the intrinsic dissolution rate of the CBZ-NIC cocrystal and an investigation by HPLC of the release profiles of the CBZ-NIC cocrystal in solution and sustained release matrix tablets.

Chapter 6 covers the influence of coformers on the phase transformation and release profiles of CBZ-SAC and CBZ-CIN cocrystals in HPMC solution and in sustained release matrix tablets. The examination by DSC, XRPD and SEM of the polymorphic transitions of the CBZ-SAC and CBZ-CIN cocrystals and their crystalline properties, the investigation of the powder dissolution studies of CBZ-SAC and CBZ-CIN cocrystals in HPMC solutions and the investigation by HPLC of solubility and release profiles of the CBZ-SAC and CBZ-CIN cocrystals in solution and sustained release matrix tablets are all detailed.

Chapter 7 deals with the influence of the polymers of HPMCAS, Polyethylene Glycol 4000 (PEG) and Polyvinvlpyrrolidone K30 (PVP) on the phase transformation and release profiles of CBZ cocrystals in solution and in tablets, and with the examination by DSC, XRPD and SEM of the polymorphic transition of the CBZ cocrystals and their crystalline properties, together with the investigation of the powder dissolution tests of CBZ cocrystals in polymer solutions and the investigation by HPLC of the release profiles of tablets.

In Chapter 8, QbD principles and tools were used to develop a tablet formulation that ensures the quality, safety and efficacy of CBZ-NIC cocrystal sustained release tablets.

Chapter 9 summarizes the present work and the results obtained from my research. Further work in the area of pharmaceutical cocrystal research is also discussed in this chapter.

Chapter 2 Literature Review

2.1 Chapter overview

In this chapter, some basic termaqueos in pharmaceutical physical chemistry are defined. A brief review of strategies to overcome poorly-water solubility are then presented, including prodrug, salt formation, high-energy amorphous forms, particle size reduction, cyclodextrin complexation and pharmaceutical cocrystals, the last of which are presented in detail. Secondly, the formulation of tablets using the QbD method was introduced [11], including the drug delivery system-tablets and some definitions and basic concepts of QbD. This presents general knowledge about QbD, the advantages and the types of tablets, tablet excipients and tablet production via direct compression. Finally, a brief review of CBZ incorporates a CBZ pharmaceutical cocrystal case study and a summary of CBZ sustained/controlled release formulations.

2.2 Definitions of basic concepts relating to pharmaceutical physical chemistry

Equilibrium Solubility

The extent to which dissolution proceeds under a given set of experimental conditions is referred to as the solubility of the solute in the solvent. Thus, the solubility of a substance is the amount that passes into solution when equilibrium is established between the solution and excess substance [12].

Apparent solubility

Apparent solubility refers to the concentration of material at apparent equilibrium (supersaturation). Apparent solubility is distinct from true thermodynamic solubility, which is reached at infinite equilibrium time [13].

Polymorphism and transformation

Polymorphism is a solid crystalline phenomenon of a given compound that results from the ability of at least two crystal structures of that compound’s molecules in its solid state. There are two types of polymorphism: the monotropic system, in which the transition between different polymorphs is irreversible, and the enantiotropic system, where the two polymorphs can repeatedly interchange forms on heating and cooling [12].

Bioavailability

Two aspects of drug absorption are important in clinical practice: the rate at which, and the extent to which, the administered dose is absorbed. The fraction of an administered dose of drug that reaches the systemic circulation in an unchanged form is known as the bioavailable dose. Bioavailability is concerned with the quantity and rate at which the intact form of a particular drug appears in the systemic circulation following administration of that drug [14].

2.3 Strategies to overcome poor water solubility

The drugs are classified by the biopharmaceutics classification system (BCS) into four categories based on their aqueous solubility and permeability [15], as shown in Fig.2.1.

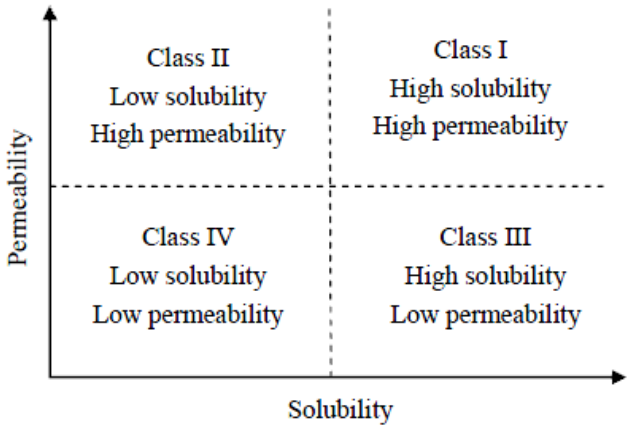

Fig.2.1 Four classes drugs: ClassI, Class II, Class III and Class IV [15]

For Class II and Class IV drugs, the bioavailability can be improved by the enhancement of solubility, especially for Class II drugs. It is reported that nearly 40%-70% of newly developed chemical compounds are not aqueous soluble enough to ensure therapeutic efficacy in gastrointestinal (GI) absorption [15]. The poor solubility that may obstruct development of parenteral products and limit bioavailability of oral ones has been of concern regarding formulations. There are generally two methods for changing Active Pharmaceutical Ingredient (API) solubility or dissolution: material engineering of the API (prodrug, salt formation and pharmaceutical cocrystal) and formulation approaches (high-energy amorphous formation, particle size reduction and cyclodextrin complexation).

2.3.1 Prodrug strategy

Prodrug strategy is applied as a chemical/biochemical method to overcome many barriers to drug delivery [16]. A prodrug is a medication that is administered in an inactive or less than fully active form, and is then converted to its active form through a normal metabolic process. An example would be hydrolysis of an ester form of the drug [17].

Fosamprenavir provides an illustration of this process. A prodrug of the HIV protease inhibitor, amprenavie, fosamprenavir takes the form of a calcium salt which is about 10 times more soluble than amprenavir. Because of this superior solubility, patients need just two tablets twice a day instead of eight capsules of amprenavir twice a day. It is more convenient for patients, and provides a longer patent clock [18-22].

2.3.2 Salt formation

The most common method of increasing the solubility of acidic and basic drugs is salt formation. Salts are formed through proton transfer from an acid to a base. In general, if the difference of pKa is greater than 3 between an acid and a base, a stable ionic bond could be formed [23]. For example, the dissolution rate and oral bioavailability of celecoxib, a poorly water-soluble weak acidic drug, is greatly enhanced by being combined with sodium salt formation [24].

2.3.3 High-energy amorphous forms

Because of the higher energy of amorphous solids, they are generally up to 10 times more soluble [25]. Many solid dispersion techniques such as the melting and solvent methods could be used to achieve a stable amorphous formulation. The intrinsic dissolution rate of Ritonavir, a Class IV drug with low solubility and permeability, for example, is 10 times that of crystalline solids [26].

2.3.4 Particle size reduction

A drug's dissolution rate rises as the surface area of its particles increases [24]. A reduction in particle size is thus the most common method of improving the bioavailability of drugs in the pharmaceutical industry. The micronized drug particles, which are 2-3 μm, can be achieved by conventional milling. However, the nanocrystal particles, which are smaller than 1 μm, are produced by wet-milling with beads. Particle size reduction can result in an increase in surface area and a decrease in the thickness of the diffusion layer, which can enhance a drug's dissolution rate.

8.7-fold and 5.5-fold enhancements in C_{max} and AUC were found in nitrendipine's nanocrystal formulation compared with micro-particle size crystal formulation, for example [27-29].

2.3.5 Cyclodextrin complexation

Cyclodextrins (CD) are oligosaccharides containing a relatively hydrophobic central cavity and a hydrophilic outer surface. A lipophilic microenvironment is provided by the central CD cavity, into which any suitably-sized drug may enter and include. There are no covalent bonds formed or broken between the API/CD complex formation and in aqueous solutions. The apparent solubility of poorly water-soluble drugs, and consequently their dissolution rate, is improved. CD intervention is thus well suited to Class II and IV drugs, of which 35 marketed formulations already exist [30].

2.3.6 Pharmaceutical cocrystals

A pharmaceutical cocrystal is a crystalline single phase material containing two or more components, one of which is an API, generally in a stoichiometric ratio amount [8].

2.3.6.1 Design of cocrystals

The components in a cocrystal exist in a definite stoichiometric ratio, and are assembled via non-convalent interactions such as hydrogen bonds, ionic bonds, π-π and van der Waals interactions rather than by ion pairing [31]. Hydrogen bonding is the most common bonding for cocrystals. Some commonly found synthons are shown in Fig.2.2 [32].

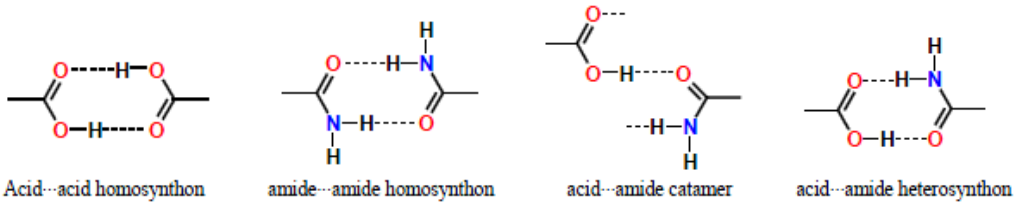

Fig.2.2 Common synthons between carboxylic acid and amide functional groups [32]

A design strategy is required to obtain the desired cocrystals. A practical screening paradigm is shown in Fig.2.3.

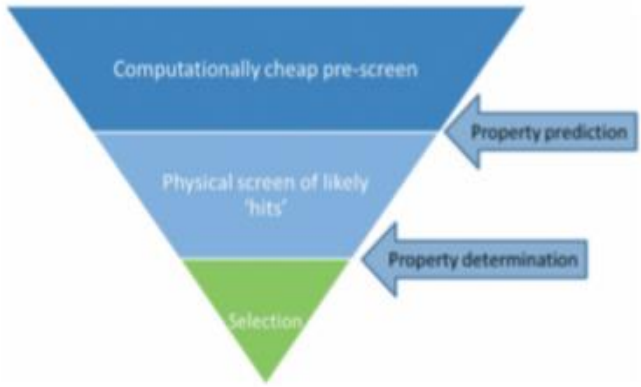

Fig.2.3 Cocrystal screening protocol [5]

Computational screening of cocrystals uses summative surface interaction via electrostatic potential surfaces to predict of the H-bond propensity based on Cambridge Structural Database (CSD) statistics [5]. Charges across the surface of the molecule can interact in pairwise fashion, as a result of which the a strongest hydrogen bond donor to strongest hydrogen bond accepter interaction takes place (Fig.2.4) [5, 33]. This summative energy is then compared to the sum of self:self interactions for both components. The lower energy, more likely structure is then ranked against others to predict the most likely cocrystals or lack of them [5].

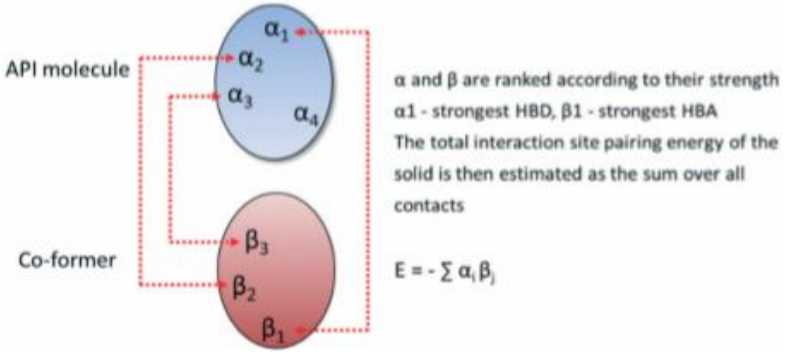

Fig.2.4 Summary surface energy approach to screening [5]

The solvent-assisted grinding is the most common method for cocrystal physical screening due to the inherent propensity of the technique to function in the region of ternary phase space, where cocrystal stability is readily accessible [33, 34].

The aim of the selection is to investigate the physiochemical and crystallographic properties. The physicochemical properties included stability, solubility, dissolution rate and compaction behaviours. Both *in vitro* and *in vivo* tests were used to evaluate the performance of formed cocrystals [35].

2.3.6.2 Cocrystal formation methods

Cocrystals can be prepared using the solution method or by grinding the components together. Sublimation, cocrystals using supercritical fluid, hot-stage microscopy and slurry preparation have also been reported [26, 36].

Solution methods

Slow evaporation from solutions with equimolar or stoichiometric concentrations of cocrystals is one of the most important solution methods. There is, however, a risk of crystallizing the single component phase [1].

The grinding method [37]

Patil et als' preparation of quinhydrone cocrystal products was the first time cocrystals were prepared by cocrystallization without a solution. Instead, reactants were ground together [37, 38]. There are two techniques for cocrystal synthesis by grinding. The first is dry grinding [39], in which the mixtures of cocrystal components are ground mechanically or manually [40], and the second is liquid-assisted grinding [41].

Other methods

Several new methods relating to pharmaceutical cocrystals have also been proposed. Sjoljar et al. prepared 1:1 or 1:2 molar ratio CBZ and NIC cocrystals by a gas anti-solvent method of supercritical fluid process [42]. Lehmann was the first to describe the mixed fusion method in 1877 [43], a methodology refined by Kofler [44]. Because of its use in screening, it is recognized as an effective method by which to identify phase behaviour in a two-component system [45]. David used hot-stage microscopy to screen a potential cocrystal system [45], employing NIC as coformer with a range of APIs with the functionalities of carboxylic acid and amide. Cocrystallization by the slurry technique has been used as a new method for several cocrystals [46]. Noriyuki et al. successfully utilized it for the cocrystal screening of two pharmaceutical chemicals with 11 coformers [47].

2.3.6.3 Properties of cocrystals

Physical and chemical properties of cocrystals are the most important for drug development. The aim of studying pharmaceutical cocrystals is to find a new method to change physicochemical

properties in order to improve the stability and efficacy of a dosage form [1, 48]. The main properties of pharmaceutical cocrystal are as follows:

Melting point

The melting point of a compound is generally used as a means of characterization or purity identification; however because hydrogen bonding networks along with intermolecular forces are known to contribute to physical properties of solids such as enthalpy of fusion, it is also valuable in the pharmaceutical sciences. It is thus very advantageous to tailor the melting point toward a particular coformer of a cocrystal before it is synthesized by the melting point. For example, AMG 517 was selected as the model drug (API) and 10 cocrystals with respective coformers were synthesized. The authors compared their melting points and the results show that those of 10 cocrystals are all between that of AMG 517 (API) and their correspondent coformers [49].

Stability

Physical and chemical stability is very important during storage. Water must also be added in some processes such as wet granulation. The stability of a drug in high humidity is therefore very important. Pharmaceutical cocrystals have an obvious advantage over other strategies. The synthesis of most cocrystals is based on hydrogen bonding, so solvate formation that relies on such bonding will be inhibited by the formation of cocrystals if the interaction between the drug and coformer is stronger than between the drug and solvent molecules. Taking CBZ as an example, even though it is transformed to CBZ dihydrate when exposed to high relative humidity, the cocrystals of CBZ-NIC and CBZ-SAC are not [50], as shown in Fig.2.5.

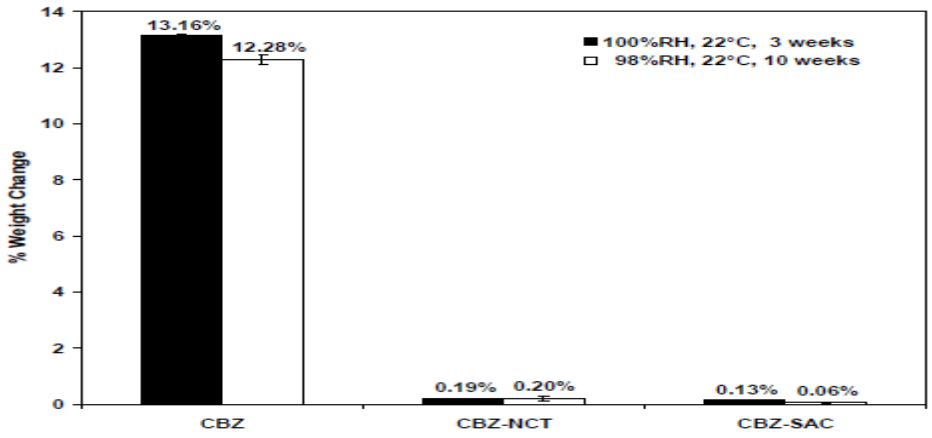

Fig.2.5 Moisture uptake of CBZ III, CBZ-NIC and CBZ-SAC cocrystals at room temperature for three weeks at 100% RH or 10 weeks at 98% RH. Equilibration time represents the rate of transformation from CBZ III to CBZ DH [50]

Compaction behaviours

Pharmaceutical cocrystals have been shown to be a valid method for the improvement of tablet performance. For example, tablet strength was demonstrably improved for ibuprofen and flurbiprofen when cocrystallised with NIC [25].

Dissolution

A dissolution improvement in ibuprofen-nicotinamide cocrystals is shown in Fig.2.6. Based on the spring and parachute model, if the transient improvement in concentration is great and is maintained over a bio-relevant timescale for administration, pharmaceutical cocrystals will be a potential method by which to improve drug bioavailability [25].

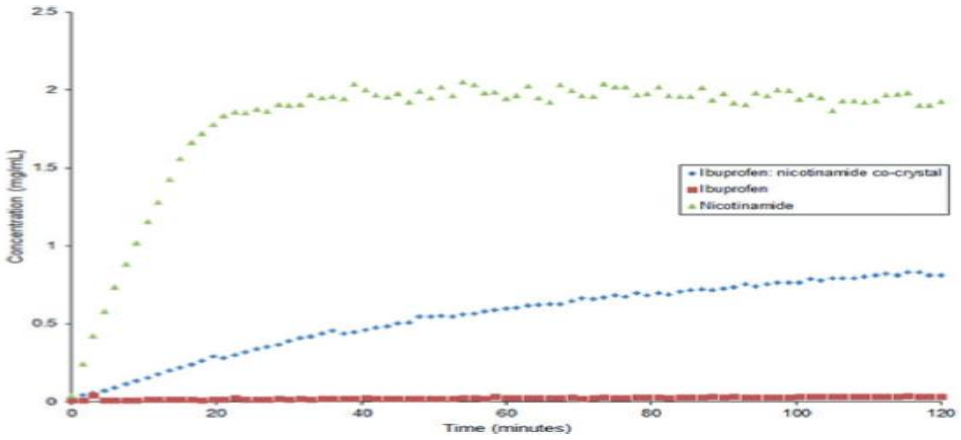

Fig.2.6 Comparison of dissolution of ibuprofen, Nicotinamideand ibuprofen-nicotinamide cocrystals [25]

2.3.6.4 Cocrystal characterization techniques

In generally, the most common techniques used to characterize cocrystal are Raman, Differential Scanning Salorimetry (DSC), Infrared Spectroscopy (IR), XRPD, SEM and Solid State Nuclear Magnetic Resonance Spectroscopy (SSNMR).

2.3.6.5 Theoretical development in the solubility prediction of pharmaceutical cocrystals

Prediction of cocrystal solubility

Pharmaceutical cocrystals can improve the solubility, dissolution and bioavailability of poorly water-soluble drugs. However, true cocrystal solubility is not readily measured for highly soluble cocrystals because they can transform to the most stable drug form in solution. The theoretical

solubility of cocrystals has been the subject of much research. Rodr ́guez-Hornedo's research group has contributed greatly to the study of cocrystal solubility [9] investigating inter alia the solubility advantage of pharmaceutical cocrystals and the predicted solubility of cocrystals based on eutectic point constants, [9, 51].

Cocrystal eutectic point

The cocrystal transition concentration or eutectic point is a key parameter that establishes the regions of thermodynamic stability of cocrystals relative to their components. It is an isothermally invariant point where two solid phases coexist in equilibrium with the solution [9].

Prediction of solubility behaviour by cocrystal eutectic constants [9, 51]

The cocrystal to drug solubility ratio (α) is shown to determine the excess eutectic coformer concentration and the eutectic constant (K_{eu}), which is the ratio of solution concentrations of cocrystal components at the eutectic point. The composition of the eutectic solution and the cocrystal solubility ratio are a function of component ionization, complexation, solvent and stoichiometry.

For cocrystal A_yB_z, where A is the drug and B the coformer, its solubility, eutectic composition and solution complexation from the eutectic of the solid drug A and the cocrystal are predicted by three equations and equilibrium constants

$$A_{solid} \rightleftharpoons A_{soln} \qquad S_{drug} = a_{drug} \tag{Equ.2.1}$$

$$A_yB_{zsolid} \rightleftharpoons yA_{soln} + zB_{soln} \quad K_{sp} = a_{drug}^{y} a_{coformer}^{z} \tag{Equ.2.2}$$

$$A_{soln} + B_{soln} \rightleftharpoons AB_{soln} \qquad K_{11} = \frac{a_{complex}}{a_{drug} a_{coformer}} \tag{Equ.2.3}$$

where S_{drug}, K_{sp} and K_{11} are the intrinsic drug solubility in a pure solvent, the cocrystal solubility product and the complexation constant respectively. Activity coefficients are relatively constant for the dilute solution. By combining Equations 2.1, 2.2 and 2.3, the concentration of the complex at eutectic can be written in Equ.2.4.

$$[AB]_{soln} = K_{11} \left(K_{sp} S_{drug}^{(z-y)} \right)^{1/z} \tag{Equ.2.4}$$

As described in the definition of the cocrystal eutectic point, for poorly water-soluble drugs and more soluble coformers, the eutectic should be for solid drugs and cocrystals in equilibrium with the solution. The solubility, stability and equilibrium behaviour are all relevant to the eutectic constant (K_{eu}), which is the concentration ratio of total coformer to total drug that satisfies equilibrium equations Equ.2.1 to Equ.2.5

$$K_{eu} = \frac{[B]_{eu}}{[A]_{eu}} = \frac{[B] + [AB]}{[A] + [AB]}$$

$$= \left[\frac{\left(K_{sp}/S_{drug}^{y}\right)^{1/z} + K_{11}\left(K_{sp}S_{drug}^{(z-y)}\right)^{1/z}}{S_{drug} + K_{11}\left(K_{sp}S_{drug}^{(z-y)}\right)^{1/z}}\right] \quad \text{Equ.2.5}$$

The cocrystal K_{sp} and drug solubility represent the eutectic concentrations of free components. Considerations of ionization for either component can be added to this equation. For a monoprotic acidic coformer and basic drug, Equ.2.5 is rewritten as

$$K_{eu} = \frac{[B]_{eu}}{[A]_{eu}} = \frac{[B]_{unionized} + [B]_{ionized} + [AB]}{[A]_{unionized} + [A]_{ionized} + [AB]}$$

$$= \left[\frac{\left(\frac{K_{sp}}{S_{drug}^{y}}\right)^{1/z}\left(1+\frac{Ka_{coformer}}{[H^+]}\right) + K_{11}\left(K_{sp}S_{drug}^{(z-y)}\right)^{1/z}}{S_{drug}\left(1+\frac{[H^+]}{Ka_{drug}}\right) + K_{11}\left(K_{sp}S_{drug}^{(z-y)}\right)^{1/z}}\right] \quad \text{Equ.2.6}$$

where $[H^+]$ is the hydrogen ion concentration and K_a is the dissociation constant for the acidic conformer or the conjugate acid of the basic drug. Considering the case of components with multiple Ka values and negligible solution complexation, the K_{eu} as a function of pH is

$$K_{eu} = \frac{\left(\frac{K_{sp}}{S_{drug}^{y}}\right)^{1/z}\left(1+\sum_{f=1}^{g}\frac{\prod_{h=1}^{f} Ka_h^{acidic}}{[H^+]^f} + \sum_{i=1}^{j}\frac{[H^+]^i}{\prod_{k=1}^{i} Ka_k^{basic}}\right)_{coformer}}{S_{drug}\left(1+\sum_{l=1}^{m}\frac{\prod_{n=1}^{l} Ka_n^{acidic}}{[H^+]^l} + \sum_{p=1}^{q}\frac{[H^+]^p}{\prod_{r=1}^{p} Ka_r^{basic}}\right)_{drug}} \quad \text{Equ.2.7}$$

where g and m are the total number of acidic groups for each component and j and q are the total number of basic groups. In this case the eutectic constant is a function of the cocrystal solubility product, drug solubility and ionization. Letting the ionization terms for drug and coformer equal δ_{drug} and $\delta_{coformer}$, Equ.2.7 simplifies to

$$K_{eu} = \left(\frac{K_{sp}\delta_{coformer}^{z}}{S_{drug}^{(y+z)}\delta_{drug}^{z}} \right)^{1/z} \quad \text{Equ.2.8}$$

K_{eu} can also be expressed as a function of the cocrystal to drug solubility ratio (α) in pure solvent using the previously described equation for cocrystal solubility [9]

$$K_{eu} = zy^{y/z}\alpha^{(y+z)/z} \quad \text{Equ.2.9}$$

$$where \quad \alpha = \frac{S_{cocrystal}}{S_{drug}\delta_{drug}} \quad \text{Equ.2.10}$$

$$and \ S_{cocrystal} = \sqrt[y+z]{K_{sp}\delta_{coformer}^{z}\delta_{drug}^{y}/(y^{y}z^{z})} \quad \text{Equ.2.11}$$

For a drug with known solubility, Equ.2.9 allows the cocrystal solubility to be predicted from the eutectic constant or vice versa. For a 1:1 cocrystal (i.e. y=z=1), Equ.2.9 becomes $K_{eu} = \alpha^2$, indicating that K_{eu} is the square of the solubility ratio of cocrystal to drug in a pure solvent. A K_{eu} greater than 1 thus indicates that the 1:1 cocrystal is more soluble than the drug, while a less soluble one would have K_{eu} values of less than 1.

The prediction solubility of cocrystals CBZ-NIC, CBZ-SAC and CBZ-CIN is discussed in the Appendiceses.

Cocrystal Solubility (Scc) and the Phase Solubility Diagram (PSD) [9, 51]

The solubility and stability of cocrystals can be explained by phase solubility diagrams. One stable cocrystal (Case 1) and one metastable cocrystal (Case 2) in solvent are shown in Fig.2.7. The solubility product behaviour of the cocrystal with the drug concentration as a function of the coformer (ligand) is shown by these curves based on $[drug]^y = K_{sp}/[coformer]^z$ from Equ.2.2. The drug solubility, shown by the horizontal line, is assumed to be much lower than the ligand (coformer) solubility, which is not shown. A dashed line represents stoichiometric solution concentrations or stoichiometric dissolution of cocrystals in pure solvent, and their intersection with the cocrystal solubility curves (marked by circles) indicates the maximum drug concentration associated with the cocrystal solubilities. For a metastable cocrystal (Case 2), the drug concentration associated with the cocrystal solubility is greater than the solubility of the stable drug form (the horizontal line). The solubility of a metastable cocrystal is not typically a measurable equilibrium, and these cocrystals are referred to as incogruently saturating. As a metastable

cocrystal dissolves, the drug released into the solution can crystallize because of supersaturation. This supersaturation is a necessary, but not sufficient condition for crystallization. In certain instances, slow nucleation might delay crystallization of the favoured thermodynamic form and enable measurement of the true equilibrium, solubility. In Case 1, a congruently saturating cocrystal has a lower drug concentration than the pure drug form at their respectively solubility values. The solubility of congruently saturating cocrystals can therefore be readily measured from solid cocrystals dissolved and equilibrated in solution.

For both congruently and incongruently saturating cocrystals, eutectic points, indicated by Xs in Fig.2.8, are the points where both solid drug and cocrystal are in equilibrium with a solution containing drug and coformer. The drug and conformer solution concentrations at the eutectic point are together referred to as the transition concentration (C_{tr}).

The solubility product expresses all possible solution concentrations of the drug and the ligand (coformer) in equilibrium with the solid cocrystal, and is directly related to cocrystal solubility by Equ.2.11. Inserting the cocrystal transition concentration ($[A]_{tr}$ and $[B]_{tr}$) into Equ.2.11 allows Equ.2.12 to be rewritten as

$$S_{A_yB_z} = \sqrt[y+z]{[A]_{tr}^{y}[B]_{tr}^{z}\delta_{coformer}^{z}\delta_{drug}^{y} \Big/ y^y z^z} \qquad \text{Equ.2.12}$$

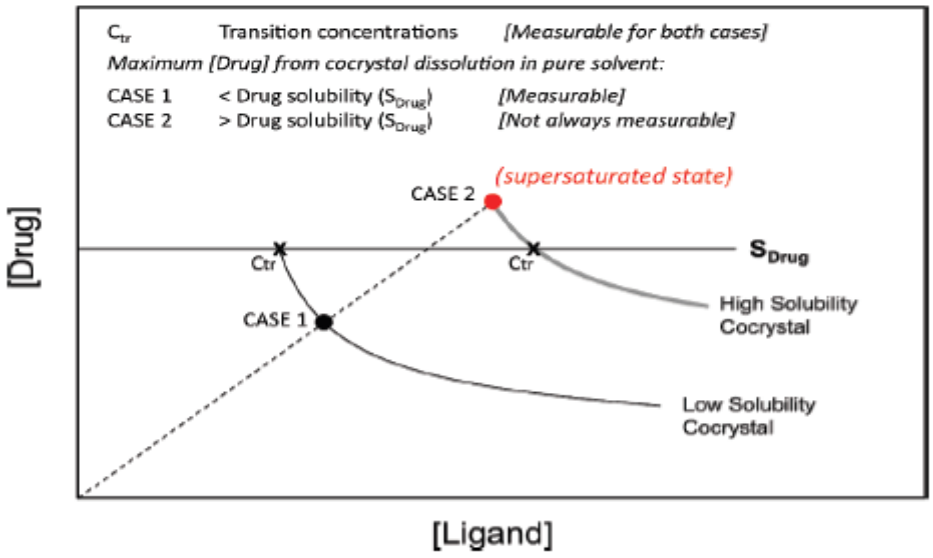

Fig.2.7 Schematic phase solubility diagram of two different cocrystals based on the K_{sp} for a stable (Case 1) or metastable (Case 2) cocrystal [9]

Methods used to determine the transition concentration C_{tr} have been investigated [9]. A flowchart of two methods used to determine cocrystal transition concentrations is shown in Fig 2.8. Method 1: Cocrystal C_{tr} was measured by adding the drug to a near saturated coformer solution and slurring for 24 hours. Method 2: The same cocrystal was measured by dissolving it in a saturated drug solution and then slurring it for 24 hours. There should be two solid phases (cocrystal and drug) in the collected samples after this period. The drug and coformer (ligand) concentration were analysed by High-Performance Liquid Chromatography (HPLC).

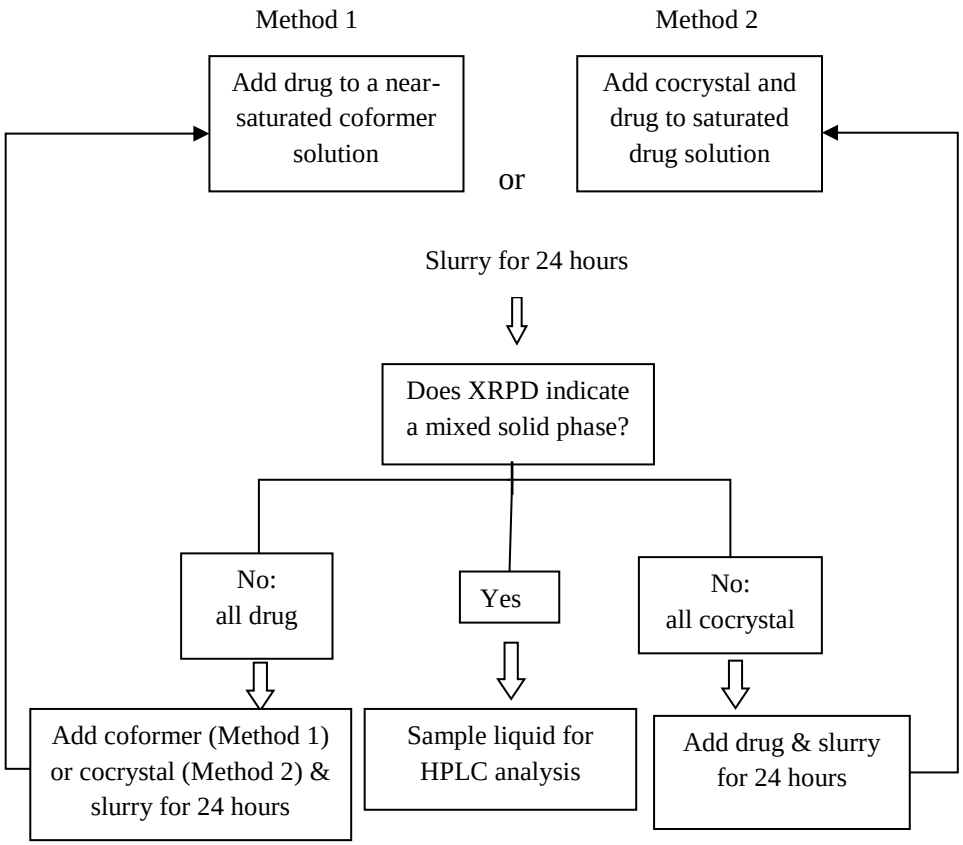

Fig.2.8 Flowchart of method used to establish the invariant point and determine equilibrium solubility transition concentration of cocrystal components [9]

Solution Mediated Phase Transformation (SMPT)

Many approaches have been used to improve the solubility of poorly water-soluble drugs. However, these approaches all result in a phenomenon called "Solution Mediated Phase Transformation" (SMPT), the crystallization of a stable solid phase during dissolution of a metastable phase caused by supersaturation conditions in solution or at the surface of the dissolving solid, as shown in Fig.2.9. The dissolution advantage is therefore lost during dissolution resulting from the crystallization of a stable phase.

Many important properties of solid materials are determined by crystal packing, so crystal polymorphism has been increasly recognized. For example, more than one crystalline polymorph may exist in pharmaceutical supramolecular isomers. The dissolution rate, equilibrium solubility and absorption may differ significantly [52].

In a monotropic polymorphic system this compound has two forms, Phases I and II. As the metastable solid (Phase I) dissolves, the solution is supersaturated with respect to Phase II, leading to precipitate Phase II and growth [53]. SMPT has been extensively examined for many years as regards amorphous solids, polymorphs and salts [54-56]. However, only a few studies have focused on the SMPT of cocrystals during dissolution.

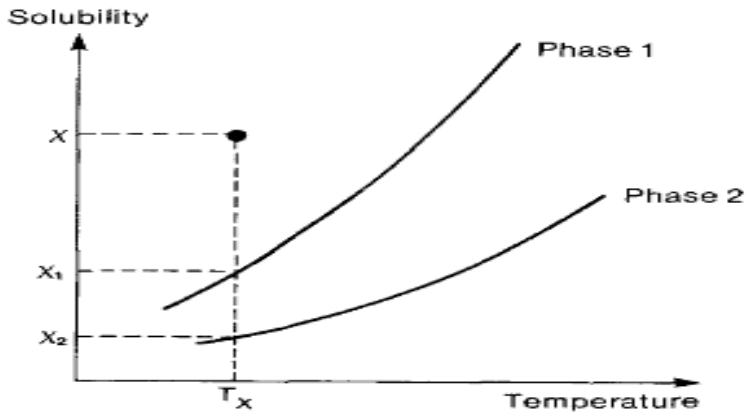

Fig.2.9 Phase diagram for a monotropic system [57]

In our previous lab works, different forms of CBZ (Form I, Form III and CBZ DH, CBZ-NIC cocrystals and physical mixtures) were studied *in situ* using UV imaging techniques. Within the first three minutes all intrinsic dissolution rates (IDRs) of the test samples reached their maximum values. During the three-hour dissolution test the IDR of CBZ DH was almost constant at 0.0065 mg/min/cm^2. The IDR profiles of CBZ I and CBZ III were similar, with the maximum IDRs being reached in two minutes and then decreasing quickly to relatively stable values. The greatest variability in IDR of the CBZ-NIC mixture is shown in Fig.2.10. Its IDR_{max} is the highest of the five test samples due to the effect of a very high concentration of NIC in the solution. Compared with CBZ I, CBZ III and the CBZ-NIC mixture, the IDR of CBZ-NIC cocrystals decreased slowly during dissolution, so it has the highest IDR from the eighth minute among all the samples [8].

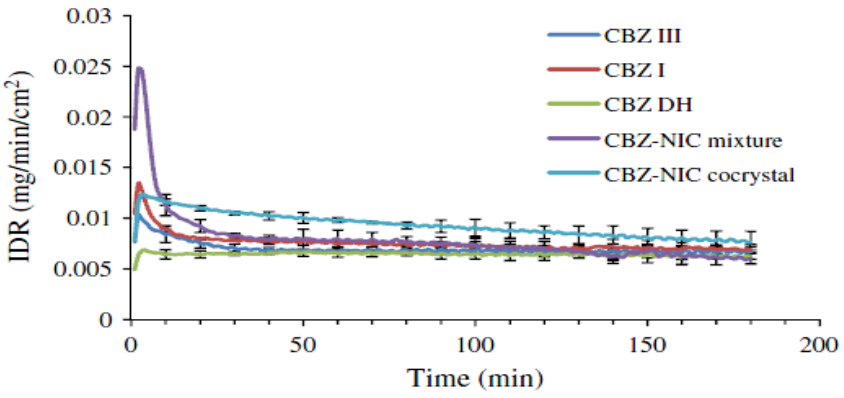

Fig.2.10 Intrinsic dissolution rates as a function of dissolution time obtained by UV imaging at a flow rate of 0.2 mL/min (n=3) [8]

Studies of the effects of surfactants and polymers on cocrystal dissolution has shown that they can impart thermodynamic stability to cocrystals that otherwise convert to a stable phase in aqueous solution [58].

Effects of polymers and surfactants on the transformation of cocrystals

The means of maintaining the solubility advantage of cocrystals is very important. The "spring and parachute model" has been widely used in cocrystal systems. This behaviour is characterised by a transient improvement in concentration and a subsequent drop, normally to the solubility limits of the free form in that pH environment [5]. The usefulness of pharmaceutical cocrystals depends on the timescale and extent of any improvement in concentration [25]. If such improvement occurs over a bio-relevant timescale, it is believed to improve bioavailability [5].

Mechanisms for stabilizing supersaturation cocrystals in a polymer solution may result from the stabilization of its supersaturation by intermolecular H-bonding between drug and polymers [59], and the prevention of transformation by delaying nucleation or inhibiting crystal growth [60]. The effect of polymers on the dissolution behaviour of indomethacin-saccharin (IND-SAC) cocrystals has been investigated by Amjad [61]. Predissolved PVP was used to examine polymer inhibition of indomethacin crystallization. PVP was chosen because it forms hydrogen bonds with solid forms of IND [62]. The dissolution behaviour of IND-SAC cocrystals was studied in buffer, predissolved 250 ug/mL PVP and 2% w/v PVP as shown in Fig.2.11. The results indicate that conversion of cocrystals takes place, but that PVP can kinetically inhibit indomethacin crystallization at higher concentrations and can maintain a supersaturation level at these concentrations for a certain time.

The maintenance of supersaturation is of great importance in order to avoid erratic absorption of the drug [61].

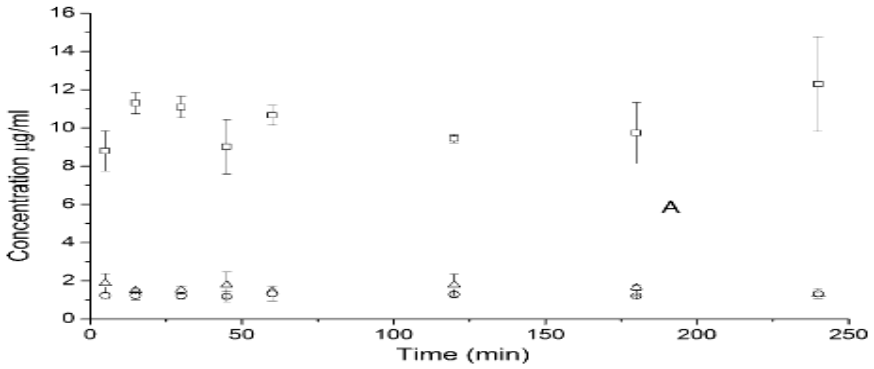

Fig.2.11 The concentration of indomethacin resulting from indomethacin-saccharin cocrystals at various times in PB at pH3. (△) in buffer only (○) in predissolved 250 ug/mL PVP (□) in predissolved 2% w/v PVP [61]

The mechanism for stabilizing supersaturation cocrystals in surfactant solution differs from polymer solution. The solubility of poorly soluble drugs was increased by micellar surfactant solubilisation through micelle formation [61]. This approach is based on the differential solubilisation of the cocrystal components, where the surfactant preferentially increase the solubility of the poorly soluble component through micelle formation, resulting in the stabilization or minimization of the thermodynamic driving force behind conversion of the cocrystal. The effect of the surfactant on the dissolution behaviour of IND-SAC cocrystals was also investigated by Amjad [61]. The surfactant SLS was predissolved at various concentration in the range of 0-800 mM, and the eutectic points were determined. The Fig.2.12 shows the concentration of IND and SAC as a function of SLS concentration at the eutectic points. It can be seen that concentration of IND dramatically increased relatively to that of SAC with increasing SLS concentrations.

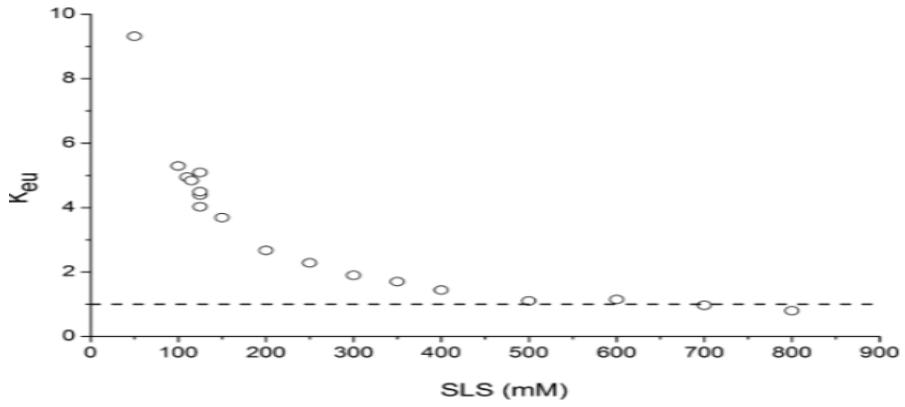

Fig.2.12 K_{eu} values (○) as a function of SLS concentration, The dotted line represents the theoretical presentation of K_{eu} =1 at various concentration of SLS

The dissolution behaviour of CBZ-SAC cocrystals in predissolved 25 mM SLS and 100 mM SLS is shown in Fig.2.13. The results indicate that the concentration of IND increases dramatically with increased SLS concentrations. The concentrated IND exhibited a parachuting effect with 25 mM SLS, dropping after the first measurement (two minutes) and continuing to decrease. With 100 mM SLS, IND reached a supersaturated state in 10 minutes [61].

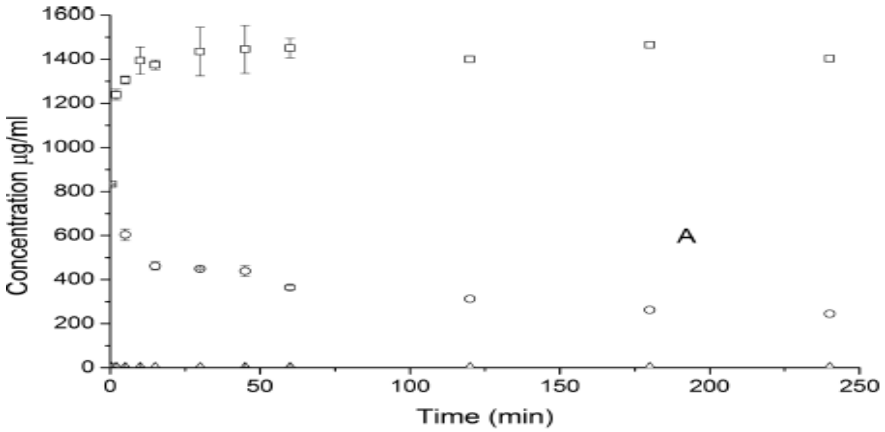

Fig.2.13 The concentration of indomethacin resulting from indomethacin-saccharin cocrystals at various times in PB at pH3 (△) in buffer only (○) in predissolved 25 mM SLS (□) in predissolved 100 mM SLS [61]

2.4 The formulation of tablets by QbD

2.4.1 Drug delivery system-Tablets

Tablets were the most common form of dosage. It has many advantages over other forms, including simplicity of administration, ease of portability by the patient, simplicity and speed of mass production and markedly lower manufacturing cost [14].

2.4.1.1 Types of tablets [14]

The commonest type is those intended to be swallowed whole. Many tablets are formulated to be effervescent because of their more rapid release of medicament and reduced chance of causing gastric irritation. Some tablets are designed to be chewed and used where buccal absorption is desired. There are now many types of tablets that provide for the release of the drug to be delayed or that allow a controlled, sustained rate of release.

2.4.1.2 Tablet excipients

A tablet does not contain only the active ingredient, but also other substances known as excipients, which have specific functions.

Diluents

Diluents are inert substances that are added to the active ingredient in sufficient quantity to make a reasonably sized tablet. Lactose, dicalcium phosphate and microcrystalline cellulose are used extensively as tablet diluents.

Binder agents

The substances that act as adhesives to bind powders together in the wet granulation process are known as binders. They are also used to bind granules together during compression. If the binding is too little in a formulation, soft granules result. Conversely, too much binding produces large, hard granules. The most common binders are glucose, starch and polyvinylpyrrolidone.

Glidants

Glidants are materials added to tablet formulations to improve the flow properties of the granulations. The most commonly used and effective glidant is colloidal silica.

Lubricants

These agents are required to prevent adherence of the granules to the punch faces and dies. They also ensure smooth ejection of the tablet from the die. Talc and magnesium stearate appear to be effective as punch lubricants.

Disintegrants

Disintegrants are always added to tablets to promote their breakup when they are placed in an aqueous environment. The object of a disintegrant is to cause the tablet to disintegrate rapidly so as to increase the surface area of the tablet fragments and so promote rapid release of the drug. Starch, cross-linked polyvinypyrrolidone and cellulose materials are commonly-used disintegrants.

2.4.1.3 Tablet preparation

The two methods of tablet preparation are dry and wet, with direct compression and wet granulation being the most common respective examples. Their details are as follows:

Direct compression

The steps involved in direct compression are shown in Fig.2.14. The potential of this method lies in the discovery of directly compressible fillers or diluents which produce good quality tablets without prior manipulation. The direct compression diluents include microcrystalline cellulose, lactose, modified starch and dicalcium phosphate.

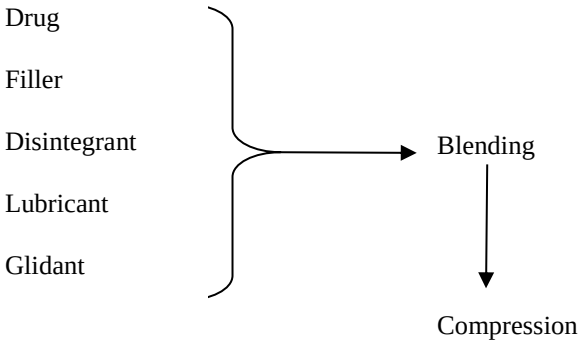

Fig.2.14 Tablet production by direct compression [14]

Direct compression offers several advantages: the small number of stages involved, the low cost of appliances and handling, and stability due to the fact that no heat and water are involved. Although it is a simple method, there are, however, limitations to its use. The difference in particle size and bulk density between the diluent and the drug may result in variations in the drug content of the tablets.

Wet granulations

This is the traditional method of giving a particulate solid those properties needed for it to produce satisfactory tablets. The process essentially consists of sticking the particles together using an adhesive material, thereby increasing particle size and improving flow properties. The enlarged particles are termed granules. Other additives are usually also incorporated at some stage. The process is represented in Fig.2.15.

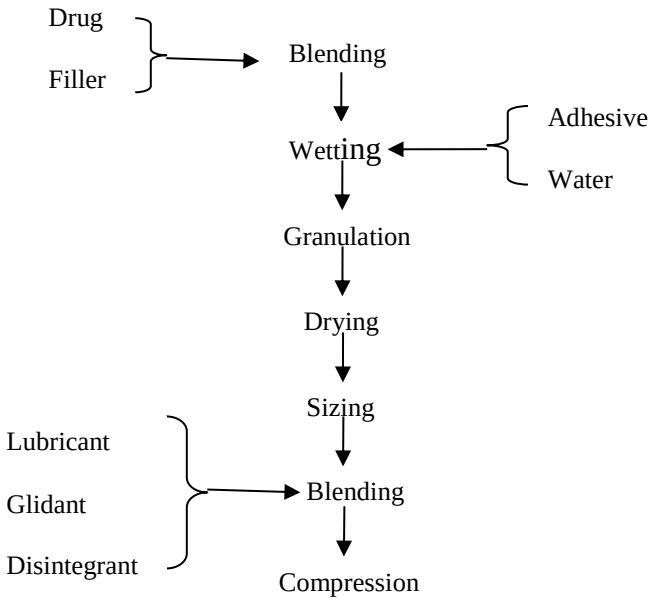

Fig.2.15 Tablet production by wet granulation [14]

2.4.2 QbD

2.4.2.1 Introduction of QbD

Pharmaceutical development involves traditional and systematic approaches. The former mainly depends on empirical evaluation of product and process performance. Product quality is tested at the end of the process or sometimes at a specific stage during production, rather than being designed into the process [63]. The aim of QbD, on the other hand, is to make more effective use of the latest pharmaceutical science and engineering principles and knowledge throughout the lifecycle of a product [64]. The difference between traditional approach and systematic (QbD) approaches are summarized in Table 2.1.

Table 2.1 Difference between traditional and QbD approaches [65]

Aspects	**Traditional**	**QbD**
Pharmaceutical development	Empirical	Systematic; multivariate experiments
Manufacturing process	Fixed	Adjustable within design space; opportunities for innovation
Process control	In process testing for go/on-go; offline analysis wide or slow response	PAT utilized for feedback and feed forward at real time
Product	Primary means of quality control; based	Part of the overall control strategy, based

specification	on batch data	on the desired product performance
Control strategy	Mainly by intermediate product and end product testing	Risk based; controlled shifted up stream, real time release
Lifecycle Management	Reactive time problem; Post approval changes needed	Continual improvement enabled within design space

QbD should include some basic elements. The Quality Target Product Profile (QTPP) forms the basis of design for the development of the product; it is a summary of the quality characteristics of product. Critical Quality Attributes (CQAs) are physical, chemical, biological or microbiological properties or characteristics that should fall within an appropriate limit range or distribution to ensure the desired product quality. Table S.2.1 in the Appendices summarizes the quality attributes of Example sustained release tablets and indicated which attributes were classified as drug product CQAs. For this product, physical attributes, assay, content uniformity and drug release are investigated and discussed in detail. Risk Assessment (RA) is a valuable science-based process used in quality risk management that can help identify which material attributes and critical process parameters (CPPs) could affect product CQAs [66]. Fig.2.16 presents a simplified flow-chart of the QbD process.

Statistical Design of Experiment (DoE) is a valuable tool with which to establish in mathematical form the relationships between CQAs and CPPs. The main purpose of DoE is to find the design space (DS). Regardless of how a DS is developed, it is expected that operation within it will result in a product matching the defined quality [65]. A control strategy is designed to ensure that a product of the required quality will produced consistently. Such a strategy can include, but is not limited to, the control of input material attributes, in-process or real-time release testing in lieu of end-product testing, and a monitoring program for verifying multivariate prediction models [66]. Working within the DS is not considered to be a change [67].

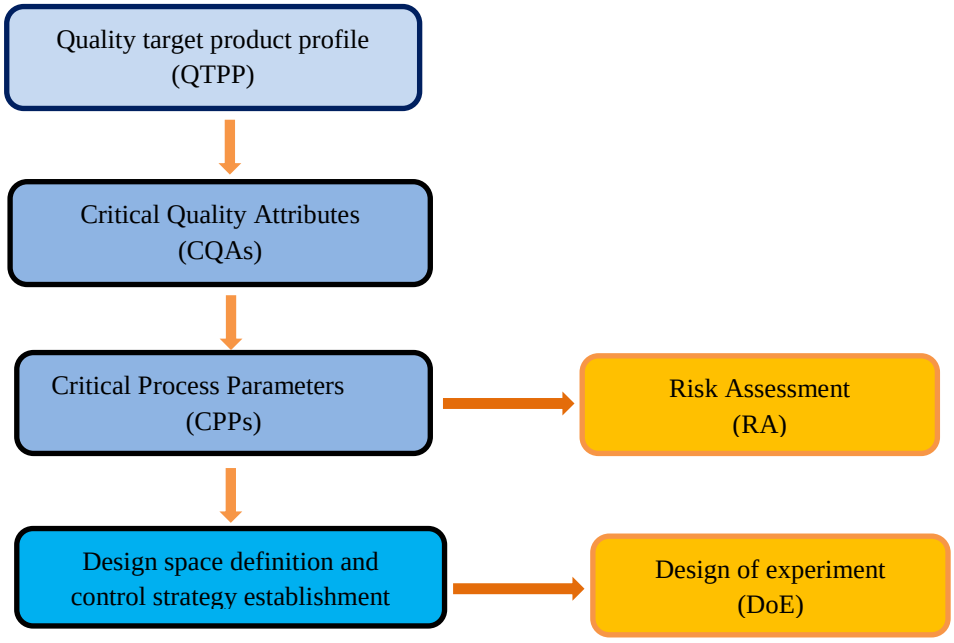

Fig.2.16 Simplified flow-chart of the QbD process

2.4.2.2 Design of Experiments (DoE)

Design of Experiments (DoE) techniques enable designers to determine simultaneously the individual and interactive effects of the factors that could affect the output results in any design. These techniques therefore help pinpoint the sensitive parts and areas in designs that cause problems in yield. Designers are then able to fix these problems and produce robust and higher-yield designs prior to going into production [68].

Basically, there are two kinds of DoE: screening and optimization. The former is the ultimate fractional factorial experiments, which assume that the interactions are not significant. Critical variables which will affect the output are determined by literally screening the factors [69]. Optimization DoE aims to determine the range of operating parameters for design space and to consider more complex simulations such as the quadratic terms of variables.

Full Factorials Design

As the name implies, full factorials experiments examine all the factors involved completely, together with all possible combinations associated with those factors and their levels. They look at the effects of the main factors and all interactions between them on the responses [69]. The sample size is the product of the numbers of levels of the factors. For example, a factorial experiment with two-level, three-level and four-level factors has 2 x 3 x 4 = 24 runs. Full factorial designs are the

most conservative of all design types. There is little scope for ambiguity when all combinations of the factors' settings are tried. Unfortunately, the sample size grows exponentially according to the number of factors, so full factorial designs are too expensive to run for most practical purposes [70].

Response Surface Methodology (RSM) [71]

Response surface designs are useful for modelling curved quadratic surfaces to continuous factors. A response surface model can pinpoint a minimum or maximum response, if one exists inside the factor region. It includes three kinds of central composite designs together with the Box-Behnken design, as shown in Fig.2.17.

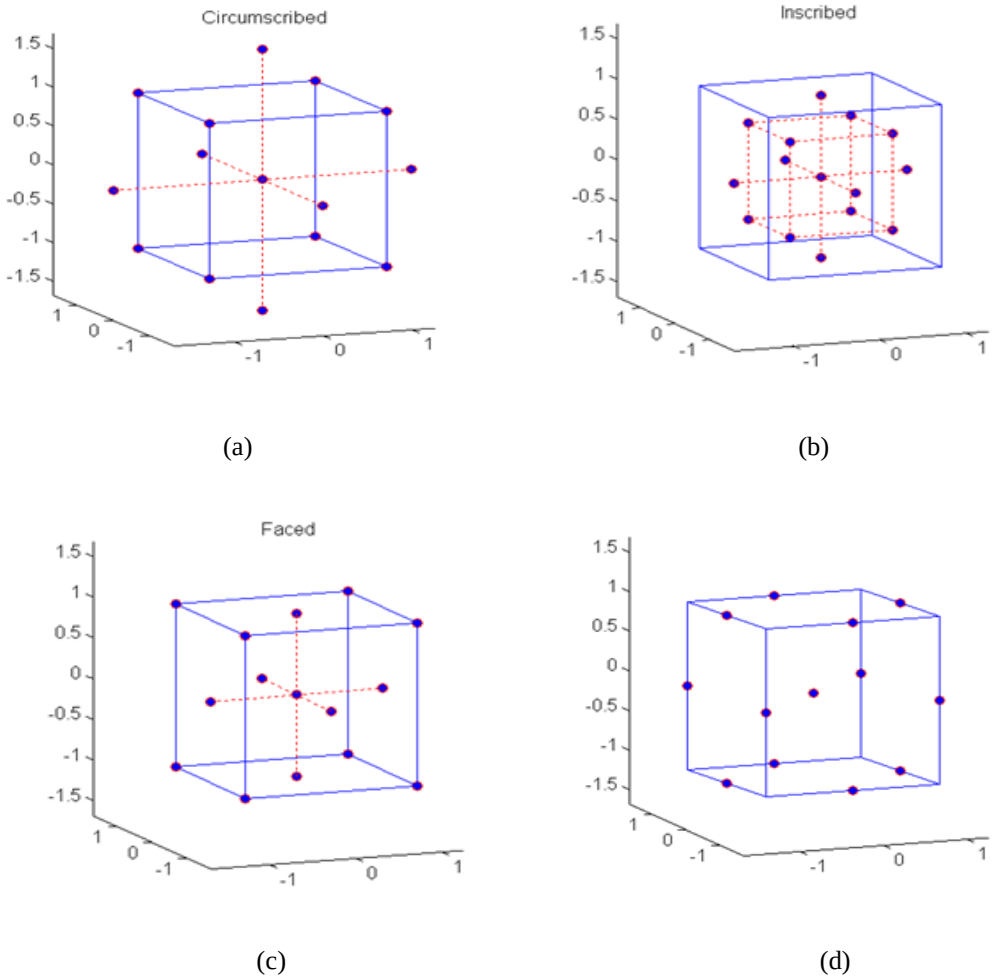

Fig.2.17 Response surface designs: (a) Circumscribed (b) Inscribed (c) Faced (d) Box-Behnken [72]

The Box-Behnken statistical design is one type of RSM design. It is an independent, rotatable or nearly rotatable, quadratic design having the treatment combinations at the midpoints of the edges of the process space and at the centre [73, 74]. The present author used it to optimize and evaluate the main, interaction and quadratic effects of the formulation variables on the quality of tablets in

her research. Because fewer experiments are run and less time is consequently required for the optimization of a formulation compared with other techniques, it is more cost-effective.

One distinguishing feature of the Box-Behnken design is that there are only three levels per factor; another is that no points at the vertices of the cube are defined by the ranges of the factors. This is sometimes useful when it is desirable to avoid these points because of engineering considerations.

For the response surface methodology involving Box-Behnken design, a total of 15 experiments are designed for 3 factors at 3 levels of each parameter shown in Table 2.2.

Table 2.2 Box-Behnken experiment design

Run	Independent variables (levels)			
	Mode	X_1	X_2	X_3
1	−−0	-1	-1	0
2	−0−	-1	0	-1
3	−0+	-1	0	1
4	−+0	-1	1	0
5	0−−	0	-1	-1
6	0−+	0	-1	1
7	000	0	0	0
8	000	0	0	0
9	000	0	0	0
10	0+−	0	1	-1
11	0++	0	1	1
12	+−0	1	-1	0
13	+0−	1	0	-1
14	+0+	1	0	1
15	++0	1	1	0

The design is equal to the three replicated centre points and the set of points are lying at the midpoint of each surface of the cube defining the region of interest of each parameter, as described by the red points in Fig.16 (d). The non-linear quadratic model generated by the design is given as below

$$Y = b_0 + b_1X_1 + b_2X_2 + b_3X_3 + b_{12}X_1X_2 + b_{13}X_1X_3 + b_{23}X_2X_3 + b_{11}X_1^2 + b_{22}X_2^2 + b_{33}X_3^2 \qquad \text{Equ.2.13}$$

where, Y is a measured response associated with each factor level combination; b_0 is an intercept; b_1 to b_{33} are regression coefficients calculated from the observed experimental values of Y; and X_1, X_2 and X_3 are the coded levels of independent variables. The terms X_1X_2, X_1X_3, X_2X_3 and X_i^2 (i=*1, 2, 3*) represent the interaction and quadratic terms, respectively.

2.5 CBZ studies

2.5.1 CBZ cocrystals

2.5.1.1 Introduction

CBZ was discovered by chemist Walter Schindler in 1953 [75], and now is a well-established drug used in the treatment of epilepsy and trigeminal neuralgia [76]. CBZ is a white or off-white powder crystal. The molecule structure of CBZ is shown in Fig.2.18. It has at least four anhydrous polymorphs: triclinic (Form I), trigonal (Form II), monoclinic (Form III and IV) and a dihydrate as well as other solvates [55, 77]. Form I crystallizes in a triclinic cell (*P-1*) having four inequivalent molecules with the lattice parameters a=5.1706(6), b=20.574(2), c=22.452(2) Å, $\alpha = 84.12(4)$, $\beta = 88.01(4)$ and $\gamma = 85.19(4)°$. The asymmetric unit consists of four molecules (Fig.2.19) that each form hydrogen-bonded *anti* dimers through the carboxamide donor and carbonyl acceptor, as in the other three modifications of the drug [52]. Graph set analysis [78] reveals that these are R2,2(8) dimers. However, only two dimers are centrosymmetric, formed between identical residues (Fig.2.20), whereas the other unique dimer is pseudocentrosymmetric and consists of inequivalent 1,3 residue pairs, where the two N-H··· O hydrogen bonds differ by <0.1 Å [52].

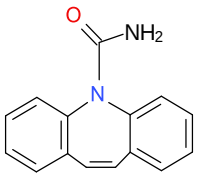

Fig.2.18 Molecular structure of CBZ

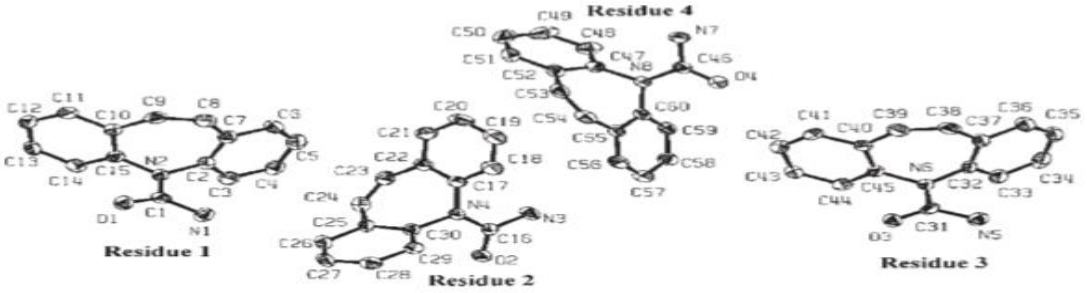

Fig.2.19 Thermal ellipsoid plot of triclinic CBZ showing the four inequivalent molecules in the unit cell [52]

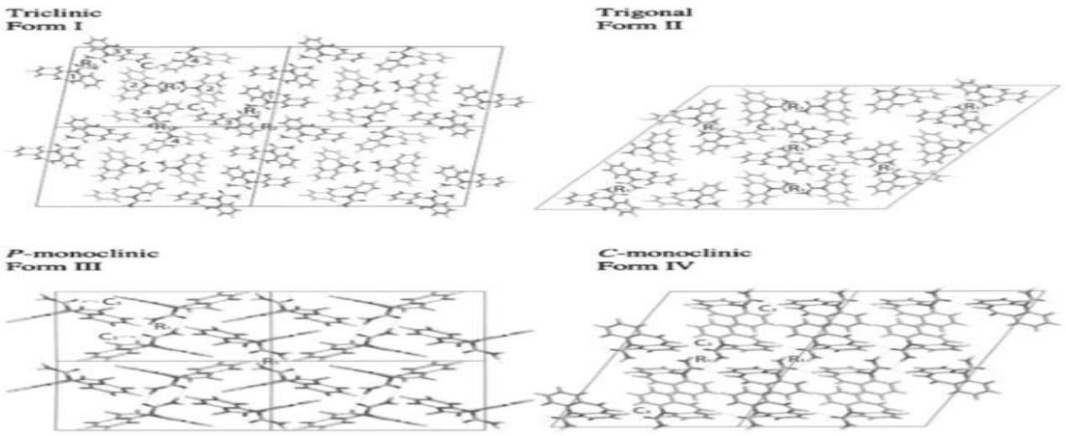

Fig.2.20 Packing diagrams of all four forms of CBZ showing hydrogen-bonding patterns. The notation indicates the position of important hydrogen-bonding patterns, and is as follows: R_1=R2,2(8); R_2=R2,4(20); C_1=C3,6(24); C_2=C1,2(8); C_3=C(7). The Arabic numbers on Form I correspond to the respective residues [52]

2.5.1.2 Current research

Given that pharmaceutical scientists are always seeking to improve the quality of their drug substances, it is not surprising that cocrystal systems of pharmaceutical interest have begun to receive extensive attention [79]. In recent years there has been much research into improving CBZ solubility and dissolution rates [80-82]. The database of 50 crystal structures containing the CBZ molecule are summarized in Table 2.3 [83].

Table 2.3 A summary of CBZ cocrystals [52]

	CBZ cocrystals	**references**
1	CBZ Form I	
2	CBZ Form II	
3	CBZ Form III	
4	CBZ Form IV	
5	CBZ/actone (1:1)	[84]
6	CBZ/water (1:2)	[85]
7	CBZ./furfural (1:0.5)	[86]
8	CBZ/trifluoroacetic acid (1:1)	[87]
9	CBZ/10,11-dihydrocarbamazepine (1:1)	[88]
10	CBZ/*N*,*N*-dimethylformamide (1:1)	[89]
11	CBZ/2,2,2-trifluoroethanol (1:1)	[90]
12	CBZ/aspirin (1:1)	[91]
13	CBZ/dimethylsulfoxide (1:1)	[84]
14	CBZ/benzoquinone (1:0.5)	[84]

15	CBZ/terepthalaldehydr (1:0.5)	[84]
16	CBZ/saccharin (1:1)	[84]
17	CBZ/nicotinamide (1:1)	[84]
18	CBZ/acetic acid (1:1)	[84]
19	CBZ/formic acid (1:1)	[84]
20	CBZ/butyric acid (1:1)	[84]
21	CBZ/trimesic acid/water (1:1:1)	[84]
22	CBZ/5-nitroisophthalic acid/methanol (1:1:1)	[84]
23	CBZ/adamantine-1,3,5,7-tetracarboxylic acid (1:0.5)	[84]
24	CBZ/formamidine (1:1)	[84]
25	CBZ/quinoxaline-*N,N'*-dioxide (1:1)	[92]
26	CBZ/hemikis (pyrazine-*N,N'*-dioxide) (1:1)	[92]
27	CBZ/ammonium chloride (1:1)	[93]
28	CBZ/ammonium bromide (1:1)	[93]
29	CBZ/4,4'-bipyridine (1:1)	[94]
30	CBZ/4-aminobenzoic acid (1:0.5)	[94]
31	CBZ/4-aminobenzoic acid/water (1:0.5:0.5)	[94]
32	CBZ/2,6-pyridinedicarboxylic acid (1:1)	[94]
33	CBZ/*N,N*-dimethylacetamide (1:1)	[95]
34	CBZ/*N*-methylpyrrolidine (1:1)	[95]
35	CBZ/nitromethane (1:1)	[95]
36	CBZ/benzoic acid (1:1)	[83]
37	CBZ/adipic acid (2:1)	[83]
38	CBZ/succinic acid (1:0.5)	[96]
39	CBZ/4-hydroxybenzoic acid (1:1) form A	[83]
40	CBZ/4-hydroxybenzoic acid (1:0.5) form C	[83]
41	CBZ/4-hydroxybenzoic acid (1:X) form B	[83]
42	CBZ/glutaric acid (1:1)	[83]
43	CBZ/malonic acid (1:0.5) form A	[96]
44	CBZ/malonic acid (1:X) form B	[83]
45	CBZ/salicylic acid (1:1)	[83]
46	CBZ-/$_{L}$-hydroxy-2-naphthoic acid (1:1)	[83]
47	CBZ/$_{DL}$-tartaric acid (1:X)	[83]
48	CBZ/maleic acid (1:X)	[83]
49	CBZ/oxalic acid (1:X)	[83]
50	CBZ/(+)-camphoric acid (1:1)	[83]

The tree diagram (Fig.2.21) was generated using the Crystal Packing Similarity tool, based on the size of the cluster that relates them as a group. The data in Fig.2.21 indicates that all the structures with blue dots share an identical cluster of three CBZ molecules. 12, 39, 3, 29, 5 and 13 all contain

similar clusters of three CBZ molecules, while 32, 25, 16, 33 and 34 each contain a third unique cluster of three CBZ molecules. The remaining eight structures do not have clusters of three CBZ molecules that match any other structures [52].

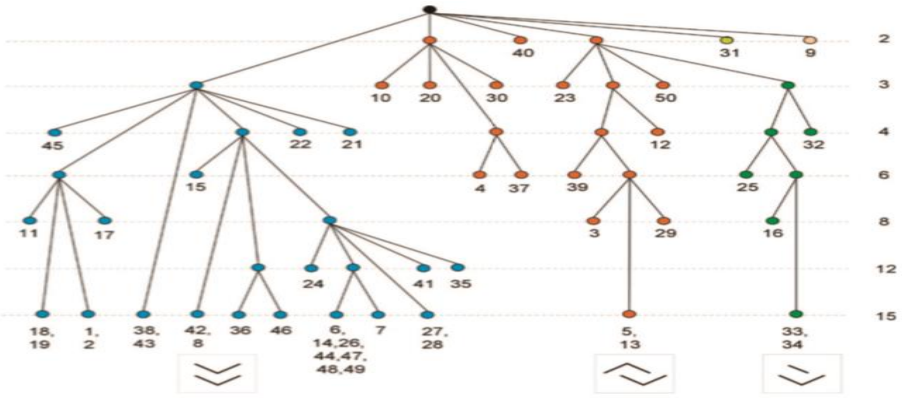

Fig.2.21 A tree diagram based on the results of the Crystal Packing Similarity tool [52]

2.5.1.3 CBZ cocrystal preparation methods

CBZ cocrystals have been prepared by a variety of methods. In Rahman's study [97], CBZ-NIC cocrystals were prepared by solution cooling crystallization, solvent evaporation and melting and cryomilling methods. Solvent drop grinding (SDG) is a new method of cocrystal preparation. For example, CBZ was chosen as a model drug to investigate whether SDG could prepare CBZ cocrystals. The results indicate that eight CBZ cocrystals could be prepared by SDG methods. SDG therefore appears to be a cost-effective, green and reliable method for the discovery of new cocrystals as well as for the preparation of existing ones [98].

2.5.2 CBZ sustained/controlled release tablets/capsules

CBZ sustained/extended release tablets can be formulated by direct compression, wet granulation methods and the oral osmotic system. Table 2.4 summarizes the research and patents on CBZ sustained/extended release formulation.

The tablets were prepared by direct compression, and hydroxypropyl methylcellulose (HPMC) was used as the matrix excipient in U.S. Patent 5980942 [99] and the research by Soravoot [100].

In U.S. Patent 5284662, CBZ was prepared using the osmotic system. An oral sustained release composition for slightly-soluble pharmaceutical active agents comprises a core with a wall around it and a bore through the wall connecting the core and the environment outside the wall. The core

comprises a slightly soluble active agent, optionally a crystal habit modifier, at least two osmotic driving agents, at least two different versions of hydroxyalkyl cellulose, and optionally lubricants, wetting agents and carriers. The wall is substantially impermeable to the core components but permeable to water and gastro-intestinal fluids. It was found CBZ from an oral osmotic dosage form approximately zero-order release of active agent [101].

In both U.S. Patent 20070071819 A1 and U.S. Patent 20090143362 A1, CBZ is prepared by the wet granulation method. In the two patents, extended release and enteric release units in ratio by weight are mixed and filled into a capsule [102, 103].

In U.S. Patent WO 2003084513 A1 and U.S. Patent 6162466 and the papers published by Barakat and Mohammed, CBZ is prepared by wet granulation followed by direct compression [104-107].

Table 2.4 Summary of CBZ sustained/extended release formulations

Method of tablet formulation	**Research/Patent**	**Excipients**	**Dissolution testing**
Direct compression	U.S. Patent 5980942	HPMC different grade	USP basket Apparatus I;700 ml1% SDS aqueous solution; 100 rev/min
	"Modified release from hydroxypropyl methylcellulose compression-coated tablets"	Tablet core: Ludipress, magnesium state. Tablet: core above, different grade of HPMC	Drug release was studied in a paddle apparatus at 37±0.1 ℃, 900 mL, 50 mM of phosphate buffer pH7.4.
Osmotic system	U.S. Patent 5284662	Core: Hydroxypropylmethy cellulose, Hydroxyethylcellulose 250LNF, Hydroxyethycellulose 250HNF, Mannitol, Dextrates NF, Na Lauryl sulphate NF, Iron Oxide yellow, Magnesium Stearate NF Semipermeable wall: Cellulose acetate 320S NF, Cellulose acetate 398-10NF, Hydroxypropylmethyl cellulose 2910 15cps, Polymethyleneglycol 8000NF	Not mentioned

Wet granulation	U.S. Patent 20070071819 A1	Coated with enteric polymer Coated with extended polymer, acceptable excipients	Not mentioned
	U.S. Patent 20090143362 A1	Granulation: microcrystalline cellulose, lactose, citric acid, sodium lauryl sulfate, hydroxypropylcellulose and a part of polyvinylpyrrolidone were mixed and granulated with granulating dispersion	0.1N HCL for 4 hours and phosphate buffer, pH6.8 with 0.5% sodium lauryl sulfate for remaining time using USP-2 dissolution apparatus at 100 rpm
Wet granulation followed by direct compression	U.S. Patent WO 2003084513 A1	Core: polyethylene glycol (PEG), magnesium Stearate Tablet: core above, granulated lactose, Carbopol 71 G polymer and sodium lauryl sulfate	The dissolution test was performed in USP Apparatus 1, 900ml water
	U.S. Patent 6162466	coated with Eurdrgit RS and RL and then in a disintegrating tablet	Dissolution testing was performed in 1% Sodium Lauryl Sulphate (SLS) water
	"Controlled-release carbamazepine matrix granules and tablets comprising lipophilic and hydrophilic components"	Compriol 888 ATO HPMC and Avicel	900 mL of 1% sodium lauryl sulphate (SLS) aqueous solution at 37 ± 0.5 ℃. Rotational speed 75 rpm
	"Formulation and evaluation of carbamazepine extended release release tablets USP 200 mg"	HPMC E5, PVP K30 were prepared by wet granulation. The granulations, Talc and Magnesium state were mixed uniformly and then prepared by direct compression.	USP II apparatus at 37 ^{o}C and 100 rpm speed.

Chapter 3 Materials and Method

3.1 Chapter overview

This chapter covers materials and analytical methods used in the present research. Firstly, all materials were introduced in detail, including the name, level of purity and the manufacturers. Secondly, analytical methods including Raman, DSC, IR, XRPD, SEM, Thermal Gravimetric Analysis (TGA), UV-imaging system, HPLC and Hot Stage Polarized optical Microscopy (HSPM). These methods were used to identify the cocrystals and characterise their physicochemical properties. DSC, TGA, FTIR and Raman were used to perform qualitative analysis of formed samples, and the Raman spectrometer was also used for quantitative analysis of the phase transition of samples during the dissolution process. SEM and HSPM were used to characterize the morphology of solid compacts. HPLC was used to measure the dissolution rate, solubility and release profiles. The UV-imaging system was used to measure the intrinsic dissolution rate. In this chapter, the principles of the most methods are outlined and the methods for the measurement of intrinsic dissolution, powder dissolution and solubility of cocrystals described. Finally, the preparation work for the present research is presented. The preparation of dissolution media included double-distilled water, pH 6.8 phosphate buffer solution (PBS) and 1% (w/v) sodium lauryl sulphate (SLS) pH 6.8 PBS. Three coformers (NIC, SAC and CIN) were used to form CBZ cocrystals. Four polymers HPMC, HPMCAS AS-MF, PEG 4000 and PVP K30 were utilized to investigate the phase transformation and release profiles of CBZ cocrystals. These are microcrystalline cellulose (MCC), lactose, colloidal silicon dioxide and stearic acid, which were used as excipients in the CBZ sustained release tablets.

3.2 Materials

All materials were used as received, without further processing. Table 3.1 summarizes these materials.

Table 3.1 Materials

Materials	Purity/grade	Manufacturer
carbamazepine form III	≥99.0%	Sigma-Aldrich Company Ltd.,Dorset , UK
NIC	≥99.5%	Sigma-Aldrich Company Ltd.,Dorset , UK
SAC	≥98%	Sigma-Aldrich Company Ltd.,Dorset , UK
CIN	≥99%	Sigma-Aldrich Company Ltd.,Dorset , UK

Ethyl acetate	≥99%	Fisher Scientific, Loughborough, UK
Ethanol	≥99%	Fisher Scientific, Loughborough, UK
Methanol	HPLC grade	Fisher Scientific, Loughborough, UK
Double distilled water		Bi-Distiller (WSC044. Fistreem International Limited, Loughborough, UK)
Sodium lauryl sulfate	>99%	Fisher Scientific, Loughborough, UK
Potassium phosphate monobasic	≥99%	Sigma-Aldrich Company Ltd.,Dorset , UK
Sodium hydroxide	0.2M	Fisher Scientific, Loughborough, UK
HPMC K4M		Shin-Etsu Pharma&Food Materials Distribution GmbH (Stevenage, UK)
HPMCAS (AS-MF)		Shin-Etsu Pharma&Food Materials Distribution GmbH (Stevenage, UK)
HPMCP (HP-55)		Shin-Etsu Pharma&Food Materials Distribution GmbH (Stevenage, UK)
PEG 4000		Fisher Scientific, Loughborough, UK
PVP K30		Fisher Scientific, Loughborough, UK
MCC		Blackbum Distributions Ltd,UK
Lactose		Blackbum Distributions Ltd,UK
Stearic acid		Sigma-Aldrich Company Ltd.,Dorset , UK
Colloidal silicon dioxide		Degussa
0.45 um nylon syringe filter		Thermo Scientific Naglene, Rochesterm, NY, USA
Carbamazepine Tegretol Prolonged Release tablets, 200mg		Pharmacy

3.2.1 Coformers

In this study, three coformers with different solubilities were selected to make CBZ cocrystals.

NIC is generally recognized as a safe Class I chemical and is often utilized in much larger doses than seen in cocrystal formation to treat high cholesterol [97]. It has four known polymorphs, I-IV, with the room temperature stable and a Phase I melting point of 129.5^{o}C [108]. The molecular structure for NIC is shown in Fig.3.1. NIC has been utilized as a coformer for the cocrystallization of theophylline [4], ibuprofen [45] and 3-hydroxybenzoic acid, 4-hydroxybenzoic acid and gentisic acid . The solubility of NIC in water is about 570 mg/ml at 37^{o}C.

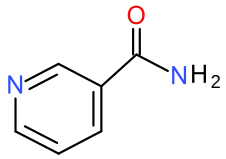

Fig.3.1 Molecular structure of NIC

SAC is a white crystalline solid and a sulphonic acid derivation used as an artificial sweetener in pharmaceutical formulation because it is a GRAS category excipient. Its melting point is about 228.8-229.7^{o}C [109]. Its molecular structure is shown in Fig.3.2. Many SAC cocrystals such as indomethacin-SAC [110], CBZ-SAC [109] and ethenzamide-saccharin [111] have been successfully prepared. The solubility of SAC in water is about 4 mg/ml at 37^{o}C.

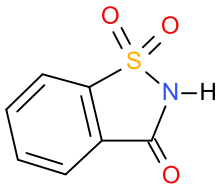

Fig.3.2 Molecular structure of SAC

CIN is an organic, white crystalline compound that is slightly soluble in water, at about 0.4 mg/ml at 37^{o}C. Its melting point is 133^{o}C [112]. CIN possesses anti-bacterial, antifungal and anti-parasitic capabilities. A derivative of CIN is an important pharmaceutical excipient for high blood pressure and stroke prevention and possesses antitumour activity [113]. Its molecular structure is shown in Fig.3.3. CIN is used as a coformer for many cocrystals such as CBZ-CIN [114] and AMG-571-cinnamic acid [49].

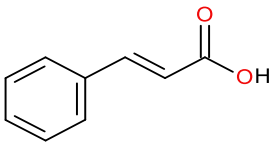

Fig.3.3 Molecular structure of CIN

3.2.2 Polymers

Hydroxypropyl Methylcellulose K4M (HPMC K4M) [115]

HPMC is the most widely used of the cellulosic controlled-release agents. It is a well-known excipient with an excellent safety record. HPMC polymers are non-ionic, so they minimize interaction problems when used in acidic, basic or other electrolytic systems. HPMC polymers work well with soluble and insoluble drugs and at both high and low dosage levels. To achieve controlled release through the use of HPMC, the polymer must quickly hydrate on the outer tablet skin to form a gelatinous layer, the rapid formation of which is critical to prevent wetting of the interior and disintegration of the tablet core. Once the original protective gel layer is formed, it controls the penetration of additional water into the tablet. As the outer gel layer fully hydrates and dissolves, a new inner layer cohesive and continuous enough to retard the influx of water and control drug diffusion must replace it. HPMC K4M's apparent viscosity at 2% in water at 20^{o}C is 4000 mPa.s. Its pH value of 1% in water is 5.5-8.0.

Hypromellose Acetate Succinateby AS-MF (HPMCAS) [116]

The appearance of HPMCAS is a white powder with a faint, acetic acid-like odour, but tasteless. The average molecular weight is 18000. The pH solubility of HPMCAS AS-MF is no less than 6.0. The labelled viscosity is 3 mPa.s. HPMCAS is used as an enteric coating material, and was first approved in Japan in 1987. Recently, HPMCAS was also used to play the role of taste masking and sustained release [117].

Polyethylene Glycol 4000 (PEG 4000) [118]

PEG is designated by a number that roughly equates to average molecular weight. As the molecular weight increases, so does PEG's viscosity. PEG 4000 has a melting point of 53-56^{o}C and is easily extracted by common solvents. Its molecular weight is about 3500-4500 and its solubility in water is 50 mg/ml at 25^{o}C. PEG has been extensively used as carriers for solid dispersion due to its favourable solution properties. Its pH value of 50 mg/ml in water at 25^{o}C is 5.5-7.0.

Polyvinvlpyrrolidone K30 (PVP K30) [119]

Polymerization of vinylpyrrolidone leads to polyvinylpyrrolidone (PVP) of molecular weights ranging from 2500-3000000. The can be classified according to the K value, which is calculated using Fikentsche's equation. The average molecular weight of PVP K30 is about 50000. Due to its good solubility in a wide variety of organic solvents, it is particularly suitable for the preparation of solid dispersions by the solvent method. PVP is widely used in the pharmaceutical sector as an excipient. When given orally, it is not regarded as toxic, partly because it has too high a MW to be

absorbed from the GI tract. Its viscosity of 1% solution at 25^{o}C is 26-35 mPa.s and its pH value of 5% aqueous solution is 3 to7.

3.3 Methods

3.3.1 Raman spectroscopy

Raman spectroscopy is a technique used to observe vibrational, rotational and other low-frequency modes in systems. It relies on inelastic, or Raman, scattering of monochromatic light, usually from a laser in the visible, near-infrared or near-ultraviolet ranges. The Raman effect occurs when electromagnetic radiation impinges on a molecule and interacts with the polarisable electron density and the bonds of the molecule. For the spontaneous Raman effect, which is a form of inelastic light scattering, a photon excites the molecule from the ground state to a virtual energy state for a short period of time shown in Fig.3.4. When the molecule relaxes it emits a photo and it returns to a different rotation or vibration state. The resulting inelastically scattered photon which is "emitted" or "scatted" can be of either higher (anti-Stokes) or lower (Stokes) energy than the incoming photon. In Raman scattering the final vibrational state of the molecule is in a different rotational or vibrational state than the one in which the molecule was originally, before interacting with the incoming photon. The difference in energy between the original state and this final state gives information about the vibration modes in the system, since the vibration information is specific to the chemical bonds and symmetry of molecules. It therefore provides a fingerprint by which the molecule can be identified [120].

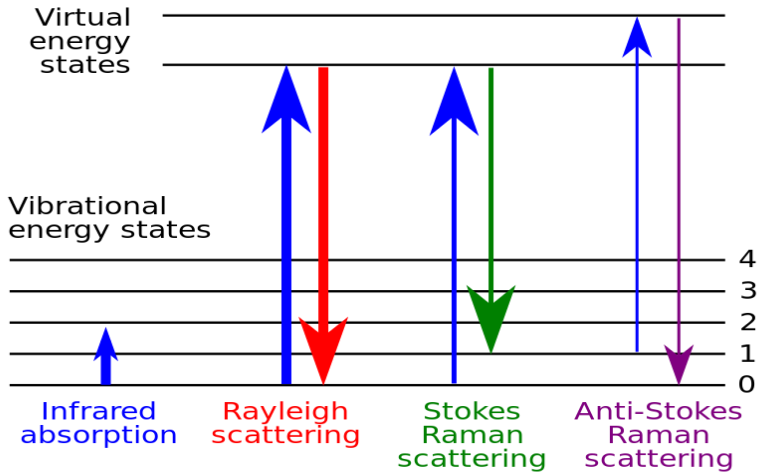

Fig.3.4 Energy level diagram showing the states involved in Raman [121]

EnSpectcter R532® Raman spectrometer (Enhanced Spectrometry, Inc., Torrance, USA), shown in Fig.3.5, is used for measuring the Raman spectra of solids. The equipment includes a 20-30 MW output powder laser source with a wavelength of 532 nm, a Czerny-Turner spectrometer, a scattered light collection and analysis system. In the present study, Raman spectra were obtained using an EnSpectcter R532® Raman spectrometer. The integration time was 200 milliseconds and each spectrum was obtained based on an average of 100 scans.

Fig.3.5 EnSpectr R532® Raman spectrometer

Raman spectroscopy quantitative characterisation [8]

In order to quantify the percentage of CBZ DH crystallised during the dissolution of CBZ III and CBZ-NIC cocrystal, Raman calibration is done as follows: CBZ III and CBZ-NIC cocrystal were blended with CBZ DH separately to form binary physical mixtures at 20% (w/w) intervals from 0 to 100% of CBZ DH in the test samples. Each sample was prepared in triplicate and measured by Raman spectroscopy. Ratios of characteristic peak intensities were used to construct the calibration models. For CBZ III and CBZ DH mixture, the ratio of peak intensity at 1040 to 1025 cm^{-1} were used to make calibration curve; for CBZ-NIC cocrystal and CBZ DH mixture, the ratio of peak intensity at 1035 to 1025 cm^{-1} were used to make calibration curve. Calibration curves for CBZ III and CBZ DH mixture, CBZ-NIC cocrystal and CBZ DH mixture were obtained and shown in Fig.3.6. Equation fitted for the calibration curves were shown in Table 3.2. The calibration equation were validated by mixtures with known proportions, and the results for validation were shown in Table 3.2

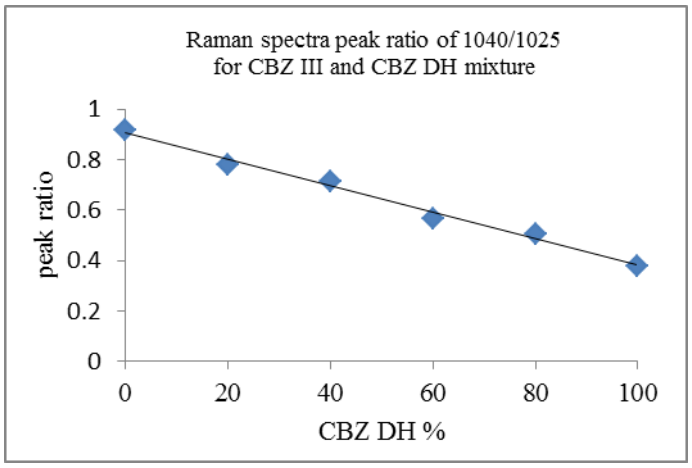

(a)

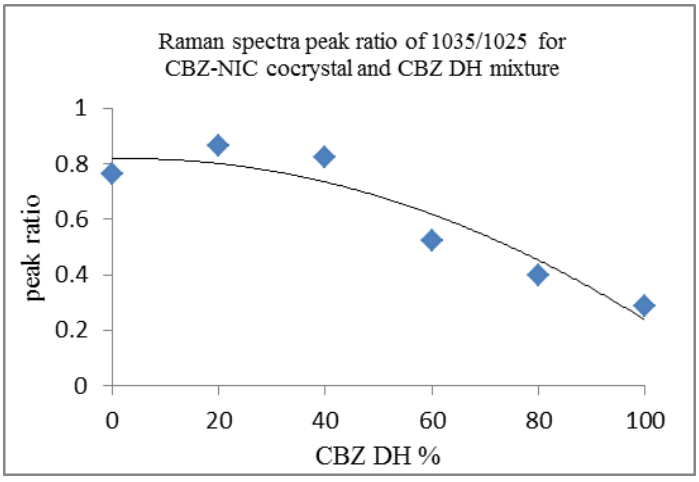

(b)

Fig.3.6 Raman calibration curve for (a) mixture of CBZ III and CBZ DH; (b) mixture of CBZ-NIC cocrystal and CBZ DH [8]

Table 3.2 Raman calibration equations and validations [8]

mixture	calib equations	validation		
		P_{DH}^{r}	P_{DH}^{m}	$\lvert P_{DH}^{m} - P_{DH}^{r} \rvert / P_{DH}^{r}\%$
CBZ III and CBZ DH	y = -0.0053x + 0.9057 R^2= 0.9894	70	73	4
CBZ-NIC cocrystal and CBZ DH	y = -6E-05x^2 + 0.0004x + 0.8171 R^2= 0.896	70	82	17

y: characteristic peak ratio of 1040/1025 for CBZ III and CBZ DH mixture, and 1035/1025 for CBZ-NIC cocrystal and CBZ DH mixture

x: percentage of CBZ DH in the mixture

P_{DH}^{r}: real DH percentage

P_{DH}^{m}: measured DH percentage

3.3.2 DSC

DSC is a thermoanalytical technique in which the amount of heat required to increase the temperature of a sample and a reference is measured as a function of temperature. Both the sample and reference are maintained at nearly the same temperature throughout the experiment. Generally, the temperature program for a DSC analysis is designed so that the sample holder temperature increases linearly as a function of time. The reference sample should have a well-defined heat capacity over the range of temperatures to be scanned [122].

In the present study a Perkin Elmer Jade DSC (PerkinElmer Ltd, Beaconsfield, UK) was used to test samples. The Jade DSC was controlled by Pyris Software. The temperature and heat flow of the instrument were calibrated using an indium and zinc standards. The samples (8-10 mg) were analysed in crimped aluminium pans with pin-hole pierced lids. Measurements were carried out at a heating rate of 20^{o}C/min under a nitrogen flow rate of 20 ml/min.

3.3.3 IR

IR is the spectroscopy that deals with the infrared region of the electromagnetic spectrum, namely light with a longer wavelength and lower frequency than visible light. The theory of infrared spectroscopy is that molecules absorb specific frequencies that are characteristic of their structures. These absorptions are resonant frequencies, i.e. those in which the frequency of the absorbed radiation matches the transition energy of the bond or group that vibrates. The energies are determined by the shape of the molecular potential energy surfaces, the masses of the atoms and the associated vibronic coupling. The infrared spectrum of a sample is recorded by passing a beam of infrared light through the sample. When the frequency of the IR is the same as the vibrational frequency of a bond, absorption occurs. Fourier Transform Infrared Spectroscopy (FTIR) is a measurement technique that allows one to record infrared spectra infrared light guided through an interferometer and then through the sample. A moving mirror inside the apparatus alters the distribution of infrared light that passes through the interferometer. The signal directly recorded, called an “interferogram”, represents light output as a function of mirror position. A data-processing technique called Fourier Transform turns this raw data into the desired result: light output as a function of infrared wavelength [123].

The current study used an ALPHA A4 sized Benchtop ATR-FTIR spectrometer for IR spectra measurement. ATR is the abbreviation of Attenuated Total Reflectance. It is a sampling technique used in conjunction with IR which enables samples to be taken directly in the solid or liquid state

without further preparation. Measurement settings are a resolution of 2 cm^{-1} and a data range of 4000-400 cm^{-1}. The ATR-FTIR spectrometer was equipped with a single-reflection diamond ATR sampling module, which greatly simplifies sample handing.

3.3.4 X-ray diffraction

X-ray crystallography is used to identify the atomic and molecular structure of a crystal. It is a tool in which the crystalline atoms cause a beam of incident X-rays to diffract in many specific directions. By measuring the angles and intensities of these diffracted beams, a crystallographer can produce a three-dimensional picture of the density of the electrons within the crystal, from which the mean positions of the atoms in the crystal can be determined as well as their chemical bonds, their states of disorder and a variety of other information [124].

Crystals are regular arrays of atoms, and X-rays can be considered waves of electromagnetic radiation. Atoms scatter X-ray waves, primarily through the atoms' electrons. Just as an ocean wave striking a lighthouse produces secondary circular waves emanating from the lighthouse, so an X-ray striking an electron produces secondary spherical waves emanating from the electron. This phenomenon is known as elastic scattering, and the electron is known as the scatter. A regular array of scatterers produces a regular array of spherical waves. Although these waves cancel one another out in most direction through destructive interference, they add constructively in a few directions, determined by Bragg's Law:

$$2\mathrm{d}\sin\theta = n\lambda \qquad \text{Equ.3.1}$$

Here d is the spacing between diffracting planes, θ is the incident angle, n is any integer, and λ is the wavelength of the beam. These specific directions appear as spots on the diffraction pattern called reflections. Thus, X-ray diffraction results from an electromagnetic wave impinging on a regular array of scatterers [125].

XRPD patterns of the samples were recorded at a scanning rate of $0.5°\ 2\Theta\mathrm{min}^{-1}$ by a Philipsautomated diffractometer. Cu Kα radiation was used with 40 kV voltage and 35 mA current.

3.3.5 SEM

A scanning electron microscope (SEM) is a type of electron microscope that produces images of a sample by scanning it with a focused beam of electrons. The electrons interact with atoms in the sample, producing various detectable signals containing information about the sample's surface

topography and composition. The electron beam is generally scanned in a raster scan pattern, and the beam's position is combined with the detected signal to produce an image [126].

In this study, SEM micrographs were photographed by a ZEISS EVO HD 15 scanning electron microscope (Carl Zeiss NTS Ltd., Cambridge, UK). The sample compacts were mounted with Agar Scientific G3347N carbon adhesive tab on Agar Scientific G301 0.5" aluminium specimen stub (Agar Scientific Ltd., Stansted, UK) and photographed at a voltage of 10.00 kV. The manual sputter coating S150B was used for gold sputtering of SEM samples.

3.3.6 TGA

The principle underlying TGA is that of a high degree of precision when making three measurements: mass change, temperature and temperature change. The basic parts of the TGA apparatus are thus in precise balance with a pan loaded with the sample, a programmable furnace. The furnace can be programmed in two ways: heating at a constant rate or heating to acquire a constant mass loss over time. For a thermal gravimetric analysis using the TGA apparatus, the sample is continuously weighed as it is heated. As the temperature increases, components of the samples are decomposed so that the weight percentage of each mass change can be measured and recorded. TGA testing results are plotted with mass loss on the Y-axis versus temperature on the X-axis [127].

In this study, a Perkin Elmer Pyris 1 TGA (PerkinElmer Ltd, Beaconsfield UK) was used. Samples (8-10 mg) in crucible baskets were used for TGA runs from 25-190^{o}C with a constant heating rate of 20^{o}C/min under a nitrogen purge flow rate of 20 ml/min.

3.3.7 Intrinsic dissolution study by UV imagine system

The ActiPix SDI 300 UV imaging system comprises a sample flow cell, syringe pump, temperature control unit, UV lamp and detector and a control and data analysis system, as shown in Fig.3.7. The instrumentation records absorbance maps with a high spatial and temporal resolution, facilitating the collection of an abundance of information on the evolving solution concentrations [128]. With spatially resolved absorbance and concentration data, a UV imaging system can give information on the concentration gradient and how it changes with different experimental conditions.

Fig.3.7 ActiPis SDI 200 UV surface imaging dissolution system

The dissolution behavior of CBZ III and CBZ-NIC cocrystals in pure water and different concentrations of HPMC solutions was studied using an ActiPis SDI 300 UV imaging system (Paraytec Ltd., York, UK). A UV imagine calibration was performed by imagining a series of CBZ standard solutions in pure water with concentrations of 4.23×10^{-3} mM, 2.12×10^{-2} mM, 4.23×10^{-2} mM, 8.46×10^{-2} mM, 1.69×10^{-1} mM and 2.54×10^{-1} mM. A standard curve was constructed by plotting the absorbance against concentration of each standard solution based on three repeated experiments as shown in Fig.3.8. The calibration curve was validated by a series of CBZ standard solutions with different HPMC concentrations, showing that HPMC did not affect the accuracy of the model and that the calibration curve was applicable for the dissolution test with HPMC solutions. The sample compact in a dissolution test was made by filling around 5 mg of the sample into a stainless steel cylinder with an inner diameter of 2 mm and compressed by a Quickset MINOR torque screwdriver (Torqueleader, M.H.H. engineering Co. Ltd., England) for one minute at a constant torque of 40 cNm. All dissolution tests were performed at 37±0.5°C and the flow rate of a dissolution medium was set at 0.4 ml/min. The concentrations of HPMC solutions were 0, 0.5, 1, 2 and 5 mg/ml. Each sample had been been tested for one hour in triplicate. A UV filter with a wavelength of 300 nm was used for this study.

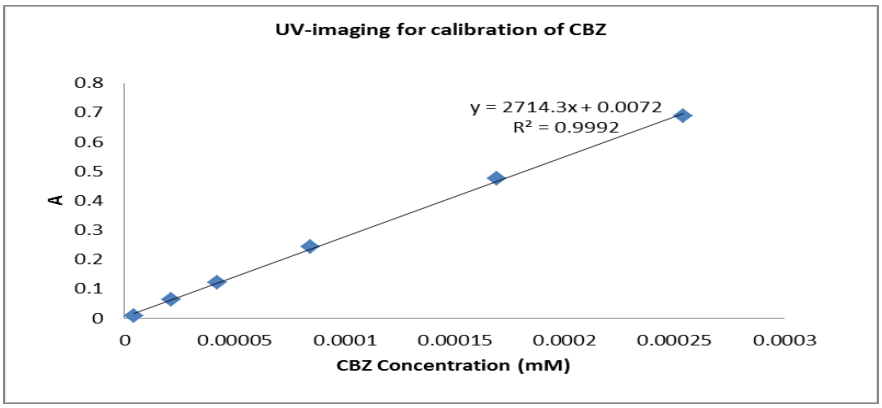

Fig.3.8 UV-imagine calibration of CBZ

UV-imaging calibration curves were validated by standard solutions of CBZ with known concentrations and by running the standard solutions and calculating their concentrations using calibration curves. The calculated concentrations were compared with real ones; the results are shown in Table 3.3.

Table 3.3 UV-imagine calibration equations of CBZ

test sample	**calib equations**	**validation**		
		C_r	C_m	$\lvert C_m - C_r \rvert / C_r$%
CBZ	y = 2714.3x+0.0072, R ²= 0.9992	8.46×10^{-2} mM	8.70×10^{-2} mM	2.76

3.3.8 HPLC

In this study, the concentrations of samples were analysed using the Perkin Elmer series 200 HPLC system. A HAISLL 100 C18 column (5 μm, 250×4.6 mm, Higgins Analytical, Inc. USA) at ambient temperature was set. The mobile phase was composed of 70% methanol and 30% water, and the flow rate was 1 ml/min using an isocratic method. Concentrations of CBZ, NIC, SAC and CIN were measured using a wavelength of 254 nm. HPLC calibration was performed for the four chemicals. The standard curves are shown in Fig.3.9. HPLC calibration curves were validated by standard solutions of CBZ, NIC, SAC and CIN with known concentrations, the standard solutions run and their concentrations calculated using calibration curves. The calculated concentrations were compared with real ones, the results being shown in Table 3.4.

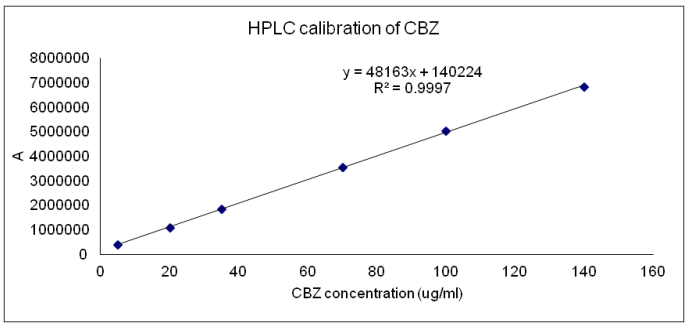

(a)

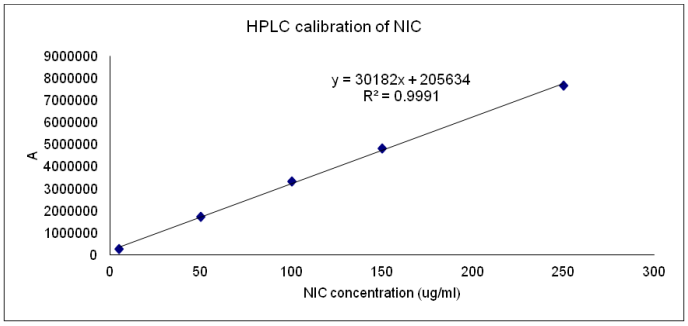

(b)

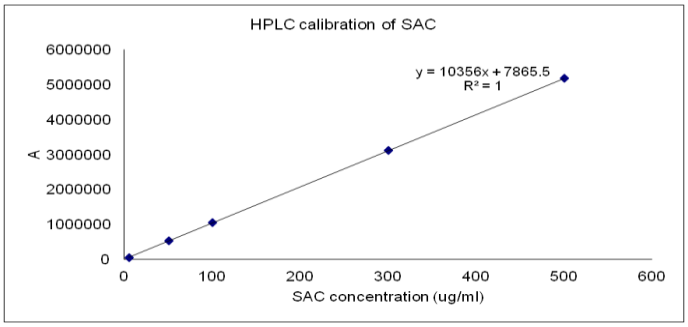

(c)

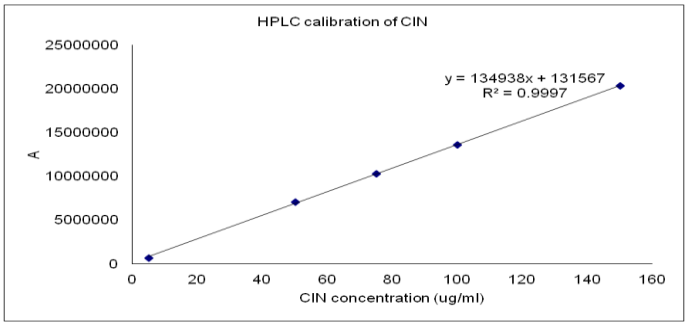

(d)

Fig.3.9 HPLC calibration of (a) CBZ; (b) NIC; (c) SAC; and (d) CIN

Table 3.4 Calibration equations of CBZ, NIC, SAC and CIN

test sample	calib equations	validation		
		C_r	C_m	$\lvert C_m - C_r \rvert / C_r \%$
CBZ	y = 48163x+140224, R^2= 0.9997	100	98	2
NIC	y = 30182x+205634, R^2= 0.9991	100	102	2
SAC	y = 10356x+7865.5, R^2= 1	100	103	3
CIN	y = 134938x+131567, R^2= 0.9997	100	98	2

3.3.9 HSPM

In this study, HSPM studies were conducted on a Leica polarizing optical microscope (Leica Microsystems DM750). The samples were placed between a glass slide and a cover glass and then fixed on a METTLER TOLEDO FP90 hot stage. The sample was then heated from 35°C to 240 ℃ at 10 ℃/min. The morphology changes during the heating process were recorded by camera for further analysis.

3.3.10 Equilibrium solubility test

In this study, all solubility tests were determined using an air-shaking bath method. Excess amounts of samples were added for 20 seconds into a small vial containing a certain volume of media and vortexes. The vials were placed in a horizontal air-shaking bath at 37°C at 100 rpm for 24 hours. Aliquots were filtered through 0.45 um filters and diluted properly for determination of the concentration of samples by HPLC. Solid residues were retrieved from the solubility tests, dried at room temperature for one day and analyzed using DSC, Raman and SEM.

3.3.11 Powder dissolution test

In this study, powder dissolution rates were investigated. In order to reduce the effect of particle size on the dissolution rates, all powders were slightly ground and sieved through a 60 mesh sieve before the dissolution tests. Powders with a 20 mg equivalent of CBZ III were added to beakers containing 200 ml of dissolution media. The dissolution tests were conducted at 37±0.5°C with the aid of magnetic stirring at 125 rpm. Samples of 2±0.1 ml were taken manually at 5, 15, 30, 45, 60,

75 and 90 minutes. The samples were filtered and measured using HPLC to determine the concentrations of samples. Each dissolution test was carried out in triplicate.

3.3.12 Dissolution studies of formulated tablets

The dissolution tests of the tablets were carried out by the USP 1 basket or USP II paddle methods for six hours. The rotation speed was 100rpm and the dissolution medium was 700 ml of 1% SLS aqueous solution (in Chapters 5 and 6) and 1% (w/v) SLS pH 6.8 PBS (in Chapters 7 and 8) to achieve sink conditions, maintained at 37^{o}C. Each profile is the average of six individual tablets.

After a dissolution test, the solid residues were collected and dried at room temperature for at least 24 hours for the further analysis of XRPD, DSC and SEM.

3.3.13 Physical tests of tablets

The diameter, hardness and thickness of tablets were tested in the Dual Tablet Hardness/Thickness tester (Pharmacist/IS0 9001/ Germany).

Friability testing is a laboratory technique used by the pharmaceutical industry to test the likelihood of a tablet breaking into smaller pieces during transit. It involves repeatedly dropping a sample of tablets over a fixed time, using a rotating wheel with a baffle, and afterwards checking whether any tablet are broken and what percentage of the initial mass of the tablets has been lost [129].

The friability test was conducted using a friabilator (Pharma test/ 1S09001/ Germany). Six tablets of each formulation were initially weighed and placed in the friabilator, the drum of which was allowed to run at 30 rpm for one minute. Any loose dust was then removed with a soft brush and the tablets were weighed again. The percentage friability was then calculated using the formula

$$F = \frac{initial\ weight - final\ weight}{initial\ weight} \times 100 \qquad \text{Equ.3.2}$$

3.3.14 Preparation of tablets

Cylindrical tablets were prepared by direct compression of the blends, using a laboratory press fitted with a 13 mm flat-faced punch and die set and applying one ton of force. All tablets contained the equivalent of 200 mg of CBZ III.

3.3.15 Statistical analysis

The differences in solubility and release profiles of the samples were analysed by one-way analysis variance (ANOVA) (the significance level was 0.05) using JMP 11 software.

3.4 Preparations

3.4.1 Media

pH 6.8 PBS: Mix 250 ml of 0.2 M potassium dihydrogen phosphate (KH_2PO_4) and 112 ml of 0.2 M sodium hydroxide and dilute to 1000.0 ml with water [130].

1% (w/v) SLS aqueous solution: dissolve 10 g SLS in 1000.0 ml water.

1% (w/v) SLS pH 6.8 PBS: dissolve 10 g SLS in 1000.0 ml pH 6.8 PBS.

0.5, 1.0, 2.0, 5.0 mg/ml HPMC aqueous solution: dissolve 50, 100, 200, 500 mg HPMC in four beakers with 100 ml of water respectively, and stir the four solutions until all are clear.

0.5, 1.0, 2.0, 5.0 mg/ml HPMCAS/PVP/PEG pH 6.8 PBS: dissolve 50, 100, 200, 500 mg HPMCAS/PVP/PEG in four beakers with 100 ml pH 6.8 PBS respectively, and stir the four solutions until all are clear.

3.4.2 Test samples

Preparation of CBZ DH

Excess amount of anhydrous CBZ III was added to double distilled water and stirred for 48 hours at a constant temperature of 37^{o}C. The suspension was filtered and dried for 30 minutes on the filter. TGA was used to determine the water content in the isolated solid and confirm complete conversion to the hydrate.

Preparation of CBZ-NIC 1:1 cocrystal

CBZ-NIC cocrystals were prepared by the reaction crystallisation method. A 1:1 molar ratio mixture of CBZ III and NIC was completely dissolved in Ethyl Acetate (EtOAc) by stirring at 70 ℃. The solution was put in an ice bath for two hours and the suspension was then filtered through 0.45 μm filters (thermo Scientific Nalgene) to collect the solid residue of CBZ-NIC cocrystals.

Preparation of physical mixture of CBZ III and NIC (CBZ-NIC mixture)

A 1:1 molar ratio mixture of CBZ III and NIC was prepared by thoroughly mixing 1 mmol CBZ III (23.6 mg) and 1 mmol NIC (12.2 mg).

Preparation of CBZ-SAC 1:1 cocrystal

A CBZ-SAC cocrystal was prepared by the reaction crystallisation method. A 1:1 molar ratio mixture of CBZ III and SAC was completely dissolved in Ethyl Acetate (EtOAc) by stirring at 70 ℃. The solution was put in an ice bath for two hours and the suspension was then filtered through 0.45 μm filters (thermo Scientific Nalgene) to collect the solid residue of CBZ-SAC cocrystals.

Preparation of physical mixture of CBZ III and SAC (CBZ-SAC mixture)

A 1:1 molar ratio mixture of CBZ III and SAC was prepared by thoroughly mixing 1 mmol CBZ III (23.6 mg) and 1 mmol SAC (18.3 mg).

Preparation of CBZ-CIN 1:1 cocrystals

Carbamazepine and cinnamic acid (CBZ-CIN) cocrystals were prepared using the slow evaporation method. A 1:1 molar ratio mixture of CBZ and CIN was completely dissolved in methanol by stirring and slight heating. The solutions were allowed to evaporate slowly in a controlled fume hood (room temperature, air flow 0.50-1.0 m/s). When all the solvent had evaporated, the solid product was obtained from the bottom of the flask.

Preparation of physical mixture of CBZ III and CIN (CBZ-CIN mixture)

A 1:1 molar ratio mixture of CBZ III and CIN was prepared by thoroughly mixing 1 mmol CBZ III (23.6 mg) and 1 mmol CIN (14.6 mg).

3.5 Conclusion

This chapter introduced all the materials, methods and sample preparations used in this study. Details of all the materials were firstly presented, including their names, purities and producers. Secondly, the research methods including analytical techniques and experiments were introduced. DSC, TGA, ATR-FTIR, Raman and SEM were used to identify the formation of test samples. The UV-imagine method was used in the intrinsic dissolution rate study of CBZ-NIC cocrystals. A

powder dissolution test was carried out to study the dissolution rates of CBZ-SAC and CBZ-CIN cocrystals. The air-shaking bath method was used in the equilibrium solubility test. Finally, test samples and dissolution media preparation methods were outlined. Several media were used in this study: water, 1% SLS water, pH 6.8 PBS, 1% SLS pH 6.8 PBS, different concentrations of HPMC aqueous solutions and different concentrations of HPMCAS/PVP/PEG pH 6.8 PBS. The preparation methods for CBZ samples, which are, CBZ DH, CBZ-NIC, CBZ-SAC and CBZ-CIN cocrystals and their mixtures, were introduced.

Chapter 4 Sample Characterisations

4.1 Chapter overview

In this chapter, test samples prepared for this study were characterised. These are CBZ III and CBZ DH, and the CBZ-NIC, CBZ-SAC and CBZ-CIN cocrystals. Various techniques such as TGA, DSC, IR spectroscopy, Raman, XRPD and HSPM were used to characterise these products.

4.2 Materials and methods

4.2.1 Materials

Anhydrous CBZ III, NIC, SAC, CIN, EtOAc, methanol and distilled water were used in this chapter; details of these materials can be found in Chapter 3.

4.2.2 Methods

ATR-FTIR, Raman, DSC, TGA, HSPM, XPRD were used for the characterisation. Details of these techniques can be found in Chapter 3.

4.3 Results

4.3.1 TGA analysis of CBZ DH

The TGA thermograph of CBZ DH is shown in Fig.4.1. The result shows that the water content of CBZ DH is 13.286%. This is similar to the theoretical stoichiometric water content of 13.2% w/w. The TGA result demonstrates the formation of CBZ DH.

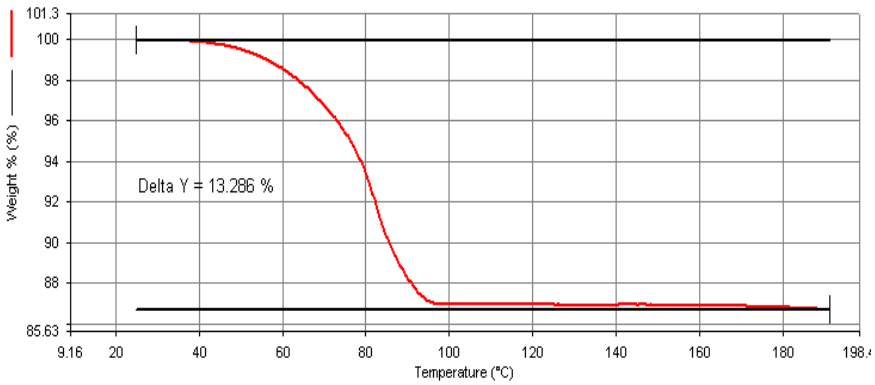

Fig.4.1 TGA thermograph of CBZ DH

4.3.2 DSC analysis of CBZ III, CBZ cocrystals and physical mixtures

4.3.2.1 CBZ-NIC cocrystals and a mixture

DSC curves patterns of CBZ III, NIC, CBZ-NIC cocrystals and a CBZ-NIC mixture are shown in Fig.4.2 and DSC data shown in Table 4.1.

Table 4.1 The thermal data of CBZ III, NIC, CBZ-NIC cocrystal and a mixture

Sample	Onset (^{o}C)	Peak(^{o}C)
CBZ III	160;189	167;195
NIC	128	133
CBZ-NIC cocrystals	159	162
CBZ-NIC mixture	121;158	128;162

The DSC curve shows that CBZ III melted at around 167^{o}C and then recrystallized in the more stable form CBZ I, which melted at around 195^{o}C; NIC melted at around 133^{o}C; CBZ-NIC cocrystals had a single melted point of around 162^{o}C; and the CBZ-NIC mixture exhibited two major thermal events: the first endothermic-exothermic one was around 120-140^{o}C because of the melting of NIC and the cocrystallisation of CBZ-NIC cocrystals, while the second endothermic peak, at around 162^{o}C, resulted from the melting of newly formed CBZ-NIC cocrystals under DSC heating. These results are identical to those reported [8, 52].

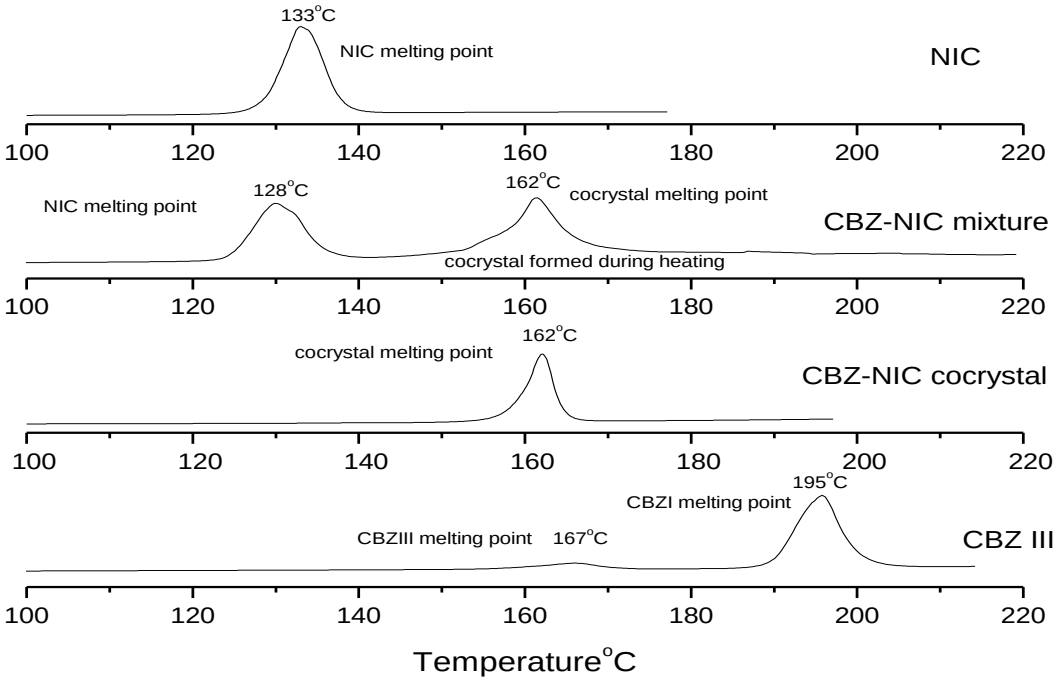

Fig.4.2 DSC thermograms for CBZ III, CBZ-NIC cocrystal and a mixture, and NIC

4.3.2.2 CBZ-SAC cocrystals and a mixture

DSC curves patterns of CBZ III, SAC, CBZ-SAC cocrystals and CBZ-SAC a mixture are shown in Fig.4.3 and DSC data shown in Table 4.2.

Table 4.2 The thermal data of CBZ III, SAC, CBZ-SAC cocrystals and a mixture

Sample	Onset (^{o}C)	Peak(^{o}C)
CBZ III	160;189	167;195
SAC	227	231
CBZ-SAC cocrystals	173	177
CBZ-SAC mixture	166	177

The DSC curve shows that SAC melted at around 231^{o}C, while CBZ-SAC cocrystals showed a sharp endothermic peak at around 177^{o}C. For the physical mixture of CBZ-SAC, the major peaks were between 160^{o}C and 180^{o}C because of the melted CBZ III for cocrystallisation of CBZ-SAC cocrystals and the newly formed cocrystals melting again under DSC heating.

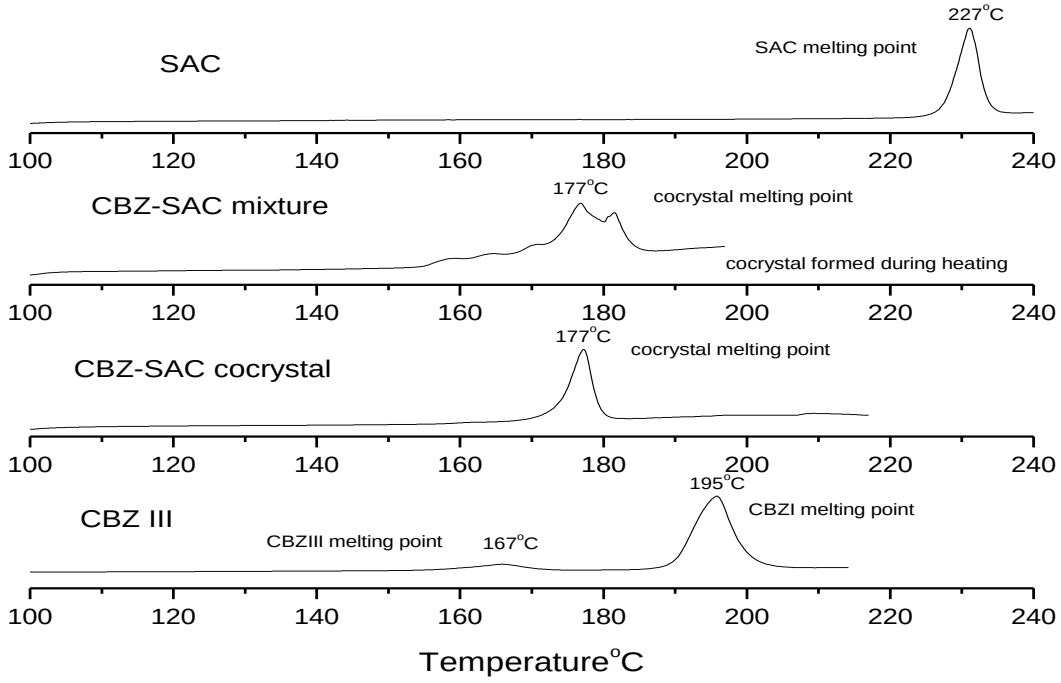

Fig.4.3 DSC thermograms of CBZ III, CBZ-SAC cocrystals and a mixture, and SAC

4.3.2.3 CBZ-CIN cocrystal and mixture

DSC curves patterns of CBZ III, CIN, CBZ-CIN cocrystals and the CBZ-CIN mixture are shown in Fig.4.4 and DSC data in Table 4.3.

Table 4.3 The thermal data of CBZ III, CIN, CBZ-CIN cocrystals and a mixture

Sample	Onset (^{o}C)	Peak (^{o}C)
CBZ	160;189	167;195
CIN	134	137
CBZ-CIN cocrystals	142	145
CBZ-CIN mixture	121;139	125;142

The DSC curve shows that CIN melted at around 137^{o}C and that CBZ-CIN cocrystals had a single endothermic peak at around 145^{o}C. For the CBZ-CIN physical mixture, the first endothermic peak was at approximately 125^{o}C because of the melting of CIN and the second endothermic peak was at around 142^{o}C, a result of the melting of the newly formed CBZ-CIN cocrystal.

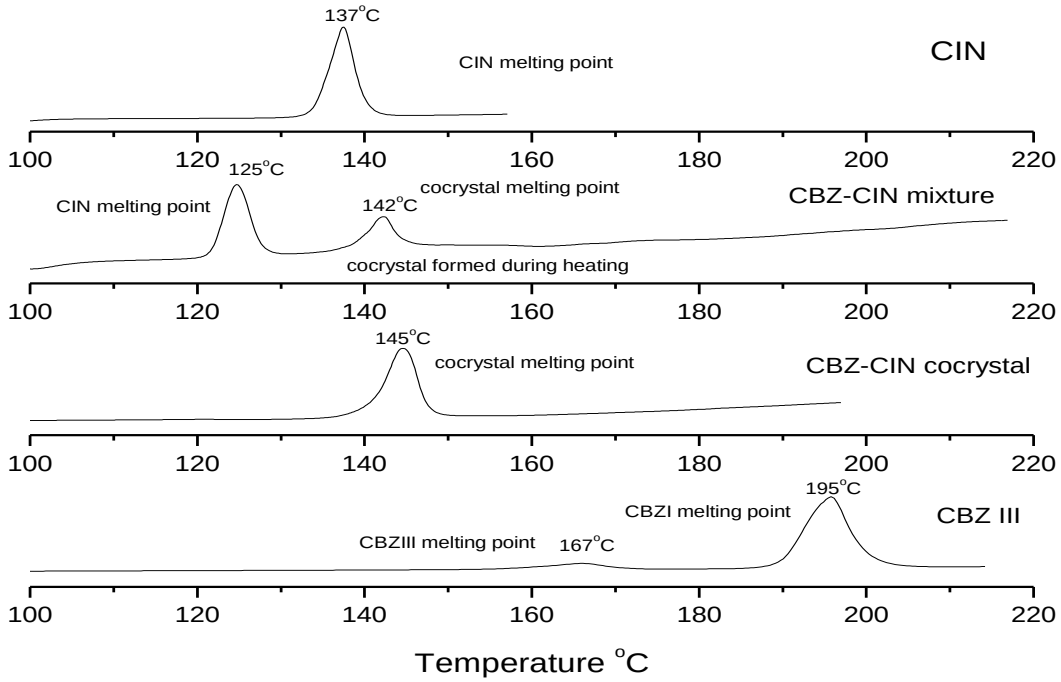

Fig.4.4 DSC thermograms for CBZ III, CBZ-CIN cocrystals and a mixture, and CIN

4.3.3 IR analysis of CBZ III, CBZ cocrystals and physical mixtures

4.3.3.1 CBZ-NIC cocrystals

The structure of CBZ, NIC and CBZ-NIC cocrystals has been the subject of study. It has an amide-to amide structure as shown in Fig.4.5 [131].

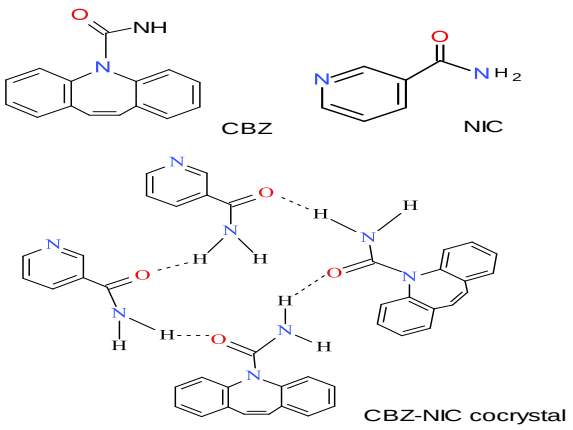

Fig.4.5 Structure of CBZ, NIC and CBZ-NIC cocrystals [132]

CBZ-NIC cocrystals are formed via hydrogen bonds in which the carboxamide groups from both CBZ and NIC provide hydrogen bonding donors and acceptors. The IR spectra for CBZ, NIC, CBZ-NIC cocrystals and the physical mixture are shown in Fig.4.6.

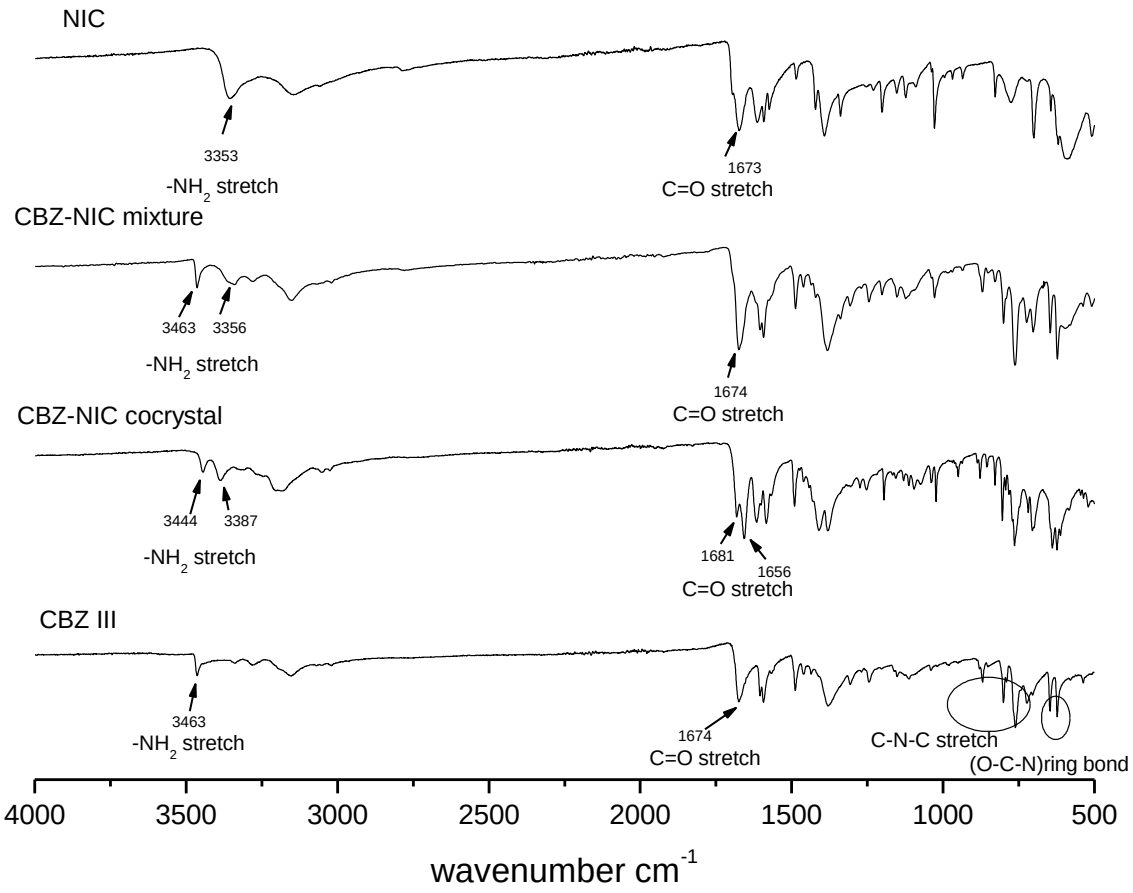

Fig.4.6 IR spectrum of CBZ III, NIC, CBZ-NIC cocrystals and a mixture

The IR spectrum for CBZ III has peaks at 3463 and 1674 cm^{-1}, corresponding to carboxamide N-H and C=O stretch respectively. The spectrum of NIC has a peak corresponding to carboxamide N-H

stretch at 3353 cm^{-1} and a peak at around 1673 cm^{-1} for C=O stretch. The spectrum of CBZ-NIC cocrystals is different from those of CBZ and NIC, suggesting that both molecules are present in a new phase. CBZ's carboxamide N-H and C=O stretching frequencies shifted to 3444 and 1656 cm^{-1} respectively. While NIC's N-H stretching frequency shifted to a higher position at 3387 cm^{-1}, the C=O stretching peak frequency moved to 1681 cm^{-1}. The spectrum of the CBZ-NIC physical mixture peaked at 3463 and 1674 cm^{-1} as a result of CBZ III, and 3356 cm^{-1} from NIC. A summary of IR peak identities for CBZ III, NIC and CBZ-NIC cocrystals and a mixture is shown in Table 4.4.

Table 4.4 Summary of IR peak identities of CBZ III, NIC and CBZ-NIC cocrystals and a mixture

	Peak position(cm^{-1})	**Assignment**
CBZ III	3463	$-NH_2$
	1674	-(C=O)-
NIC	3353	$-NH_2$
	1673	-(C=O)-
CBZ-NIC cocrystals	3444	$-NH_2$ of CBZ
	3387	$-NH_2$ of NIC
	1681	-(C=O)- of CBZ
	1656	-(C=O)- of NIC
CBZ-NIC mixture	3463	$-NH_2$ of CBZ
	3356	$-NH_2$ of NIC
	1674	-(C=O)- of CBZ

4.3.3.2 CBZ-SAC cocrystal

The structure of CBZ III, SAC and CBZ-SAC cocrystals, the structure of which is shown in Fig.4.7, has been the subject of study [133].

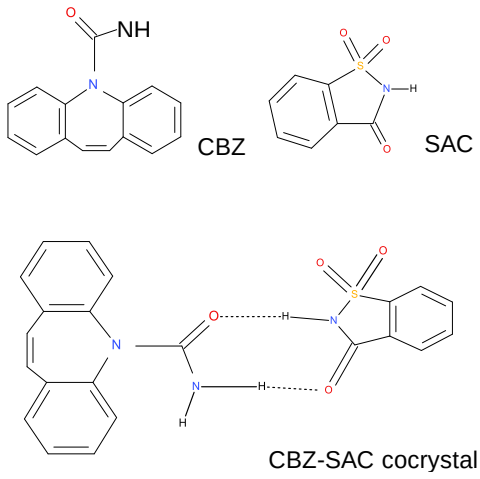

Fig.4.7 Structure of CBZ, SAC and CBZ-SAC cocrystals

The IR spectrum of CBZ III, SAC, CBZ-SAC cocrystals and a physical mixture are shown in Fig.4.8.

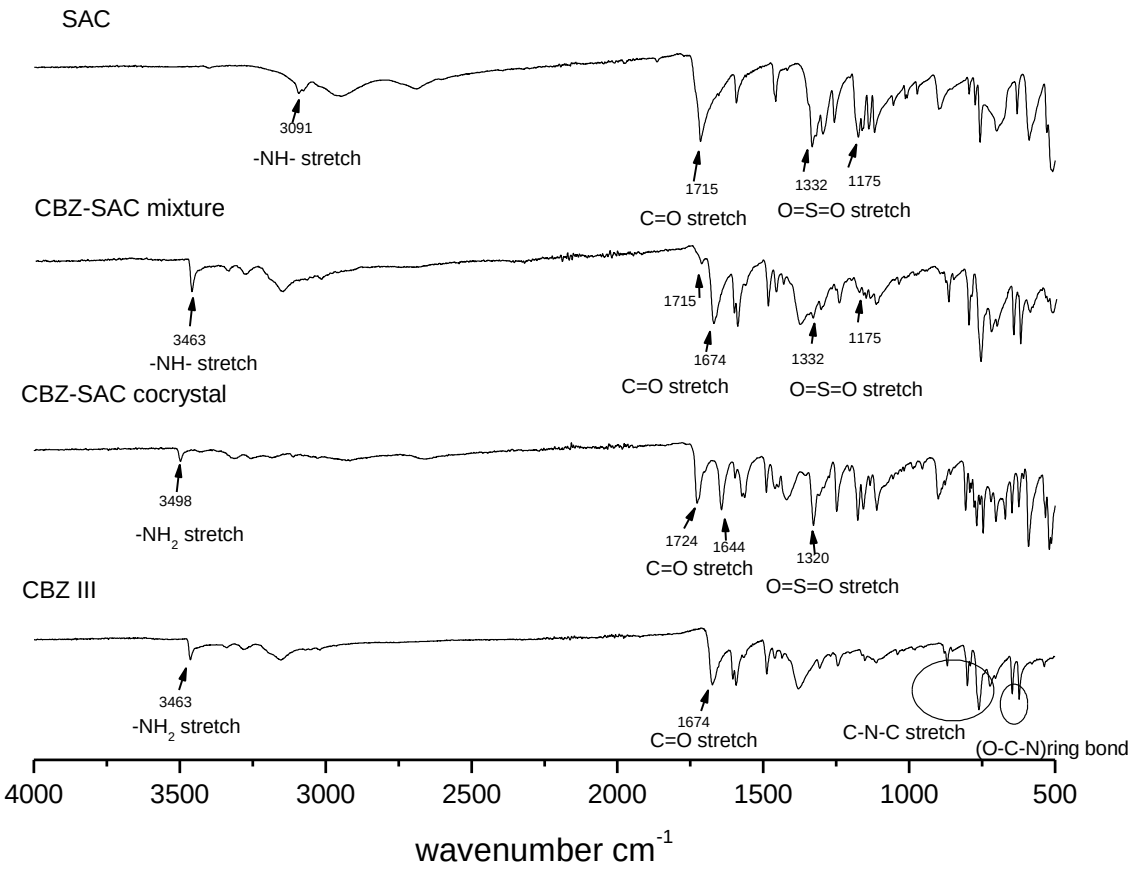

Fig.4.8 IR spectrum of CBZ III, SAC, CBZ-SAC cocrystals and a mixture

The IR spectrum of pure SAC demonstrates the peaks resulting from secondary amide and carbonyl stretching at 3091 and 1715 cm^{-1} respectively [134, 135]. Additionally, peaks corresponding to an

asymmetric stretching of the -SO_2 group in the SAC was also observed at 1332 and 1175 cm^{-1} respectively [134]. The IR spectra of CBZ-SAC cocrystals exhibited a shift in peaks of carbonyl, amide and –SO_2 regions that indicated the hydrogen bonding interaction between CBZ III and SAC. A shift in the carbonyl stretching of CBZ III was observed at 1644 cm^{-1} and the stretching due to the primary –NH group of CBZ III had shifted to 3498 cm^{-1}, a return that agrees with its report data [136]. Similarly, the peak of the free carbonyl group had shifted to 1724 instead of 1715 cm^{-1}, as seen in the SAC result. This also exhibited a shift in the asymmetric stretching from 1332 to 1320 cm^{-1}because of the –SO_2 group of SAC. All these change in the IR spectra indicated interaction between the SAC and CBZ molecules in their solid state, and hence the formation of cocrystals [134]. The IR spectra of the CBZ-SAC physical mixture peaked at 3463 and 1674 cm^{-1} as a result of CBZ III, 1715, 1332 and 1175 cm^{-1} from SAC. These IR peak identities of CBZ III, SAC, CBZ-SAC cocrystals and a mixture is shown in Table 4.5.

Table 4.5 Summary of IR peak identities of CBZ III, SAC and CBZ-SAC cocrystals and a mixture

	Peak position(cm^{-1})	**assignment**
CBZ III	3463	-NH_2
	1674	-(C=O)-
SAC	1715	-(C=O)-
	1332 and 1175	-SO_2-
	3091	-NH-
CBZ-SAC cocrystals	3498	N-H of CBZ
	1644	-(C=O)- of CBZ
	1320	O=S=O of SAC
	1724	-(C=O)- of SAC
CBZ-SAC mixture	3463	-NH_2 of CBZ
	1674	-(C=O)- of CBZ
	1715	-(C=O)- of SAC
	1332 and 1175	-SO_2- of SAC

4.3.3.3 CBZ-CIN cocrystals

The structure of CBZ, CIN and CBZ-CIN cocrystals is shown in Fig.4.9.

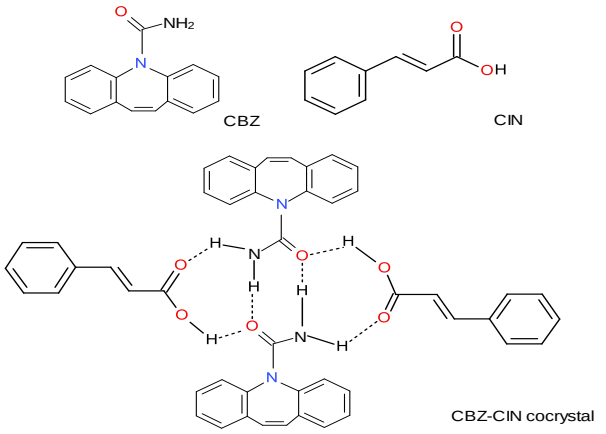

Fig.4.9 Structure of CBZ, CIN and CBZ-CIN cocrystals

The IR spectrum of CBZ III, CIN, CBZ-CIN cocrystals and a physical mixture are shown in Fig.4.10.

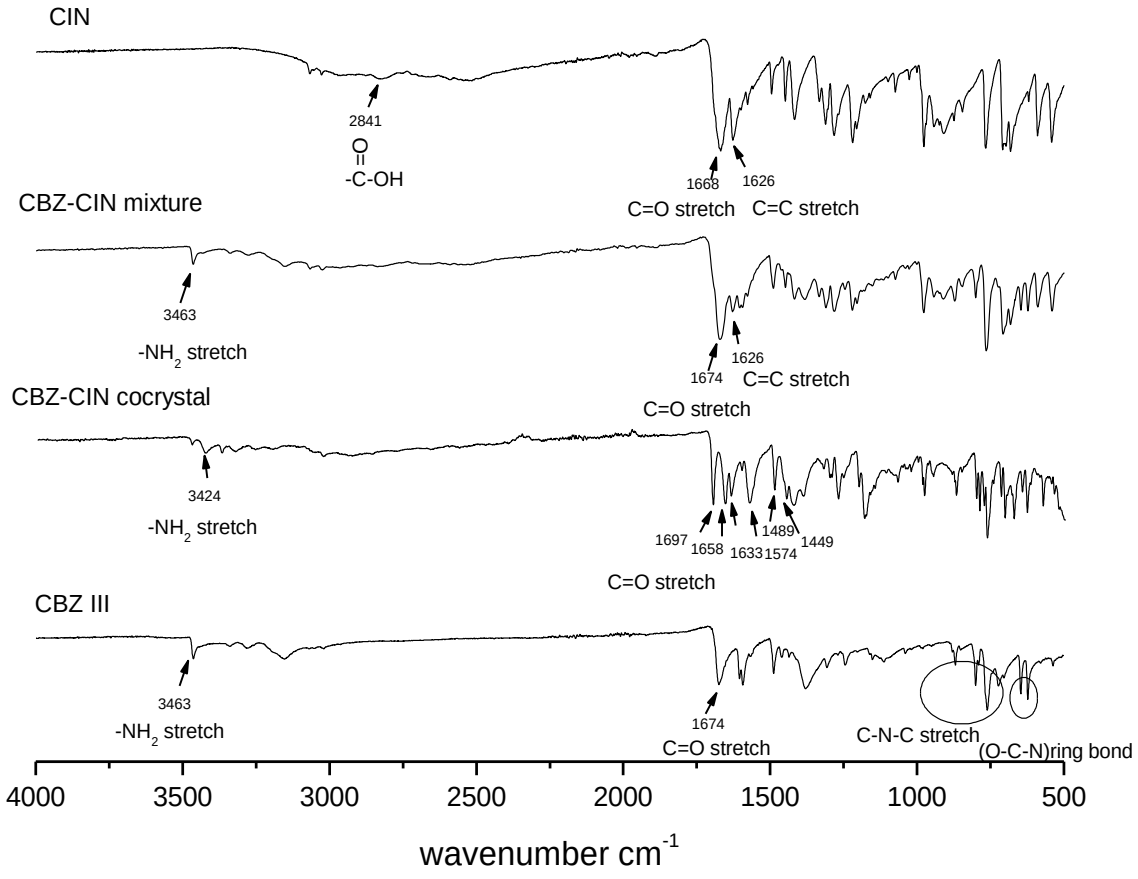

Fig.4.10 IR spectrum of CBZ III, CIN, CBZ-CIN cocrystals and a mixture

CIN's IR spectrum exhibited medium strong and broad peaks at around 2542-2985 cm^{-1} corresponding to -OH- stretch. Peaks corresponding to the stretching of C=O and C=C in CIN were also observed at around 1668 and 1626 cm^{-1} respectively, which agrees with the published data

[137]. The cocrystals' IR spectra peaks showed shifts in the C=O, C=C and –NH regions. Shifts in CBZ III's amide-NH stretching were observed at 3424 cm^{-1}. The peak of CBZ III and CIN's C=O stretch had shifted to 1697 cm^{-1}. It also exhibited a shift in the stretching from 1626 to 1633 cm^{-1} because of the C=C group of CIN. All these changes in the IR spectra indicated interaction between the CIN and CBZ III molecule in their solid state, and hence the formation of cocrystals. The CBZ-CIN cocrystals can be characterized by any one or more of the IR peaks including, but not limited to, 1658, 1633, 1574, 1489 and 1449 cm^{-1}. This agrees with the published data [138]. The CBZ-CIN physical mixture's IR spectra showed peaks of 3463 and 1674 cm^{-1} resulting from CBZ III, and 1626 cm^{-1} from CIN. The IR peak identities of CBZ III, CIN, the CBZ-CIN cocrystals and a mixture are summarized in Table 4.6.

Table 4.6 Summary of IR peak identities of CBZ III, CIN, CBZ-CIN cocrystals and a mixture

	Peak position(cm^{-1})	**assignment**
CBZ III	3463	-NH2
	1674	-(C=O)-
CIN	2841	-OH- of carboxylic acid
	1668	-C=O-
	1626	-C=C- conjugated with aromatic rings
CBZ-CIN cocrystals	3424	-NH2 of CBZ
	1633	-C=C- of CIN
	1697	-(C=O)- of CBZ, CIN
	1658,1633,1574,1489,1449 [138]	
CBZ-CIN mixture	3463	-NH2 of CBZ
	1675	-(C=O)- of CBZ
	1626	-C=C- of CIN

4.3.4 Raman analysis of CBZ III, CBZ cocrystals and physical mixtures

4.3.4.1 CBZ-NIC cocrystals

Raman spectra of CBZ III, NIC, CBZ-NIC cocrystals and a physical mixture are shown in Fig.4.11, and spectra data shown in Table 4.7.

Several characteristic peaks can identify CBZ samples. CBZ III's double peak at 272 cm^{-1} and 253 cm^{-1} is caused by lattice vibration. CBZ III exhibits triple peaks in the range of wavenumbers 3070-3020 cm^{-1} and one aromatic asymmetric stretch peak around 3071 cm^{-1}. The two most significant peaks for NIC are the pyridine ring stretch peak at 1042 cm^{-1} and the C-H stretching peak at 3060 cm^{-1}.

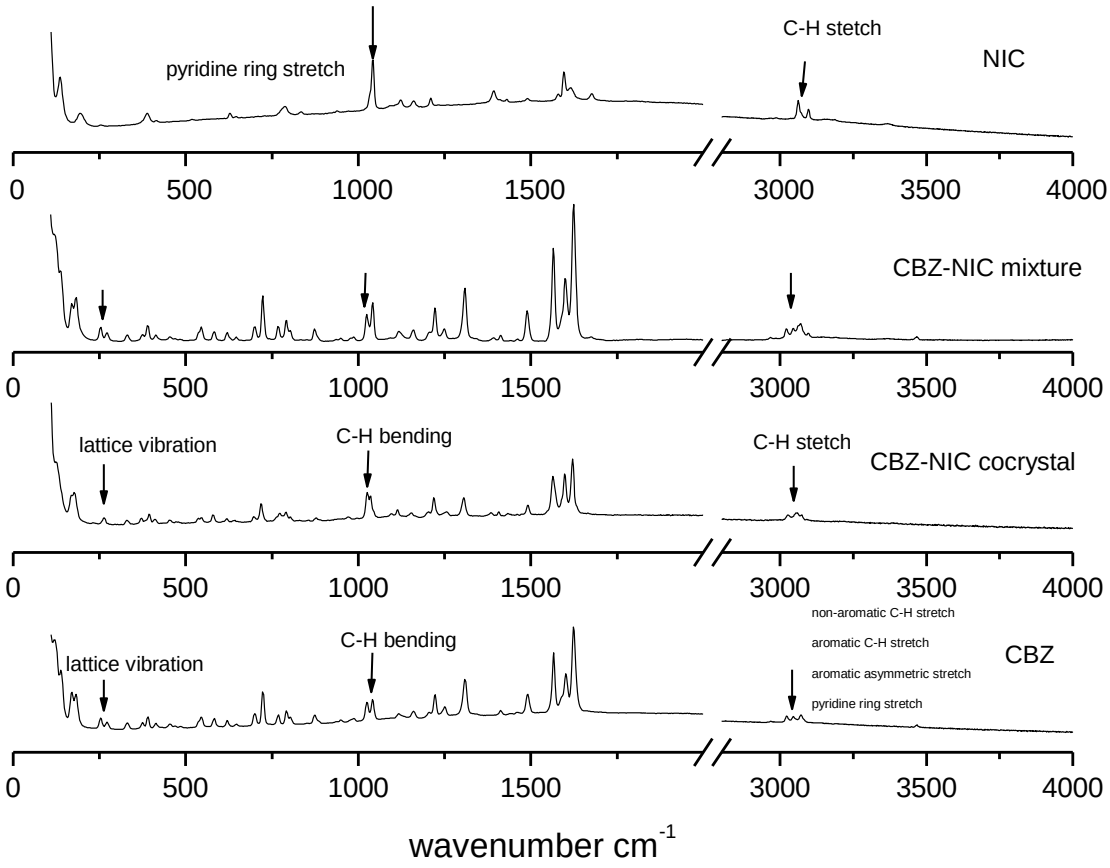

Fig.4.11 Raman spectra for CBZ III, NIC, CBZ-NIC cocrystals and a mixture

Characteristic peaks of CBZ and NIC both showed in the Raman spectrum of the CBZ-NIC physical mixture. This double peak, at 272 and 253 cm^{-1}, as a result of CBZ; the ratio of the peak intensity at 1040 cm^{-1} to that at 1025 cm^{-1} increases due to NIC's strong ring stretch peak at 1042 cm^{-1}. The CBZ-NIC cocrystals' Raman spectrum has a single peak at around 264 cm^{-1} and a spectrum pattern in the ranges of 1020-1040 cm^{-1} and 2950-3500 cm^{-1}. Differences among the Raman spectra of CBZ, NIC, CBZ-NIC cocrystals and a physical mixture demonstrate that CBZ-NIC cocrystals are not just a physical mixture of the two components; rather, a new solid-state formation has been generated [132].

4.3.4.2 CBZ-SAC cocrystals

Raman spectra of CBZ III, SAC, CBZ-SAC cocrystals and a physical mixture are shown in Fig.4.12, and the spectra data is shown in Table 4.7.

A strong band characteristic of SAC's C=O stretching mode was observed near 1697 cm^{-1}, which agrees with published data [139]. The Raman spectrum for the CBZ-SAC physical mixture shows both characteristic peaks CBZ III and SAC. Its double peak at 272 and 253 cm^{-1} results from CBZ III, and its single peak near 1697 cm^{-1} from SAC. The Raman spectrum of CBZ-SAC cocrystals contained a single peak at around 1715 cm^{-1}, which differs from SAC's stretching frequency 1697 cm^{-1}. The pattern of spectrum in the ranges of 2950-3500 cm^{-1} is different from those of the physical mixture. Differences among the Raman spectra of CBZ III, SAC, CBZ-SAC cocrystals and a physical mixture demonstrate that CBZ-SAC cocrystals are not just a physical mixture of the two components; rather, a new solid-state formation has been generated.

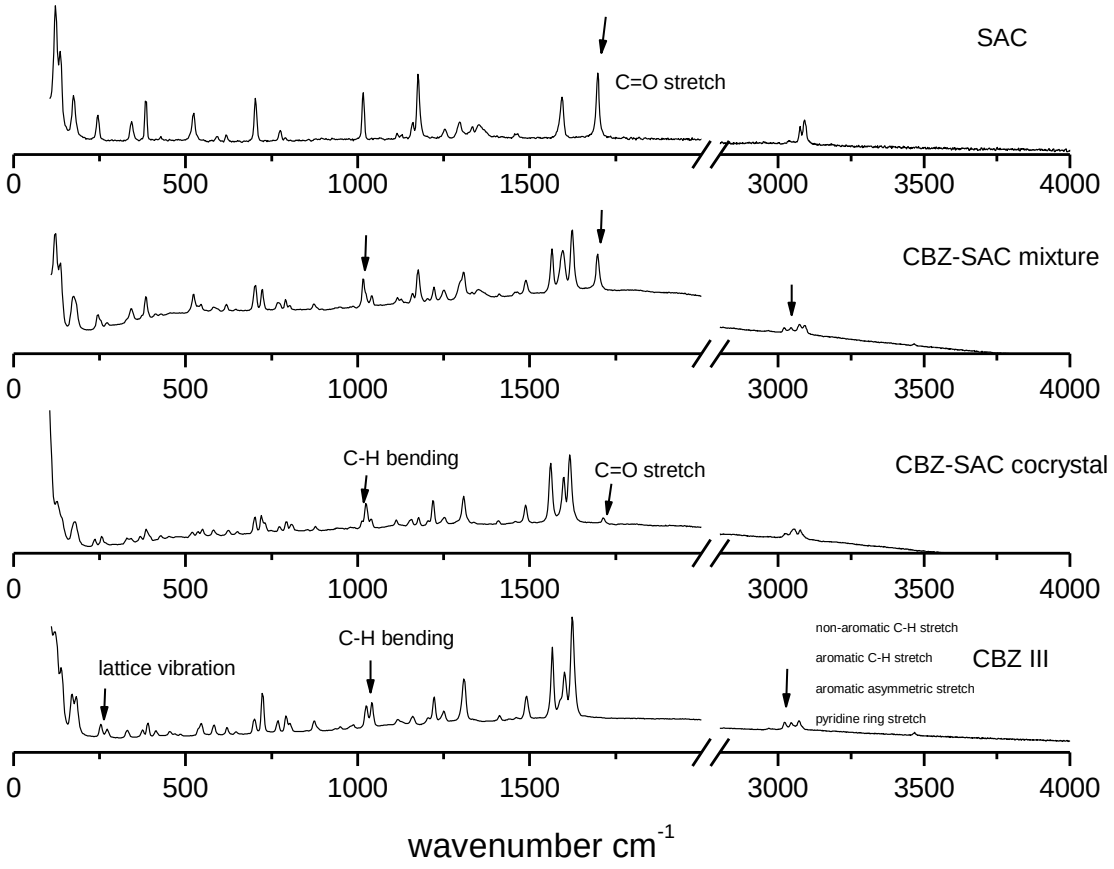

Fig.4.12 Raman spectra for CBZ III, SAC, CBZ-SAC cocrystals and a mixture

4.3.4.3 CBZ-CIN cocrystals

The Raman spectra of CBZ III, CIN, CBZ-CIN cocrystals and a physical mixture are shown in Fig.4.13 and the spectra data in Table 4.7.

A very strong characteristic of CIN's C=C stretching mode was observed near 1637 cm^{-1} and a weak characteristic of CIN's C-O stretch near 1292 cm^{-1}, both of which agree with published data [137]. The Raman spectrum of the CBZ-CIN physical mixture demonstrates the characteristic peaks of both CBZ III and CIN. It exhibits a double peak at 272 and 253 cm^{-1} as a result of CBZ III, and single peaks near 1637 cm^{-1} and 1292 cm^{-1} as a result of CIN. The Raman spectrum of CBZ-CIN cocrystals show a single peak at around 255 cm^{-1} instead of a double one at 272 and 253 cm^{-1}. The spectrum pattern in the range 2950-3500 cm^{-1} is different from that of the physical mixture. A single peak near 1699 cm^{-1} was observed in the cocrystals but not in CBZ III or CIN. Differences among the Raman spectra of CBZ III, CIN, CBZ-CIN cocrystals and a physical mixture demonstrate that the CBZ-CIN cocrystals are not just a physical mixture of the two components; rather, as before, a new solid-state formation has been generated.

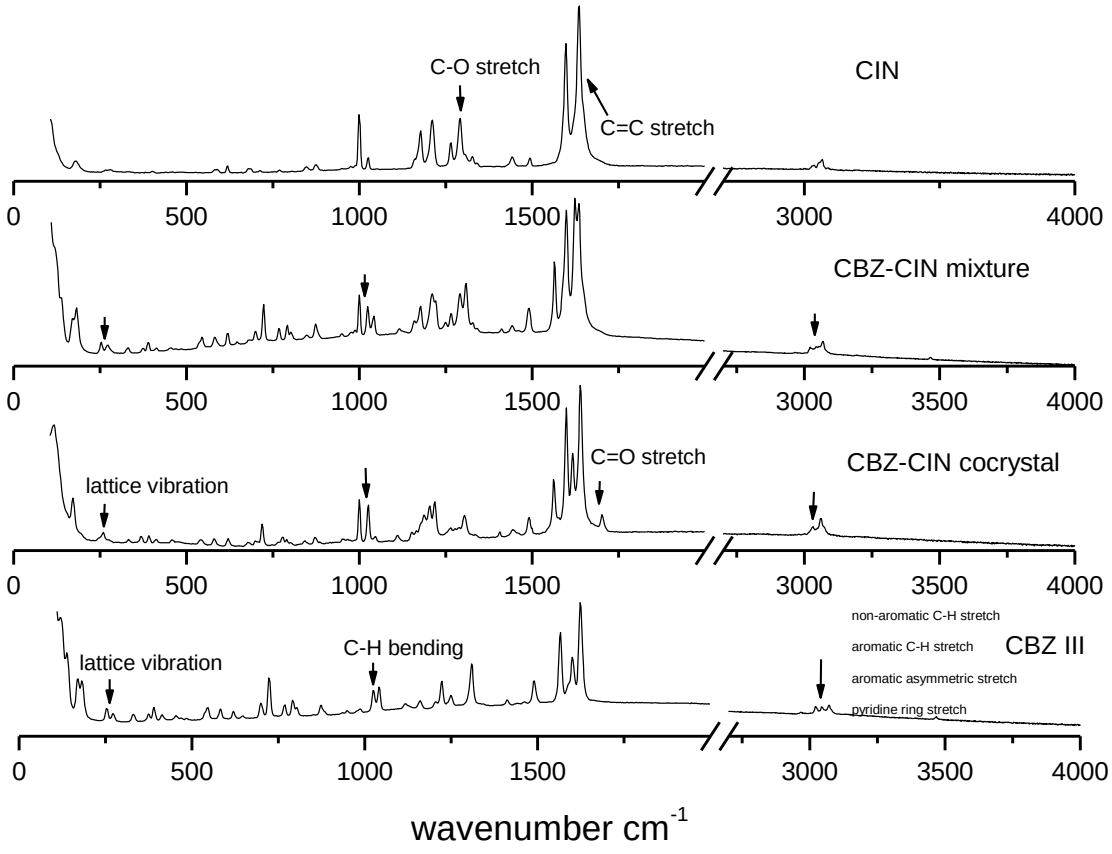

Fig.4.13 Raman spectra for CBZ III, CIN, CBZ-CIN cocrystals and a mixture

The Raman spectra data of CBZ III, NIC, SAC, CIN and the CBZ-NIC, CBZ-SAC and CBZ-CIN cocrystals is summarized in Table 4.7.

Table 4.7 Raman peaks for CBZ III, NIC, SAC, CIN and CBZ-NIC, CBZ-SAC and CBZ-CIN cocrystals

Compound	**Peak position (cm^{-1})**	**Assignment**
CBZ III	double peaks at 272 and 253	lattice vibration
	1040,1025, peak intensity ratio 0.97	C-H bending
	triple peaks at 3020, 3043 and 3071	non-aromatic C-H stretch
		aromatic C-H stretch
		aromatic asymmetric stretch
NIC	1042	pyridine ring stretch
	3060	C-H stretch
SAC	1697	C=O stretch
CIN	1637	C=C stretch
	1292	C-O stretch
CBZ-NIC cocrystals	single peak at 264	lattice vibration
	distinctive peaks at 1020-1040	C- H bending
	distinctive peaks at 2950-3500	C-H stretch
CBZ-SAC cocrystals	1715	C=O stretch
CBZ-CIN cocrystals	255	lattice vibration
	1700-1720	C=O

4.3.5 XRPD analysis of CBZ III, CBZ cocrystals and physical mixtures

4.3.5.1 CBZ-NIC cocrystals

Fig.4.14 presents the corresponding XRPD patterns of the crystals of CBZ III, NIC, CBZ-NIC cocrystals and a physical mixture. The characteristic diffraction peaks of CBZ III are at $2\theta=13.1^{o}$, 15.3^{o}, 19.6^{o} and 20.1^{o}, all of which are identical to those of the reported data [52, 140-142]. NIC's characteristic diffraction peaks are at $2\theta=14.9^{o}$ and 23.5^{o}. CBZ-NIC cocrystals show the characteristic diffraction peaks at $2\theta=6.7^{o}$, 9.0^{o}, 10.3^{o}, 13.5^{o} and 20.6^{o}, which agrees with previous reports [140, 143]. The physical mixtures showed the characteristic peaks of both CBZ III and NIC.

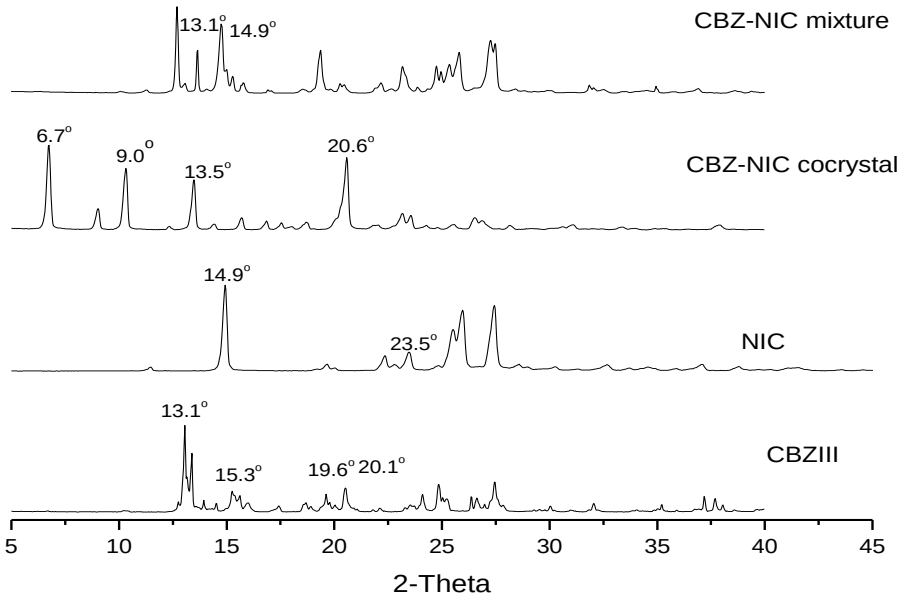

Fig.4.14 XRPD of CBZ III, NIC, CBZ-NIC cocrystals and a mixture

4.3.5.2 CBZ-SAC cocrystals

Fig.4.15 presents the corresponding XRPD patterns of the crystals of CBZ III, SAC, CBZ-SAC cocrystals and a physical mixture. SAC's characteristic diffraction peaks are at 2θ=9.8°, 16.3°, 19.4° and 25.4°. CBZ-SAC cocrystals show the characteristic diffraction peaks at 2θ=6.8°, 9.0°, 12.3° and 14.0°, all of which agrees with the reported data [144]. The physical mixtures showed the characteristic peaks of both CBZ III and SAC.

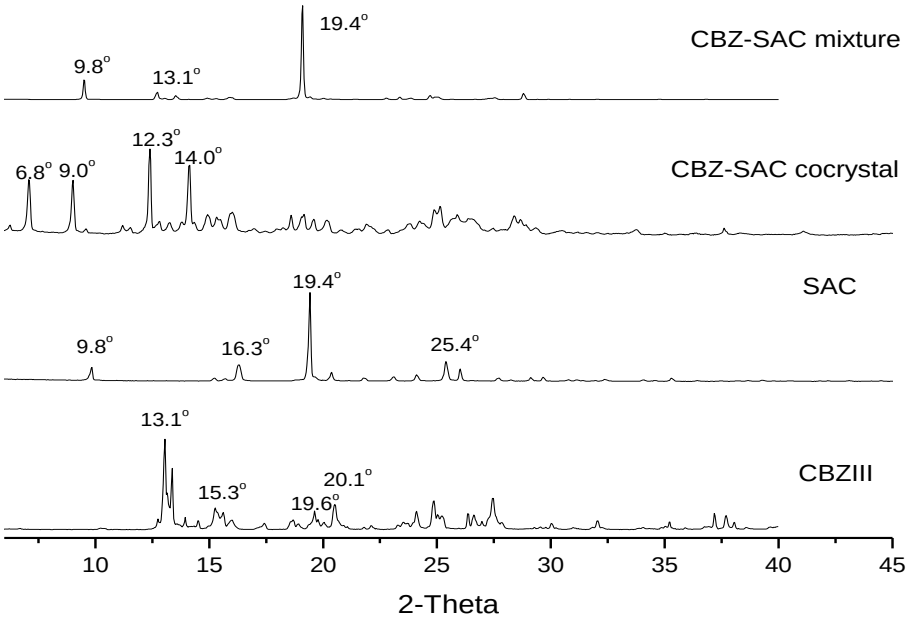

Fig.4.15 XRPD of CBZ III, SAC, CBZ-SAC cocrystals and a mixture

4.3.5.3 CBZ-CIN cocrystals

Fig.4.16 presents the corresponding XRPD patterns of the crystals of CBZ III, CIN, CBZ-CIN cocrystal and a physical mixture. The characteristic diffraction peaks of CIN are at 2θ=9.7°, 18.3°, 25.2° and 29.2° [145]. CBZ-CIN cocrystal shows the characteristic diffraction peaks at 2θ=5.8°, 7.6°, 9.9°, 16.7° and 21.8° which are identical to the reported data [146]. The physical mixtures showed characteristic peaks of both CBZ III and CIN.

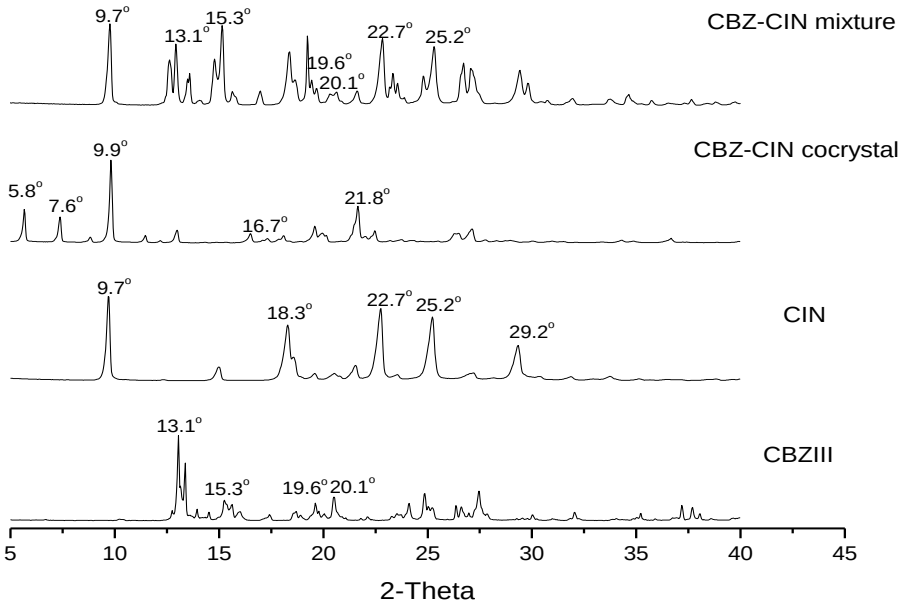

Fig.4.16 XRPD of CBZ III, CIN, CBZ-CIN cocrystals and a mixture

4.3.6 HSPM analysis of CBZ III, CBZ cocrystals and physical mixtures

4.3.6.1 CBZ-NIC cocrystals

The crystallization pathways of CBZ III and NIC were investigated using HSPM and the photomicrographs obtained are shown in Fig.4.17. For CBZ, the agglomerates of prismatic crystal corresponding to Form III converted to small needle-like crystal corresponding to Form I from 176 ℃ [147], which finally melted at 193 ℃ as shown in Fig.4.17 (a). For NIC, the crystalline completely melted at 130 ℃, as shown in Fig.4.17 (b). For CBZ-NIC cocrystals, the crystalline completely melted at 161 ℃ as shown in Fig.4.17 (c). For CBZ-NIC physical mixture, NIC melted from 130 ℃ and CBZ dissolved into this melt. The CBZ-NIC cocrystals then began to grow until 157 ℃ and completely melted at 162 ℃. The results of HSPM analysis indicated that physical mixture of CBZ and NIC could form cocrystals during the heating process. The newly generated cocrystals melted at 162 ℃, as shown in Fig.4.17 (d).

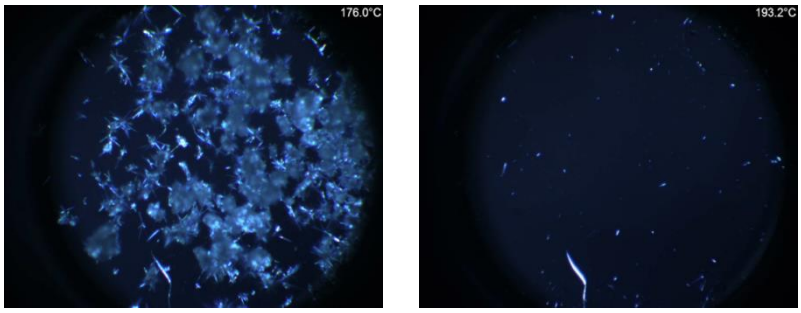

(a) CBZ III

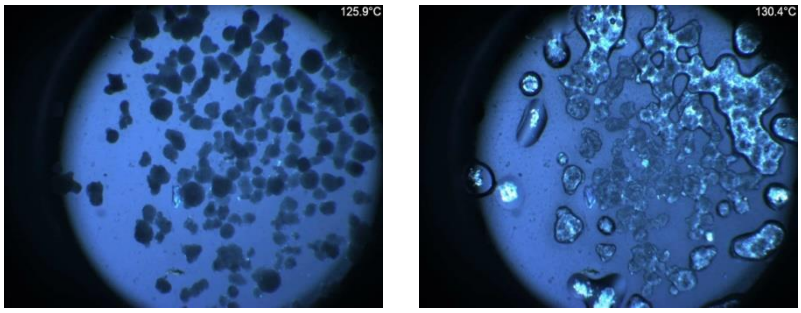

(b) NIC

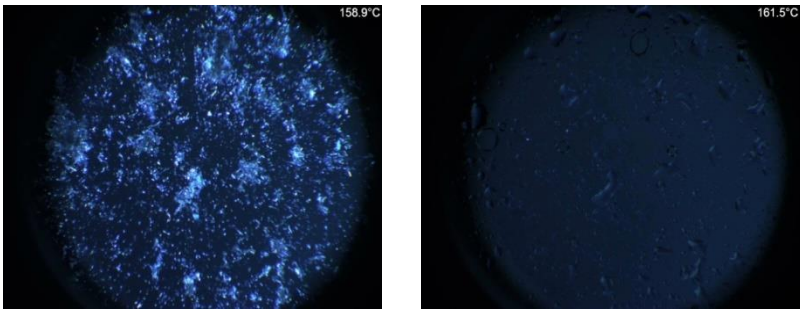

(c) CBZ-NIC cocrystals

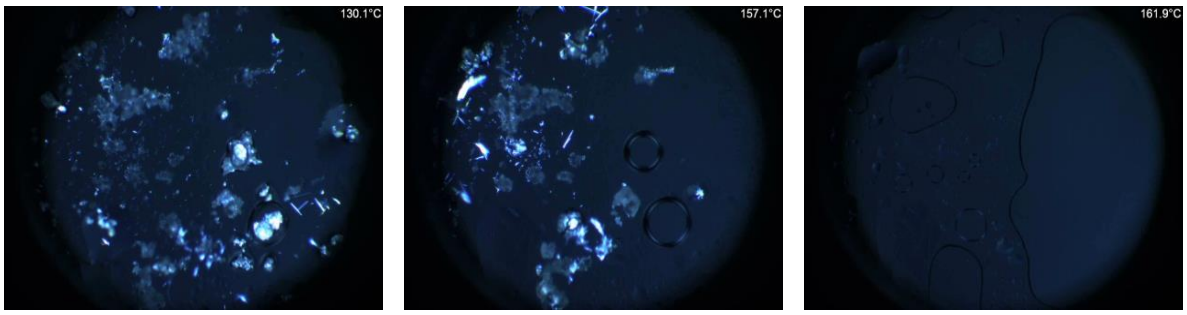

(d) CBZ and NIC mixture

Fig.4.17 HSPM micrographs of phase transition during heating processes: (a) CBZ III; (b) NIC; (c) CBZ-NIC cocrystals; (d) CBZ and NIC mixture.

4.3.6.2 CBZ-SAC cocrystals

The crystallization pathways of CBZ III and SAC were investigated using HSPM and the photomicrographs obtained are shown in Fig.4.18. For SAC, the crystalline completely melted at 230 ℃, as shown in Fig.4.18 (a). For CBZ-SAC cocrystals, the crystalline completely melted at 177 ℃ as shown in Fig.4.18 (b). For CBZ-SAC physical mixture, new crystalline was generated from 130 ℃; this began to grow until 150 ℃ and completely melted at 178 ℃ as shown in Fig.4.18 (c). The results of the HSPM analysis indicated that the physical mixture CBZ and SAC could form cocrystal during the heating process.

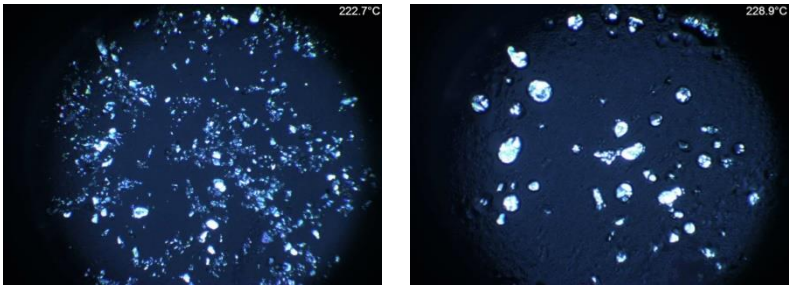

(a) SAC

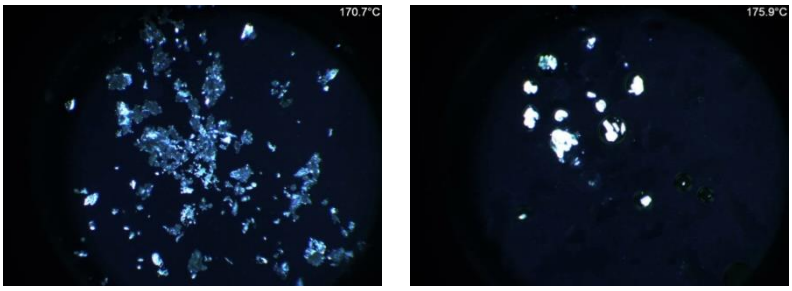

(b) CBZ-SAC cocrystals

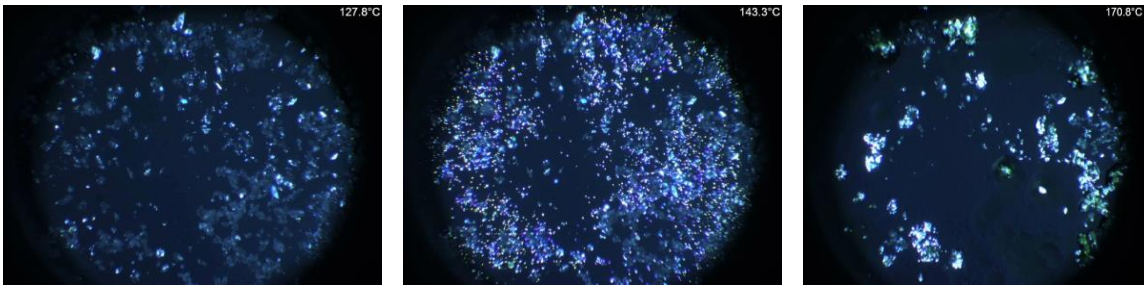

(c) CBZ-SAC mixture

Fig.4.18 HSPM micrographs of phase transition during heating processes: (a) SAC; (b) CBZ-SAC cocrystals; (c) CBZ-SAC mixture

4.3.6.3 CBZ-CIN cocrystals

The crystallization pathways of CBZ III and CIN were investigated using HSPM and the photomicrographs obtained are shown in Fig.4.19. For CIN, the crystalline completely melted at 136 ℃ as shown in Fig.4.19 (a). For CBZ-CIN cocrystals, the crystalline completely melted at 147 ℃ as shown in Fig.4.19 (b). For CBZ-CIN physical mixture, some crystalline melt from 110 ℃ and new crystalline was generated from 120 ℃. This then began to grow until 127 ℃ and completely melted at 144 ℃, as shown in Fig.4.19 (c). The results of HSPM analysis indicated that CBZ and CIN could form cocrystal during the heating process.

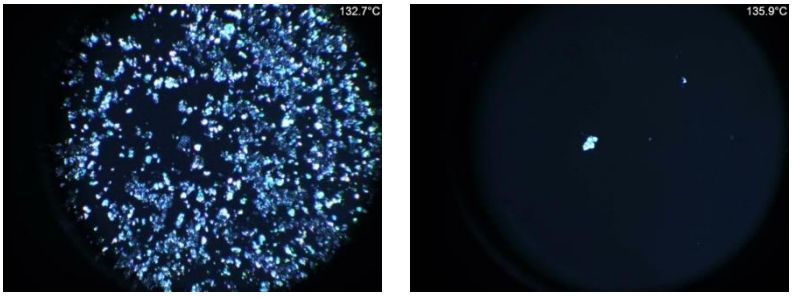

(a) CIN

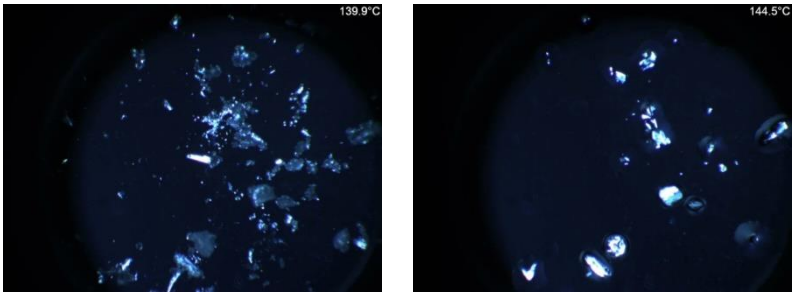

(b) CBZ-CIN cocrystal

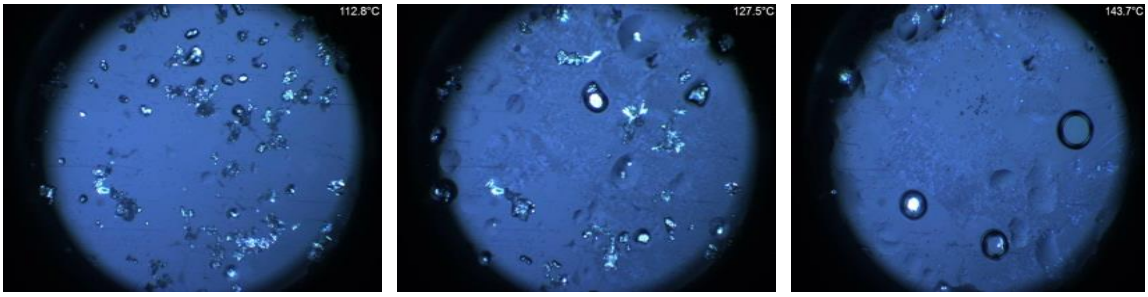

(c) CBZ-CIN mixture

Fig.4.19 HSPM micrographs of phase transition during heating processes: (a) CIN; (b) CBZ-CIN cocrystals; (c) CBZ-CIN mixture

4.4 Chapter conclusions

In this chapter, various samples of CBZ DH, cocrystals of CBZ-NIC, CBZ-SAC and CBZ-CIN were successfully prepared. The CBZ-NIC cocrystals were prepared using the solvent evaporation method and the CBZ-SAC and CBZ-CIN cocrystals using the cooling crystallization method. All the prepared samples were the characterized using a variety of techniques. The DSC results indicate that the physical mixtures of CBZ and the coformer formed CBZ cocrystals during the heating process. The Raman and FTIR results indicate that the CBZ cocrystals had formed through the H-bonding acceptors and donors of groups $–NH_2$ and –(C=O)-. The patterns of the CBZ cocrystals were different from the physical mixtures of CBZ and the coformer by XRPD, indicating that the CBZ cocrystals were not just a physical mixture of the two components but rather that a new solid-state formation had been generated. The HSPM micrographs further prove that the physical mixtures of CBZ and the coformer form a new solid-state formation during the heating process. The molecular structure of the cocrystals CBZ-NIC, CBZ-SAC and CBZ-CIN were also described in this chapter, which gives readers a better understanding of cocrystal structure formation.

Chapter 5 Investigation of the effect of Hydroxypropyl Methylcellulose on the phase transformation and release profiles of CBZ-NIC cocrystals

5.1 Chapter overview

In this chapter the effect of Hydroxypropyl Methylcellulose (HPMC) on the phase transformation and release profile of CBZ-NIC cocrystals in solution and in sustained release matrix tablets were investigated. The polymorphic transitions of the CBZ-NIC cocrystals and their crystalline properties were examined using DSC, XRPD, Raman spectroscopy and SEM. The intrinsic dissolution study was investigated using the UV imaging system. The release profiles of the CBZ-NIC cocrystals in solution and sustained release matrix tablets were investigated using the dissolution method.

5.2 Materials and methods

5.2.1 Materials

Anhydrous CBZ III, NIC, Ethyl acetate, double distilled water, HPMC K4M, SLS and methanol were used in this chapter; details of these materials can be found in Chapter 3.

5.2.2 Methods

5.2.2.1 Formation of the CBZ-NIC cocrystals

This chapter describes the preparation of the CBZ-NIC cocrystals. The details of the formation method can be found in Chapter 3

5.2.2.2 Preparation of tablets

The formulations of the matrix tablets are provided in Table 5.1. The details of the method can be found in Chapter 3.

Table 5.1 Matrix tablet composition (mg)

Component	**Formulation**					
	F1	**F2**	**F3**	**F4**	**F5**	**F6**
CBZ III	200			200		
CBZ-NIC cocrystals		304			304	
Equal molar mixture of CBZ III and NIC			304			304
HPMC K4M	100	100	100	200	200	200

5.2.2.3 Intrinsic dissolution study by the UV imaging system

The dissolution behaviours of CBZ III and CBZ-NIC cocrystals in pure water and different concentrations of HPMC solutions were studied in this study. The details of this method can be found in Chapter 3. The media used for the tests included water and 0.5, 1, 2 and 5 mg/ml HPMC aqueous solutions.

5.2.2.4 Solubility analysis of CBZ-NIC cocrystals and mixture, CBZ III in HPMC solutions

The equilibrium solubilities of CBZ-NIC cocrystals and a mixture, as well as CBZ III in HPMC aqueous solution, were tested in this chapter. The details of this method can be found in Chapter 3. The media used for the tests included water and 0.5, 1, 2 and 5 mg/ml HPMC aqueous solutions.

5.2.2.5 Dissolution studies of formulated HPMC matrix tablets

The results of dissolution studies of formulated HPMC tablets are presented in this chapter. The details of this method can be found in Chapter 3. The medium used for the test was 1% SLS water.

5.2.2.6 Physical properties characterisation techniques

HPLC and statistical analysis were used to study the solubility and dissolution behaviour of tablets. UV imaging was used to study the intrinsic dissolution rate. SEM, XRPD and DSC were used in this chapter for characterisation. Details of these techniques can be found in Chapter 3.

5.3 Results

5.3.1 Phase transformation

Fig.5.1 shows the CBZ solubility of CBZ-NIC cocrystals, CBZ III and a physical mixture of CBZ III and NIC at different HPMC concentration solutions at equilibrium after 24 hours. In pure water, there was no significant difference in equilibrium solubility between CBZ III, CBZ-NIC cocrystals and a physical mixture of CBZ III and NIC ($P>0.05$).

It was found that a small amount of HPMC in solution can increase the CBZ solubility of CBZ III and a physical mixture of CBZ III and NIC significantly, indicating a higher degree of interaction between CBZ and HPMC to form a soluble complex. No difference in the equilibrium solubility of CBZ III and the physical mixture ($P>0.05$) at different HPMC concentration solutions was observed, indicating that NIC had no effect on the solubility of CBZ because of the low concentration of NIC in the solution, which is consistent with the present researchers' previous results [148]. The solubility of CBZ III and a physical mixture of CBZ III and NIC increased initially with increasing HPMC concentration in solution to a maximum at 2 mg/ml HPMC concentration, and then decreased slightly. This suggests that the soluble complex of CBZ and HPMC reached its solubility limit at 2 mg/ml HPMC in solution.

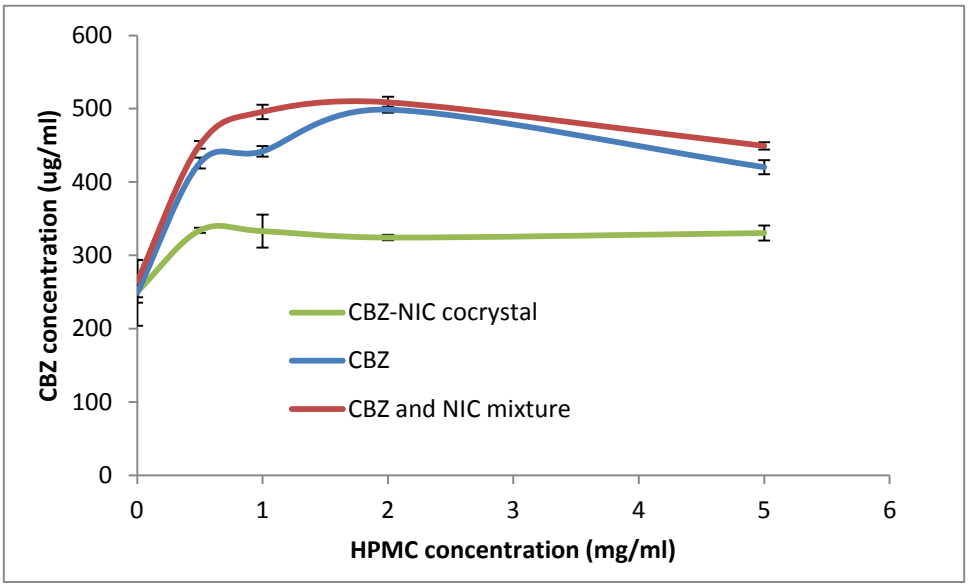

Fig.5.1 CBZ concentration of CBZ-NIC cocrystals, CBZ III, and a physical mixture of CBZ III and NIC in different HPMC solution concentration solutions

The CBZ solubility of CBZ-NIC cocrystals exhibits behaviour different to those of CBZ III and a physical mixture ($P<0.05$) i.e. its value was significantly lower than that of CBZ III; indeed, it was

nearly constant with increasing HPMC concentrations, indicating that the amount of a soluble complex of CBZ-HPMC formed in solution was not significant.

Solid residues retrieved from each of the solubility tests were analysed using DSC, Raman and SEM. The DSC thermographs of individual components are given in Fig.5.2 (a) for comparison, showing that the dehydration process of CBZ DH occurred in the range 80-120^{o}C. After a dehydration process under DSC heating conditions, CBZ DH converted back to CBZ III which melted at around 175^{o}C and recrystallized to CBZ I, which in turn melted at around 195^{o}C. The DSC thermographs of the solid residues from different HPMC concentration solutions were examined as shown in Fig.5.2 (b). It can clearly be seen that the CBZ DH crystals were found in the solid residues of CBZ-NIC cocrystals in different HPMC concentration solutions because there was a clear dehydration process with a sharp endothermic between 80-120 ℃ in each DSC thermograph. This is analogous to that seen with CBZ DH in Fig.5.2 (a), indicating that HPMC did not inhibit the crystallisation of CBZ DH from solution. As expected, the solid residues of CBZ III and a physical mixture in water were converted to CBZ DH after 24 hours, showing the same DSC thermographs as that of CBZ DH alone. It can be seen that at 2 mg/ml of HPMC concentration and above, CBZ III alone or in physical mixture did not convert to dihydrate after 24 hours because no dehydration event occurred in the DSC thermographs, indicating that HPMC completely inhibited the transformation of CBZ III to CBZ DH. Furthermore, more thermal events occurred at temperatures of between 175^{o}C and 185^{o}C; the present researchers believe that this was caused by the CBZ IV melting and simultaneously recrystallizing to CBZ I. This is discussed in greater depth in the following section.

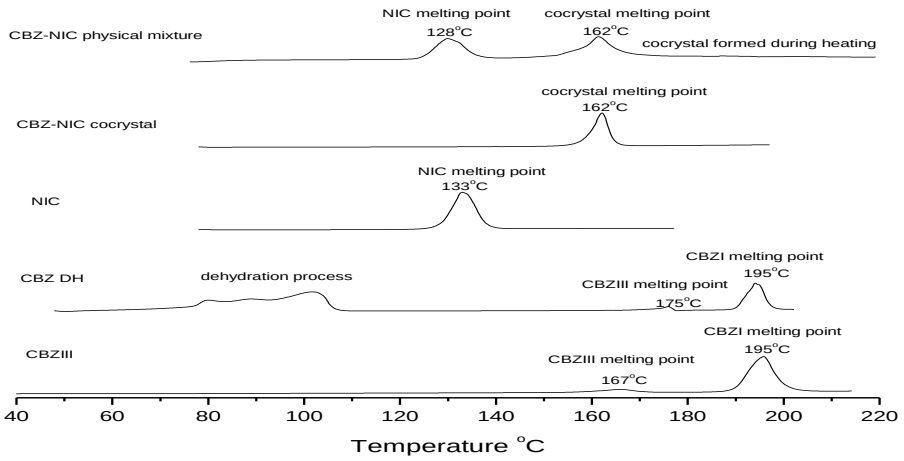

(a)

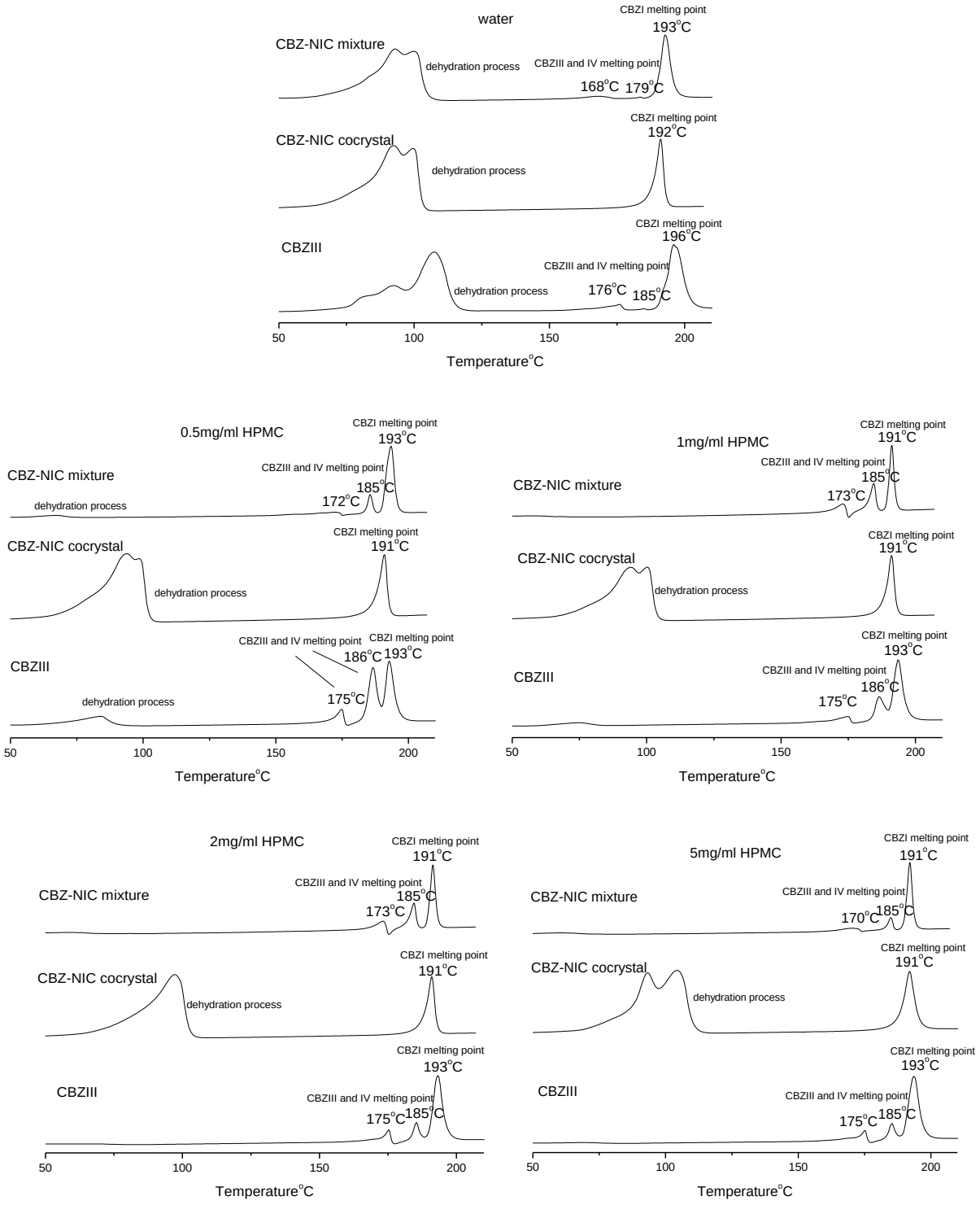

(b)

Fig.5.2 DSC thermographs of solid residues obtained from different HPMC concentration solutions: (a) original samples; (b) solid residues of CBZ III, CBZ-NIC cocrystals and a physical mixture of CBZ and NIC

Fig.5.3 illustrates the influence between various HPMC concentrations on the degree of conversion to CBZ DH analysed by Raman spectroscopy. As expected, the solid residues of CBZ III, CBZ-NIC

cocrystals and a physical mixture in water were completely converted to CBZ DH after 24 hours. HPMC did not show any influence on the transformation of CBZ-NIC cocrystals to CBZ DH at any concentrations between the 0.5 to 5 mg/ml studied, showing the same conversion rate of around 95% CBZ DH in the solid residues. At 2 mg/ml of HPMC concentration and above, the conversion rate of CBZ DH for anhydrous CBZ III alone or in physical mixture was zero, which was consistent with the DSC results. The conversion rates of CBZ DH for CBZ III alone and in physical mixture were also same at the other HPMC concentrations – i.e. around 10% in the 0.5 mg/ml HPMC concentration solution and 5% in the 1mg/ml HPMC concentration solution – indicating that HPMC partly inhibited the transformation to CBZ DH. It is also interesting to note that NIC did not affect the conversion rate for CBZ III in a physical mixture.

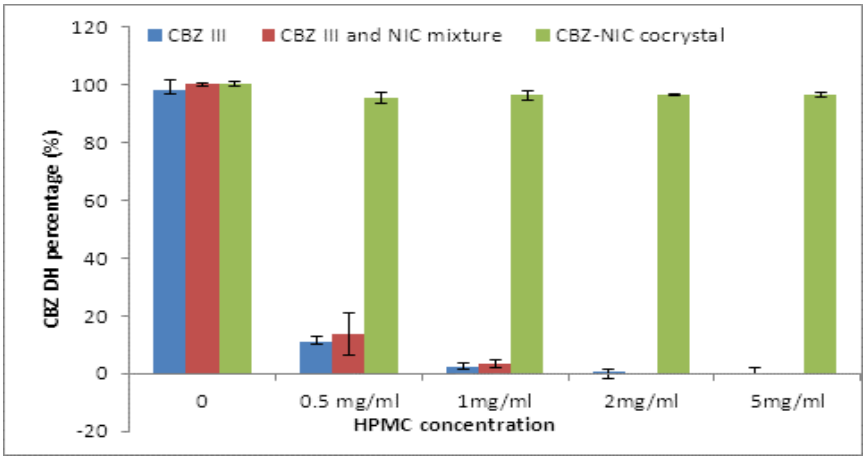

Fig.5.3 Influence of HPMC concentration on conversion of CBZ to CBZ DH after 24 hours

Fig.5.4 shows SEM photographs of solid residues obtained from different HPMC concentration solutions. CBZ III samples used appeared to be prismatic, showing a wide range of size and shape. Small cylindrical NIC particles could be seen to mix with CBZ III particles in the physical mixture samples. CBZ-NIC cocrystals show a thin needle-like shape in a wide range of sizes. It can be seen that HPMC has a significant influence on the morphology of the crystals shown in the SEM photographs. In water, prism-like CBZ III crystals have become transformed into needle-like CBZ DH crystals. At different HPMC concentration solutions there was no significant change in morphology for most residual crystals compared with the starting materials of CBZ III. However, it can clearly be seen that some spherical aggregates appeared to be amorphous in the residuals, all of which are consistent with previous findings [149]. The morphology of the residues for the physical mixture of CBZ III and NIC was similar to those of CBZ III in different concentrations of HPMC solutions, indicating that all NIC samples had dissolved and that NIC had no effect on the phase transformation of CBZ III. For the CBZ-NIC cocrystals, the residues up to 1 mg/ml HPMC

concentration solutions show the needle-like shape as that of pure CBZ DH, whose size distribution is much more even and narrow than that of the CBZ-NIC cocrystals. This indicates that HPMC did not inhibit the crystallisation of CBZ DH from the solution. At concentrations of 2 and 5 mg/ml HPMC solution, the CBZ DH crystals were thicker than the CBZ DH crystals precipitated from pure water, and some aggregates composed of small crystals also appeared with the needle-like shape of the CBZ DH crystals.

	CBZ-NIC cocrystals	**CBZ III**	**CBZ III and NIC mixture**
original material	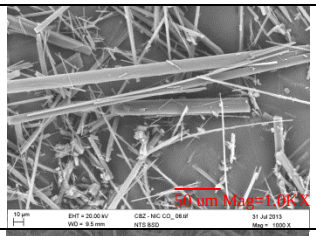	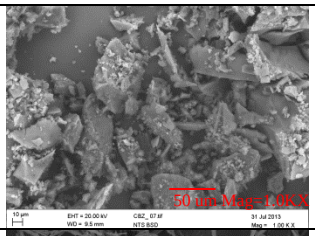	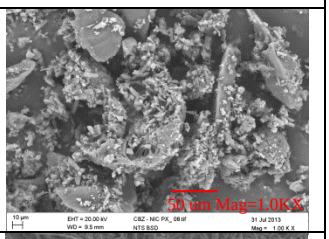
water	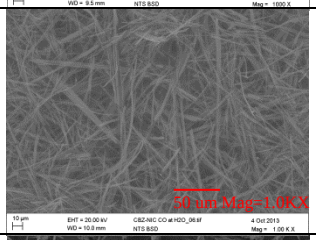	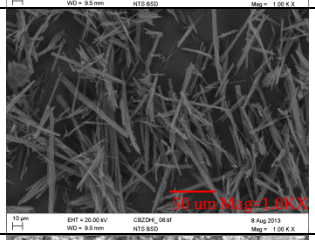	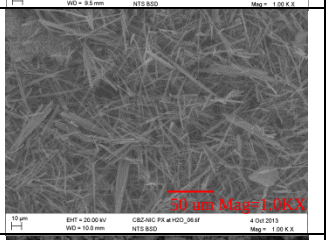
0.5 mg/ml HPMC	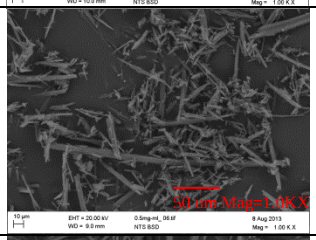	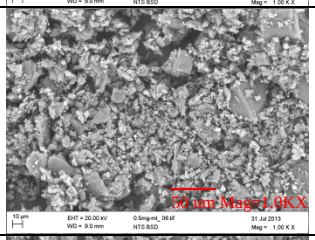	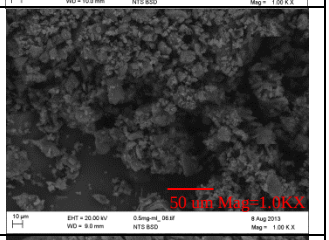
1 mg/ml HPMC	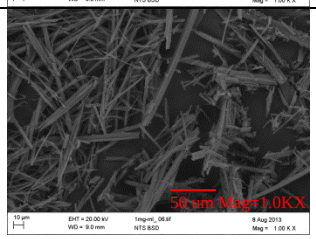	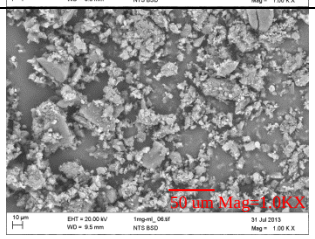	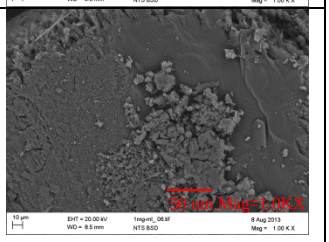
2 mg/ml HPMC	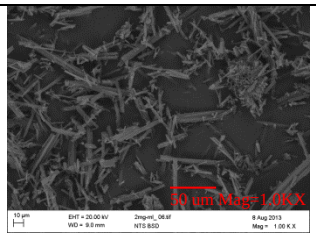	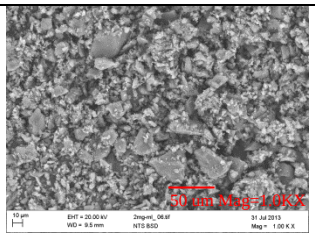	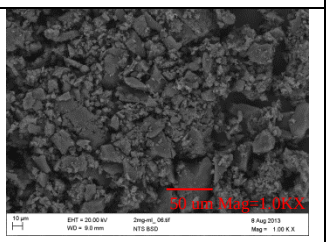
5 mg/ml HPMC	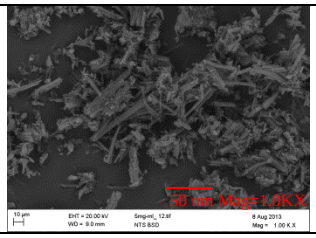	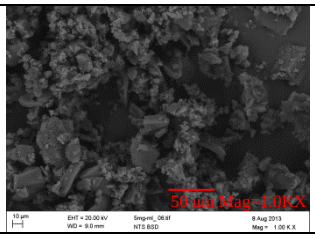	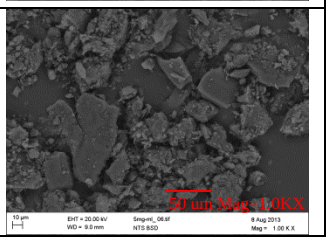

Fig.5.4 SEM photographs of solid residues obtained from CBZIII, CBZ-NIC cocrystal and physical mixture at different HPMC concentration solutions

The IDR profiles of the compacts of the CBZ III (dashed lines) and CBZ-NIC cocrystals (solid lines) at different HPMC concentration dissolution medium are shown in Fig.5.5. It can be seen that all IDRs decreased quickly within 10 minutes, reaching their static values after 30. No differences between the IDR profiles of the CBZ-NIC cocrystals at different HPMC concentration dissolution medium ($P>0.05$) were found. Prior to the dissolution tests, all the compact surfaces of CBZ-NIC cocrystals were smooth. After those tests, the SEM photographs (Fig.S5.1 in the Appendices) show that small needle-shaped CBZ DH crystals had appeared on the compact surfaces of the CBZ-NIC cocrystals, indicating that HPMC did not inhibit the recrystallization of CBZ DH crystals from the solutions. Different dissolution behaviours ($P<0.05$) of CBZ III at different HPMC concentration dissolution medium were observed. When the dissolution medium was water, the IDR of CBZ III decreased quickly because of the precipitation of CBZ DH on the compact surface (shown in the SEM photographs in Fig.S5.1 in the Appendices). The IDR of CBZ III increased significantly when the HPMC was added in the dissolution medium, as shown in Fig.5.5, and there were no CBZ DH crystals on the compact surfaces in Fig.S5.1 in the Appendices, indicating that HPMC inhibited the recrystallization of CBZ DH crystals from the solutions. It can be also shown that the CBZ-NIC cocrystals had an improved dissolution rate in water when compared with CBZ III, but also that this advantage was completely lost (when compared with CBZ III) when HPMC was included in a dissolution medium.

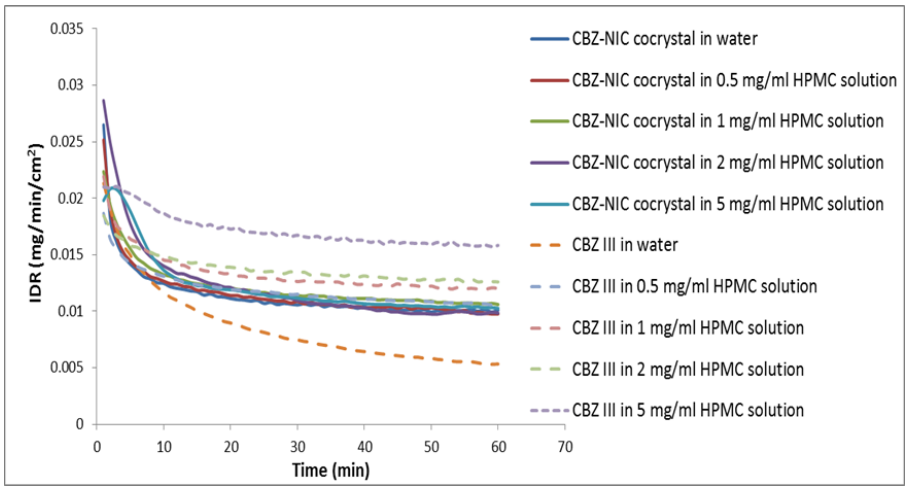

Fig.5.5 Intrinsic dissolution rates obtained by UV imaging (n=3)

The results of IDR have the same ranking as the solubility – i.e. in different HPMC solutions, CBZ III> CBZ-NIC cocrystals (Fig.5.1). The turning point on the IDR curves indicates where the slope changed from the dissolution of CBZ III or CBZ-NIC cocrystals to that of CBZ DH. The highest slope means that the sample has the ability to undergo the fastest transformation to the CBZ DH

form [150]. The results of the IDR curves indicate that CBZ-NIC cocrystals transformed into CBZ DH faster than CBZ III in HPMC solutions.

5.3.2 CBZ release profiles in HPMC matrices

Fig.5.6 (a) presents the CBZ release profiles of CBZ-NIC cocrystals, CBZ III and a physical mixture of CBZ III and NIC from the 100 mg HPMC matrices. This demonstrates that the release of CBZ from the CBZ-NIC cocrystal formulation is significant different from those of the CBZ III and physical mixture formations ($P<0.05$). It is interesting to note that the significantly higher release of CBZ from the CBZ-NIC cocrystal formulation occurred at the early stage of the dissolution (up to one hour). However, the CBZ release rate from the cocrystal formulation changed significantly, gradually decreasing to a lower value than that of the CBZ III and physical mixture formulations after 2.5 hours, indicating significant changes to the cocrystal properties in the matrix. The difference in the CBZ releases from the CBZ III and physical mixture formulations was significant during dissolution up to three hours ($P<0.05$), after which both formulations' CBZ release profiles were identical ($P>0.05$). It can be seen that during the first hour of the dissolution test the CBZ release rate from the CBZ III formulation was the lowest, which is explained by HPMC's initially slower hydration and gel layer formation processes. Once the tablet's hydration process was completed, the CBZ release rate remained constant. For the physical mixture of CBZ and NIC formulations, HPMC's hydration and gel layer formation processes was much faster than that of the CBZ III formulation alone because the quickly dissolved NIC acted as a channel agent to speed up the water uptake process, resulting in a higher release rate. Once all of NIC had dissolved, both formations showed similar dissolution profiles.

Fig.5.6 (b) presents the CBZ release profiles of CBZ-NIC cocrystals, CBZ III and a physical mixture of CBZ III and NIC from the 200 mg HPMC matrices. Overall, the results show that increasing HPMC in all three formulations resulted in reduced CBZ release rates, indicating that HPMC slowed down drug dissolution. It shows that the CBZ release from the CBZ-NIC cocrystal formulation is much higher than those of the other two formulations of CBZ III and a physical mixture, demonstrating the advantage of CBZ-NIC cocrystal formulation. Incorporation of NIC in the formulation produced no change in CBZ III release rate ($P>0.05$), thereby demonstrating NIC's complete lack of effect on the enhancement of CBZ III dissolution in the formation. The CBZ release rate of each of three formulations was nearly constant.

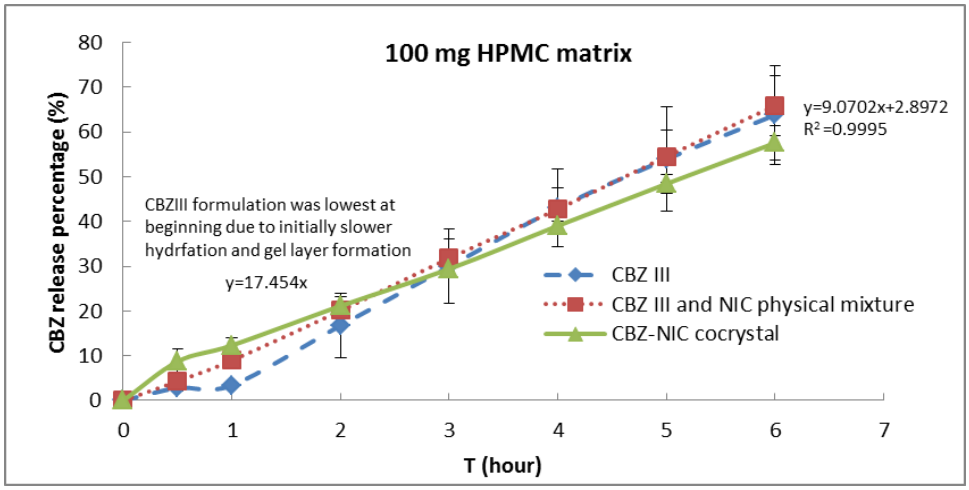

(a)

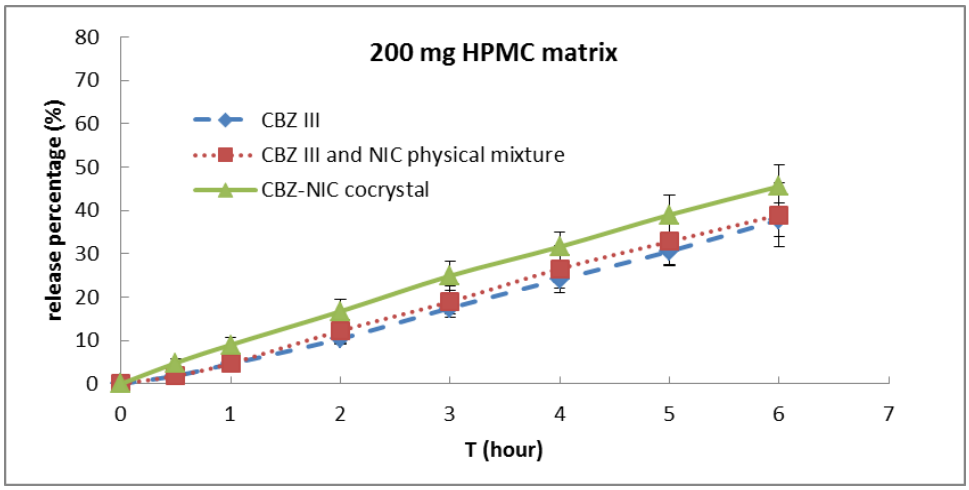

(b)

Fig.5.6 CBZ release profiles of CBZ-NIC cocrystals, CBZ III and a physical mixture of CBZ III and NIC formulations: (a) in a 100 mg HPMC matrix; (b) in a 200 mg HPMC matrix

The solid crystal properties in the gel layer were examined using XRPD, SEM and DSC in order to understand the mechanisms involved in the CBZ release of CBZ-NIC cocrystals from a HPMC Fig.5.7 (e)-(j) illustrates the corresponding XRPD patterns of the crystals in the gel layers of different formulations. The XRPD patterns of the individual components of CBZ III, CBZ DH, NIC and CBZ-NIC cocrystals are also shown in Fig.5.7 (a)-(d). The characteristic diffraction peaks of CBZ III are at 2θ=13.1 °, 15.3 °, 19.6 ° and 20.1 °, being identical to those in published data [52, 140-142]. The molecular of CBZ III arrangements along the three crystal faces [(100), (010) and (001)] was carried out: fewer polar groups were exposed on the (100) face than on the (001) and (010) faces, which explains the comparatively weak interaction of the (100) face with water during hydration [151]. The reflections at 9.0 °, 12.4 °, 18.8 ° and 19.0 ° are especially characteristic peaks

of CBZ DH. NIC shows the characteristic diffraction peaks at 2θ=14.9 ° and 23.5 °. The characteristic diffraction peaks of CBZ-NIC cocrystals were exhibited at 2θ=6.7 °, 9.0 °, 10.3 °, 13.5 ° and 20.6 °, which agrees with previous reports [140, 143].

The significant, characteristic peaks of CBZ III, without any characteristic peaks of CBZ DH, were observed in the gels of CBZ III tablets in both 100 mg and 200 mg HPMC matrices, implying that there was no change in CBZ III's crystalline state. In the gel layers of the physical mixture of CBZ III and NIC in both 100 mg and 200 mg matrices, only the characteristic peaks of CBZ III appear; no diffraction peaks of NIC or CBZ DH are evident, indicating that NIC had dissolved completely and that its existence had no effect in the formulation on CBZ III's crystalline properties. Furthermore, the XRPD diffraction patterns of CBZ III obtained from the formulations of CBZ III and a physical mixture of CBZ III and NIC in Fig.5.7 (e), (f), (i) and (j) revealed the characteristic peaks of CBZ IV at 2θ=14.4 and 17.4 ° [52], indicating that a new form of CBZ IV crystal had been crystallised during the dissolution of the tablets. In the meantime, those XRPD diffraction patterns showed the significantly weaker and broader peaks compared with that of CBZ III powder in Fig.5.7 (a), which can be attributed to smaller particle size and increased defect density of CBZ crystals.

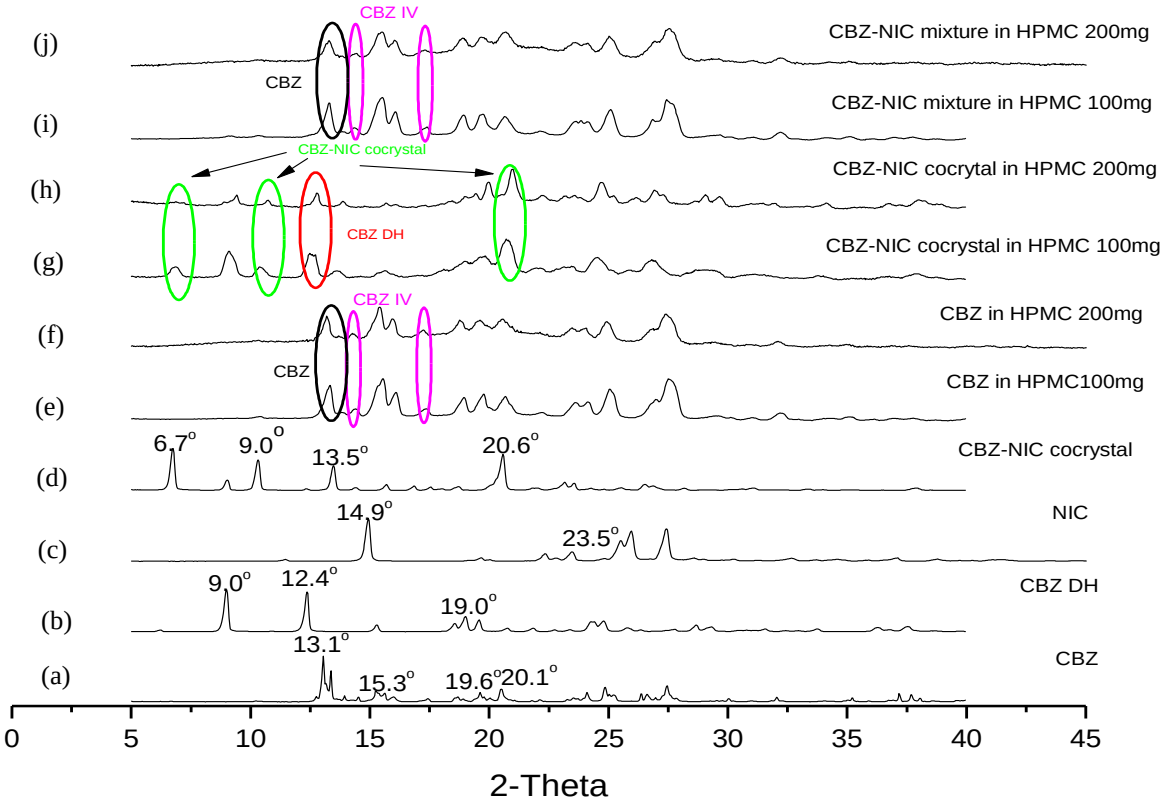

Fig.5.7 XRPD patterns

Both CBZ-NIC cocrystals and CBZ DH characteristic peaks were observed in the CBZ-NIC cocrystal formulations of the 100 mg and 200 mg HPMC matrices, indicating recrystallization of CBZ DH from the solution. However, diffraction peaks of CBZ DH in the 100 mg HPMC matrix are stronger, indicating that more CBZ DH had been recrystallized. The broad peaks of CBZ DH compared with the X-ray patterns of pure CBZ DH indicate a decrease in crystallinity of the crystals with the formation of a less ordered structure.

The gels' SEM morphologies after the dissolution tests are shown in Fig.5.8. These make it clear both that there are many CBZ DH particles dispersed in the gels for the CBZ-NIC cocrystal formulations in both 100 mg and 200 mg HPMC matrices, and that needle-shaped CBZ DH particles were not found in a formulation of either CBZ III or a physical mixture of CBZ III and NIC.

	CBZ-NIC cocrystals	**CBZ III**	**CBZ III and NIC mixture**
Gel of 100 mg HPMC matrix after dissolution	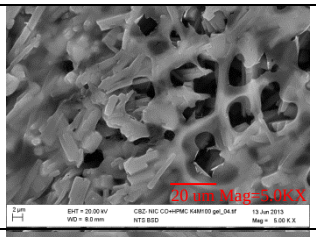	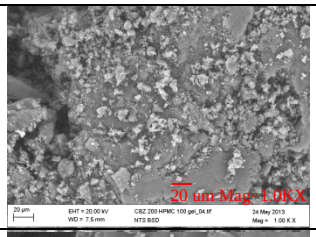	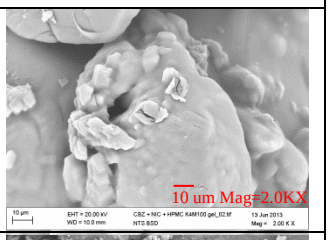
Gel of 200 mg HPMC matrix after dissolution	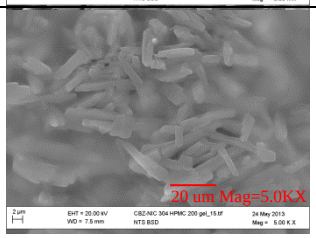	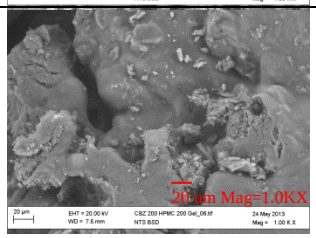	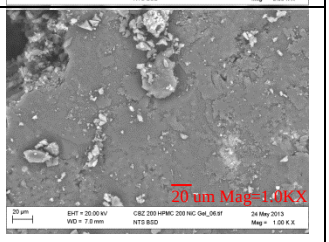

Fig.5.8 SEM photographs of layers after dissolution tests

DSC results are also similar to those in Fig.S5.2 in the Appendices, which supports XRPD and SEM analysis.

5.4 Discussion

The inhibition of CBZ III phase transition to CBZ DH and the amorphism induced in the presence of low concentrations of HPMC and in the gel layer of hydrated tablets has been extensively studied [149]. It is known that hydroxyl groups of HPMC attach to CBZ at the site of water binding and therefore that its transformation to the dihydrate form is inhibited. HPMC was also expected to inhibit the transformation of CBZ-NIC cocrystals to CBZ DH during dissolution because the change in crystalline properties of CBZ-NIC cocrystals during this process can reduce the

advantages of the improved dissolution rate and solubility, resulting in poor drug absorption and bioavailability [8, 148]. Unfortunately, this study shows that HPMC did not inhibit the phase transformation of CBZ-NIC cocrystals to CBZ DH in either the aqueous solutions or the sustained-release HPMC matrix tablets. It also indicated that the CBZ release profile of CBZ-NIC cocrystals was significantly affected by the percentage of HPMC in the formulation.

In fusion, the competition mechanism between CBZ and NIC with HPMC to form hydrogen bonds has been proposed [140]. When the physical mixture of CBZ III, NIC and HPMC was heated, NIC melted first, allowing both CBZ III and HPMC subsequently to dissolve in molten NIC and form intermolecular hydrogen bonds between the three components [152].

The solubility study of CBZ III in different concentrations of HPMC solutions found that CBZ's apparent solubility initially increased with the increasing concentration of HPMC in solution, as shown in Fig.5.1, implying a soluble complex formation between CBZ and HPMC in solution. When the concentration of HPMC was higher than 1mg/ml, the solubility limit of the complex formed was reached and the total apparent solubility of CBZ in solution did not change significantly, as represented by the plateau in Fig.5.1. The sole phase of CBZ III appears as solid residues when the concentration of HPMC was above 1 mg/ml, as is evident from the results of the DSC and Raman spectroscopy in Fig.5.2 and Fig.5.3. This indicates that HPMC can inhibit the precipitation of CBZ DH. The most reasonable explanation is probably two-fold:. a stronger interaction between CBZ and HPMC involving hydrogen bonding interaction occurring at the site where water molecules attack CBZ to form a CBZ-HPMC association, resulting in inhibition of the formation of CBZ DH in solution, and the formation of a soluble complex of CBZ-HPMC in the solution being faster than the rate of CBZ III dissolution.

The formation of the soluble complex CBZ-HPMC in solution has been studied extensively [149, 153-155]. The molecular structure of CBZ DH and a part of the hydrogen bond system is shown in Fig.5.9. Like the crystalline structure of the non-hydrated form, intermolecular hydrogen bonding between carboxamide groups builds centrosymmetric dimers with N17-H…O18'. The two independent water molecules, W1 and W2, are linked to the CBZ molecules by the bridge N17-H…OW1 and OW2-H…O18. The structural formula of HPMC is present in Fig.5.10, which has a high content of OH groups. The formation of CBZ-HPMC association which hydrogen bonding interaction occurs at the site where water molecules are attached to CBZ, thus inhibit the transformation of CBZ to CBZ DH. This interaction may occur at different sites on HPMC molecules that contain hydroxyl groups [149].

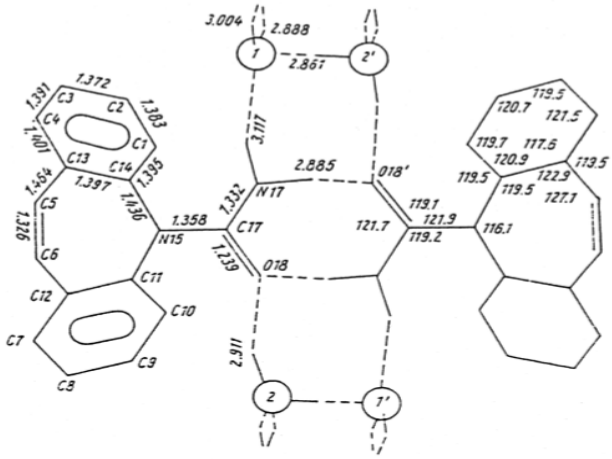

Fig.5.9 The structure of CBZ DH [149]

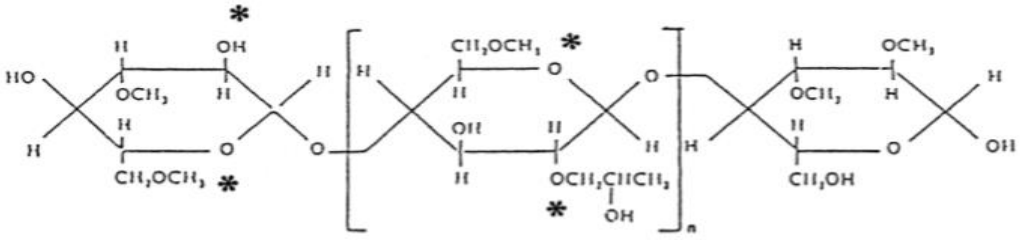

Fig.5.10 HPMC's molecular structure, possible sites of interaction are indicated by * [149]

When the HPMC concentration was higher than 2 mg/ml, the solubility limit of the complex of CBZ-HPMC formed was exceeded, resulting in the precipitation of the complex of CBZ-HPMC showing induction of amorphism of CBZ III crystals in the solid residues. The apparent CBZ solubility therefore decreased, as shown in Fig.5.1. The SEM images in Fig.5.4 illustrate larger agglomerated particles in the solid residuals of the 5 mg/ml HPMC solution. The UV imaging intrinsic dissolution study of CBZ III compacts also supports this explanation. When the dissolution medium was water, the IDR of CBZ III decreased quickly because of precipitation of CBZ DH on the compact surface. This in turn was caused by supersaturation of the CBZ solution around the compact surface. CBZ III's IDR increased with increasing HPMC concentration and no CBZ DH was precipitated on the sample compact surface when HPMC was included in the dissolution medium. The CBZ solubility profile was the same as the physical mixture of CBZ III and NIC, suggesting that NIC had not been incorporated into the complex with CBZ or HPMC in solution. The reason is that the interaction force between NIC and water is much stronger than between the other two components as a result of the large incongruent solubility difference between NIC and CBZ or HPMC in water. This is consistent with the authors' previous report [148], which found no soluble complex of NIC and CBZ formed in solution at a low NIC concentration (up to 40 mM).

The apparent CBZ solubility of CBZ-NIC cocrystals was same as the solubility of CBZ III alone or a physical mixture of CBZ III and NIC because the interaction force of CBZ and NIC was much weaker than that of NIC with water, resulting in the failure in formation of the soluble complex of CBZ-NIC at a low NIC concentration. The apparent CBZ solubility of CBZ-NIC cocryrstals at different concentrations of HPMC solutions was constant, increasing slightly compared with that of CBZ-NIC cocrystals in water. This can be explained by the rate differences between the cocrystal dissolution and formation of a soluble complex of CBZ and HPMC in solution. The solubility of the CBZ-NIC cocrystals was higher and their dissolution rate faster, making it possible to generate a higher supersaturation of CBZ in solution during dissolution. Although the soluble complex of CBZ-HPMC can be formed to stabilize CBZ in the solution, the rate of CBZ from the dissolved CBZ-NIC cocrystals entering the solution was much faster than the rate of CBZ-HPMC complex formation, leading to precipitation of CBZ DH. The Raman analysis shown in Fig.5.3 indicates that nearly 95% of the CBZ DH crystals in the solid residues and SEM images in Fig.5.4 show the needle-shaped particles precipitated on the surfaces of sample compacts. Previous studies have shown that CBZ IV (C-monoclinic) can be crystallized by the slow evaporation of an ethanol solution in the presence of polymers such as hydroxypropyl cellulose, poly(4-methylpentene), poly(α-methylstyrene), and poly(p-phenylene ether-sulfone) [52, 156]. The present study finds that CBZ IV can also be crystallized by dissolving CBZ III in HPMC solution. The DSC results of the solid residues from the both CBZ III and a physical mixture of CBZ III and NIC in different concentrations of HPMC solutions, as shown in Fig.5.2 (b), reveal an additional endothermic-exothermic thermal event between 175^{o}C and 185^{o}C corresponding to the melting point of CBZ IV [52], indicating that HPMC has been docked on the surfaces of CBZ III crystals, as heteronucleito induces defects in crystallinity. Although some aggregates appeared in the solid residuals of CBZ-NIC cocrystals at different concentrations of HPMC solution, the DSC thermograms are same as those shown in Fig.5.2, indicating that HPMC was not crystallised in the crystal units of CBZ dihydrate. It did, however, affect the morphology of CBZ DH crystals.

When the CBZ-NIC cocrystals were formulated into sustained release HPMC matrix tablets, the change in the cocrystals' crystalline properties was affected not only by interaction forces among the components in solution but also by the matrix hydration and erosion characteristics of the drug delivery system. The reduction in CBZ-NIC cocrystal dissolution through HPMC was affected by drug loading: higher drug loading resulted in a weaker reduction effect, exhibiting high CBZ release rates for all three formulations at 100 mg HPMC matrices.

In a lower percentage of 100 mg HPMC matrixes the CBZ release profiles of CBZ-NIC cocrystals, CBZ III and a physical mixture display behaviour similar to that of their IDRs in solution, as found in the authors' previous study [8]. The CBZ-NIC cocrystals in a 100 mg HPMC matrix exhibits the highest release rate compared with the other two formulations at the early stage of the dissolution (up to two hours) because of the improved dissolution rate and the solubility of CBZ-NIC cocrystals. The study has shown that the solubility of CBZ-NIC was approximately 130 to 319 times that of CBZ III alone in water [148]. However, the dissolution profile of CBZ-NIC cocrystals was nonlinear and the release rate declined over time, as shown in Fig.5.6 (a). The slope of the CBZ-NIC cocrystal release rate was 17.454 for the first 0.5 hours, decreasing to 9.0702 thereafter. The XRPD analysis of the gel layer showed that CBZ DH crystals recrystallized from the solution. Similar as the solubility study of CBZ-NIC cocrystals, HPMC in solution failed to stabilize CBZ in solution because the formation rate of the soluble complex of CBZ-HPMC was slower compared with the dissolution rate of CBZ-NIC cocrystals. Because of solid phase transformation of CBZ-NIC cocrystals, the CBZ release rate from the cocrystal formation was lower than that of the formation of CBZ III alone, or of a physical mixture after two hours in the dissolution tests.

By contrast, the CBZ release rate of the physical mixture in the HPMC matrix was linear. When the more soluble component of NIC dissolved rapidly from the matrix, pores could be formed to bring more water into the matrix to increase the dissolution rate of both HPMC and CBZ, resulting in higher CBZ dissolution rates compared with that of the pure CBZ III formulation. A significant delay in the release stage of the pure CBZ III formulation was observed because of the hydration of the HPMC matrix. When NIC dissolved and the HPMC matrix was hydrated, the two formulations exhibited the same CBZ release rates.

With an increased HPMC (200 mg) content in the tablets, it was observed that the release rate of CBZ from various formulations was reduced. The CBZ release profiles of CBZ-NIC cocrystals, CBZ III and a physical mixture in the 200 mg HPMC matrix tablets were controlled mainly by the matrix bulk erosion, indicating that the kinetics of the CBZ release rate were of zero order. Although the XRPD diffraction patterns of the gels of the CBZ-NIC cocrystal formulation indicate the crystallisation of CBZ DH crystals, the CBZ release is less influenced by the change of the crystalline properties of CBZ-NIC cocrystals. When a matrix tablet is immersed in the dissolution medium, wetting occurs at the surface and then progresses into the matrix to form an entangled three-dimensional gel structure in HPMC. Molecules undergoing chain entanglement are characterized by strong viscosity dependence on concentration. An increase in the HPMC percentage in the formulation can lead to an increase in gel viscosity, suppressing the dissolution of

the CBZ-NIC cocrystals. Dissolution of most of CBZ-NIC cocrystals can occur only at the outer surface of the matrix when HPMC undergoes a process of disentanglement in order to be released from the matrix. A similar hydration process also occurred for the CBZ III and physical formulations in 200 mg HPMC matrices. The CBZ release from the CBZ-NIC cocrystal formulation is therefore much higher than those of the other two formulations.

The matrices of the six formulations maintained their structural integrity after six hours of dissolution tests. CBZ III's XRPD diffraction patterns produced by the formulations of CBZ III and a physical mixture of CBZ III and NIC revealed the defect of crystallinity, because CBZ IV appeared in the gel layers, indicating weaker and broader peaks compared with CBZ III powder. The broad peaks of CBZ dihydrate obtained from the gel of CBZ-NIC cocrystal formulations compared with those of pure CBZ DH indicated a change in the crystallinity of crystals with the formation of less ordered structures.

5.5 Chapter conclusion

The influence of HPMC on the phase transformation and release profiles of CBZ-NIC cocrystals in solution and in sustained release matrix tablets was investigated using DSC, XRPD, Raman spectroscopy and SEM. The results indicate that HPMC cannot inhibit the transformation of CBZ-NIC cocrystals to CBZ DH in solution or in the gel layer of the matrix, by contrast with its ability to inhibit CBZ III phase transition to CBZ DH. Based on this conclusion, we propose a possible mechanism for HPMC's inability to inhibit CBZ dihydrate during CBZ-NIC cocrystal dissolution: it is caused by the rate differences between CBZ-NIC cocrystal dissolution and formation of a CBZ-HPMC soluble complex in the solution. For CBZ III, alone or in a physical mixture of CBZ III and NIC, the rate of CBZ III dissolution was slower than the rate of formation of a CBZ-HPMC association in solution, involving a hydrogen bonding interaction at the site where water molecules attach CBZ. The supersaturation level of the soluble complex of CBZ-HPMC was exceeded first, causing the precipitation of CBZ IV crystals because HPMC had been docked on the surfaces of CBZ III crystals as heteronuclei to induce defects of crystallinity. Because of the significantly improved dissolution rate of CBZ-NIC cocrystals, the rate at which CBZ entered the solution was significantly faster than the rate of formation of the CBZ-HPMC soluble complex, leading to high supersaturation levels of CBZ and subsequently precipitation of CBZ DH. Therefore, the apparent solubility and dissolution rates of CBZ of CBZ-NIC cocrystals were constant at different concentrations of HPMC solutions. In a lower percentage of 100 mg HPMC matrixes, the CBZ release profile of CBZ-NIC cocrystals was nonlinear and declined over time, a profile that was

affected significantly by the change of the crystalline properties of CBZ-NIC cocrystals. With an increased HPMC content in the tablets, dissolution of CBZ-NIC cocrystals can only occur at the outer surface of the matrix when HPMC undergoes a process of disentanglement, resulting in a significantly higher CBZ release rate in comparison with the other two formulations of CBZ III and a physical mixture. In conclusion, there can be no doubt that cocrystals offer great advantages with regard to the fine-tuning of physicochemical properties of drug compounds, and in particular to improved solubility and dissolution rates of poorly water-soluble drugs. However, the means by which to maintain drug supersaturation level after the cocrystals are dissolved is a different matter, requiring much more research.

Chapter 6 Effects of coformers on phase transformation and release profiles of CBZ-SAC and CBZ-CIN cocrystals in HPMC based matrix tablets

6.1 Chapter overview

This chapter investigates the effects of coformers on the phase transformation and release profiles of CBZ-SAC and CBZ-CIN cocrystals in both HPMC solution and sustained release matrix tablets. The polymorphic transitions of the CBZ-SAC and CBZ-CIN cocrystals and their crystalline properties were examined using DSC, XRPD and SEM. The release profiles of the CBZ-SAC and CBZ-CIN cocrystals in solution and sustained release matrix tablets were investigated using the dissolution method.

6.2 Materials and methods

6.2.1 Materials

Anhydrous CBZ III, SAC, CIN, HPMC K4M, SLS, methanol, EtOAc and doubly-distilled water were used in this chapter. Details can be found in Chapter 3.

6.2.2 Methods

6.2.2.1 Formation of the CBZ-SAC and CBZ-CIN cocrystals

CBZ-SAC and CBZ-CIN cocrystals were used in this chapter. The details of the formation method can be found in Chapter 3.

6.2.2.2 Preparation of tablets

The formulations of the matrix tablets are provided in Table 6.1. The details of the method can be found in Chapter 3.

Table 6.1 Matrix tablet composition (mg)

Component	Formulation									
	F1	**F2**	**F3**	**F4**	**F5**	**F6**	**F7**	**F8**	**F9**	**F10**
CBZ III	200					200				
CBZ-SAC cocrystals		355					355			
equal molar mixture of CBZ III and SAC			355					355		
CBZ-CIN cocrystals				325					325	
equal molar mixture of CBZ III and CIN					325					325
HPMC K4M	100	100	100	100	100	200	200	200	200	200

6.2.2.3 Powder dissolution study

The powder dissolution rates of CBZ-SAC and CBZ-CIN cocrystals and CBZ III were studied. The details of this method can be found in Chapter 3. The concentrations of HPMC solutions were 0, 0.5 and 2 mg/ml. Each dissolution test was carried out in triplicate.

6.2.2.4 Solubility analysis of CBZ-SAC cocrystal, CBZ-CIN cocrystal and CBZ III in HPMC solutions

The equilibrium solubility of CBZ-SAC and CBZ-CIN cocrystals and of CBZ III in HPMC aqueous solutions was tested in this chapter. The details of this method can be found in Chapter 3. The medium used for the tests included 0, 0.5, 2 and 5 mg/ml HPMC aqueous solutions.

6.2.2.5 Dissolution studies of formulated HPMC matrix tablets

Dissolution studies of formulated HPMC tablets were studied. The details of this method can be found in Chapter 3. The medium used for the test was 1% SLS water.

6.2.2.6 Physical properties characterisation techniques

HPLC and statistical analysis were used to study the solubility, powder dissolution rates and dissolution behaviour of tablets. SEM, XRPD and DSC were used in this chapter for characterisation. Details of these techniques can be found in Chapter 3.

6.3 Results

6.3.1 Phase transformation

Fig.6.1 (a)-(b) shows the CBZ and coformer concentrations after the solubility tests of CBZ III, SAC and CIN and of CBZ-SAC and CBZ-CIN cocrystals at various concentrations of HPMC solutions at equilibrium after 24 hours.

The solubility of CBZ III as shown in Fig.6.1 (a) increased significantly with increasing HPMC concentrations in solution as the result of the formation of the soluble complex CBZ-HPMC, reaching its maximum at 2 mg/ml HPMC in solution and then decreasing slightly because of the inhibition effect of HPMC on the phase transformation of CBZ DH, as discussed in Chapter 5 [157]. SAC's solubility decreased slightly in different concentrations of HPMC solutions, as shown in Fig.6.1 (b), indicating that there was no complex formation between SAC and HPMC in solution. Similarly to SAC, there was no interaction between CIN and HPMC in solution because the solubility of CIN in water or in different concentrations of HPMC solutions was almost constant (p>0.05).

For CBZ-SAC cocrystals, the concentration of CBZ was the same as that of CBZ III in water (p>0.05). It increased slightly (from 1.19 mM to 1.56 mM) with increasing HPMC concentration up to 2 mg/ml, after which point it remained constant as shown in Fig.6.1 (a). The SAC concentration of CBZ-SAC cocrystals decreased slightly in solution as HPMC concentrations rose, as shown in Fig.6.1 (b).

For CBZ-CIN cocrystals, the concentration of CBZ in water was significantly lower than that of CBZ III alone. The CBZ concentrations of CBZ-CIN cocrystals in various concentrations of HPMC solutions remained constant (p>0.05), as shown in Fig.6.1 (a). The CIN concentration profile of CBZ-CIN cocrystals was similar to that of CBZ, as shown in Fig.6.1 (b). Fig.6.1 (c) shows the eutectic constant K_{eu} of CBZ-SAC and CBZ-CIN cocrystals decreasing with an increase in HPMC concentrations in solution, indicating that HPMC can change the stability of the cocrystals in solution during dissolution. More details will be given in the discussion section.

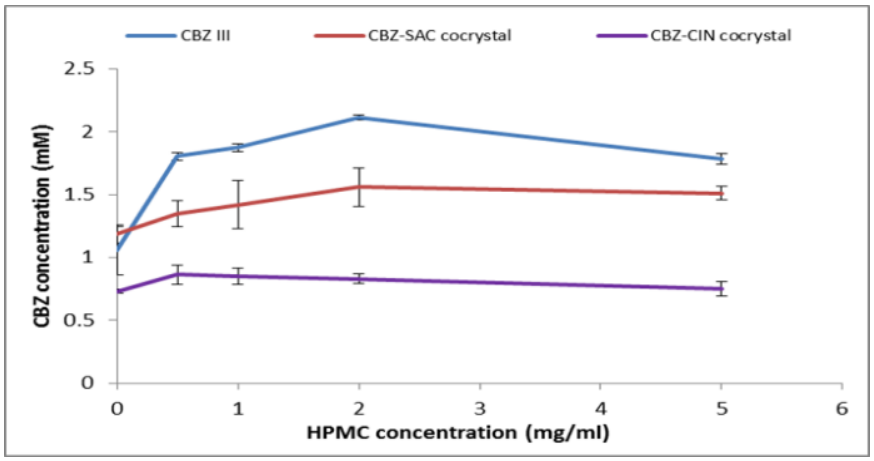

(a)

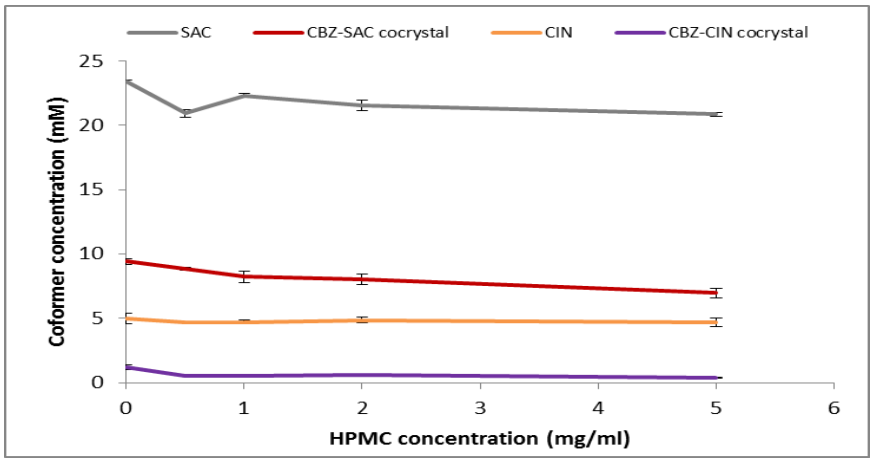

(b)

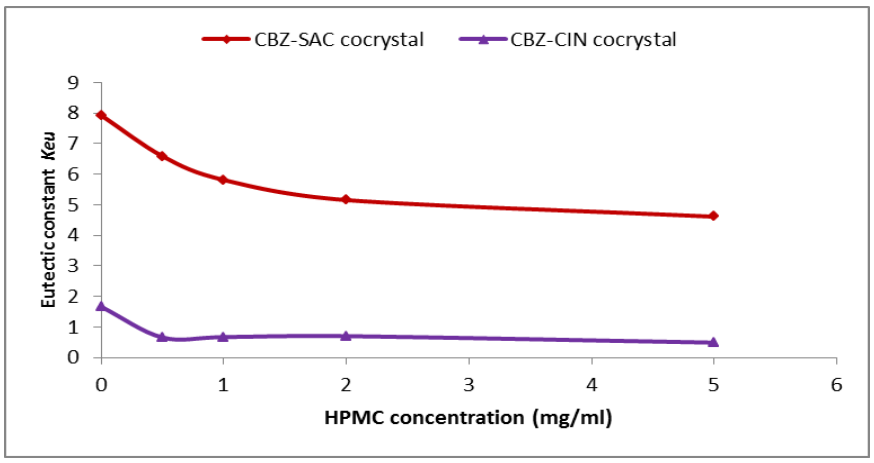

(c)

Fig.6.1 Concentration of solubility tests: (a) CBZ concentrations; (b) coformer concentrations; (c) Eutectic constant K_{eu} as a function of HPMC concentration

Solid residues retrieved from each of the solubility tests were analysed using DSC and SEM. The DSC thermographs of individual components are given in Fig.6.2 (a). DSC thermographs of the

solid residuals retrieved from the solubility tests are shown in Fig.6.2 (b). CBZ DH crystals were found in the solid residues of HPMC solutions up to 1 mg/ml after the solubility test of CBZ III alone, but the dehydration peak decreased significantly with increased HPMC concentrations in solution, indicating a reduction in the percentage of CBZ DH in the solid residue due to HPMC's inhibition effects. There was no CBZ DH in the solid residuals retrieved from the solubility tests of a higher HPMC solution of 2 mg/ml, indicating that HPMC can completely inhibit the transformation of CBZ to CBZ DH in solution during the dissolution of CBZ III.

It is clear that CBZ DH crystals were found in the solid residues of CBZ-SAC cocrystal solubility tests at different HPMC concentration solutions. This can be explained by the existence of a clear dehydration process of CBZ DH with a sharp endothermic peak between 80 and 120°C in each DSC thermograph, indicating that HPMC cannot inhibit the crystallisation of CBZ DH from solution during the dissolution of CBZ-SAC cocrystals. It also shows that the solid residues left by the solubility tests of CBZ-SAC cocrystals in various dissolution medium were a mixture of CBZ DH and CBZ-SAC cocrystals: the peak melting point of CBZ-SAC cocrystals occurred between 174°C and 177°C, as shown in the DSC thermographs in Fig.6.2 (b). It seems that there was no significant change in the percentage of CBZ DH in the solid residues, indicating that HPMC has no significant effect on the transformation of CBZ to CBZ DH in solution during dissolution of CBZ-SAC cocrystals.

The DSC thermographs for the solid residuals retrieved from the solubility tests of CBZ-CIN cocrystals (Fig.6.3 (b)) show a single peak between 143°C and 150°C, corresponding to the melting point of CBZ-CIN cocrystals, as shown in Fig.6.2 (a). This illustrates that there was no change of the solid form of CBZ-CIN cocrystals after the solubility tests. There was a small change in the DSC thermographs of the solid residuals retrieved from the CBZ-CIN cocrystal solubility tests at around 75°C, which the authors believe resulted from the evaporation of free water in the solid residues. HPMC in solution therefore had no effect on the solid form change of CBZ-CIN cocrystals in the solubility tests.

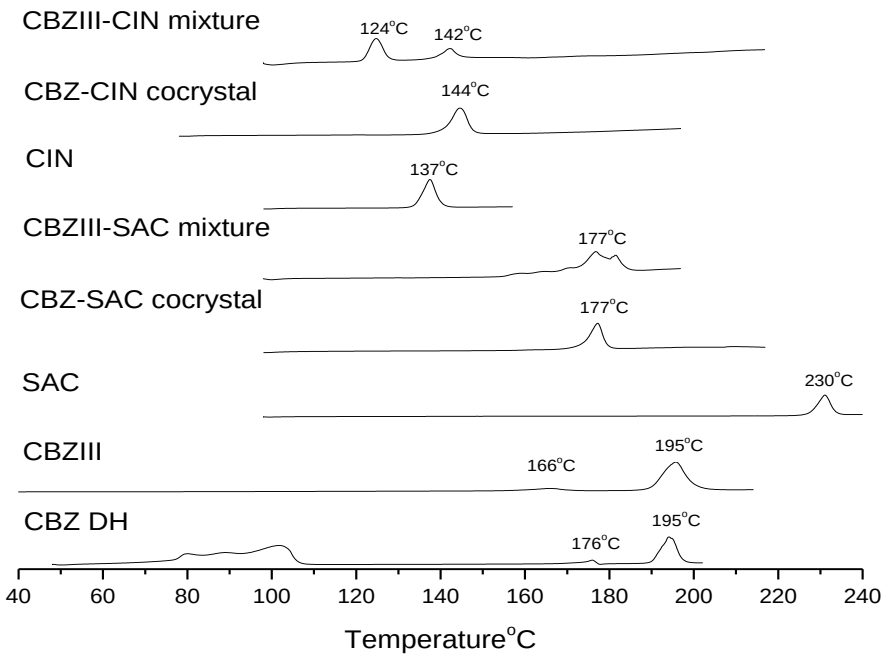

(a)

	CBZ III	CBZ-SAC cocrystals	CBZ-CIN cocrystals
water	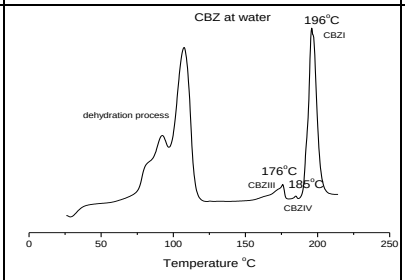	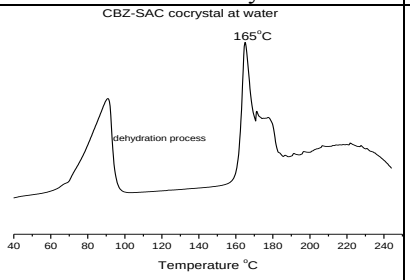	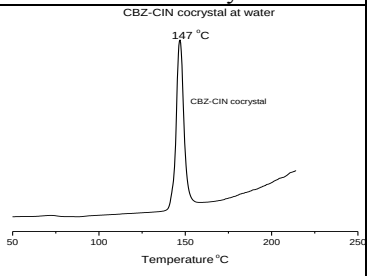
0.5 mg/ml HPMC	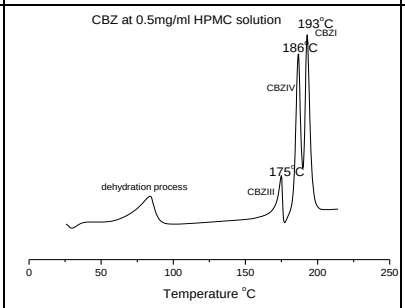	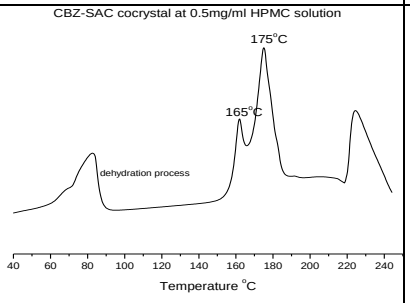	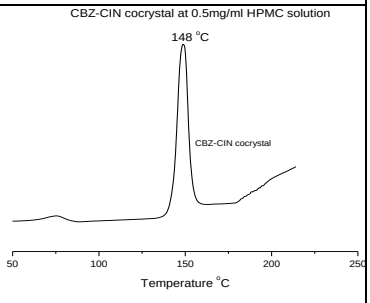
1 mg/ml HPMC	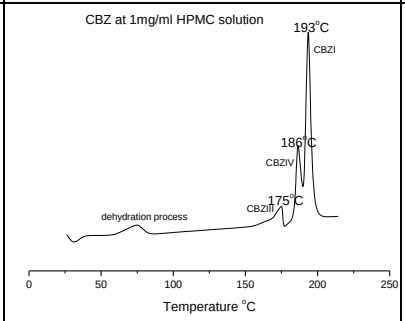	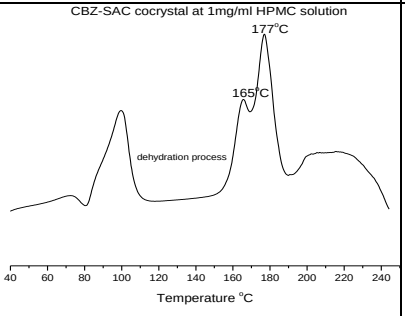	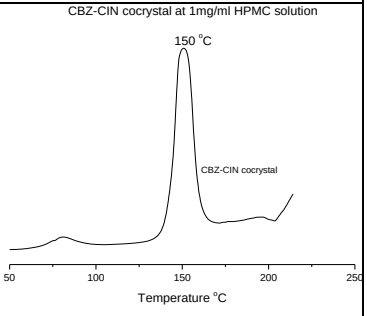

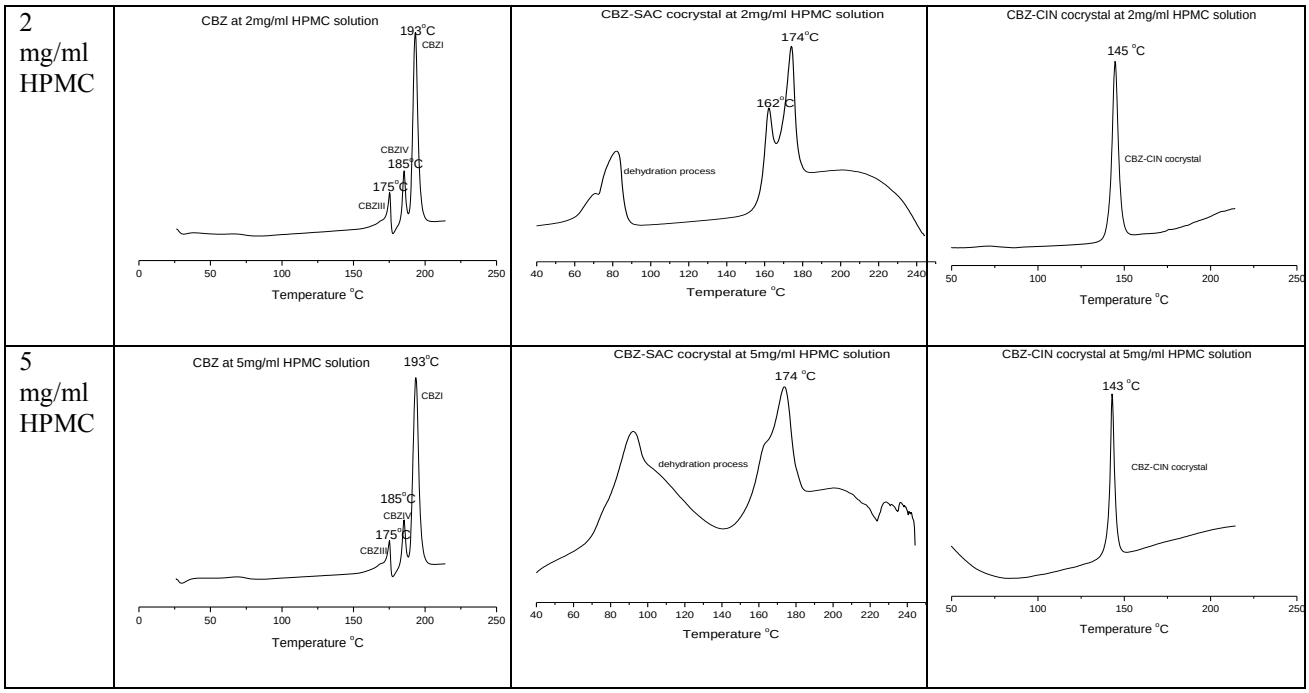

(b)

Fig.6.2 DSC thermographs: (a) original samples; (b) solid residues of solubility test

Fig.6.3 shows the SEM photographs of the solid residuals. In water, CBZ III has completely transformed into needle-like CBZ DH crystals. A large amount of CBZ DH crystals were found in the solid residuals after the tests of CBZ-SAC cocrystals in water. Needle-like CBZ DH crystals were clearly observed in the solid residues of the CBZ-SAC cocrystal solubility tests in different concentrations of HPMC solutions, but the amount of CBZ DH was significantly reduced. Some CBZ-SAC cocrystals can clearly be seen in the solid residuals after solubility tests, indicating that HPMC can partly inhibit the transformation of CBZ-SAC cocrystals into CBZ DH. CBZ-CIN cocrystals did not change their form after the solubility tests.

The XRPD results shown in Fig.S6.1 in the Appendices also support the above analysis.

	CBZ III	CBZ-SAC cocrystals	CBZ-CIN cocrystals
Original material	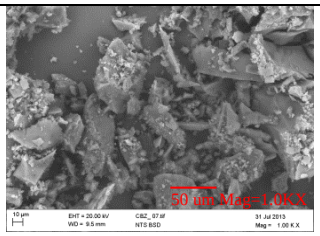	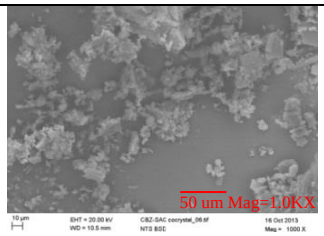	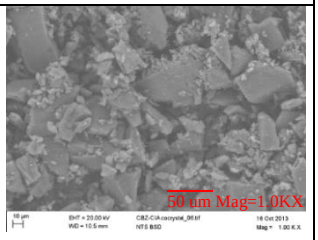

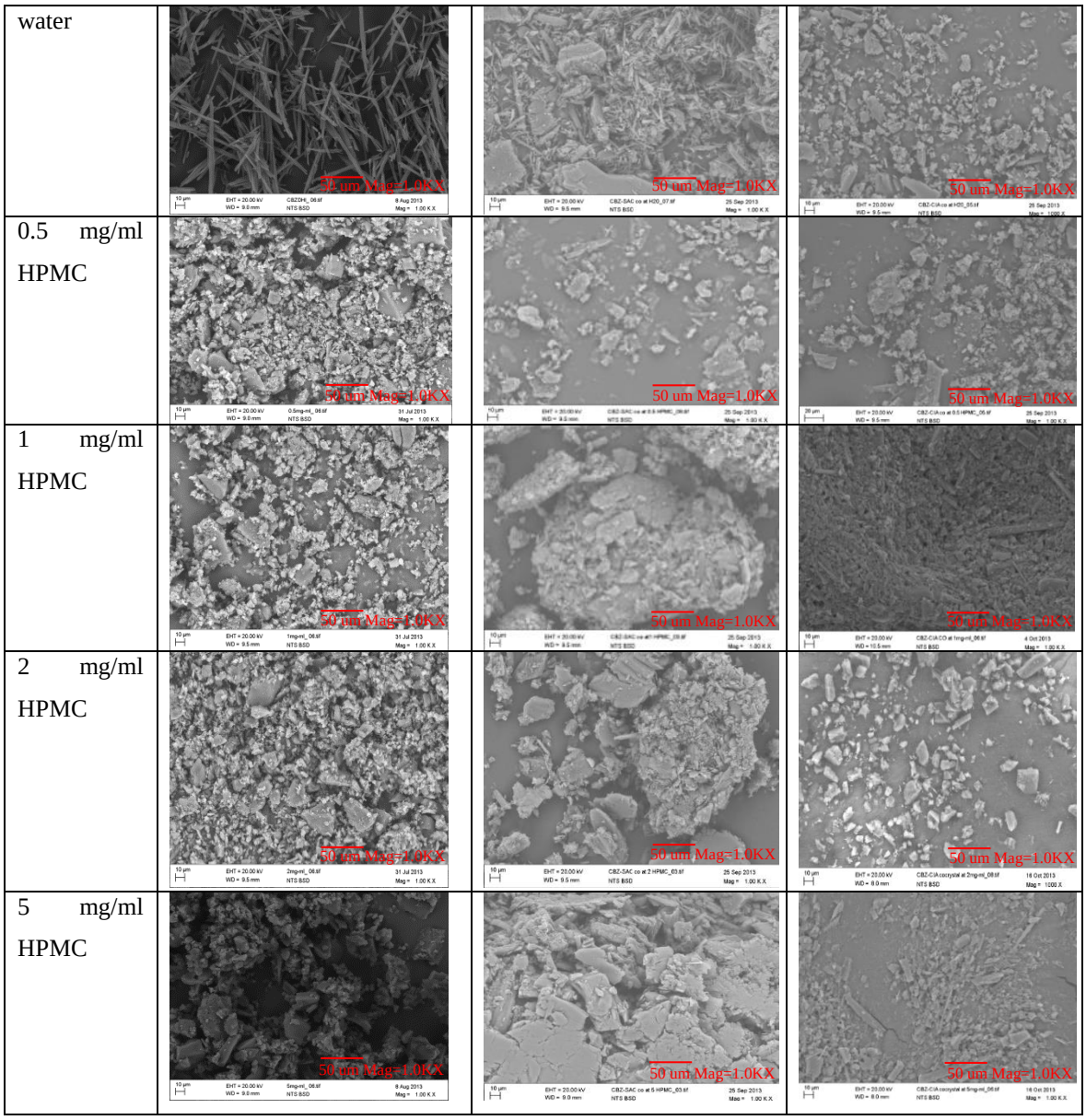

Fig.6.3 SEM photographs of solid residues of soubility tests at different HPMC concentration solutions

6.3.2 Powder dissolution study

Fig.6.4 (a)-(c) show the results of the powder dissolution studies of CBZ III alone and of CBZ-SAC and CBZ-CIN cocrystals in various dissolution medium including water and 0.5 mg/ml and 2 mg/ml HPMC solutions. It was observed that the CBZ release profile of CBZ III alone was significantly affected by the concentration of HPMC in solution ($p<0.05$), as shown in Fig.6.4 (a). Increasing the HPMC concentration in the dissolution medium can reduce the amount of CBZ dissolved in solution from CBZ III powders. By contrast, the CBZ release profile of CBZ-CIN cocrystal was insensitive to HPMC in solution, remaining constant in different concentrations of HPMC solutions for up to 30 minutes ($p>0.05$). The effect of HPMC in solution on the CBZ release of CBZ-SAC cocrystals was complex: the CBZ release profile in a lower HPMC dissolution

medium of 0.5 mg/ml was higher than those in both in water and a higher HPMC concentration solution of 2 mg/ml. A nonlinear CBZ release rate was also observed, both for CBZ III in water and for cocrystals of CBZ-SAC and CBZ-CIN in various dissolution medium. This indicates that the solids changed their properties. However, in 0.5 mg/ml or 2 mg/ml HPMC dissolution medium, the CBZ release rate of CBZ III was nearly linear, as illustrated in Fig.6.4 (a) (The linear regression coefficients (R^2) are 0.9762 and 0.9889 in 0.5 mg/ml and 2 mg/ml HPMC dissolution medium), indicating no change in the form of CBZ III solids.)

CBZ-CIN cocrystals' dissolution rate in various dissolution medium proved better (i.e. greater) than those for both CBZ III and CBZ-SAC cocrystals. In water, the amount of dissolved CBZ was 65% from CBZ-CIN cocrystal after 30 minutes, which was significantly higher than those of CBZ III (around 45%) and CBZ-SAC cocrystals (around 40%). CBZ-SAC cocrystals had the advantage over CBZ III in an improved dissolution rate in water for a very short period of around 15 minutes, after which the release percentage of CBZ from CBZ-SAC cocrystals was lower than that from CBZ III alone. In a 0.5 mg/ml HPMC solution, both CBZ-CIN and CBZ-SAC cocrystals showed similar dissolution profiles, which were significant higher than that of CBZ III. In the higher 2 mg/ml HPMC solution, the dissolution rates of both CBZ III and CBZ-SAC cocrystals were lower than that of CBZ-CIN cocrystals, whose dissolution profile remained constant. Fig.6.4 (d) shows the change of the eutectic constant K_{eu} of CBZ-SAC and CBZ-CIN cocrystals with various HPMC concentrations during powder dissolution. More details will be given in the discussion section.

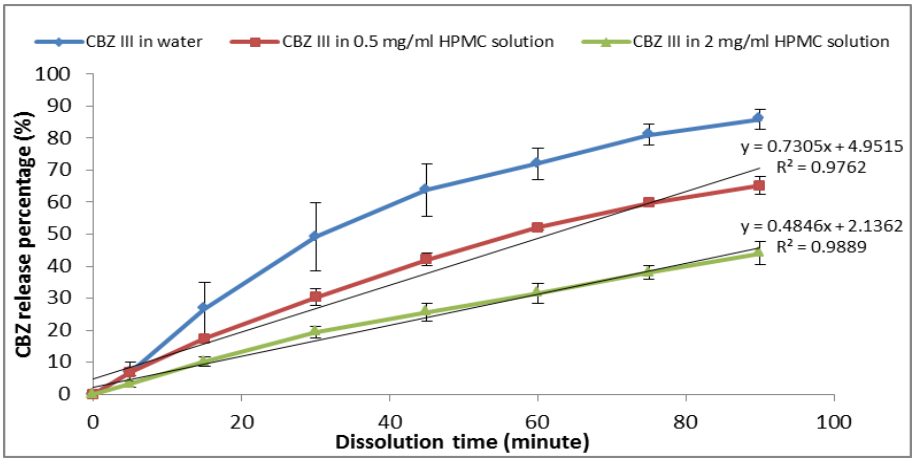

(a)

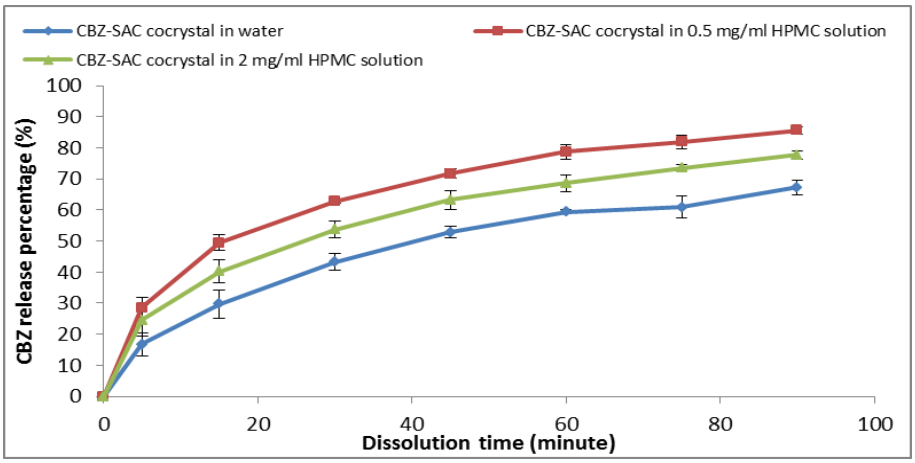

(b)

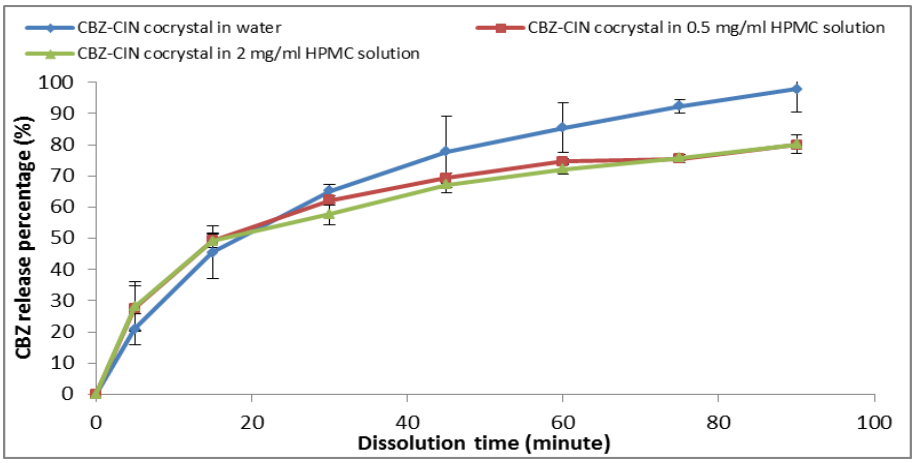

(c)

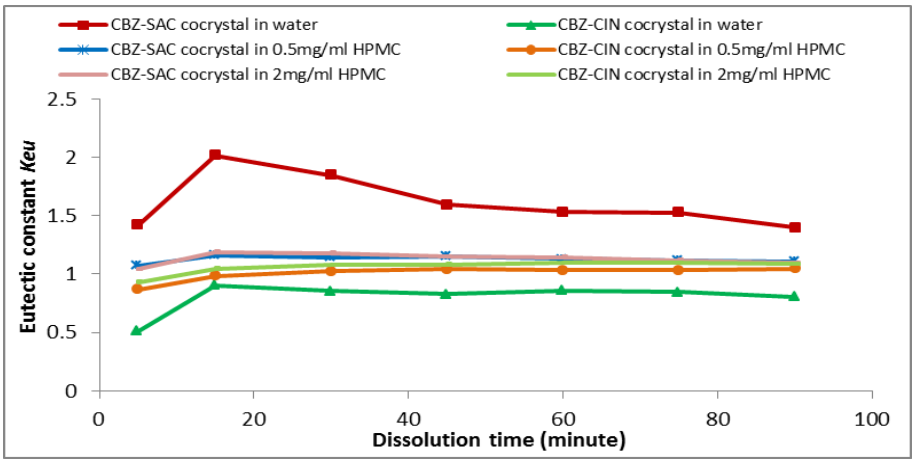

(d)

Fig.6.4 Comparison of powder dissolution profiles for various HPMC concentration solutions: (a) CBZ III release profiles; (b) CBZ-SAC cocrystal release profiles; (c) CBZ-CIN cocrystal release profiles; (d) Eutectic constant

6.3.3 CBZ release from HPMC matrices

Fig.6.5 (a) shows the CBZ release profiles of CBZ III, CBZ-SAC cocrystals, CBZ-CIN cocrystals and their physical mixtures from the 100 mg HPMC matrices. It was found that the physical mixture of CBZ III and SAC had the highest CBZ release rate. The rate of release of CBZ from the CBZ-CIN cocrystal formulation was significantly higher than that of their physical mixture of CBZ III and CIN ($p<0.05$). In the early stages of dissolution (up to 2 hours), the CBZ releases from both of the cocrystal formulations were similar ($p>0.05$). After that, the formulations of CBZ-SAC cocrystals and CBZ III exhibited similar CBZ release profiles, while the release rate for the CBZ-CIN formulations was much lower.

Fig.6.5 (b) shows that the CBZ release profiles of CBZ III, CBZ-SAC and CBZ-CIN cocrystals and their physical mixtures from the 200 mg HPMC matrices. It was observed that the CBZ release from the CBZ-CIN cocrystal formulation was much faster than those of the other four formulations. Interestingly, the CBZ release profiles of the three formulations of CBZ-SAC cocrystal and the physical mixtures of CBZ III and SAC, CBZ III and CIN were all similar ($p>0.05$), being lower than that of the CBZ III formulation. Fig.6.5 (c) illustrates the change of the eutectic constant K_{eu} of CBZ-SAC and CBZ-CIN cocrystals in HPMC tablets during dissolution. It was found that the eutectic constant K_{eu} of CBZ-SAC cocrystal tablets changed significantly during dissolution by comparison with a nearly constant value of K_{eu} for CBZ-CIN cocrystal tablets.

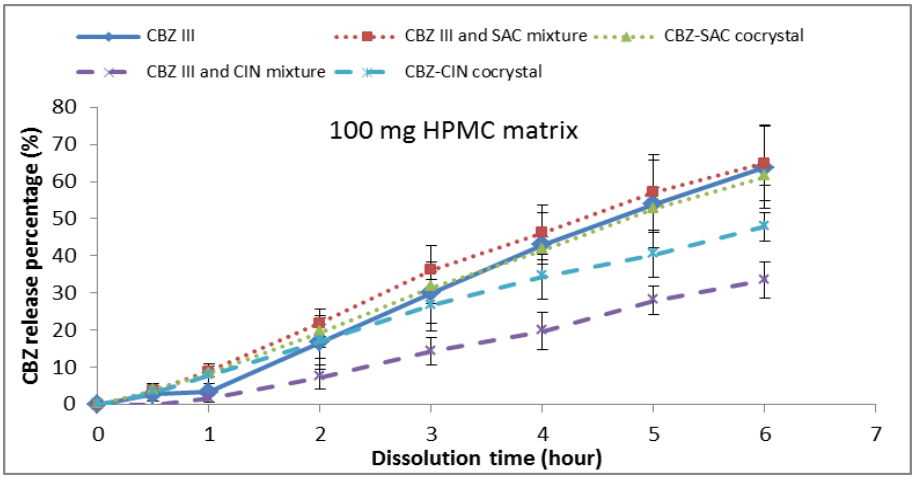

(a)

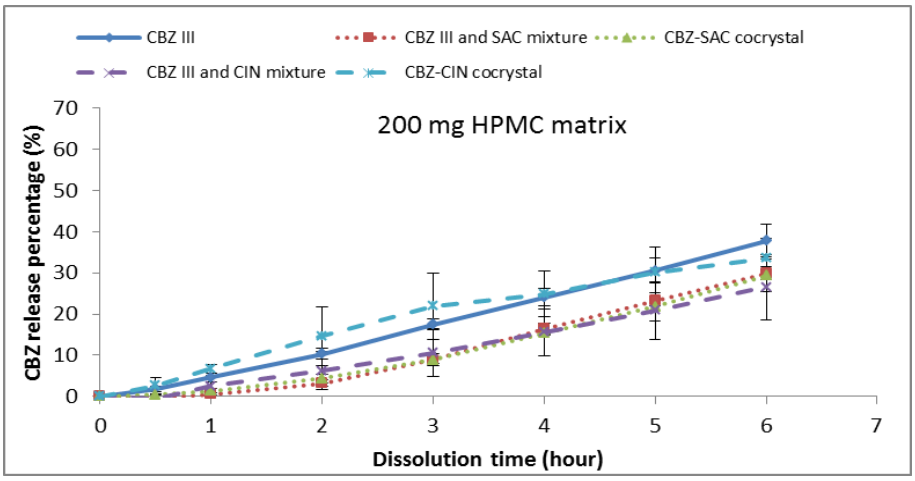

(b)

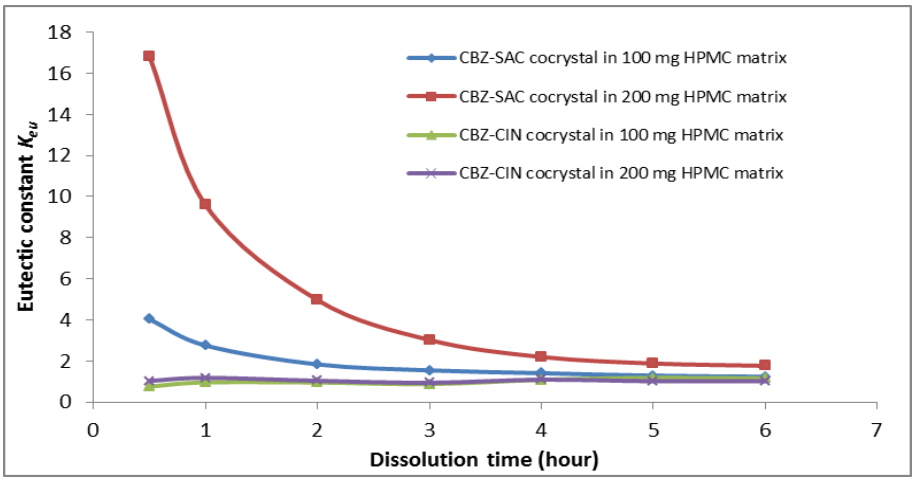

(c)

Fig.6.5 Comparison of CBZ release profiles of CBZ III, physical mixtures and cocrystals in various percentages of HPMC matrices: (a) 100mg HPMC matrix; (b) 200mg HPMC matrix; (c) Eutectic constant

The solid residuals of various formulations after the dissolution tests were analysed using XRPD are shown in Fig.6.6; the DSC analysis is shown in Fig.S6.2 in the Appendices. It was observed that CBZ DH crystals were precipitated from the CBZ-SAC cocrystal formulation during dissolution. There was no solid phase change for the other formulations, including the physical mixtures of CBZ III and SAC, CBZ III and CIN, CBZ-CIN cocrystals and CBZ III.

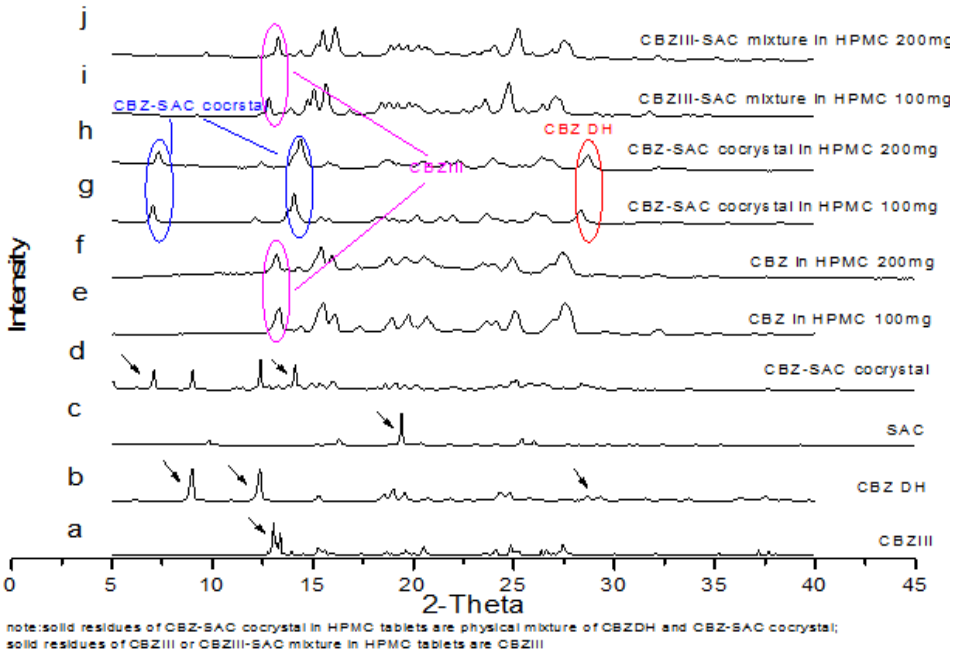

(a)

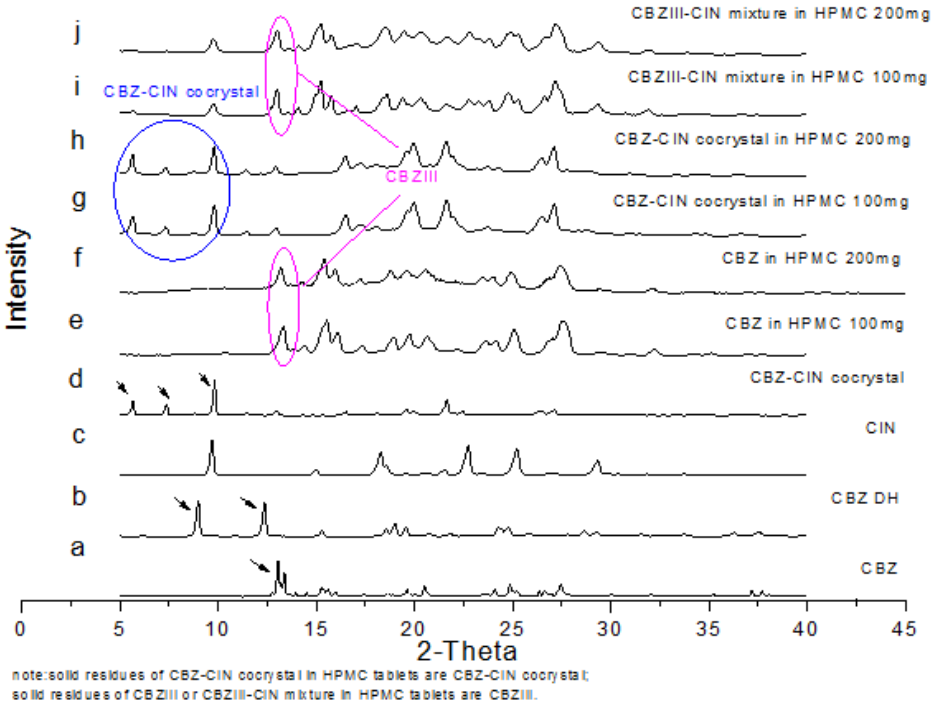

(b)

Fig.6.6 XRPD patterns of solid residues of various formulations after dissolution tests: (a) CBZ-SAC cocrystals and physical mixture formulations; (b) CBZ-CIN cocrystals and physical mixture formulations

6.4 Discussion

It is well documented that pharmaceutical cocrystals can improve the solubility of both ionisable and noionizable drug compounds, in particular that of BCS II APIs with low aqueous solubility. However, the supersaturated solution generated from the dissolution of cocrystals is unstable. This results in the crystallisation of a stable solid phase with less solubility, and subsequently the loss of the solubility advantage offered by cocrystals [158]. It is believed that the addition of the excipients of polymers and/or surfactants in a formulation could inhibit the crystallisation of the parent drug from solution by the formation of a soluble complex of the drug and polymer to maintain the drug's supersaturation [61, 159-161]. Unfortunately, most studies have not demonstrated the effectiveness of the polymers and/or surfactants in inhibiting the phase transformation of cocrystals [61, 157, 161]. A possible reason for this could be the "rate difference between cocrystal dissolution and formation of the soluble complex", as revealed in our previous study [157]. In order for the inhibition function of a selected polymer in a formulation to be activated, the cocrystal dissolution rate must be lower than the rate of formation of the soluble complex of the parent drug and polymer in solution. The present authors expected this to be achieved through selection of a coformer with low water solubility to form relative stable CBZ cocrystals, in contrast to CBZ-NIC cocrystals in solution.

SAC is soluble (its apparent solubility is 23.4 mM at 37°C, as shown in Fig.6.1 (b)), whereas CBZ is only a slightly soluble drug (its apparent solubility is 1.1 mM at 37°C, as shown in Fig.6.1(a)). According to the theory of cocrystal solubility based on the transition concentration measurements of the parent drug and coformer [162], the solubility of CBZ-SAC cocrystals in water at 37°C as calculated in the present study is 3.34 Mm, i.e. around 3.2 times the apparent solubility of CBZ III at equilibrium. This agrees well with the previous published data of 2.6 times. Because of CBZ-SAC cocrystals' improved solubility, CBZ-SAC cocrystals are thermodynamically unstable in various HPMC concentration solutions, and CBZ DH crystals have therefore crystallized from solution as shown in the DSC thermographs of the solid residues in Fig.6.2 (b). The effect of the various HPMC concentrations in solution on the stability of CBZ-SAC cocrystals in solution is indicated by the cocrystal eutectic constant K_{eu}, which can be determined from the ratio of the concentrations of the coformer and drug at the eutectic point [163]. Fig.6.1 (c) shows the change of the eutectic constant K_{eu} of CBZ-SAC cocrystals with the HPMC concentration in solution. K_{eu} decreased with increasing HPMC concentration as a result of the reduced solubility difference between CBZ and SAC in solution, indicating that HPMC can partially solubilize CBZ-SAC

cocrystals. However, the values of K_{eu} at various concentrations of HPMC solution are well above the critical value of 1, so the conversion of CBZ-SAC cocrystals into CBZ DH duly occurs.

CIN is slightly soluble, and its apparent solubility is 5 mM at 37°C as shown in Fig.6.1 (b). By contrast to CBZ-SAC cocrystals, the solubility of CBZ-CIN cocrystals in water is 0.73 mM at 37°C (around two-thirds of the apparent solubility of CBZ III at equilibrium as observed in this study). CBZ-CIN cocrystals are therefore thermodynamically stable in various HPMC concentration solutions, and no conversion of CBZ-CIN cocrystals occurrs, as confirmed by the sole feature of CBZ-CIN cocrystals in the DSC thermographs of the solid residues in Fig.6.2 (b). CBZ-CIN cocrystals' eutectic constant K_{eu} decreases slightly when HPMC is added in solution from 1.6 in water to 0.7 at various concentrations of HPMC, as shown in Fig.6.1 (c), confirming that HPMC can also slightly increase the stability of CBZ-CIN cocrystals in solution.

Cocrystals' dissolution behaviour is crucial for the prediction of absorption and efficient formulations, and in particular for those insoluble or lightly soluble BCS II drugs whose absorption is limited by the dissolution rate. Cocrystal dissolution involves many complex processes occurring simultaneously, such as the breakdown of the crystal lattice, the dissociation of the cocrystal into its individual components and the solvation and/or crystallisation of the individual components. The cocrystal dissolution rate is the result of a combination of the properties of the cocrystal itself, formulation including excipients and manufacturing conditions, and dissolution test conditions including dissolution medium, apparatus and hydrodynamics.

The powder dissolution tests shown in Fig.6.4 can be regarded as composed of two consecutive stages: the cocrystal molecules are liberated from the solid phase (a process needed to break down the crystal lattice) and the drug molecules in the form of the pure parent drug or a complex (drug-coformer or drug-additive) migrate through the boundary layers surrounding the solid crystals to the bulk of the solution. Whether the API crystallizes into its less soluble and most stable solid form depends on the gap between supersaturation and the apparent solubility of the drug. Although CBZ-CIN cocrystals' dissolution rate is significantly better than that of the parent drug, its solubility is lower than that of CBZ III. No supersaturation of CBZ in solution is therefore generated during the dissolution of CBZ-CIN cocrystals. The eutectic constant K_{eu} of CBZ-CIN cocrystals in water is around 0.8, supporting the proposition that there is no precipitation of CBZ DH during the dissolution of CBZ-CIN cocrystals. CBZ-SAC cocrystal solubility is greater than that of the parent drug CBZ III. When it dissolves, unstable CBZ-SAC cocrystals can be dissociated into the two individual components of CBZ and SAC in solution. This process is very fast, occurring in fractions

of seconds [61, 158], and results in the local supersaturation of CBZ in solution for the crystallization of CBZ DH. The eutectic constant K_{eu} of CBZ-SAC cocrystal in water was observed as being around 1.5. It is interesting to note that the more soluble CBZ-SAC cocrystals do not exhibit a faster dissolution rate than less soluble CBZ-CIN ones as dissolution commences. This indicates that the initial rate of dissolution is not related to the stability of the cocrystals in solution.

HPMC can inhibit the transformation of CBZ III to its dihydrate form CBZ DH in solution [149, 157]. Fig.6.1 (a) shows the increased solubility of CBZ in solution. However, when HPMC is added to the dissolution medium, it slows down the dissolution of CBZ III, as shown in Fig.6.4, because the increased viscosity of a dissolution medium can suppress the dissolution of the crystals and slow the migration of the dissolved solute molecules to the bulk of the solution.

The eutectic constants K_{eu} of CBZ-SAC cocrystals at both 0.5 mg/ml and 2 mg/ml HPMC solutions are close to 1, as shown in Fig.6.4 (d), indicating that HPMC can solubilize CBZ in solution because of the formation of CBZ-HPMC complex. However, the selection of an appropriate concentration of HPMC in solution is essential to realise the improved dissolution rate of CBZ-SAC cocrystals by balancing the formation rate of the soluble complex of CBZ-HPMC in solution and the reduced cocrystal dissolution rate due to the increased viscosity of the dissolution medium. It was observed that the CBZ-SAC cocrystals' dissolution rate in 0.5 mg/ml HPMC solution is higher than that in a 2 mg/ml HPMC solution.

There is no significant change in the dissolution rate of CBZ-CIN cocrystals in various concentrations of HPMC solution due to the stability of the CBZ-CIN complex in solution, as shown by the eutectic constant K_{eu} in Fig.6.4 (d). This indicates its potential as a lead cocrystal for further product development.

In the 100 mg HPMC matrix, there was a delay in CBZ release from the CBZ III formulation because of HPMC's hydration and gel layer formation process. The release of CBZ from the matrix was subsequently constant because of the inhibition of CBZ DH during the dissolution of CBZ III [157]. For the formulation of the physical mixture of CBZ III and SAC, the latter can be regarded as a channel agent to speed up the matrix's wetting process, resulting in a higher CBZ release rate compared with CBZ III alone in the formulation. The slow dissolution of CIN in the formulation of the physical mixture of CBZ and CIN can result in the slowing of the HPMC matrix's hydration and a reduction in CBZ III's wetting surface areas. The formulation of the physical mixture of CBZ and CIN therefore exhibited the lowest CBZ release rate. Because of the improved dissolution rates,

both the CBZ-SAC and CBZ-CIN cocrystal formulations showed a higher CBZ release rate at the early stages of dissolution than that of the CBZ III formulation. As dissolution commenced, the CBZ was released from the surface of the matrix tablet, where the dissolution rate of CBZ-SAC cocrystals was higher than the formation rate of the soluble complex CBZ-HPMC because of a slower process of HPMC dissolution, resulting in the crystallisation of CBZ DH as shown in Fig.6.5 (b), and a higher value for the eutectic constant K_{eu} of CBZ-SAC cocrystals, as shown in Fig.6.5 (c). After the CBZ-SAC cocrystals were completely dissolved from the surface of the tablet, the dissolution medium had to diffuse into the matrix in order to dissolve the non-hydrated core. It can be seen that the soluble complex CBZ-HPMC was formed, as indicated by a reduced eutectic constant K_{eu} of CBZ-SAC cocrystals as dissolution proceeded, as shown in Fig.6.5 (c). In the meantime, a higher concentration of HPMC inside the matrix (which can reduce the CBZ-SAC cocrystal dissolution rate) resulted in similar release rates for the CBZ-SAC cocrystals and the CBZ III formulation after three hours.

CBZ-CIN cocrystals are stable in solution during dissolution of the CBZ-CIN cocrystal formulation, as shown by the eutectic constant K_{eu} in Fig.6.5 (c). Inside the matrix, the dissolved CBZ-CIN complex had to travel to the surface for release. This process is controlled by diffusion, and the driving force is proportional to the solubility of CBZ-CIN cocrystals. After two hours the CBZ-CIN cocrystal formulation had a lower CBZ release rate compared with the CBZ III formulation due to its lower apparent solubility.

In the higher-percentage 200 mg HPMC matrices, the rate of CBZ release from the formulations depended mainly on the erosion of the HPMC from the hydrated matrix, which can only take place at the outer surface of the tablets. Similarly to those of powder dissolution tests, the rate of CBZ release from CBZ-CIN was significantly higher than those of the other formulations. Increased viscosity in a higher HPMC percentage in the formulation can result in lower SAC dissolution rates, which cannot be treated as a channel agent to increase the hydration process of the matrix. The formulations of the physical mixtures of CBZ and SAC and of CBZ and CIN therefore exhibited a similar CBZ release profile. Furthermore, SAC and CIN can reduce the surface area of CBZ III with the dissolution medium, resulting in a lower release rate than the CBZ III formulation. CBZ-SAC cocrystal formulation is robbed of any advantage by its sensitivity to the concentration of HPMC in solution.

6.5 Chapter conclusion

The influence of HPMC on the phase transformation and release profiles of CBZ-SAC and CBZ-CIN cocrystals in solution and in sustained release matrix tablets have been investigated. The authors have found that the selection of coformers of SAC and CIN affects the stability of the cocrystals in solution, resulting in significant differences in the apparent solubility of CBZ in solution. The dissolution advantage of CBZ-SAC cocrystals is only evident for a short period during dissolution because of its rapid conversion to its dihydrate form. HPMC can partly inhibit the crystallisation of CBZ DH during the dissolution of CBZ-SAC cocrystals, but it does not display an increased CBZ release rate from the cocrystal formulations at different percentages of HPMC because the increased viscosity can result in a reduction in CBZ-SAC cocrystal dissolution. By contrast, their stability means that CBZ-CIN cocrystals' potential for improved dissolution rates can be realised in both solution and formulation. In conclusion, exploring and understanding the mechanisms of the phase transformation of pharmaceutical cocrystals in aqueous medium in order to select lead cocrystals for further development is the key for success.

Chapter 7 Role of polymers in solution and tablet based carbamazepine cocrystal formulations

7.1 Chapter overview

In this chapter, the effects of three chemically diverse polymers on the phase transformations and release profiles of three CBZ cocrystals with significantly different solubility and dissolution rates, including CBZ-NIC, CBZ-SAC and CBZ-CIN cocrystals [114, 146, 161, 164, 165], are evaluated. Three chemically diverse polymers (HPMCAS, PVP and PEG) were selected because they are widely used as precipitation inhibitors in other supersaturating drug delivery systems [166-168]. In order to evaluate the effectiveness of these polymers in inhibiting the phase transformation of cocrystals, the study has been carried out with polymers in both pre-dissolved solution and tablet formulations. Two types of dissolution testing experiment were therefore conducted: 1) cocrystal powder dissolution tests in the dissolution medium of pH 6.8 PBS in the absence and presence of pre-dissolved polymers to identify the mechanism by which drug precipitation is inhibited, and 2) dissolution tests for tablets consisting of a mixture of cocrystals (or physical mixtures of drug and coformers) and polymers in order to assess the effects of polymer release kinetics on the cocrystal release profiles. Both powder and tablet dissolution tests were carried out under sink conditions with the aim of identifying the rate of difference between cocrystal dissolution and interaction between the drug and the polymer in solution [164]. In the meantime, the equilibrium solubility of the CBZ cocrystals and the parent drug CBZ III in pH 6.8 PBS in both the absence and the presence of different concentrations of the selected polymers was measured so as to evaluate the polymer solubilization effects in solution formulations. By comparing the behaviour of cocrystals with that of physical mixtures or the pure parent drug, it was expected that the role of polymers in solution and tablet based cocrystal formulations would be elucidated.

7.2 Materials and methods

7.2.1 Materials

Anhydrous CBZ III, NIC, SAC, CIN, EtOAc, methanol, SLS, HPMCAS, PVP, PEG, potassium dihydrogen phosphate (KH_2PO_4) and sodium hydroxide (NaOH) were used in this chapter. Details of these materials can be found in Chapter 3.

7.2.2 Methods

7.2.2.1 Formation of the CBZ-NIC, CBZ-SAC and CBZ-CIN cocrystals

CBZ-NIC, CBZ-SAC and CBZ-CIN cocrystals were used in this chapter. The details of the formation methods can be found in Chapter 3.

7.2.2.2 Preparation of pH 6.8 PBS

The dissolution medium used for solubility and dissolution tests was pH 6.8 PBS, which was prepared according to British Pharmacopeia 2010. Details of this preparation can be found in Chapter 3.

7.2.2.3 Preparation of tablets

The formulations of the matrix tablets are provided in Table 7.1. The details of this method can be found in Chapter 3.

7.2.2.4 Powder dissolution study

The powder dissolution rates of CBZ-NIC, CBZ-SAC and CBZ-CIN cocrystals and CBZ III were studied in this chapter. The details of this method can be found in Chapter 3. The two dissolution medium used for the tests were pH 6.8 PBS and pH 6.8 PBS, with a pre-dissolved 2 mg/ml polymer of HPMCAS, PVP or PEG.

7.2.2.5 Solubility analysis of CBZ III, CBZ cocrystals and physical mixtures in pH 6.8 PBS with a pre-dissolved polymer of HPMCAS, PVP or PEG

The equilibrium solubility of the three cocrystals CBZ-NIC, CBZ-SAC and CBZ-CIN and their mixtures, CBZ III in pH 6.8 PBS or with a pre-dissolved polymer of HPMCAS, PVP or PEG were tested in this chapter. The details of this method can be found in Chapter 3. The concentrations of a pre-dissolved polymer of HPMCAS, PVP or PEG in pH 6.8 PBS were 0.5, 1, 2 and 5 mg/ml.

Table 7.1 Matrix tablet composition (mg)

Component	**Formulation**													
	F1	**F2**	**F3**	**F4**	**F5**	**F6**	**F7**	**F8**	**F9**	**F10**	**F11**	**F12**	**F13**	**F14**
CBZ III	200							200						
CBZ-NIC cocrystal		304							304					
equal molar mixture of CBZ III-NIC			304							304				
CBZ-SAC cocrystal				355							355			
equal molar mixture of CBZ III-SAC					355							355		
CBZ-CIN cocrystal						325							325	
equal molar mixture of CBZ III-CIN							325							325
HPMCAS /PVP /PEG	100	100	100	100	100	100	100	200	200	200	200	200	200	200

7.2.2.6 Dissolution studies of formulated HPMCAS, PEG and PVP tablets

The dissolution studies of CBZ-NIC, CBZ-SAC and CBZ-CIN cocrystals, their physical mixtures of CBZ III and coformers and CBZ III in 100 mg and 200 mg HPMCAS, PVP or PEG tablets were investigated in this study. Details can be found in Chapter 3. The dissolution medium was 700 ml, 1% (w/v) SLS pH 6.8 PBS.

7.2.2.7 Physical property characterisation techniques

HPLC and statistical analysis were used to study the solubility, powder dissolution rates and dissolution behaviours of the tablets. SEM, XRPD and DSC were used in this chapter for characterisation. Details of these techniques can be found in Chapter 3.

7.3 Results

7.3.1 Solubility studies

Fig.7.1 (a)-(d) shows the CBZ concentrations after the solubility tests of CBZ III and cocrystals of CBZ-NIC, CBZ-SAC, and CBZ-CIN in both the absence and the presence of the different concentrations of a pre-dissolved polymer of HPMCAS, PVP or PEG in pH 6.8 PBS at equilibrium after 24 hours.

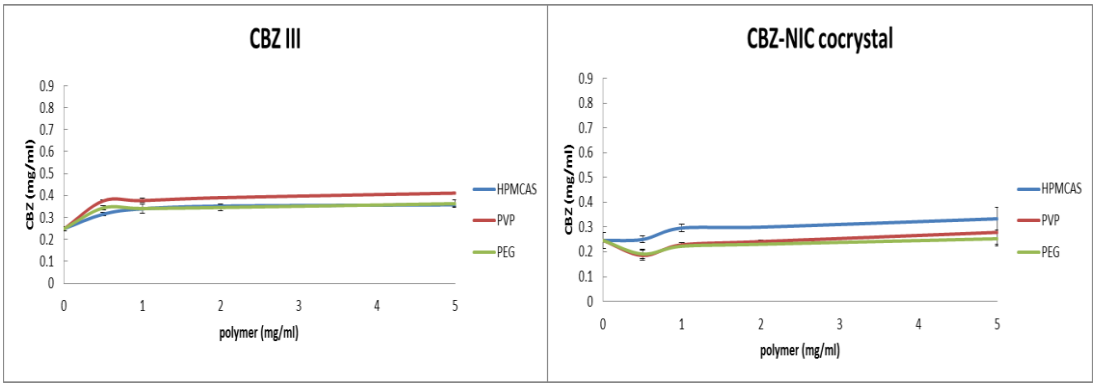

(a)

(b)

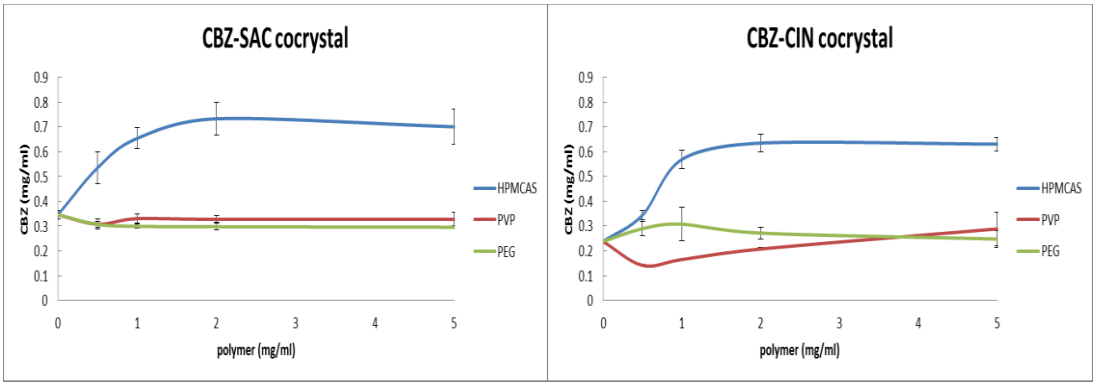

(c)

(d)

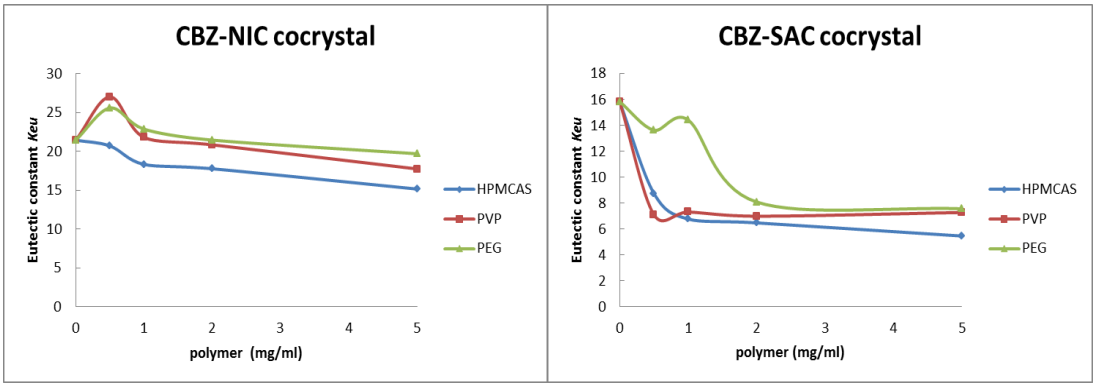

(e)

(f)

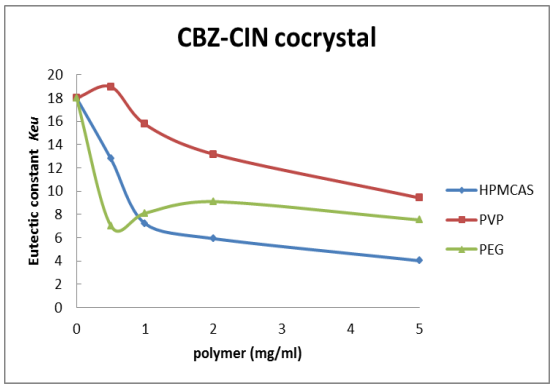

(g)

Fig.7.1 CBZ concentrations in the absence and presence of the different concentrations of pre-dissolved polymers in pH 6.8 PBS at equilibrium after 24 hours: (a) CBZ III; (b) CBZ-NIC cocrystal; (c) CBZ-SAC cocrystal; (d) CBZ-CIN cocrystal; (e) eutectic constant for CBZ-NIC cocrystal; (f) eutectic constant for CBZ-SAC cocrystal; (g) eutectic constant for CBZ-CIN cocrystal

The findings demonstrate that the three polymers HPMCAS, PVP and PEG can all enhance the solubility of CBZ III, as shown in Fig.7.1 (a). The equilibrium concentration of CBZ in solution increases with the increase in polymer concentration, its maximum at 1mg/ml for all three polymers, after which point it remained constant. The polymers' solubility enhancement was limited to a 1.5-fold increase for HPMCAS and PEG and a slightly higher increase of 1.6-fold for PVP. This enhancement of solubility is due to formation of the soluble complex through hydrogen bonding between CBZ and the polymers. However, these polymers show significantly different precipitation inhibition abilities. HPMCAS can completely inhibit the transformation of CBZ III into CBZ DH, whereas PVP and PEG can only partially inhibit such transformation. This is confirmed by DSC thermographs of the solid residues retrieved from the solubility tests.

Fig.7.2 shows the comparison of DSC thermographs of original samples and the solid residues obtained from the solubility tests in the absence and the presence of a 2 mg/ml polymer in pH 6.8 PBS. In pH 6.8 PBS without a polymer, the solid residues of the CBZ III test consisted of CBZ DH crystals, showing that the dehydration process occurred between 80 to 120°C under DSC heating. After dehydration, CBZ DH converted back to CBZ III, which melted around 175°C and then recrystallized in the more stable form of CBZ I, which melted at around 196°C [164]. In the presence of 2 mg/ml PVP or PEG in pH 6.8 PBS, CBZ DH crystals were found in the solid residues of the CBZ III test, showing a DSC thermograph similar to that of solid residues in pH 6.8 PBS in the absence of a polymer. However, the dehydration peak of the test's DSC thermograph in the presence of PVP or PEG was significantly lower than that of the solid residual in the absence of a

polymer, indicating that the solid residues comprised a mixture of CBZ DH and CBZ III. PVP or PEG can therefore partially inhibit the transformation of CBZ III into CBZ DH. In the presence of 2 mg/ml HPMCAS in pH 6.8 PBS, the DSC thermograph of the solid residues was the same as that of CBZ III, the material used at the start, due to the HPMCAS inhibition effect. In a similar fashion to HPMC, the hydroxyl groups of HPMCAS can attach to CBZ at the site of water binding to form stable CBZ-HPMCAS complexes, result in an inhibition of CBZ transformation to the dihydrate form CBZ DH [164, 165].

SEM photographs of solid residues obtained from the tests in Fig.7.3 further support these analyses. The original CBZ III samples appeared to be irregular. They were mixtures of prismatic- and rock-shaped particles, and they became CBZ DH crystals after the test in the absence of a polymer showing a needle-like shape. The solid residues in the presence of 2 mg/ml HPMCAS in pH 6.8 PBS had a shape similar to that of the original CBZ III, indicating the absence of a phase transformation. The solid residues left when the test was conducted in the presence of 2 mg/ml PVP or PEG consisted of a mixture of needle-like (CBZ DH) and prismatic/rock (CBZ III) particles. Similar results can be found in the other solubility tests conducted in the presence of different concentrations of a polymer of HPMCAS, PVP or PEG, including 0.5 mg/ml, 1 mg/ml and 5 mg/ml by the DSC thermographs of the solid residues in Fig.S7.1 and SEM photographs in Fig.S7.2 in the supplementary materials.

		CBZ III	CBZ-NIC cocrystals	CBZ-NIC mixture	CBZ-SAC cocrystals	CBZ-SAC mixture	CBZ-CIN cocrystals	CBZ-CIN mixture
original samples		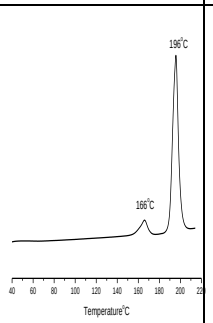	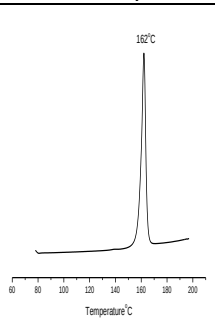	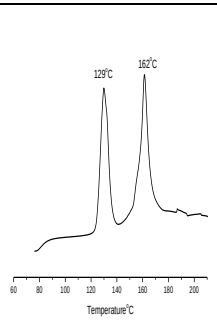	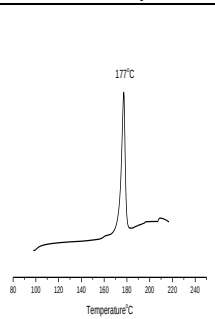	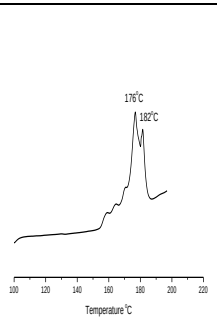	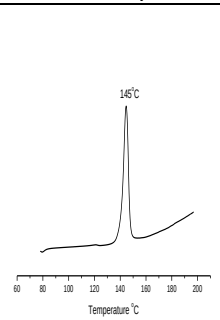	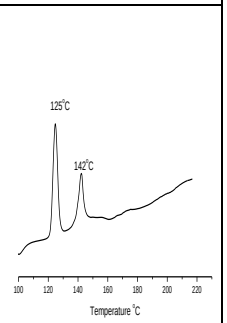
pH 6.8 PBS		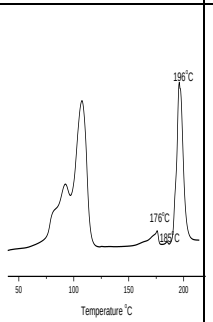	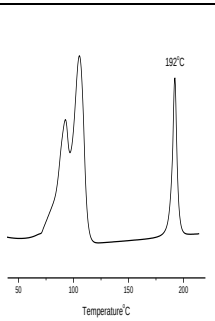	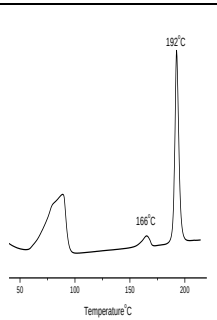	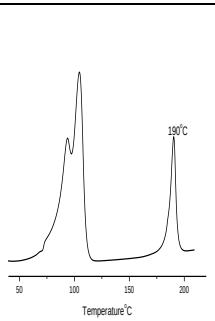	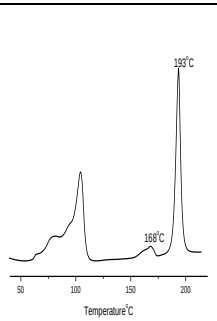	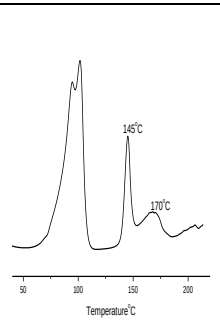	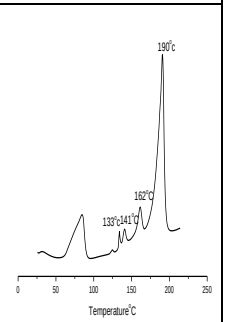
pH6.8 PBS with 2 mg/ml	HPMCAS	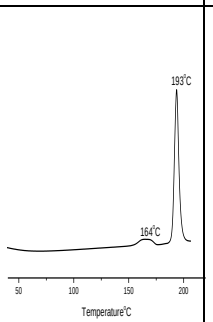	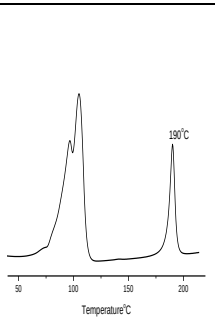	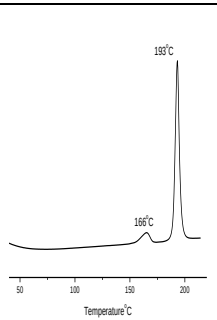	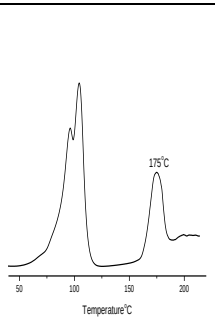	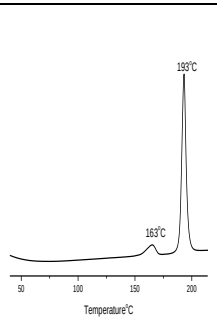	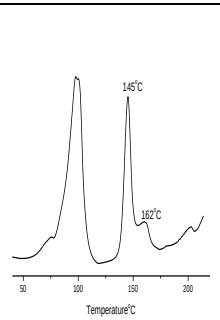	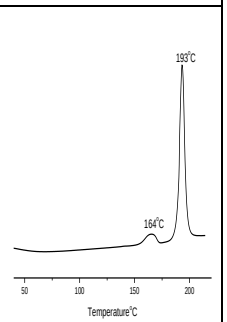

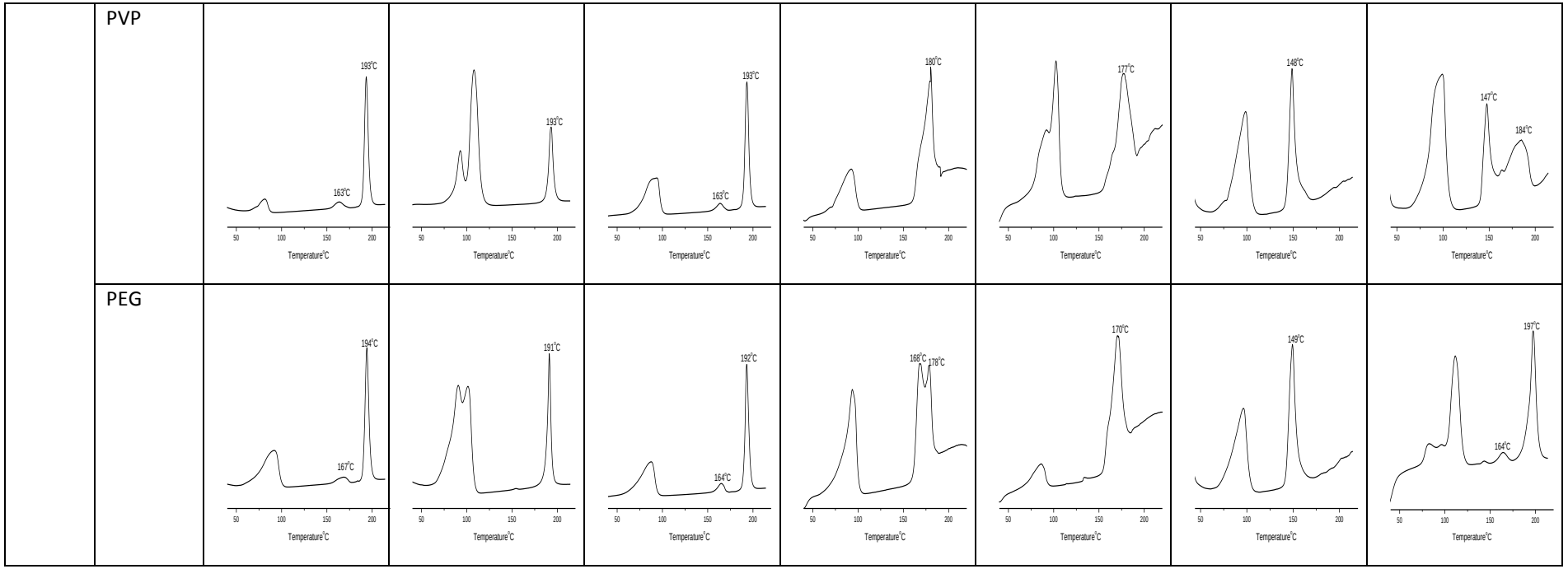

Fig.7.2 DSC thermographs of original samples and solid residues retrieved from solubility studies in the absence and presence of 2 mg/ml polymer in pH 6.8 PBS

	CBZ III	CBZ-NIC cocrystal	CBZ-NIC mixture	CBZ-SAC cocrystal	CBZ-SAC mixture	CBZ-CIN cocrystal	CBZ-CIN mixture
original	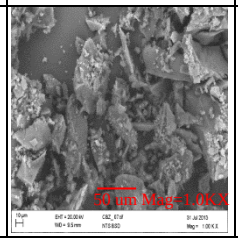	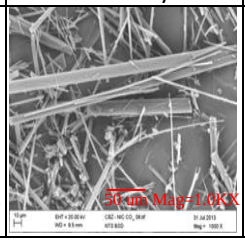	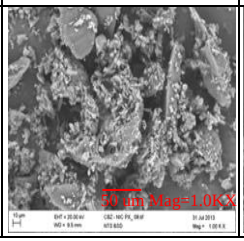	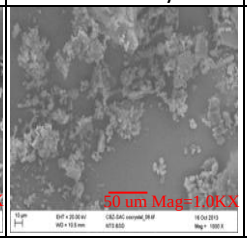	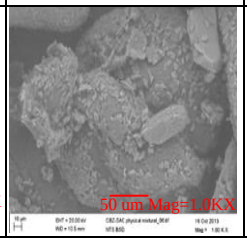	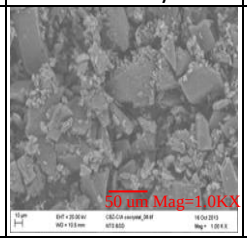	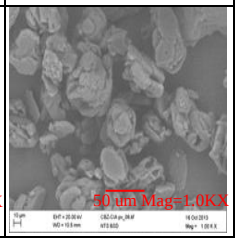

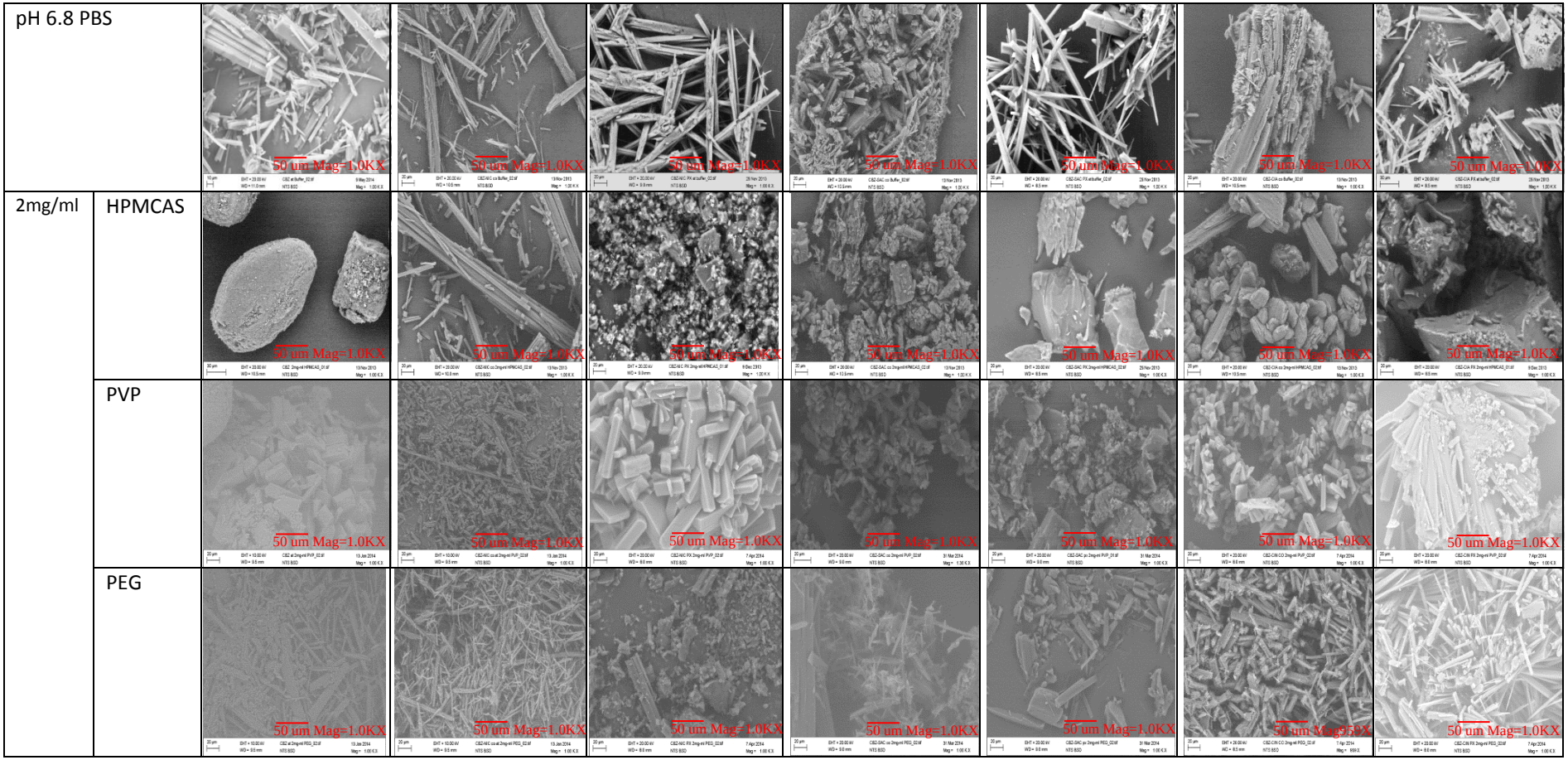

Fig.7.3 SEM photographs of original samples and solid residues retrieved from solubility studies in the absence and the presence of 2 mg/ml polymer in pH 6.8 PBS

For CBZ-NIC cocrystals, the apparent CBZ concentration was the same as that of CBZ III in pH 6.8 PBS in the absence of a polymer. This concentration rose slightly with an increase in the concentration of HPMCAS up to 1 mg/ml in pH 6.8 PBS, subsequently remaining constant. A pre-dissolved polymer of PVP or PEG in pH 6.8 PBS at any of the concentrations tested did not affect the apparent CBZ concentration of CBZ-NIC cocrystals, which was the same as the solubility of CBZ III in pH 6.8 PBS in the absence of a polymer, although the apparent CBZ concentration fell slightly in a low polymer concentration as shown in Fig.7.1 (b). The DSC thermographs and SEM photographs of solid residues after the solubility tests were conducted are shown in Fig.7.2 and Fig.7.3. Figs S7.1 and S7.2 show the results of the other polymer concentrations in the supplementary materials. It was evident that the original CBZ-NIC cocrystals were completely transformed into needle-like CBZ DH crystals, indicating that none of the polymers HPMCAS, PVP and PEG can inhibit the crystallisation of CBZ DH from solution. This is similar to the case of the polymer HPMC. The solubility test of the physical mixture of CBZ III-NIC demonstrates that NIC does not affect the apparent solubility of CBZ III in the either the absence or the presence of a polymer in pH 6.8 PBS, as shown in Fig.S7.3 in the supplementary material. Pre-dissolved HPMCAS in pH 6.8 PBS can inhibit the transformation of CBZ into CBZ DH for the physical mixture of CBZ III-NIC, as confirmed by the DSC thermographs and SEM photographs in Figs.7.2 and 7.3 (Figs.S7.1 and S7.2 in the supplementary material show the results for the other polymer concentrations).

The apparent CBZ concentration of CBZ-SAC cocrystals (about 0.35 mg/ml) in pH 6.8 PBS in the absence of a polymer was 1.4 times that of CBZ III (0.25 mg/ml), indicating the enhanced solubility advantage of the cocrystal. The SEM photograph of the solid residues after the test in Fig.7.3 shows that some of the CBZ-SAC cocrystals had transformed into needle-like CBZ DH crystals. When HPMCAS was pre-dissolved in pH 6.8 PBS, the apparent CBZ solubility of CBZ-SAC cocrystals increased significantly, reaching their maximum 0.74 mg/ml at 2 mg/ml of HPMCAS concentration. This was 2.1 times the solubility of CBZ III in the same polymer solution and three times the solubility of CBZ III in pH 6.8 PBS in the absence of HPMCAS. Although the CBZ DH crystals were found in the solid residues of the tests shown in the DSC thermographs in Fig.7.2 (other results are given in Fig.S7.1 in the supplementary material), their percentage was significantly lower than those for the absence of HPMCAS in pH 6.8 PBS, as shown in the SEM photographs in Fig.7.3 (other results are given in Fig.S7.2 in the supplementary material), indicating that HPMCAS can partially inhibit the precipitation of CBZ from solution. Pre-dissolved PVP in pH 6.8 PBS did not affect the apparent CBZ concentration of CBZ-SAC cocrystals, showing that the CBZ

concentration remains constant irrespective of the concentration of PVP, as shown in Fig.7.1. However, the solid residues consisted of a mixture of CBZ-SAC cocrystals and CBZ DH crystals, as confirmed by the DSC analysis in Fig.7.2 (other results are given in Fig.S7.1 in the supplementary material) and the SEM photographs in Fig.7.3 (other results are given in Fig.S7.2 in the supplementary material). This indicates that the pre-dissolved PVP can partially inhibit the crystallisation of CBZ DH, but less effectively than HPMCAS. Pre-dissolved PEG in pH 6.8 PBS slightly lowered the apparent CBZ concentration of CBZ-SAC cocrystals by comparison with that of CBZ-SAC cocrystals in the absence of the polymer, demonstrating that PEG enhances the precipitation of CBZ DH from solution. This is confirmed by the SEM photographs in Fig.7.3 (other results are given in Fig.S7.2 in the supplementary material), in which a large amount of needle-like CBZ DH crystals was found in the solid residues after the tests. The solubility of SAC in pH 6.8 PBS decreased slightly when a polymer of HPMCAS, PVP or PEG was pre-dissolved in solution as shown in Fig.S7.3 (a) in the supplementary material. In the absence of a polymer in pH 6.8 PBS, the CBZ concentration of the physical mixture of CBZ III-SAC was the same as that of CBZ-SAC cocrystals and higher than that of CBZ III, indicating that SAC can enhance the solubility of CBZ III. The CBZ concentration of physical mixture of CBZ III-SAC decreased in the presence of HPMCAS in solution,, as shown in Fig.S7.3 (b) in the supplementary material. By contrast, the apparent CBZ concentration of the physical mixture of CBZ III-SAC in the presence of a polymer of PVP or PEG in solution was similar to that of CBZ III in the same condition, as shown in Fig.S7.3 (b) in the supplementary material.

Fig.7.1 (d) shows the apparent CBZ concentration of CBZ-CIN cocrystals in both the absence and the presence of a polymer in solution. The apparent CBZ concentration of CBZ-CIN cocrystals in pH 6.8 PBS was same as that of CBZ III. When HPMCAS was pre-dissolved in the solution, the apparent CBZ concentration of CBZ-CIN cocrystals increased significantly. At a concentration of 2 mg/ml of HPMCAS, the solubility of CBZ-CIN cocrystals can rise to 2.7 times that of CBZ III in pH 6.8 PBS, which is slightly lower than that of CBZ-SAC cocrystals in the same condition. In the presence of PVP in pH 6.8 PBS, it is evident that PVP has a profound effect on the apparent CBZ concentration of CBZ-CIN cocrystals. At a lower concentration of 0.5 mg/ml PVP, the apparent CBZ concentration of CBZ-CIN cocrystals was significantly lower than that of CBZ III, while at a higher PVP concentration (2 mg/ml or 5 mg/ml) the CBZ concentration of CBZ-CIN cocrystals increased to the same level of solubility as CBZ III. PEG pre-dissolved in solution did not significantly affect the apparent CBZ concentration of CBZ-CIN cocrystals, displaying a nearly constant concentration of CBZ whatever the concentration of PEG. The solid residues of CBZ-CIN

cocrystals in pH 6.8 PBS in the absence and presence of a polymer of HPMCAS, PVP, or PEG consisted of physical mixtures of CBZ DH and CBZ-CIN cocrystals, as confirmed by DSC analysis in Fig.7.2 and SEM photographs in Fig.7.3. The CBZ concentration of the physical mixture of CBZ III-CIN was constant in both the absence and the presence of a polymer in pH 6.8 PBS, as shown in Fig.S7.3 in the supplementary material, which was lower than CBZ III or CBZ-CIN cocrystals. However, the components of the solid residuals from the tests were different. In the absence of a polymer, these residuals contained mixtures of CBZ DH, CIN and CBZ-CIN cocrystals. In the presence of HPMCAS in solution, the solid residuals were CBZ III, indicating that HPMCAS completely inhibits the transformation of CBZ III to CBZ DH. By contrast, both CBZ DH and CBZ-CIN cocrystals were found in the solid residuals when in the presence of PVP or PEG in solution. DSC analysis in Fig.7.2 and SEM photographs in Fig.7.3 support these conclusions.

Fig.7.1 (e)-(g) shows the ratios of CBZ and its corresponding coformer concentrations for the three CBZ cocrystals. This parameter is also called the cocrystal eutectic constant K_{eu}, which can be used as an indicator of the stability of cocrystals in solution [61, 165]. Details will be given in the discussion section.

7.3.2 Powder dissolution studies

Fig.7.4 represents the effect of a pre-dissolved 2 mg/ml concentration of HPMCAS, PVP and PEG on the powder dissolution profiles of CBZ III and cocrystals of CBZ-NIC, CBZ-SAC and CBZ-CIN. It was found that a pre-dissolved polymer did not improve the dissolution rate of CBZ III. Actually a pre-dissolved polymer of HPMCAS or PVP decreased CBZ III's release rate, while the pre-dissolved PEG did not affect CBZ III's dissolution rate. Although the final CBZ concentration of 0.1 mg/ml in solution was well below its solubility (0.25 mg/ml) in the experiments, a nonlinear release profile of CBZ III was observed, demonstrating that an increased concentration of CBZ in solution can decrease the release rate of the solids due to the reduced dissolution driving force. This reduction is most likely caused by the reduced diffusion coefficient of CBZ in solution due to the change of the bulk solution properties, in particular the increased viscosity of the solution with a pre-dissolved polymer.

By contrast, all three pre-dissolved polymers in pH 6.8 PBS could increase the dissolution rates of the three CBZ cocrystals. PEG was least able to do so, while the performances of HPMCAS and PVP were similar to each other in this regard. Although the physicochemical properties of CBZ-NIC and CBZ-CIN cocrystals are significantly different, their dissolution profiles ($p>0.05$) are

similar in the absence or the presence of a polymer of 2 mg/ml concentration in pH 6.8 PBS, both of those profiles being faster than those of CBZ-SAC cocrystals. In the meantime, all three cocrystals display a significant advantage in a better dissolution rate than that of CBZ III. In the presence of a 2 mg/ml HPMCAS in pH 6.8 PBS, the cocrystals of CBZ-NIC and CBZ-CIN can be approximately 80% dissolved within five minutes, compared to 10% of CBZ III over the same time.

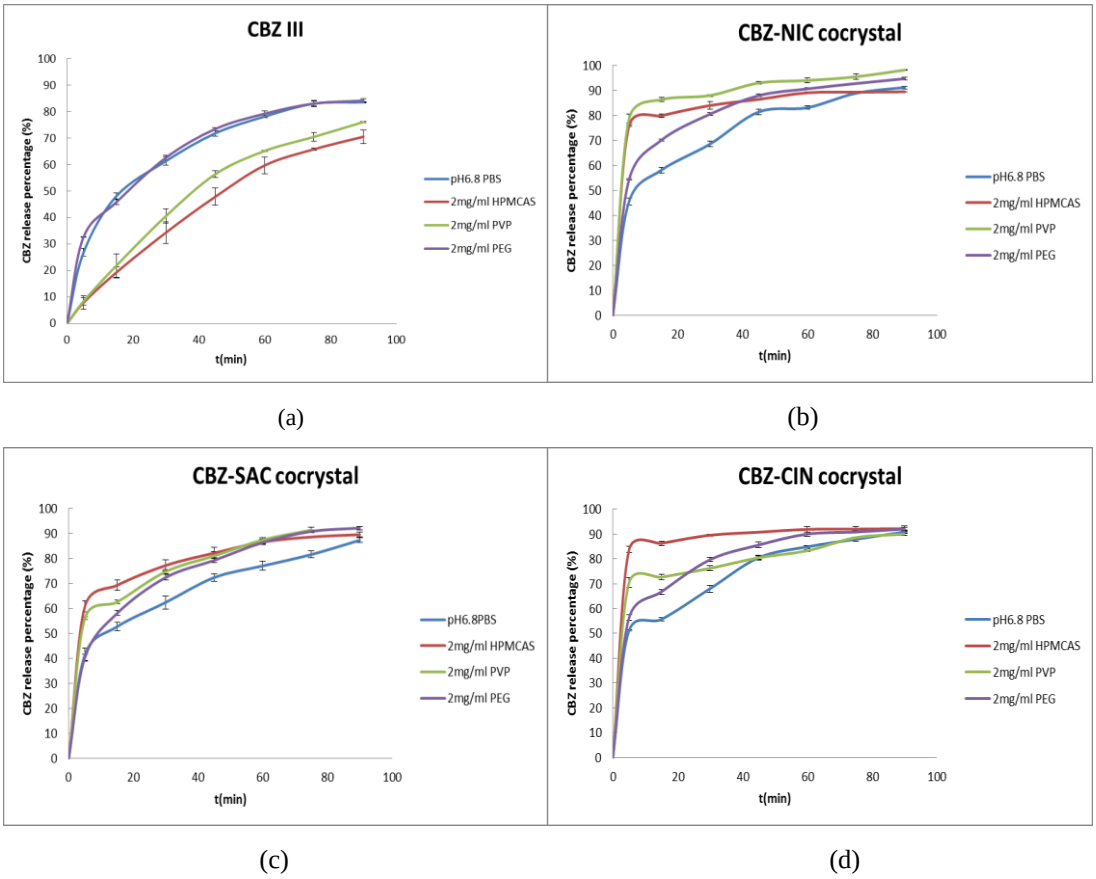

Fig.7.4 Powder dissolution profiles in the absence and the presence of a 2 mg/ml pre-dissolved polymer in pH 6.8 PBS: (a) CBZ III; (b) CBZ-NIC cocrystal; (c) CBZ-SAC cocrystal; (d) CBZ-CIN cocrystal

7.3.3 CBZ release profiles from HPMCAS, PVP and PEG based tablets

Fig.7.5 presents the comparisons of CBZ release profiles from different polymer-based tablets. The performance of none of the cocrystal formulations was observed to be better than the CBZ III formulation.

Depending on coformer, the dissolution profile of a physical mixture formulation can vary significantly. Generally, a physical mixture of a CBZ III-NIC formulation had a similar release performance to that of a CBZ III formulation. The dissolution performance of a physical mixture of CBZ III-SAC in HPMCAS or PVP tablets intermediate between those of the formulations of CBZ

III and CBZ-SAC cocrystals. For the PEG based tablets, the release profiles of the physical mixture of CBZ III-SAC were better than those of CBZ III-based formulations. The dissolution performance of a physical mixture of CBZ III-CIN varied by polymers. In HPMCAS or PVP based tablets, CIN reduced the release rate of CBZ III, indicating that the release profile of a physical mixture of CBZ III-CIN was lower than that of CBZ III alone. In a HPMCAS-based tablet, the physical mixture of CBZ III-CIN had a lower release profile than that of the cocrystal formulation for up to four hours. In a PVP based tablet, CBZ III-CIN's physical mixture had a lower release profile than that of the cocrystal formulation over the whole dissolution period, while in a PEG-based tablet, the same mixture had a higher one. For any period of dissolution of up to three hours, the physical mixture of the CBZ III-CIN formulation shows a lower rate profile than that of CBZ III alone.

The drug release profile is also affected by the percentage of a polymer in the tablet, a percentage that varies with different polymers. PEG's effects on formulation performance differ from those of HPMCAS and PVP. Increasing the percentage of PEG in a formulation increased the drug's dissolution, while the same procedure with HPMCAS or PVP had the opposite result.

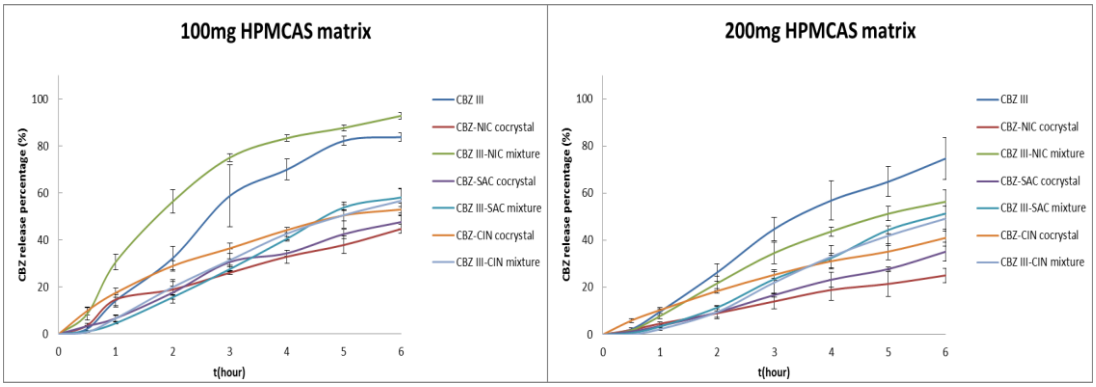

(a)

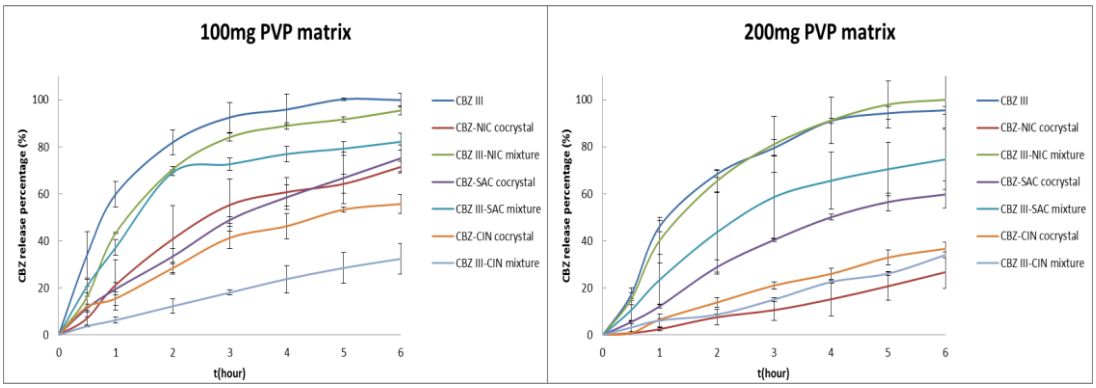

(b)

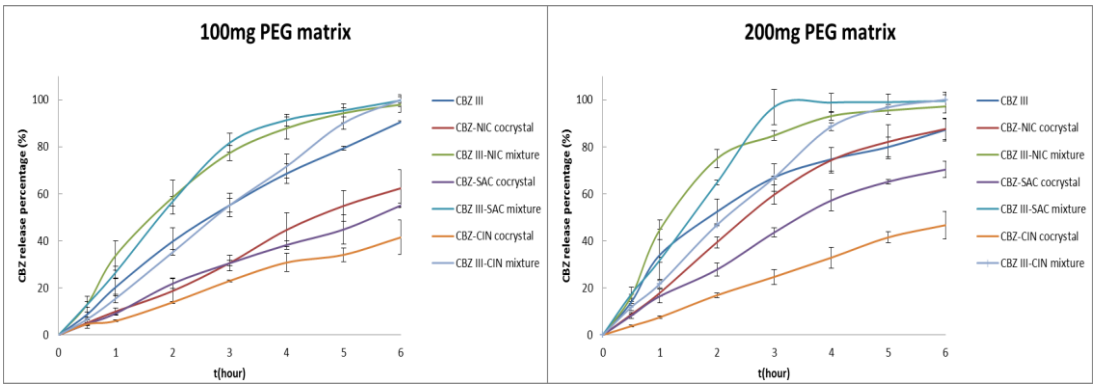

(c)

Fig.7.5 CBZ release profiles of CBZ III and cocrystals of CBZ-NIC, CBZ-SAC and CBZ-CIN from 100 mg and 200 mg polymer based tablets: (a) HPMC-based tablets; (b) PVP-based tablets; (c) PEG-based tablets

The solid residuals of different formulations after the dissolution tests (if any reasonable amounts of the solids can be collected for testing) have been analysed by DSC in Fig.7.6, XRPD in Fig.7.7 and SEM in Fig.S7.4 in the supplementary material. It has been shown that all cocrystal formulations had solid residues left after six hours dissolution except the 100 mg PVP-based CBZ-SAC cocrystal formulation. The solid residues from these cocrystal formulations comprised a mixture of CBZ cocrystals and CBZ DH crystals, as confirmed by XRPD patterns in Fig.7.7 and DSC analyses in Fig.7.6. This indicated that the CBZ DH crystals were precipitated during dissolution. Tablets of the CBZ III formulations and the physical mixture of CBZ III-NIC had dissolved completely. The solid residues collected from the 200 mg HPMCAS-based physical mixture of CBZ III-SAC consisted of CBZ III, indicating that HPMCAS can completely inhibit the transformation of CBZ III into CBZ DH during tablet dissolution. For the HPMCAS-based physical mixture of CBZ III-CIN formulations, the solid residues consisted of a mixture of the original materials of CBZ III and CIN, as shown in XRPD patterns in Fig.7.7 and DSC analyses in Fig.7.6. However, for the PVP-based physical mixture of CBZ III-CIN formulation, the solid residuals comprised a the mixture of the three components of CBZ III, CIN and CBZ DH, indicating that PVP cannot inhibit the transformation of CBZ III into CBZ DH during tablet dissolution. No solid residual was collected for any PEG-based formations because the tablet had either broken into fine particles or dissolved completely.

	CBZ III	CBZ-NIC cocrystals	CBZ-NIC mixture	CBZ-SAC cocrystals	CBZ-SAC mixture	CBZ-CIN cocrystals	CBZ-CIN mixture
100 mg HPMCAS	×	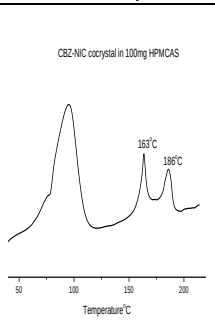	×	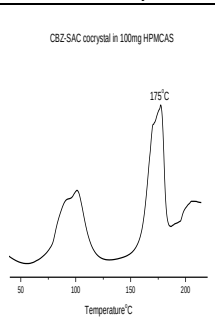	×	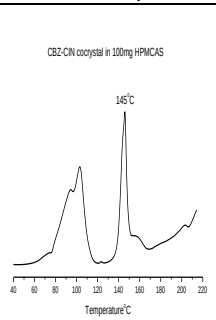	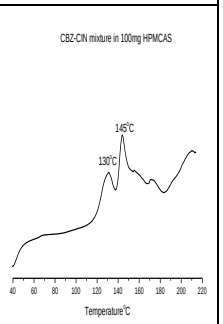
200 mg HPMCAS	×	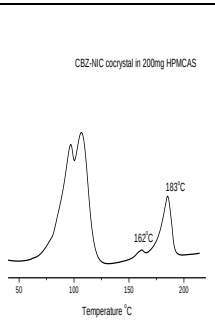	×	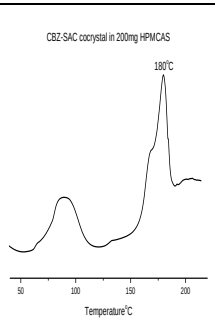	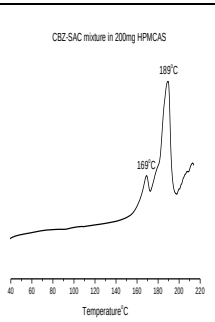	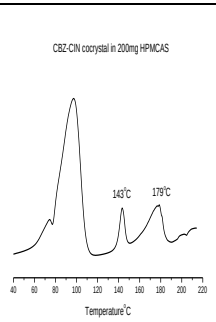	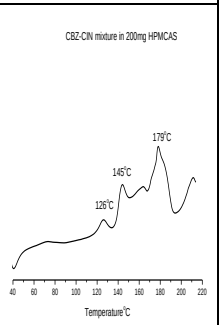
100 mg PVP	×	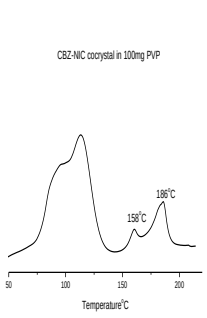	×	×	×	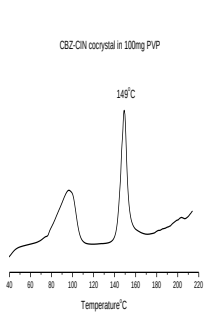	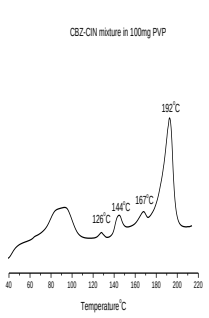

200 mg PVP	×	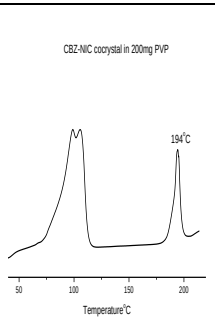	×	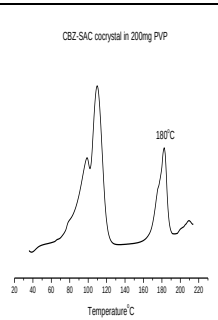	×	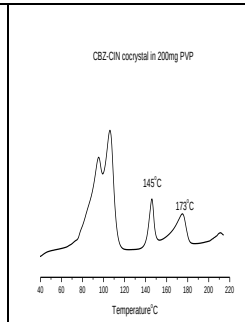	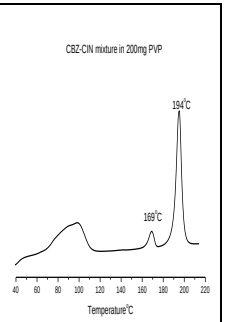
100 mg PEG	×	×	×	×	×	×	×
200 mg PEG	×	×	×	×	×	×	×

Fig.7.6 DSC thermographs of solid residues retrieved from various formulations after dissolution tests (X: no solid residues collected)

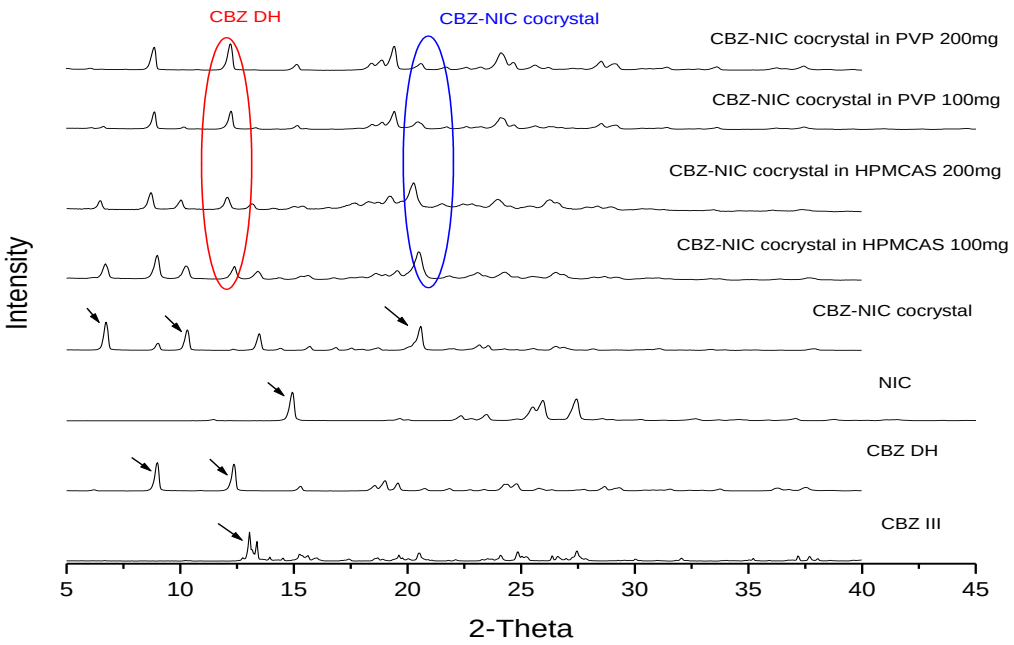

note: solid residues are physical mixture of CBZ-NIC cocrystal and CBZ DH

(a)

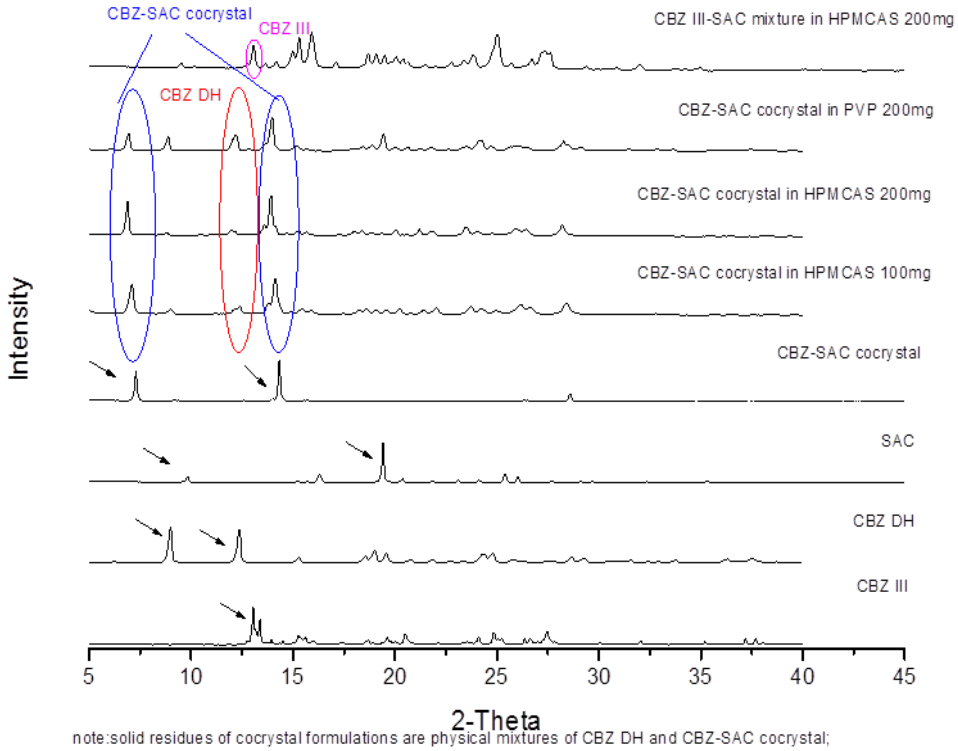

note:solid residues of cocrystal formulations are physical mixtures of CBZ DH and CBZ-SAC cocrystal;
solid residues of physical mixture formulations are CBZ III.

(b)

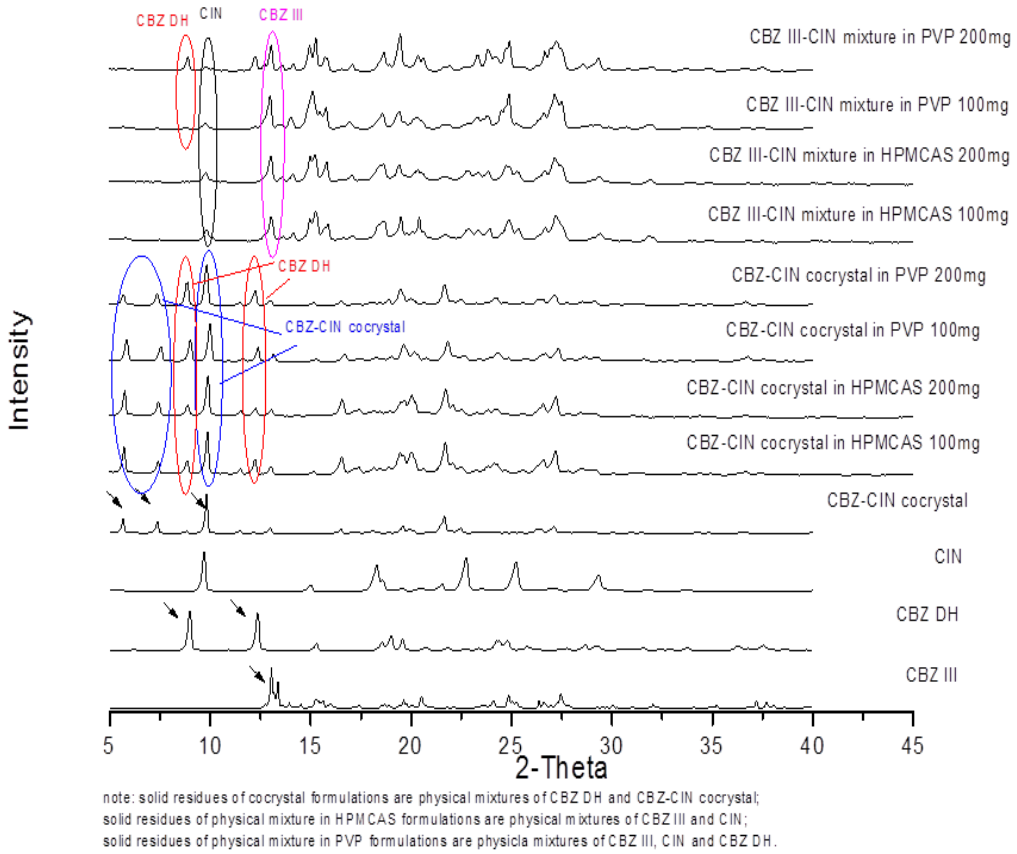

(c)

Fig.7.7 XRPD patterns of solid residues of various formulation after dissolution tests: (a) CBZ-NIC cocrystal formulations (b) CBZ-SAC cocrystal and physical mixture formulations; (c) CBZ-CIN cocrystal and physical mixture formulations

7.4 Discussion

Theoretically, cocrystals can significantly improve the solubility of drug compounds with solubility-limited bioavailability through the selection of suitable coformers [162]. In reality, however, such solubility cannot be sustained in the supersaturated solution generated because of the solution-medted phase transformation, which results in the precipitation of a less soluble solid form of the parent drug. The drug precipitation process can occur simultaneously with the dissolution of the cocrystals, demonstrating that the apparent drug solubility of cocrystals has not been improved by comparison with that of the stable form of the parent drug. Further research on maintaining the advantages of cocrystals is important [61, 159, 161, 164, 165, 169].

Cocrystals in pre-dissolved polymer solutions

In pH 6.8 PBS in the absence of a polymer, the solubility advantage of CBZ cocrystals was not in evidence: both CBZ-NIC and CBZ-CIN cocrystals generated the same apparent CBZ concentrations as that of the parent drug CBZ III while CBZ-SAC cocrystals generated a slightly higher value, as shown in Fig.7.1. This was due to crystallisation of CBZ DH from the supersaturated solution generated by the dissolution of CBZ cocrystals, as seen in the DSC and SEM analyses in Figs.7.2 and Fig.7.3. When HPMCAS with a concentration of 2 mg/ml or higher was pre-dissolved in solution, both CBZ-SAC and CBZ-CIN cocrystals could generate significantly higher CBZ supersaturated solutions with approximately three times the solubility of CBZ III. This supersaturated state had been maintained for more than 24 hours, so therefore it could certainly allow sufficient CBZ absorption for increasing bioavailability. Based on the powder dissolution studies, all three cocrystals showed at least a two-fold increase in drug release compared with that of CBZ III in pH 6.8 PBS in the absence of a polymer at five minutes. In the presence of 2 mg/ml HPMCAS in pH 6.8 PBS, the drug release of CBZ-NIC or CBZ-CIN cocrystals rose to around eight times of that of CBZ III in the same condition. These results are much better than those of previous work based on the solid dispersion approaches [170, 171]. The implication of these observations is therefore of significance because it demonstrates that cocrystals can be easily formulated through a simple solution or powder formulation to generate supersaturated concentrations and faster dissolution rates to overcome those drugs whose solubility and/or dissolution is limited. This conclusion is supported by a recent similar study of the development of an enabling danazol-vanillin cocyrstal formulation, although this research used a relatively complicated approach involving both a surfactant and polymer in the formulation [169]. As regards the formulation of drug compounds whose solubility and/or dissolution is limited, the cocrystal approach should be considered just as seriously as many other successfully supersaturating drug delivery approaches such as solubilized formulations, solid dispersions, nanoparticles and crystalline salt forms and particle size reduction [166].

In order to develop an enabling cocrystal formulation, a mechanistic understanding of the role of a polymer in inhibiting the phase transformation of cocrystals is required. This study and the authors' previous work [164, 165] has found that the key factors in controlling the maintenance of the apparent parent drug supersaturating level of a cocrystal include the cocrystal stability in solution, the rate difference between the cocrystal dissolution/dissociation and formation of a soluble complex between the parent drug and polymer, and the stability of the complexes of the drug and polymer. Fig.7.8 is a schematic diagram summarizing the important processes during dissolution of

cocrystals. It can be seen that when the cocrystal molecules are dissolved into solution, they are completely or partially dissociated into the parent drug and coformer molecules depending on the stability of the cocrystals in solution. If a pre-dissolved polymer in solution cannot form soluble complexes with the drug molecules, the solid crystals will certainly precipitate from solution due to its supersaturated states. On the other hand, although a pre-dissolved polymer can form soluble complexes with the API in solution, precipitation of the drug crystals can also occur if the rate of cocrystal dissolution and dissociation is faster than the rate at which the soluble complexes are formed. Finally, the stability of the soluble complex of the drug and polymer formed in solution is another factor by which to determine the precipitation of the drug's solid forms from solution. Two approaches can therefore be used to completely inhibit the crystallisation of the stable solid form of the parent drug in a formulation:

Scheme 1: Selecting cocrystals which are stable in solution. This can be achieved by selecting a suitable coformer. Because most cocrystals have faster dissolution rates, this scheme is particularly suitable for the formulation of drug compounds whose dissolution bioavailability is limited, although the apparent solubility of the parent drug has not been improved.

Scheme 2: Balancing the rate difference between cocrystal dissolution and the formation of a soluble complex between drug and polymer in solution. This can be realised by selecting both a polymer and a coformer. Because a stable supersaturated drug concentration can be generated to enhance drug absorption, the scheme is a particularly suitable one by which to formulate drug compounds whose solubility bioavailability is limited,.

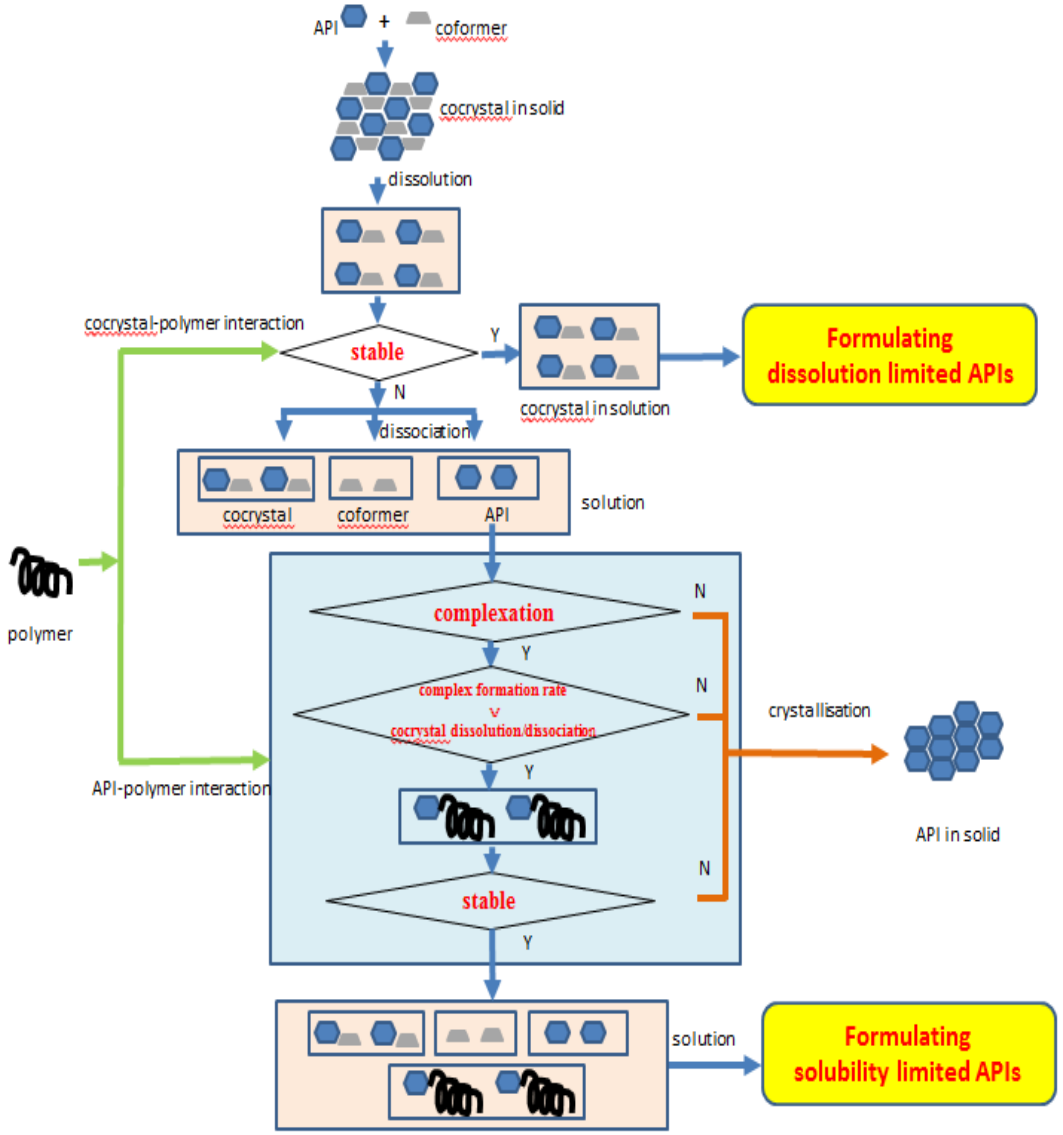

Fig.7.8 Illustration of factors affecting the phase transformation of cocrystals

It must be stressed that when a polymer is pre-dissolved in solution, both the dissolution rate of the solid cocrystals and the stability of the cocrystals in solution will be affected because of the change in the bulk properties of the dissolution medium and the solubility of both parent drug and coformer. The cocrystals in solution intend to be stable if the solubility difference between the drug and coformer in a pre-dissolved polymer solution becomes smaller, forming a congruent system.

Based on the solubility tests of CBZ III in this study, it was found that all three polymers (HPMCAS, PVP and PEG) can interact with CBZ in solution to form soluble complexes through hydrogen bonding. This indicates the increased solubility of CBZ III in pH 6.8 PBS in the presence of a pre-dissolved polymer, as shown in Fig.7.1 (a). However, the stability of the formed soluble complexes is different. Due to the rigorous structure and rich hydrogen-bond acceptors of HPMCAS in comparison to PVP and PEG, CBZ-HPMCAS complexes are stable in solution. The

supersaturated CBZ solution can therefore be stabilized, indicating that HPMCAS can completely inhibit the precipitation of CBZ from solution, as shown in the DSC and SEM analyses of the solid residues of the tests in Fig.7.2 and Fig.7.3.

The solubility tests in pH 6.8 PBS in the absence of a polymer show that all three CBZ cocrystals (CBZ-NIC, CBZ-SAC and CBZ-CIN) are not stable, indicating that the eutectic constants K_{eu} in Fig.7.1 (e)-(g) are significantly higher than the critical value of 1 [61, 165]. When they are dissolved, therefore, the cocrystal molecules are dissociated into CBZ and coformers in solution, resulting in the crystallisation of CBZ DH crystals from solution. This is confirmed by the DSC and SEM analyses in Fig.7.2 and Fig.7.3. Because the value of the eutectic constant is smaller than CBZ-NIC and CBZ-CIN cocrysatls, CBZ-SAC cocrystals in solution are relatively more stable than them, resulting in a higher apparent CBZ concentration.

A pre-dissolved polymer in pH 6.8 PBS can significantly improve the stability of CBZ-SAC and CBZ-CIN cocrystals because of the reduced solubility differences between CBZ and coformers (coformer solubility is shown in Fig.S7.3 (a) in the supplementary material), indicating decreases in the eutectic constants K_{eu}, as shown in Fig.7.1 (f)-(g). HPMCAS is also the best polymer to stabilize CBZ-SAC or CBZ-CIN cocrystals in solution because of the smallest value of the eutectic constant K_{eu}, pointing to the significant improvement of the supersaturating level of CBZ in solution shown in Fig. 7.1 (c)-(d). The values of K_{eu} in different concentrations of HPMCAS solutions are, however, e is a small change of the eutectic constants K_{eu} for CBZ-NIC cocrystals in the presence of HPMCAS, PVP or PEG in solution so that the apparent concentration of CBZ is almost constant, as shown in Fig.7.1 (b).

All three CBZ cocrystals exhibit significantly improved dissolution rates compared with that of CBZ III, based on the powder dissolution tests in pH 6.8 PBS in both the absence and the presence of a polymer, as Fig.7.4 shows. Selection of a coformer is the key factor that affects cocrystal dissolution rate. Although there is a significant difference between NIC and CIN in term of solubility, it was found that both CBZ-NIC and CBZ-CIN cocrystals have similar dissolution rates, both of them higher than that of CBZ-SAC cocrystals. A pre-dissolved polymer in the dissolution medium of pH 6.8 PBS can further improve this dissolution rate. One reasonable explanation is that the presence of a polymer in solution can increase the solubility of the cocrystals, resulting in faster dissolution. In the meantime, because of the improved stability of cocrystals in solution in the presence of a pre-dissolved polymer, the dissolved cocrystal will be stable in solution to avoid crystallisation of the parent drug, indicating that the eutectic constants K_{eu} were close to the critical

value of 1 as shown in Fig.S7.5 in the supplementary material. Generally, the experiments show that HPMCAS is the best excipient to be included in solution to improve the dissolution rates as well as solubility of the cocrystals. In contract, the presence of HPMCAS or PVP in solution decreased the dissolution rate of CBZ III, which is the similar to our previous work on HPMC [165]. This could be caused by the slightly increased viscosity of the dissolution medium, resulting in a reduction in CBZ III's molecular mobility. In the meantime, the polymers HPMCAS and PVP can also be adsorbed on the surfaces of CBZ III particles to hinder the latter's dissolution.

Cocrystals in polymer-based matrix tablets

A polymer-based cocrystal tablet formulation has not demonstrated any advantage in increasing CBZ's release rate by comparison with the formulation of CBZ III or physical mixtures of CBZ III and coformers, as shown in Fig.7.5. This is contrary to the solution behaviours of CBZ cocrystals studied in the solubility and powder dissolution tests. A tablet's drug release performance is complex and highly dependent not only on each individual component's properties (such as solubility, dissolution rate, particle size, and wettability) but also on manufacturing factors (e.g. compression forces, tablet shape and drug loads). These factors affect the kinetic processes of tablet dissolution, including the polymer dissolution kinetics, drug dissolution kinetics and kinetics of the physical form change of the tablet. Both this study and our previous work [164, 165] indicate that the polymer hydration process is the critical factor in determining cocrystal release performance.

PEG as used in this study is highly soluble and exhibits good wettability. Their poor gelling ability meant that all PEG-based tablets eroded quickly and eventually disintegrated completely, thus leaving no solid residue after dissolution. PEG-based CBZ III tablets and physical mixtures of CBZ III and coformers exhibited complete drug release because of the sink conditions. The PEG-based cocrystal tablets had an incomplete release profile, which was believed to be caused by the precipitation of CBZ DH. Once the tablet was immersed into the dissolution medium, the PEG dissolved quickly to form channels that allowed water to penetrate the tablet. Because of the faster dissolution rate, dissolution of the cocrytstal started immediately inside the tablet before its erosion and disintegration, resulting in crystallisation of CBZ DH from the micro-environmentally supersaturated states.

Similarly to PEG, PVP can dissolve quickly in water. However, PVP, which is a good gelling agent, can form a gel matrix to modify the drug release profile in an extended release formulation. Due to the loose structure of the gel matrix formed by PVP, the dissolution medium can easily penetrate

inside the tablet to dissolve the drug. The highly viscous environment inside the matrix prevented the dissolved drug from immediately diffusing into the bulk solution. When the drug concentration was built up to exceed its solubility, a stable, solid form of the drug crystallized. The three CBZ cocrystals used in this study had significantly improved dissolution rates compared with that of CBZ III, so the concentration of the cocrystals inside the tablets quickly exceeded their solubility. In the meantime, the formation of the soluble complexes between the drug and polymer was slower. PVP-based cocrystal formulation release is slower and incomplete compared with that of CBZ III or physical mixture formulations because of the crystallisation of CBZ DH inside the tablet, as shown in Fig.7.5 (b) and analyses of the DSC in Fig.7.6 and XRPD in Fig.7.7. The formulation of the physical mixture of CBZ III and CIN resulted in significantly slower release rates for CBZ. It is believed that poor solubility and a slow CIN dissolution rate retarded the hydration and dissolution of CBZ III.

HPMCAS-based cocrystal formulations display improved release rates at the early stage of the tablet dissolution test, which is similar to the authors' previous work on HPMC-based cocrystal formulations [164, 165]. This is caused by HPMCAS' slower hydration property. At the beginning of the dissolution test, cocrystal dissolution can only take place at the surface of the tablet, and the dissolved cocrystal can therefore diffuse into the bulk of the dissolution medium directly so as to avoid the supersaturated states of the drug concentration. This is similar to the powder dissolution tests. Once the gel layer has formed, water can penetrate into the inside tablet to dissolve the cocrystals, resulting in crystallisation of CBZ DH inside the tablet.

7.5 Chapter conclusion

The influence of the three chemically diverse polymers (HPMCAS, PVP and PEG) on the phase transformation of the three CBZ cocrystals (CBZ-NIC, CBZ-SAC and CBZ-CIN) in solution and tablet-based formulations has been investigated. This study has shown that the improved CBZ solubility of the three CBZ cocrystals cannot be sustained in the supersaturated solution generated due to the solution mediated phase transformation, resulting in precipitation of a less soluble solid form of CBZ DH. When HPMCAS with a concentration of 2 mg/ml or higher was pre-dissolved in solution, both CBZ-SAC and CBZ-CIN cocrystals could generate significantly higher CBZ supersaturated solutions with an approximate three-fold increase in CBZ III's solubility that can be sustained for more than 24 hours. All three cocrystals at least doubled the drug release compared with CBZ III in pH 6.8 PBS in the absence of a polymer at five minutes. In the presence of 2 mg/ml HPMCAS in pH 6.8 PBS, the drug release of CBZ-NIC or CBZ-CIN cocrystals was increased to

around eight times of that of CBZ III in the same condition. These results demonstrate that cocrystals can easily be formulated through a simple solution or powder formulation to generate supersaturated concentrations and faster dissolution rates to overcome those drugs whose solubility and/or dissolution bioavailability is limited. The cocrystal approach should therefore be taken just as seriously for formulating drug compounds with limited solubility and/or dissolution bioavailability as many other successfully supersaturating drug delivery approaches such as solubilized formulations, solid dispersions, nanoparticles and crystalline salt forms and particle size reduction. As regards improved CBZ release rates, however, a polymer tablet-based CBZ cocrystal formulation did not reveal any advantage compared with CBZ III formulations or physical mixtures of CBZ III and coformers. These findings contradict the solution behaviours of CBZ cocrystals studied in the solubility and powder dissolution tests because crystallization of the stable solid form of CBZ DH within the tablet has taken place, leading to a reduced drug release rate and incomplete release.

Chapter 8 Quality by Design approach for developing an optimal CBZ-NIC cocrystal sustained-release formulation

8.1 Chapter overview

This chapter discusses the QbD principles and tools used to develop a CBZ-NIC cocrystal formulation that ensures the quality, safety and efficacy of CBZ sustained-release tablets. Self-made tablets are compared with the CBZ commercial tablet, the 200 mg Tegretol Prolonged Release Tablet.

8.2 Materials and methods

8.2.1 Materials

CBZ, NIC, HPMC, HPMCP, EtOAc, methanol, SLS, potassium dihydrogen phosphate (KH_2PO_4) and sodium hydroxide (NaOH), double distilled water, microcrystalline (MCC), lactose, stearic acid, colloidal silicon dioxide and 200 mg CBZ Tegretol Prolonged Release Tablets, were used in the tests discussed in this chapter. Details of these materials can be found in Chapter 3.

8.2.2 Methods

8.2.2.1 Formation of CBZ-NIC cocrystal

CBZ-NIC cocrystals were used for the tests described in this chapter. The details of the formation method can be found in Chapter 3.

8.2.2.2 Tablet preparation

Tablets were prepared, the details of which can be found in Chapter 3. The total weight of each tablet was 500 mg. All tablets contained the equivalent of 304 mg CBZ-NIC cocrystals (equal to 200 mg CBZ III).

8.2.2.3 Physical tests of tablets

The tablets' diameter, hardness, thickness and friability were tested. Details can be found in Chapter 3.

8.2.2.4 Dissolution studies of tablets

The details of the dissolution studies on formulated tablets can be found in Chapter 3. The dissolution medium was 700 ml, 1% SLS pH 6.8 PBS.

8.3 Preliminary experiments

CBZ sustained-release oral tablets were formulated and tested in the early stages of development. The pharmaceutical target profile for CBZ is a safe efficacious convenient dosage form, preferably a tablet, which facilitates patient compliance. The tablet should be of appropriate size. The manufacturing process for the tablet should be robust and reproducible and should result in a product that meets the appropriate critical quality attributes. These pharmaceutical Quality Target Product Profiles (QTPPs) are summarized in Table 8.1.

Table 8.1 Quality Target Product Profile

Quality Attribute	**Target**
Dosage form	Oral sustained-release Carbamazepine Tablet
Potency	200 mg
Identity	Positive to Carbamazepine
Appearance	White round tablets
Thickness	3-3.5 mm
Diameter	12.5-13.0 mm
Friability	Not more than 1%
Release percentage	15-30% at 0.5 hours 40-60% at 2 hours not less than 75% at 6 hours

Fig.8.1 shows the CBZ release profiles of CBZ-NIC cocrystals (304 mg) in 100mg MCC or 100 mg HPMCP tablets. The CBZ release percentages of CBZ-NIC cocrystals in 100 mg MCC tablets at 0.5, 1, 2, 3, 4, 5 and 6 hours are 5.9, 9.8, 18.8, 24.7, 33.1, 38.4 and 45.0 respectively. The CBZ release percentages of CBZ-NIC cocrystals in 100 mg HPMCP tablets at 0.5, 1, 2, 3 and 4 hours are 53.9, 74.6, 90.8, 95.0 and 96.4 respectively. The results indicate that CBZ releases more slowly from MCC tablets than from HPMCP ones. Therefore, HPMCP and MCC were both used in the preliminary experiments for CBZ sustained-release tablets in order to obtain reliable dissolution profiles compared to commercial products.

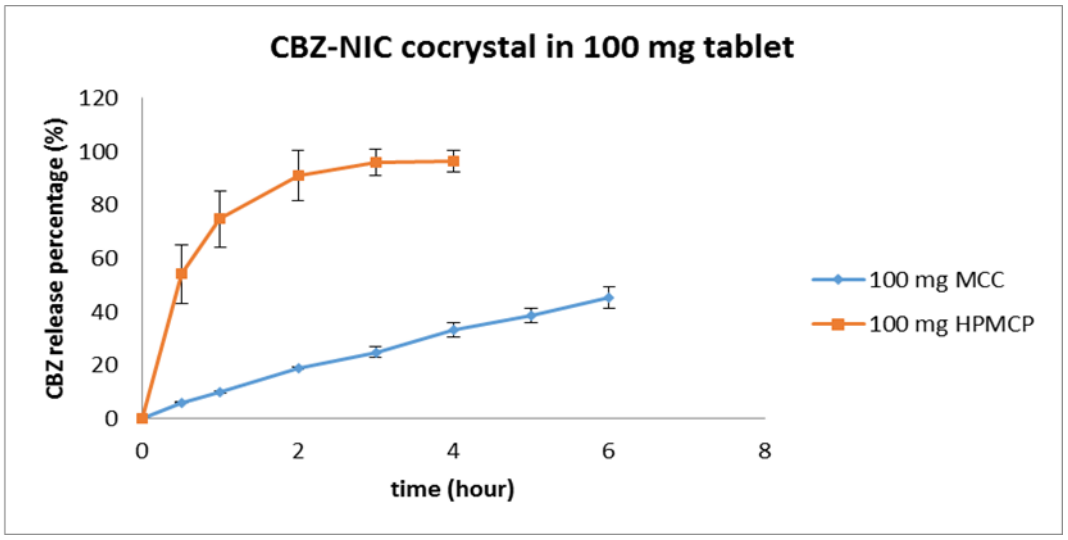

Fig.8.1 Dissolution profiles of CBZ-NIC cocrystal in 100 mg MCC and 100 mg HPMCP tablets

Four pharmaceutical formulations of CBZ sustained-release tablets have initially been developed for preliminary studies. The formulations were evaluated for their physical properties and dissolution profiles. HPMCP was used as a disintegrant, lactose as a dissolution enhancer, MCC as a filler, stearic acid as a lubricant and silica as a glidant. The drug release profiles of the four formulations were used to find the parameter ranges for the final design of experiments. Table 8.2 shows the composition of the four preliminary formulations (the total weight of tablet is 500 mg).

Table 8.2 Preliminary formulations in percentage and mass in milligrams

Raw material	**Function**	**F1**	**F2**	**F3**	**F4**
CBZ-NIC cocrystal	API	60.8%(304mg)	60.8%(304mg)	60.8%(304mg)	60.8%(304mg)
HPMCP	Disinte-grant	20%(100mg)	20%(100mg)	12%(60mg)	12%(60mg)
Lactose	Dissolution enhancer	4%(20mg)	8%(40mg)	4%(20mg)	8%(40mg)
MCC	Filler	13.95%(69.75mg)	9.95%(49.75mg)	21.95%(109.75mg)	17.95%(89.75mg)

Stearic acid	Lubricant	1%(5mg)	1%(5mg)	1%(5mg)	1%(5mg)
Silica	Glidant	0.25%(1.25mg)	0.25%(1.25mg)	0.25%(1.25mg)	0.25%(1.25mg)

The results of the thickness, hardness, diameter and friability tests on the four preliminary formulations are shown in Table 8.3.

Table 8.3 Physical tests of preliminary formulations

Formulation	**Mass (g) (±SD)**	**Thickness(mm) (±SD)**	**Diameter(mm) (±SD)**	**Hardness(N) (±SD)**	**Friability %**
1	0.499±0.013	3.510±0.010	12.673±0.015	77.967±1.686	0.335
2	0.500±0.006	3.510±0.010	12.690±0.010	92.233±0.352	0.306
3	0.504±0.012	3.460± 0.030	12.670±0.020	114.600±1.442	0.398
4	0.498±0.003	3.420±0.100	12.676±0.006	122.833±4.80	0.245

Standard deviation of the four preliminary formulations diameter was less than 1, which is close to the actual die diameter used (13 mm). The average thickness of tablets with a standard deviation of 0.01, 0.01, 0.03 and 0.10 separately, indicates good reproducibility. The hardness results showed higher standard deviation compared to the

other measurements. This could be due to poor mixing and/or different particle size distribution of the excipients.

The dissolution profiles of the four preliminary formulations and the commercial product CBZ Tegretol 200 mg Prolonged Release Tablets (Reference) are shown in Fig.8.2.

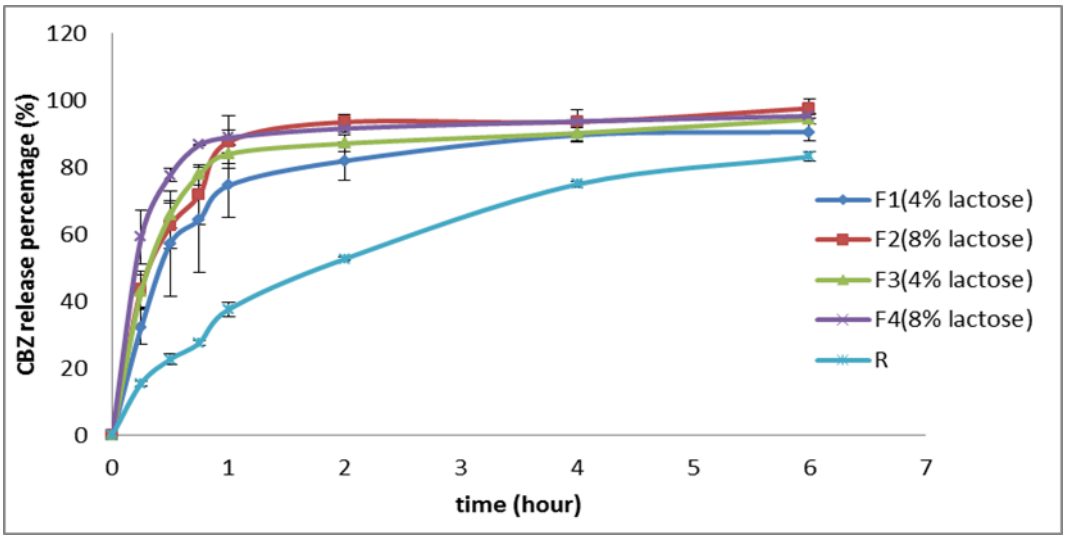

Fig.8.2 Dissolution profiles of four preliminary formulations and CBZ commercial tablet. R: (reference)

The dissolution profiles shown in Fig.8.2 indicate that, with an increase of dissolution enhancer lactose, the drug's release rate increased (F4>F3; F2>F1). The release rates of all four preliminary formulations were faster than those of the reference (i.e. commercial) tablets, signifying that when HPMCP is used in MCC tablets, they disintegrate rapidly so as to increase the surface area of their fragments and so promote rapid drug release. The pharmaceutical excipient MCC thus cannot sustain the release of CBZ from the tablets. The dissolution profiles of the four preliminary formulations suggest that a high-viscosity polymer should be used in the formulations in order to make the tablets sustained-release. Based on the previous experiments, HPMC was selected as a new excipient added to the formulation.

8.4 Risk assessments

Risk assessment aims to obtain all the potential high impact factors to be subjected to a Design of Experiment (DoE) study that establishes a product or process design space. A fish-bone diagram identifies the potential risks and corresponding causes. Friability and hardness of tablets are identified as the Critical Quality Attributes (CQAs). Based on the preliminary work, factors thought to affect dissolution are assessed and the critical attributes identified. These factors are shown in the following fish bone diagram (Fig.8.3).

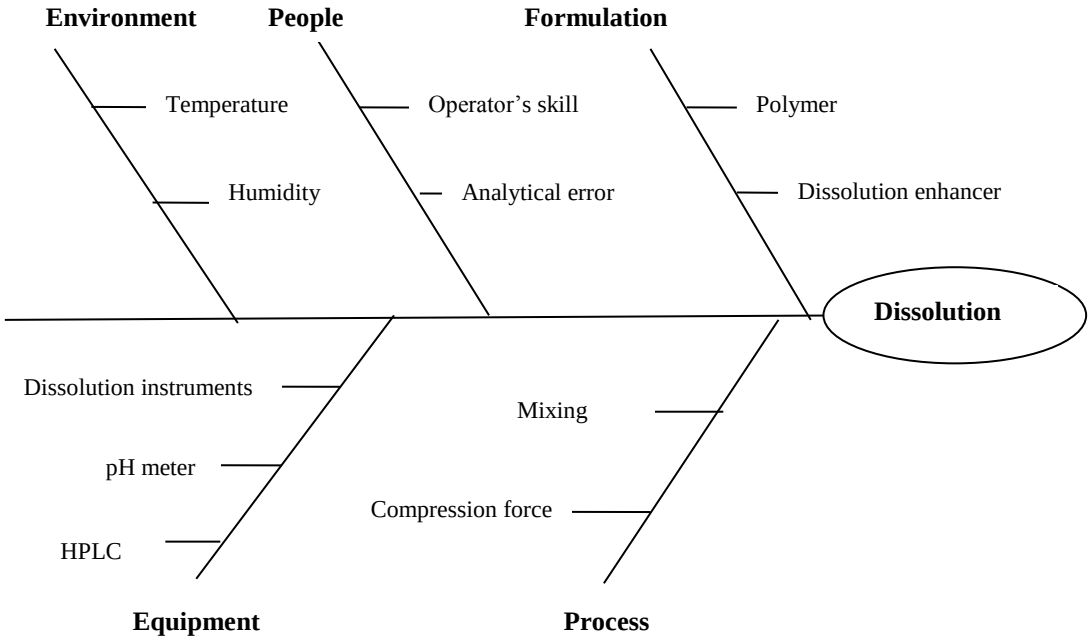

Fig.8.3 Fish bone diagram showing the possible factors that could affect CBZ's dissolution rate

8.5 Design of Experiment (DoE) [69]

The Box-Behnken experimental design was used to optimise and evaluate the main effects of HPMC, HPMCP and lactose together with their interaction effects. A three-factor, three-level design was used because it was suitable for exploring quadratic response surfaces and constructing second order polynomial models for optimisation. The independent factors and dependent variables used in this design are listed in Table 8.4. Selection of the low, medium and high levels of each independent factor was based on the results of the preliminary experiments. HPMC was used as matrix in the formulation. HPMCP, which dissolves when pH ≥5.5, was used as the formulation's

channel agent and lactose as its dissolution enhancer. For the response surface methodology involving the Box-Behnken design, a total of 15 experiments were constructed for the three factors at the three levels of each parameter, as shown in Table 8.4. Each factor was tested at three levels designated as -1, 0 and +1. HPMCP's weight percentage ranged from 5% (-1) to 15% (+1), HPMC's weight percentage from 5% (-1) to 15% (+1) and lactose's weight percentage from 2% (-1) to 6% (+1). The design was equal to the three replicated centre points and the set of points lying at the midpoint of each surface on the cube defining the region of interest of each parameter. The non-linear quadratic model generated by the design is

$$Y = b_0 + b_1x_1 + b_2x_2 + b_3x_3 + b_{12}x_1x_2 + b_{13}x_1x_3 + b_{23}x_2x_3 + b_{11}x_1^2 + b_{22}x_2^2 + b_{33}x_3^2 \qquad \text{Equ.8.1}$$

where Y is a measured response associated with each factor level combination, b_0 is an intercept, b_1 to b_{33} are regression coefficients calculated from the observed experimental values of Y, and x_1,x_2 and x_3 are the coded levels of independent variables. The terms x_1x_2, x_1x_3, x_2x_3 and x_i^2 (i=1, 2 and 3) represent the interaction and quadratic terms respectively. The response surface and analysis were carried out using JMP 11 software (SAS, SAS Institute, Cary, NC, USA).

Table 8.4 Variables and levels in the Box-Behnken experimental design

In dependent variables	**level**		
	Low (-1)	**Medium(0)**	**High(+1)**
x_1 : weight percentage of HPMCP	5	10	15
x_2: weight percentage of HPMC	5	10	15
x_3 : weight percentage of lactose	2	4	6
Dependent responses	**Goal**	**lower limit**	**upper limit**
Y_1: drug release percentage at 0.5 hours	Match Target	15	30
Y_2: drug release percentage at 2 hours	Match Target	40	60
Y_3: drug release percentage at 6 hours	Match Target	75	100

8.6 Results

The Box-Behnken design was applied in this study to optimise CBZ sustained-release tablets. A total of 15 experiments were conducted to construct the formulation. The aim of the formulation

optimisation was to determine the design space of excipients range in order to obtain a target product which releases the drug at rates of 15-30% at 0.5 hours, 40-60% at 2 hours and no less than 75% at 6 hours. The observed responses for the 15 experiments are given in Table 8.5.

Tablets produced were white, smooth, flat faced and circular. No cracks were observed. Physical tests for the 15 formulations were carried out to study the average mass, thickness, diameter, hardness and friability of the tablets. Six tablets of each formulation were tested for mass and friability, and three of each for thickness, diameter and hardness.

Table 8.5 The Box-Behnken experimental design and responses

Run	**Independent variables**				**Dependent variables**			**Hardness**	**Friability**
	mode	X_1	X_2	X_3	Y_1	Y_2	Y_3	$\overline{Y_4}$	$\overline{Y_5}$
1	--0	5	5	4	57.45	82.70	87.96	141.27	0.143
2	-0-	5	10	2	33.23	60.20	80.73	135.30	0.219
3	-0+	5	10	6	31.79	53.93	79.58	152.90	0.213
4	-+0	5	15	4	16.01	31.21	60.37	157.53	0.080
5	0--	10	5	2	63.98	85.72	89.11	140.27	0.195
6	0-+	10	5	6	66.47	88.52	89.19	134.67	0.293
7	000	10	10	4	22.16	47.80	79.43	115.97	0.253
8	000	10	10	4	29.47	52.31	88.24	140.80	0.213
9	000	10	10	4	27.51	54.94	86.18	140.73	0.207
10	0+-	10	15	2	14.17	31.83	67.15	159.40	0.040
11	0++	10	15	6	10.51	35.19	67.76	137.77	0.482
12	+-0	15	5	4	72.23	85.80	88.80	123.63	0.290
13	+0-	15	10	2	29.36	51.49	75.96	159.43	0.182
14	+0+	15	10	6	28.38	58.60	81.73	144.43	0.274
15	++0	15	15	4	13.13	32.86	64.84	129.37	0.404

Notes: "-" indicates low (-1) level; "0" indicates medium (0) level; "+" indicates high (+1) level.

The average masses of all formulations ranged between 0.501 g and 0.506 g. The average thickness of the tablets ranged from 3.307 mm to 3.563 mm. The average diameters of the tablets ranged from 12.657 mm to 12.790 mm. Friability tests showed vales less than 1% for all the formulations range between 0.080% and 0.482%. The lowest average hardness was 115.97 N and the highest was 159.43 N. The results of physical properties of the tablets produced are given in Table 8.6.

The standard deviation calculated for the average masses, thickness and diameters was less than 1%. This indicated that the reproducibility process for the tablets was good. The friability was less than 1%, which showed that the tablets' mechanical resistance was likewise good.

The hardness of Formulation 1 (HPMCP 5%, HPMC 5%, lactose 4%) was 141.27 N. Increasing the percentage of HPMCP in Formulation 12 (HPMCP 15%, HPMC 5%, lactose 4%) resulted in a hardness value of 123.63 N. This decrease in hardness can be attributed to HPMCP's poor compressibility properties, a quality which is also attested by the friability of Formulations 1 and 12, of 0.143 N and 0.290 N respectively.

The effect of HPMC on the mechanical strength of the tablets was studied by comparing Formulations 1 (HPMCP 5%, HPMC 5%, Lactose 4%) and 4 (HPMCP 5%, HPMC 15%, lactose 4%). Increasing the percentage of HPMC from 5% in the former to 15% in the latter resulted in an increase in hardness from 141.27 N to 157.53 N and a corresponding decrease in friability from 0.143 to 0.080. These two effects can be attributed to the binding property of HPMC, that tends to hold the particles together, resulting in a stronger tablet. These results accord with those of the published paper [172]. Investigation of the various polymers' structures and dry binding activities revealed that hardness and friability improved with increasing the percentage of binger HPMC.

Formulations 2 (HPMCP 5%, HPMC 10%, lactose 2%), 3 (HPMCP 5%, HPMC 10%, lactose 6%), 5 (HPMCP 10%, HPMC 5%, lactose 2%) and 6 (HPMCP 10%, HPMC 5%, lactose 6%) were compared, with no significant effect of lactose on mechanical properties being observed.

Table 8.6 Physical test showing average of tested masses, thicknesses and diameters of the 15 formulations

Form.	**Mass (g) (±SD)**	**Thickness (mm) (±SD)**	**Diameter(mm) (±SD)**
1	0.501±0.003	3.307±0.038	12.757±0.055
2	0.501±0.004	3.373±0.031	12.697±0.031
3	0.502±0.001	3.337±0.049	12.660±0.017
4	0.502±0.013	3.467±0.170	12.677±0.006
5	0.502±0.003	3.353±0.021	12.710±0.010
6	0.502±0.001	3.407±0.071	12.690 ±0.010
7	0.501±0.006	3.473±0.117	12.740±0.010

8	0.500 ±0.004	3.387 ±0.025	12.683 ±0.015
9	0.501 ±0.003	3.400 ±0.020	12.657 ±0.049
10	0.502 ±0.003	3.453 ±0.035	12.743 ±0.055
11	0.502 ±0.005	3.403 ±0.083	12.683 ±0.006
12	0.506 ±0.006	3.457 ±0.015	12.677 ±0.015
13	0.502 ±0.004	3.563 ±0.160	12.790 ±0.090
14	0.502 ±0.003	3.350 ±0.050	12.697 ±0.025
15	0.502 ±0.008	3.470 ±0.026	12.703 ±0.035

Mass N=6 tablets, thickness, diameter N=3 tablets

8.7 Discussion

8.7.1 Fitting data to model

Using a fitted full quadratic model, a response surface regression analysis for each of response Y_1-Y_3 was performed using JMP 11 software. Table 8.7 shows the values calculated for the coefficients and the *P*-value. Using a 5% significance level, a factor is considered to have a significant effect on the response if the coefficients markedly differ from zero and the *P*-value is less than 0.05 (p<0.05). A positive coefficient before a factor in the polynomial equation means that the response increases with the factor, while a negative one means that the relationship between response and factor is reciprocal. Higher order terms or more than one factor term in the regression equation represents nonlinear relationships between responses and factors.

Table 8.7 Regression coefficients and associated probability values (*P*-value) for responses of Y_1, Y_2, Y_3

Term	**release percentage at 0.5h**		**release percentage at 2h**		**release percentage at 6h**	
	Coefficient	**P-value**	**Coefficient**	**P-value**	**Coefficient**	**P-value**
Constant	26.38	<0.0001*	51.68	<0.0001*	84.62	<0.0001*
X_1	0.58	0.6968	0.09	0.9329	0.34	0.7956
X_2	-25.79	<0.0001*	-26.46	<0.0001*	-11.87	0.0002*
X_3	-0.45	0.7613	0.88	0.4229	0.66	0.6128
X_1*X_2	-4.42	0.0759	-0.36	0.8085	0.91	0.6244
X_1*X_3	0.12	0.9559	3.35	0.0649	1.73	0.3659
X_2*X_3	-1.54	0.4721	0.14	0.9252	0.13	0.9423
X_1*X_1	2.62	0.2597	1.10	0.4899	-3.96	0.0803
X_2*X_2	10.78	0.0035*	5.36	0.0151*	-5.16	0.0359*
X_3*X_3	1.69	0.4481	3.27	0.0775	-1.15	0.5524
Regression	$Y_1=26.38+0.58X_1-25.79X_2-$		$Y_2=51.68+0.09X_1-26.46X_2$		$Y_3=84.62+0.34X_1-11.87X_2+$	

$0.45X_3-4.42X_1*X_2+0.12$	$+ 0.88X_3-0.36X_1*X_2+3.35$	$0.66X_3+0.91X_1*X_2+1.73$
$X_1*X_3-1.54X_2*X_3+2.62$	$X_1*X_3+0.14X_2*X_3+1.10X_1^2$	$X_1*X_3+0.13X_2*X_3-3.96X_1^2-$
$X_1^2+10.78\ X_2^2+1.69\ X_3^2$	$+5.36X_2^2+3.27\ X_3^2$	$5.16X_2^2-1.15\ X_3^2$

P-value <0.05

It is quite evident that the factor of weight percentage of HPMC (X_2) and (X_2^2) had significant effects (*P*-value <0.05) on the drug release percentage at 0.5 hours (Y_1), 2 hours (Y_2) and 6 hours (Y_3). The weight percentage of HPMC (X_2) negatively affected the drug release percentage at 0.5 hours, 2 hours and 6 hours. As expected, increasing HPMC's weight percentage resulted in a decrease in the drug's release percentage, as has already been reported in the literature [99, 157]. When a matrix tablet is immersed in the dissolution medium, wetting occurs at the surface and then progresses into the matrix to form an entangled three-dimensional gel structure in HPMC. Molecules undergoing chain entanglement are characterized by strong viscosity dependence on the concentration. An increase in the HPMC percentage in the formulation can lead to an increase in the gel viscosity, suppressing the dissolution of the drug [157]. The interaction effect of X_1 and X_2 favoured a decrease in the drug's release percentage at 0.5 hours (Y_1) and 2 hours (Y_2) while increasing it at 6 hours (Y_3). The interaction effect of $X_1$and X_3 led to an increase in the drug's release percentage at 0.5 hours (Y_1), 2 hours (Y_2) and 6 hours (Y_3). The interaction effect of X_2 and X_3 resulted in a decrease in the drug's release percentage at 0.5 hours (Y_1) and an increase in that percentage at 2 hours (Y_2) and 6 hours (Y_3). The interaction effect of X_1^2 favoured an increase in the drug's release percentage at 0.5 hours (Y_1) and 2 hours (Y_2) while decreasing it at 6 hours (Y_3). The interaction effect of X_2^2 resulted in an increase in the drug's release percentage at 0.5 hours (Y_1) and 2 hours (Y_2) and a decrease at 6 hours (Y_3). It is also evident that the interaction effect of X_2^2 significantly affects the drug's release percentage at 0.5 hours (Y_1), 2 hours (Y_2) and 6 hours (Y_3). The interaction effect of X_3^2 favoured an increase in this percentage at 0.5 hours (Y_1) and 2 hours (Y_2) while decreasing it at 6 hours (Y_3).

Repeatability of the formulation experiments was studied by examining the results of Experiments 7 to 9. The values of the dependent responses (Y_1, Y_2 and Y_3) were similar, indicating good experimental repeatability.

8.7.2 Response contour plots

The relationship between the inputs and outputs are further elucidated using response contour plots, which are very useful in the study of the effects of two factors on a response at the same time as a third factor is kept at a constant level. The focus was to study the effects of the weight percentages of HPMCP, HPMC and lactose, and of their interactions, on the responses of the drug release percentages at 0.5 hours (Y_1), 2 hours (Y_2) and 6 hours (Y_3).

The effect of X_1 and X_2 and their interaction on the drug release percentage at 0.5 hours (Y_1), 2 hours (Y_2) and 6 hours (Y_3) at medium level of X_3 is given in Fig.8.4. In the contour plots shown in Fig.8.4 (d), the white areas show the formulation spaces which can meet the required dissolution profiles: drug release between 15 to 30% at 0.5 hours; 40 to 60% at 2 hours; above 75% at 6 hours.

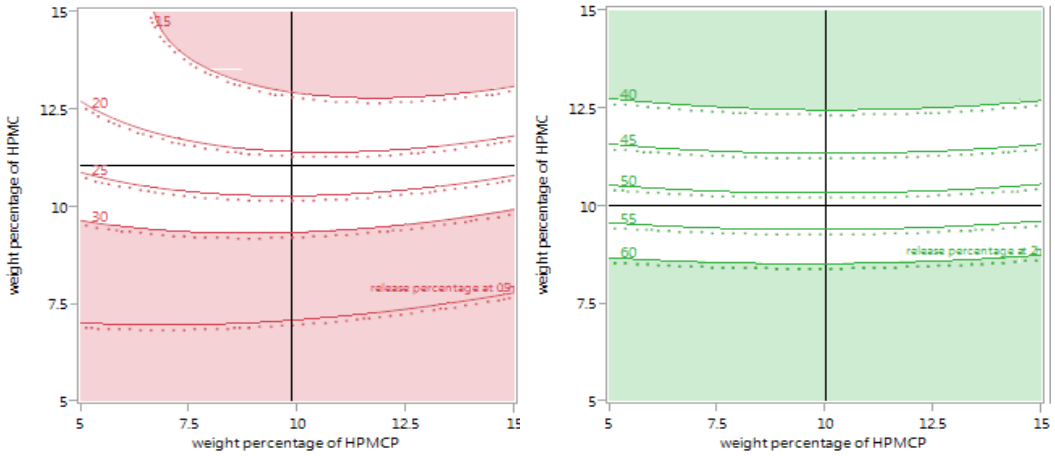

(a) (b)

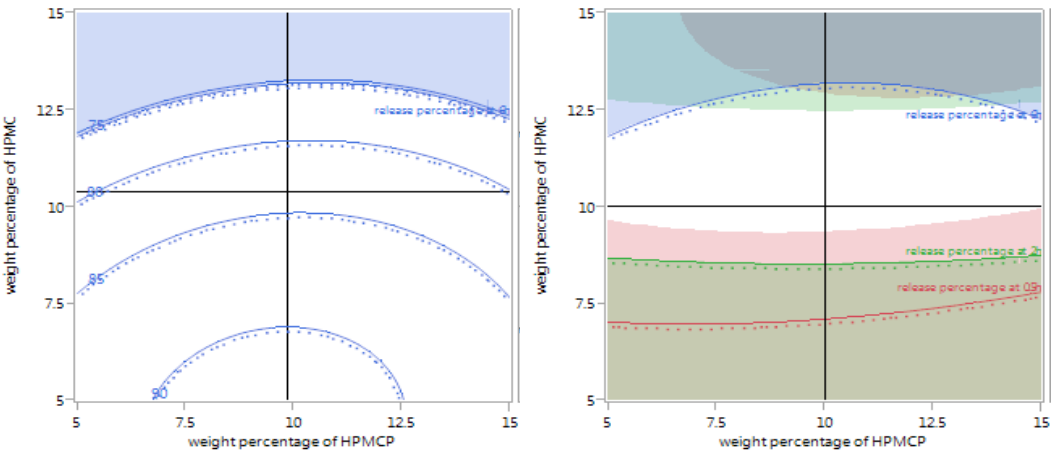

(c) (d)

Fig.8.4 Response contour plots showing the effect of weight percentages of HPMCP (X_1) and HPMC (X_2), (a) on the drug release percentage at 0.5 hours (Y_1) at a medium weight percentage of lactose (X_3); (b) on the drug release percentage at 2 hours (Y_2) at a medium weight percentage of lactose (X_3); (c) on the drug release percentage at 6 hours (Y_3) at a medium weight percentage of lactose (X_3); (d) on the drug release percentage at 0.5 hours (Y_1), 2 hours (Y_2) and 6 hours (Y_3) at a medium weight percentage of lactose (X_3).

The effect of the input variables on the output variable Y_1, Y_2 and Y_3 is summarised using a pareto chart and interaction plot in Figs.8.5–8.7. The interaction plots in Fig.8.5 show that, at a low and high level of weight percentage of HPMCP, the drug's release percentage at 0.5 hours decreased with an increase of the weight percentage of HPMC, and that the drug's release percentage at 0.5 hours remained constant with changes in the weight percentage of lactose. At a low HPMC weight percentage, the drug's release percentage at 0.5 hours increased slightly with an increase in HPMCP. At a high weight percentage of HPMC, however, the drug's release percentage at 0.5 hours was nearly constant. Its release percentage at 0.5 hours remained constant with changes in the weight percentage of lactose at both low and high levels of HPMC weight percentage. There was not much difference in the drug's release percentage at 0.5 hours, irrespective of lactose's weight percentage.

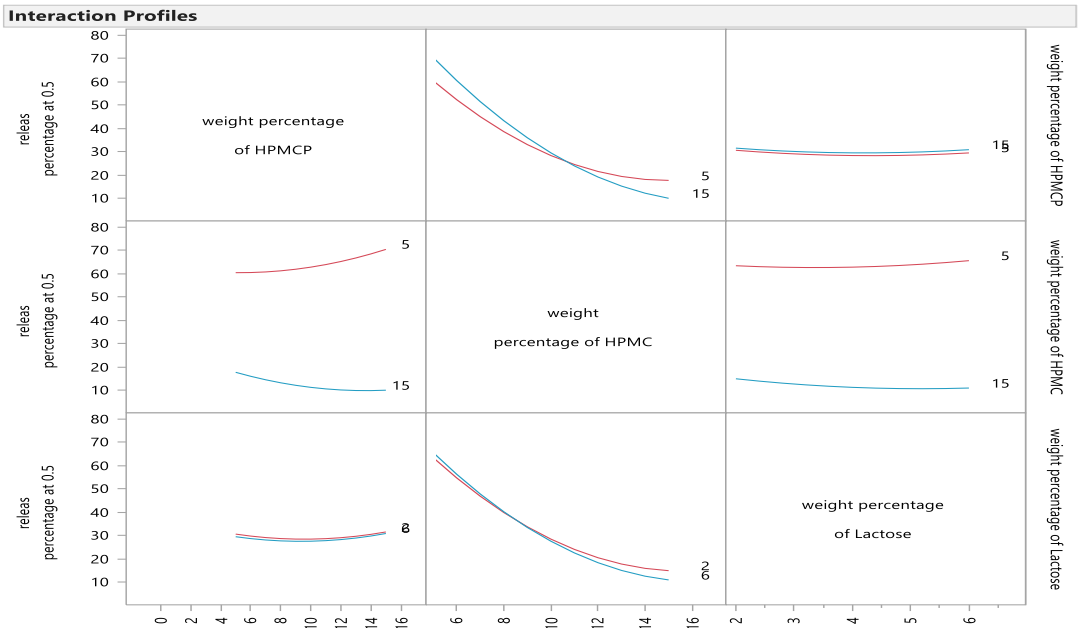

Fig.8.5 Interaction plot showing the quadratic effects on the interactions between factors on Y_1

As Fig.8.6 shows, at both low and high HPMCP weight percentages, the drug's release percentage at 2 hours remained nearly constant with increased HPMC, indicating that HPMCP was not the main influence on that percentage. At both high (15%) and low (5%) HPMCP weight percentages, the drug's release percentage at 2 hours increased slightly with an increase of lactose. At both low

and high HPMC weight percentages, there was not much difference in the drug's release percentage at 2 hours with increased HPMCP or lactose. At a high (6%) lactose weight percentage, the drug's release percentage at 2 hours increased slightly with an increase of HPMCP, while at a low level (2%), it decreased slightly with an increase in HPMCP. The figures for the drug's release percentage at 2 hours at both low and high lactose weight percentages were parallel, which indicates that lactose was the dissolution enhancer in the formulation.

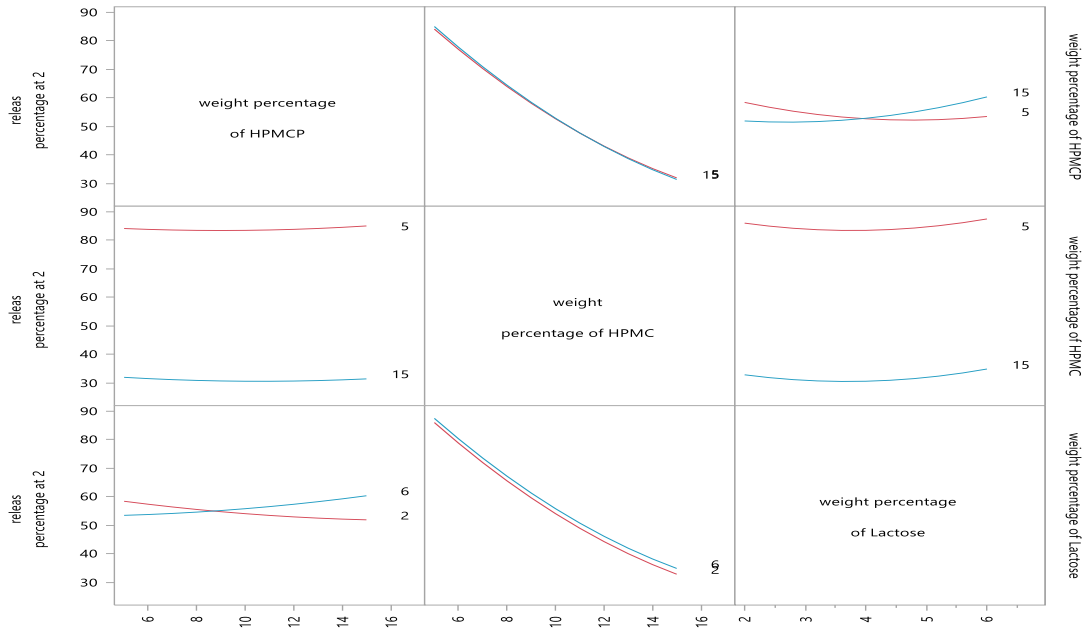

Fig.8.6 Interaction plot showing the quadratic effects on the interactions between factors on Y_2

Fig.8.7 shows that, at both low and high HPMCP weight percentages, the drug's release percentage at 6 hours was similar; it decreased with an increase in HPMC weight percentage. At a high HPMCP weight percentage, the drug's release percentage at 6 hours increased slightly with an increase of lactose, but remained constant at a low percentage. At both low and high HPMC weight percentages, the drug's release percentage at 6 hours remained largely unaffected by the change in either HPMCP or lactose, while at both low and high levels of lactose, the drug's release percentage at 6 hours increased slightly and then decreased with an increase in HPMCP. The drug's release percentage at 6 hours at both low and high lactose weight percentages were parallel, indicating that lactose was the dissolution enhancer in the formulation.

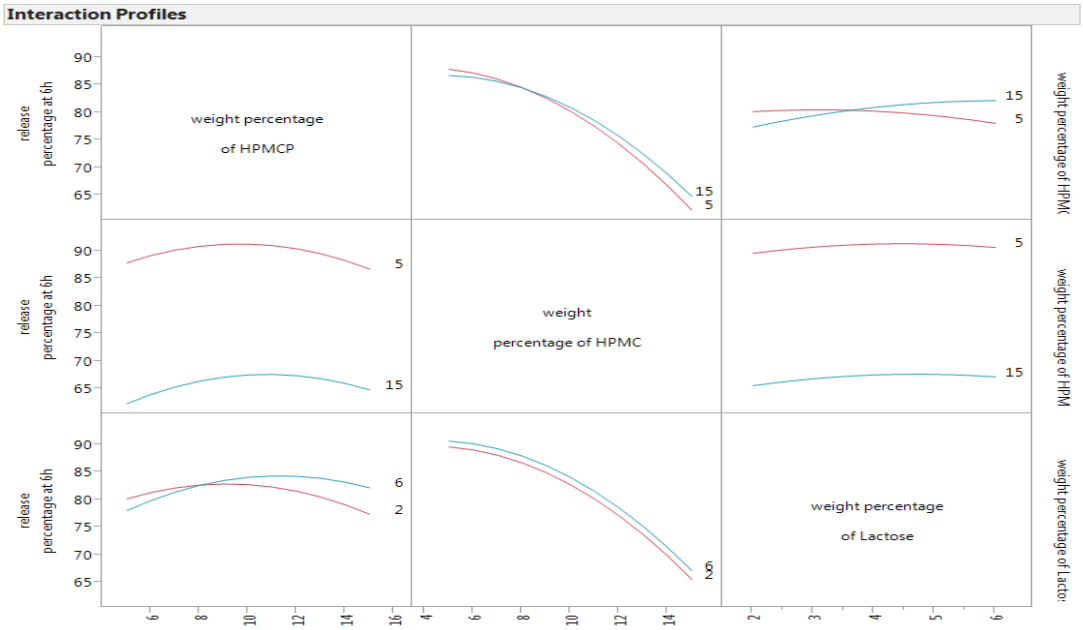

Fig.8.7 Interaction plot showing the quadratic effects on the interactions between factors on Y_3

8.7.3 Establishment and evaluation of the Design Space (DS)

Design Space (DS) is defined by ICH Q8 as "the multidimensional combination and interaction of input variables (material attributes) and process parameters that have been demonstrated to provide assurance of quality. Working within the design space is not considered as a change; however the movement out of the design space is considered a change and would normally initiate a regulatory post approval change process. Design space is proposed by the applicant and is subject to the regulatory assessment and approval" [67].

Based on the response surface models, a design space should define the ranges of the formulation, in which final tablet quality can be ensured. The objective of optimization is to maximize the range of input variables for meeting a goal. The desired response values were 15%<Y_1<30%, 40%<Y_2<60% and Y_3>75%. When lactose was at the medium level set for the experiment, Fig.8.4 (a), (b) and (c) show the proposed design space of Y_1, Y_2 and Y_3. As depicted in Fig.8.4(d), the blank region satisfied both 15%<Y_1<30%, 40%<Y_2<60% and Y_3>75%.

In order to evaluate the accuracy and robustness of the derived model, two further experiments were carried out with all three factors in the ranges of design space. Table 8.8 shows the three factors, the experimental and predicted values of all the response variables and their percentage errors. The results show that the prediction error between the experimental values of the responses and those of

the anticipated values was small. The prediction error varied between 1.74% and 4.46% for Y_1, 0.48% and 1.46% for Y_2 and 0.28% and 1.04% for Y_3.

Table 8.8 Confirmation tests

weight percentage of HPMCP,HPMC, lactose (X_1,X_2,X_3)	**Response variable**	**Experimental value (Y)**	**Model prediction value ($\widehat{Y}$)**	**Percentage of predication error $\frac{[Y-\hat{Y}]}{Y}$%**
(6%, 10.5%, 2%)	drug released % at 0.5 hours (Y_1)	28.35	27.86	1.74
	drug released % at 2 hours (Y_2)	54.02	54.81	1.46
	drug released % at 6 hours (Y_3)	79.82	80.05	0.28
(14%, 12%, 6%)	drug released % at 0.5 hours (Y_1)	20.12	19.22	4.46
	drug released % at 2 hours (Y_2)	49.26	49.50	0.48
	drug released % at 6 hours (Y_3)	78.83	78.01	1.04

8.8 Chapter conclusion

In this chapter, the influence factors of the HPMCP, HPMC and lactose weight percentages of the CBZ-NIC cocrystal sustained-release tablet formulation were studied using the Box-Behnken experimental design method. The results show that the level of HPMC (X_2) and (X_2^2) have a significant effect (P-value <0.05) on the drug's release percentage at 0.5 hours (Y_1), 2 hours (Y_2) and 6 hours (Y_3). The weight percentage of HPMC (X_2) has negative effects on the drug's release percentage at 0.5 hours, 2 hours and 6 hours. As expected, increasing HPMC's weight percentage resulted in a decrease in the drug's release percentage.

Different mathematical models were developed to predict the drug's release percentage at 0.5 hours, 2 hours and 6 hours. The validation of the mathematical model showed that the variation between experimental value and model prediction was from 1.74% to 4.46% for Y_1, 1.46% to 0.48% for Y_2 and 0.28% to1.04% for Y_3. The high degree of prediction obtained from validation experiments has demonstrated the reliability and effectiveness of the Box-Behnken experimental design method for the study of the CBZ sustained-release tablet.

Chapter 9 Conclusion and Future Work

This chapter summarizes the work and its main findings. The limitations of the research are briefly discussed, along with potential areas for further research.

9.1 Summary of the work

This research has investigated the effect of coformers and polymers on the phase transformation and release profiles of CBZ cocrystals, which can explain the mechanism by which CBZ cocrystals dissolve in polymer solutions and tablets.

The research commenced by reviewing some of the strategies to overcome poor water solubility. One of these, pharmaceutical cocrystals, was introduced in detail, including discussion of cocrystals design, formation and characterization methods, physicochemical properties, theoretical development on stability prediction and recent progress. Secondly, the formulation of tablets by the QbD method was introduced, and the drug delivery system-tablets and some definitions and basics of QbD were discussed. Finally, CBZ was briefly reviewed, a CBZ pharmaceutical cocrystal case study was presented and CBZ sustained/controlled release formulations were summarized.

This research subsequently studied the effects of polymer HPMC on the phase transformation and release profiles of CBZ-NIC cocrystals. Solution-mediated phase transformation of CBZ-NIC cocrystals, which could greatly reduce the enhancement of its apparent solubility, was discussed in this part of the research.

The effect of coformers on the phase transformation and release profiles of CBZ-SAC and CBZ-CIN cocrystals in HPMC-based matrix tablets were further investigated.

The polymer screening method was used to determine the polymers of HPMCAS, PVP, PEG that optimize the extent and stability supersaturation of CBZ cocrystals in solution. By comparing the behaviour of cocrystals with that of physical mixtures or the pure parent drug, the role of polymers in solution and tablet-based cocrystal formulations was investigated.

This research finally studied the QbD approach to developing a CBZ-NIC cocrystal formulation that ensures the quality, safety and efficacy of CBZ sustained release tablets.

9.2 Conclusions

This thesis investigated the effect of coformers and polymers on the phase transformation and release profiles of CBZ cocrystals in solution and in tablets, which can provide a comprehensive understanding of the mechanisms for phase transformation of CBZ cocrystals.

The influence of HPMC on the phase transformation and release profiles of CBZ-NIC cocrystals in solution and in sustained release matrix tablets was investigated. The results indicate that HPMC cannot inhibit the transformation of CBZ-NIC cocrystals to CBZ DH in solution or in the gel layer of the matrix, as opposed to its ability to inhibit CBZ III phase transition to CBZ DH. HPMC's inability to inhibit CBZ dihydrate during CBZ-NIC cocrystal dissolution is caused by the rate differences between CBZ-NIC cocrystal dissolution and formation of a CBZ-HPMC soluble complex in solution.

The influence of HPMC on the phase transformation and release profiles of CBZ-SAC and CBZ-CIN cocrystals in solution and in sustained release matrix tablets was also investigated, the finding being that the selection of different coformers of SAC and CIN affects the stability of the cocrystals in solution, resulting in significant differences in the apparent solubility of CBZ in solution. The dissolution advantage of CBZ-SAC cocrystals only lasts for a short period because of the speed of its conversion to its dihydrate form. HPMC can to some degree inhibit the crystallisation of CBZ DH during dissolution of CBZ-SAC cocrystals. By contrast, the improved dissolution rate of CBZ-CIN cocrystals can be realised in both solution and formulation due to their stability.

The influence of three polymers, HPMCAS, PVP and PEG, on the phase transformation of the three CBZ cocrystals CBZ-NIC, CBZ-SAC and CBZ-CIN in solution and tablet based formulations was also investigated. The study has shown that when HPMCAS with a concentration of 2 mg/ml or higher was pre-dissolved in solution, both CBZ-SAC and CBZ-CIN cocrystals can generate significantly higher CBZ supersaturated solutions with an increase of around three times the solubility of CBZ III, which can be sustained for more than 24 hours. All three cocrystals showed at least a two-fold increase in drug release compared with that of CBZ III in pH 6.8 PBS in the absence of a polymer at five minutes. These results demonstrate that cocrystals can be easily formulated through a simple solution formulation or powder formulation to generate a supersaturated concentration and faster dissolution rates to overcome those drugs with solubility- and/or dissolution-limited bioavailability.

The CBZ-NIC cocrystal sustained release tablets were developed using the QbD method. Different mathematical models were developed to predict the drug release percentage at 0.5 hours, 2 hours and 6 hours. A high degree of predictiveness was obtained from validation experiments, demonstrating the reliability and effectiveness of QbD method in studying the CBZ sustained release tablet.

9.3 Future work

Future research into pharmaceutical cocrystals in the author's laboratory will focus on preparation scale-up, a large amount of polymer screening and formulation, and the use of FTIR or Raman spectroscopy to characterize polymer-cocrystal and polymer-API interactions in solution.

Although cocrystals can offer the advantage of providing a higher dissolution rate and greater apparent solubility to improve the bioavailability of a poorly water-soluble drug, a key limitation is that a stable form of the drug can be recrystallized during dissolution. The selection of both the cocrystal form and the excipients in formulations to maximise the benefit is an important part of successful product development. To achieve the target, it will first be necessary to scale up cocrystal preparation. The amount of cocrystal needed in the research, especially in the formulation study, is large, which makes it difficult to provide by slow evaporation and reaction crystallisation methods.

More work on cocrystal formulation is then required. The recognition and adoption of cocrystals as an alternative formulation strategies for drugs' low bioavailability faces several obstacles. More laboratory work should be done on long-term stability, coformer toxicity and regulatory issues. In particular, *in vivo* experiments should be done to demonstrate the cocrystals' performance is comparable to other approaches. The author hopes to develop different cocrystal formulations such as solutions, immediate-release tablets or capsules and sustained-release tablets or capsules. In addition, the investigation of the *in vitro-in vivo correlation* (IVIVC) should be studied.

There is still much to learn about how crystals actually grow: it is not clear how they change from a liquid to a solid state. This process is called "nucleation". It is the first step in crystallisation, determining whether a crystal can form from a liquid state. Even though the present study has used sufficient instrumentation techniques, however, the mechanism by which polymers affect the phase transformation of cocrystals is based on the assumption of existing "API-polymer" or "cocrystal-polymer" complexes for which there is no direct experimental evidence. Developments in advanced

techniques such as FT-Raman microscopy should be used to provide insight into how molecules interact in solution and ultimately form crystals.

The powder-stir method was used to investigate the powder dissolution rate of CBZ-SAC and CBZ-CIN cocrystals. Even before experiments were conducted, all the powders were lightly ground and sieved through a 60 mesh sieve in order to reduce the effect of particle size on dissolution rates. This rate still depended on particle size. A rotating disk IDR apparatus, monitored in real time by an *in situ* dip-probe fiber optic UV method, could be used in future to investigate the powder dissolution rate. It would reduce the effects of particle size by supporting a constant surface area while requiring a much smaller sample size. Further advantages of this method are that any polymorph changes during dissolution can be recognized, and the longer incubation time needed to establish the true equilibrium of the most stable form of a solid may become evident in the dissolution curve.

REFERENCES

1. Qiao, N., et al., *Pharmaceutical cocrystals: an overview.* International Journal of Pharmaceutics, 2011. **419**(1): p. 1-11.
2. PhRMA. *Pharmaceutical Industry Profile 2006*. 2006. Washington,DC.
3. Thakuria, R., et al., *Pharmaceutical cocrystals and poorly soluble drugs.* International Journal of Pharmaceutics, 2013. **453**(1): p. 101-125.
4. Lu, J. and S. Rohani, *Preparation and characterization of theophylline− nicotinamide cocrystal.* Organic Process Research & Development, 2009. **13**(6): p. 1269-1275.
5. Blagden, N., S.J. Coles, and D.J. Berry, *Pharmaceutical co-crystals – are we there yet?* CrystEngComm, 2014. **16**: p. 5753-5761.
6. Cheney, M.L., et al., *Coformer selection in pharmaceutical cocrystal development: A case study of a meloxicam aspirin cocrystal that exhibits enhanced solubility and pharmacokinetics.* Journal of pharmaceutical sciences, 2011. **100**(6): p. 2172-2181.
7. Gao, Y., et al., *Coformer selection based on degradation pathway of drugs: A case study of adefovir dipivoxil–saccharin and adefovir dipivoxil–nicotinamide cocrystals.* International Journal of Pharmaceutics, 2012. **438**(1–2): p. 327-335.
8. Qiao, N., et al., *In situ monitoring of carbamazepine-nicotinamide cocrystal intrinsic dissolution behaviour.* European Journal of Pharmaceutics and Biopharmaceutics, 2013. **83**(3): p. 415-426.
9. Good, D.J. and N.r. Rodríguez-Hornedo, *Solubility advantage of pharmaceutical cocrystals.* Crystal Growth and Design, 2009. **9**(5): p. 2252-2264.
10. Takagi, T., et al., *A Provisional Biopharmaceutical Classification of the Top 200 Oral Drug Products in the United States, Great Britain, Spain, and Japan.* Mol Pharm, 2006. **3**(6): p. 631-643.
11. Yu, L.X., *Pharmaceutical Quality by Design: Product and Process Development, Understanding, and Control.* Pharmaceutical Research, 2008. **25**(4): p. 781-791.
12. Wells, J.I., *Pharmaceutical preformulation : the physicochemical properties of drug substances*1988.
13. *Guidance for Industry ANDAs: Pharmaceutical Solid Polymorphism Chemistry, Manufacturing, and Controls Information*, FDA, Editor 2007. p. 1-13.
14. Aulton, M.E., ed. *Pharmaceutics:The science of dosage form design*. 1998.
15. Hauss, D.J., *Oral lipid-based formulations.* Advanced Drug Delivery Reviews, 2007. **59**(7): p. 667-676.
16. Testa, B., *Prodrug research: futile or fertile?* Biochemical pharmacology, 2004. **68**(11): p. 2097-2106.
17. Stella, V.J. and K.W. Nti-Addae, *Prodrug strategies to overcome poor water solubility.* Advanced Drug Delivery Reviews, 2007. **59**(7): p. 677–694.
18. Stella, V.J. and K.W. Nti-Addae, *Prodrug strategies to overcome poor water solubility.* Advanced Drug Delivery Reviews, 2007. **59**(7): p. 677-694.
19. Y.sohma, Y.H., T.Ito,H.Matsumoto,T.Kimura,Y.Kiso, *Development of water-soluble prodrug of the HIV-1 protease inhibitor KNI-727:importance of the conversion time for higher gastrointestinal absorption of prodrugs based on spontaneous chemical cleavage.* J.Med.Chem, 2003. **46**(19): p. 4124-4135.
20. P.Vierling, J.G., *Prodrugs of HIV protease inhibitors.* Curr.Pharm.Des., 2003. **9**(22): p. 1755-1770.
21. C.Falcoz, J.M.J., C.Bye,T.C.Hardman,K.B.Kenney,S.Studenberg,H.Fuder,W.T.Prince, *Pharmacokinetics of GW433908,a prodrug of amprenavir,in healthy male volunteers.* J.Clin.Pharmacol., 2002. **42**(8): p. 887-898.
22. J.Brouwers, J.T., P.Augustijins, *In vitro behavior of a phosphate ester prodrug of amprenavir in human intestinal fluids and in the caco-2 system:Illustration of intraluminal supersaturation.* Int.J.Pharm., 2007. **366**(2): p. 302-309.
23. Childs, S.L., G.P. Stahly, and A. Park, *The salt-cocrystal continuum: the influence of crystal structure on ionization state.* Molecular Pharmaceutics, 2007. **4**(3): p. 323-338.

24. Kawabata, Y., et al., *Formulation design for poorly water-soluble drugs based on biopharmaceutics classification system: Basic approaches and practical applications.* International Journal of Pharmaceutics, 2011. **420**(1): p. 1-10.
25. Blagden, N., S.J. Coles, and D.J. Berry, *Pharmaceutical co-crystals - are we there yet?* CrystEngComm, 2014. **16**(26): p. 5753-5761.
26. Blagden, N., et al., *Crystal engineering of active pharmaceutical ingredients to improve solubility and dissolution rates.* Advanced Drug Delivery Reviews, 2007. **59**(7): p. 617-630.
27. Kesisoglou, F., S. Panmai, and Y. Wu, *Nanosizing—oral formulation development and biopharmaceutical evaluation.* Advanced Drug Delivery Reviews, 2007. **59**(7): p. 631-644.
28. Patravale, V. and R. Kulkarni, *Nanosuspensions: a promising drug delivery strategy.* Journal of Pharmacy and Pharmacology, 2004. **56**(7): p. 827-840.
29. Xia, D., et al., *Effect of crystal size on the in vitro dissolution and oral absorption of nitrendipine in rats.* Pharmaceutical Research, 2010. **27**(9): p. 1965-1976.
30. Brewster, M.E. and T. Loftsson, *Cyclodextrins as pharmaceutical solubilizers.* Advanced Drug Delivery Reviews, 2007. **59**(7): p. 645-666.
31. Aakeroy, C.B. and D.J. Salmon, *Building co-crystals with molecular sense and supramolecular sensibility.* CrystEngComm, 2005. **7**(72): p. 439-448.
32. Bethune, S.J., *Thermodynamic and kinetic parameters that explain crystallization and solubility of pharmaceutical cocrystals*2009: ProQuest.
33. Musumeci, D., et al., *Virtual cocrystal screening.* Chemical Science, 2011. **5**(5): p. 883-890.
34. Delori, A., T. Friscic, and W. Jones, *The role of mechanochemistry and supramolecular design in the development of pharmaceutical materials.* CrystEngComm, 2012. **14**(7): p. 2350-2362.
35. Gad, S.C., *Preclinical development handbook ; ADME and biopharmaceutical properties.* Preclinical development handbook ; ADME and biopharmaceutical properties, 2008.
36. Zaworotko, M. *Polymorphism in co-crystals and pharmacuetical cocrystals*. in *XX Congress of the International Union of Crystallography, Florence*. 2005.
37. Rodríguez-Hornedo, N., et al., *Reaction crystallization of pharmaceutical molecular complexes.* Molecular Pharmaceutics, 2006. **3**(3): p. 362-367.
38. Patil, A., D. Curtin, and I. Paul, *Solid-state formation of quinhydrones from their components. Use of solid-solid reactions to prepare compounds not accessible from solution.* Journal of the American Chemical Society, 1984. **106**(2): p. 348-353.
39. Pedireddi, V.R., et al., *Creation of crystalline supramolecular arrays: a comparison of co-crystal formation from solution and by solid-state grinding.* Chemical Communications, 1996(8): p. 987-988.
40. Brown, M.E., et al., *Superstructure Topologies and Host–Guest Interactions in Commensurate Inclusion Compounds of Urea with Bis(methyl ketone)s.* Chemistry of Materials, 1996. **8**(8): p. 1588-1591.
41. Friščić, T., et al., *Screening for Inclusion Compounds and Systematic Construction of Three-Component Solids by Liquid-Assisted Grinding.* Angewandte Chemie, 2006. **118**(45): p. 7708-7712.
42. Shikhar, A., et al., *Formulation development of Carbamazepine–Nicotinamide co-crystals complexed with γ-cyclodextrin using supercritical fluid process.* The Journal of Supercritical Fluids, 2011. **55**(3): p. 1070-1078.
43. Lehmann, O., *Molekular Physik, Vol. 1.* Engelmann, Leipzig, 1888: p. 193.
44. Kofler, L. and A. Kofler, *Thermal Micromethods for the Study of Organic Compounds and Their Mixtures, Wagner, Innsbruck (1952), translated by McCrone, WC; McCrone Research Institute: Chicago, 1980.*
45. Berry, D.J., et al., *Applying hot-stage microscopy to co-crystal screening: a study of nicotinamide with seven active pharmaceutical ingredients.* Crystal Growth and Design, 2008. **8**(5): p. 1697-1712.
46. Zhang, G.G., et al., *Efficient co‐crystal screening using solution‐mediated phase transformation.* Journal of Pharmaceutical Sciences, 2007. **96**(5): p. 990-995.

47. Takata, N., et al., *Cocrystal screening of stanolone and mestanolone using slurry crystallization.* Crystal Growth and Design, 2008. **8**(8): p. 3032-3037.
48. Blagden, N., et al., *Current directions in co-crystal growth.* New Journal of Chemistry, 2008. **32**(10): p. 1659-1672.
49. Stanton, M.K. and A. Bak, *Physicochemical Properties of Pharmaceutical Co-Crystals: A Case Study of Ten AMG 517 Co-Crystals.* Crystal Growth & Design, 2008. **8**(10): p. 3856-3862.
50. Spong, B.R., *Enhancing the pharmaceutical behavior of poorly soluble drugs through the formation of cocrystals and mesophases*, 2005, University of Michigan.
51. Good, D.J. and N. Rodríguez-Hornedo, *Cocrystal eutectic constants and prediction of solubility behavior.* Crystal Growth & Design, 2010. **10**(3): p. 1028-1032.
52. Grzesiak, A.L., et al., *Comparison of the four anhydrous polymorphs of carbamazepine and the crystal structure of form I.* Journal of Pharmaceutical Sciences, 2003. **92**(11): p. 2260-2271.
53. Greco, K. and R. Bogner, *Solution‐mediated phase transformation: Significance during dissolution and implications for bioavailability.* Journal of Pharmaceutical Sciences, 2012. **101**(9): p. 2996-3018.
54. Greco, K., D.P. Mcnamara, and R. Bogner, *Solution‐mediated phase transformation of salts during dissolution: Investigation using haloperidol as a model drug.* Journal of pharmaceutical sciences, 2011. **100**(7): p. 2755-2768.
55. Kobayashi, Y., et al., *Physicochemical properties and bioavailability of carbamazepine polymorphs and dihydrate.* International Journal of Pharmaceutics, 2000. **193**(2): p. 137-146.
56. Konno, H., et al., *Effect of polymer type on the dissolution profile of amorphous solid dispersions containing felodipine.* European journal of pharmaceutics and biopharmaceutics, 2008. **70**(2): p. 493-499.
57. Davey, R.J., et al., *Rate controlling processes in solvent-mediated phase transformations.* Journal of Crystal Growth, 1986. **79**(1–3, Part 2): p. 648-653.
58. Alhalaweh, A., H.R.H. Ali, and S.P. Velaga, *Effects of polymer and surfactant on the dissolution and transformation profiles of cocrystals in aqueous media.* Crystal Growth & Design, 2013.
59. Surikutchi, B.T., et al., *Drug-excipient behavior in polymeric amorphous solid dispersions.* Journal of Excipients and Food Chemicals, 2013. **4**(3): p. 70-94.
60. Wikström, H., W.J. Carroll, and L.S. Taylor, *Manipulating theophylline monohydrate formation during high-shear wet granulation through improved understanding of the role of pharmaceutical excipients.* Pharmaceutical Research, 2008. **25**(4): p. 923-935.
61. Alhalaweh, A., H.R.H. Ali, and S.P. Velaga, *Effects of Polymer and Surfactant on the Dissolution and Transformation Profiles of Cocrystals in Aqueous Media.* Crystal Growth & Design, 2013. **14**(2): p. 643-648.
62. Fedotov, A.P., et al., *The effects of tableting with potassium bromide on the infrared absorption spectra of indomethacin.* Pharmaceutical Chemistry Journal, 2009. **43**(1): p. 68-70.
63. Lourenço, V., et al., *A quality by design study applied to an industrial pharmaceutical fluid bed granulation.* European Journal of Pharmaceutics and Biopharmaceutics, 2012. **81**(2): p. 438-447.
64. Dickinson, P.A., et al., *Clinical relevance of dissolution testing in quality by design.* The AAPS journal, 2008. **10**(2): p. 380-390.
65. Nadpara, N.P., et al., *QUALITY BY DESIGN (QBD): A COMPLETE REVIEW.* International Journal of Pharmaceutical Sciences Review & Research, 2012. **17**(2).
66. Guideline, I.H.T., *Pharmaceutical development.* Q8 (2R). As revised in August, 2009.
67. Guideline, I.H.T., *Pharmaceutical development Q8.* Current Step, 2005. **4**: p. 11.
68. Fegadea, R. and V. Patelb, *Unbalanced Response and Design Optimization of Rotor by ANSYS and Design Of Experiments.*
69. *Design of Experiments*. Available from: http://www.qualitytrainingportal.com/newsletters/nl0207.htm.
70. *FULL FACTORIAL DESIGNS*. Available from: http://www.jmp.com/support/help/Full_Factorial_Designs.shtml.

71. *Response Surface Designs*. Available from: http://www.jmp.com/support/help/Response_Surface_Designs.shtml#67894.
72. Liu, H., *Modeling and Control of Batch Pulsed Top-spray Fluidized bed Granulation*, 2014, De Montfort University: Leicester.
73. Zidan, A.S., et al., *Quality by design: Understanding the formulation variables of a cyclosporine A self-nanoemulsified drug delivery systems by Box-Behnken design and desirability function.* International Journal of Pharmaceutics, 2007. **332**(1&2): p. 55-63.
74. Govender, S., et al., *Optimisation and characterisation of bioadhesive controlled release tetracycline microspheres.* International Journal of Pharmaceutics, 2005. **306**(1&2): p. 24-40.
75. Schindler, W. and F. Häfliger, *Über derivate des iminodibenzyls.* Helvetica Chimica Acta, 1954. **37**(2): p. 472-483.
76. Rustichelli, C., et al., *Solid-state study of polymorphic drugs: carbamazepine.* Journal of Pharmaceutical and Biomedical Analysis, 2000. **23**(1): p. 41-54.
77. Kaneniwa, N., et al., *[Dissolution behaviour of carbamazepine polymorphs].* Yakugaku zasshi: Journal of the Pharmaceutical Society of Japan, 1987. **107**(10): p. 808-813.
78. Bernstein, J., et al., *Patterns in Hydrogen Bonding: Functionality and Graph Set Analysis in Crystals 69.* Angewandte Chemie International Edition, 1995. **34**(15): p. 1555–1573.
79. Brittain, H.G., *Pharmaceutical cocrystals: The coming wave of new drug substances.* Journal of Pharmaceutical Sciences, 2013. **102**(2): p. 311-317.
80. Sethia, S. and E. Squillante, *Solid dispersion of carbamazepine in PVP K30 by conventional solvent evaporation and supercritical methods.* International Journal of Pharmaceutics, 2004. **272**(1): p. 1-10.
81. Bettini, R., et al., *Solubility and conversion of carbamazepine polymorphs in supercritical carbon dioxide.* European Journal of Pharmaceutical Sciences, 2001. **13**(3): p. 281-286.
82. Qu, H., M. Louhi-Kultanen, and J. Kallas, *Solubility and stability of anhydrate/hydrate in solvent mixtures.* International Journal of Pharmaceutics, 2006. **321**(1): p. 101-107.
83. Childs, S.L., et al., *Analysis of 50 Crystal Structures Containing Carbamazepine Using the Materials Module of Mercury CSD.* Crystal Growth & Design, 2009. **9**(4): p. 1869-1888.
84. Fleischman, S.G., et al., *Crystal Engineering of the Composition of Pharmaceutical Phases: Multiple-Component Crystalline Solids Involving Carbamazepine.* Crystal Growth & Design, 2003. **3**(6): p. 909-919.
85. Gelbrich, T. and M.B. Hursthouse, *Systematic investigation of the relationships between 25 crystal structures containing the carbamazepine molecule or a close analogue: a case study of the XPac method.* CrystEngComm, 2006. **8**(6): p. 448-460.
86. Johnston, A., A. Florence, and A. Kennedy, *Carbamazepine furfural hemisolvate.* Acta Crystallographica Section E: Structure Reports Online, 2005. **61**(6): p. o1777-o1779.
87. Fernandes, P., et al., *Carbamazepine trifluoroacetic acid solvate.* Acta Crystallographica Section E: Structure Reports Online, 2007. **63**(11): p. o4269-o4269.
88. Florence, A.J., et al., *Control and prediction of packing motifs: a rare occurrence of carbamazepine in a catemeric configuration.* CrystEngComm, 2006. **8**(10): p. 746-747.
89. Johnston, A., A.J. Florence, and A.R. Kennedy, *Carbamazepine N, N-dimethylformamide solvate.* Acta Crystallographica Section E: Structure Reports Online, 2005. **61**(5): p. o1509-o1511.
90. Lohani, S., et al., *Carbamazepine-2, 2, 2-trifluoroethanol (1/1).* Acta Crystallographica Section E: Structure Reports Online, 2005. **61**(5): p. o1310-o1312.
91. Vishweshwar, P., et al., *The Predictably Elusive Form II of Aspirin.* Journal of the American Chemical Society, 2005. **127**(48): p. 16802-16803.
92. Babu, N.J., L.S. Reddy, and A. Nangia, *Amide−N-Oxide Heterosynthon and Amide Dimer Homosynthon in Cocrystals of Carboxamide Drugs and Pyridine N-Oxides.* Molecular Pharmaceutics, 2007. **4**(3): p. 417-434.

93. Reck, G. and W. Thiel, *Crystal-structures of the adducts carbamazepine-ammonium chloride and carbamazepine-ammonium bromide and their transformation in carbamazepine dihydrate.* Pharmazie, 1991. **46**(7): p. 509-512.
94. McMahon, J.A., et al., *Crystal engineering of the composition of pharmaceutical phases. 3. Primary amide supramolecular heterosynthons and their role in the design of pharmaceutical co-crystals.* Zeitschrift für Kristallographie, 2005. **220**(4/2005): p. 340-350.
95. Johnston, A., et al., *Targeted crystallisation of novel carbamazepine solvates based on a retrospective Random Forest classification.* CrystEngComm, 2008. **10**(1): p. 23-25.
96. Lu, E., N. Rodríguez-Hornedo, and R. Suryanarayanan, *A rapid thermal method for cocrystal screening.* CrystEngComm, 2008. **10**(6): p. 665-668.
97. Rahman, Z., et al., *Physico-mechanical and stability evaluation of carbamazepine cocrystal with nicotinamide.* AAPS PharmSciTech, 2011. **12**(2): p. 693-704.
98. Weyna, D.R., et al., *Synthesis and structural characterization of cocrystals and pharmaceutical cocrystals: mechanochemistry vs slow evaporation from solution.* Crystal Growth and Design, 2009. **9**(2): p. 1106-1123.
99. Katzhendler, I. and M. Friedman, *Zero-order sustained release matrix tablet formulations of carbamazepine*, 1999, Patents.
100. Rujivipat, S. and R. Bodmeier, *Modified release from hydroxypropyl methylcellulose compression-coated tablets.* International Journal of Pharmaceutics, 2010. **402**(1): p. 72-77.
101. Koparkar, A.D. and S.B. Shah, *Core of carbamazepine, crystal habit modifiers, hydroxyalkyl c celluloses, sugar alcohol, and mono- or disacdaride, semipermeable wall and hole in wall*, 1994, Patents.
102. Kesarwani, A., et al., *Multiple unit modified release compositions of carbamazepine and process for their preparation*, 2007, Patents.
103. BARABDE, U.V., R.K. Verma, and R.S. Raghuvanshi, *Carbamazepine formulations*, 2009, Patents.
104. Jian-Hwa, G., *Controlled release solid dosage carbamazepine formulations*, 2003, Google Patents.
105. Licht, D., et al., *Sustained release formulation of carbamazepine*, 2000, Google Patents.
106. Barakat, N.S., I.M. Elbagory, and A.S. Almurshedi, *Controlled-release carbamazepine matrix granules and tablets comprising lipophilic and hydrophilic components.* Drug delivery, 2009. **16**(1): p. 57-65.
107. Mohammed, F.A. and A.Arunachalam, *Formulation and evaluation of carbamazepine extended release tablets usp 200mg.* International Journal of Biological & Pharmaceutical Research, 2012. **3**(1): p. 145-153.
108. Miroshnyk, I., S. Mirz, and N. Sandler, *Pharmaceutical co-crystals-an opportunity for drug product enhancement.* Expert Opinion on Drug Delivery, 2009. **6**(4): p. 333-41.
109. Rahman, Z., et al., *Physicochemical and mechanical properties of carbamazepine cocrystals with saccharin.* Pharmaceutical development and technology, 2012. **17**(4): p. 457-465.
110. Basavoju, S., D. Boström, and S.P. Velaga, *Indomethacin–saccharin cocrystal: design, synthesis and preliminary pharmaceutical characterization.* Pharmaceutical Research, 2008. **25**(3): p. 530-541.
111. Aitipamula, S., P.S. Chow, and R.B. Tan, *Dimorphs of a 1: 1 cocrystal of ethenzamide and saccharin: solid-state grinding methods result in metastable polymorph.* CrystEngComm, 2009. **11**(5): p. 889-895.
112. JA, M., *Crystal Engineering of Novel Pharmaceutical Forms*, in *Department of Chemistry*2006, Univeristy of South Florida, USA.
113. Kalinowska, M., R. Świsłocka, and W. Lewandowski, *The spectroscopic (FT-IR, FT-Raman and ^{1}H, ^{13}C NMR) and theoretical studies of cinnamic acid and alkali metal cinnamates.* Journal of molecular structure, 2007. **834**: p. 572-580.
114. Shayanfar, A., K. Asadpour-Zeynali, and A. Jouyban, *Solubility and dissolution rate of a carbamazepine–cinnamic acid cocrystal.* Journal of Molecular Liquids, 2013. **187**: p. 171-176.
115. *Using METHOCEL Cellulose Ethers for Controlled Release of Drugs in Hydrophilic Matrix Systems*. Available from:

http://www.colorcon.com/literature/marketing/mr/Extended%20Release/METHOCEL/English/hydroph_matrix_broch.pdf.
116. *Hypromellose Acetate Succinate Shin-Etsu AQOAT*. Available from: http://www.elementoorganika.ru/files/aqoat.
117. *Pharmaceutical Excipients Guide to Applications*. Available from: http://www.rwunwin.co.uk/excipients.aspx.
118. *CARBOWAXPolyethylene Glycol (PEG) 4000*. Available from: http://msdssearch.dow.com/PublishedLiteratureDOWCOM/dh_0887/0901b80380887910.pdf?filepath=polyglycols/pdfs/noreg/118-01804.pdf&fromPage=GetDoc.
119. *PVP Popyvinylpyrrolidong polymers*. Available from: http://www.brenntagspecialties.com/en/downloads/Products/Multi_Market_Principals/Ashland/PVP_-_PVP_VA/PVP_Brochure.pdf.
120. Mccreery, R.L., *Raman Spectroscopy for Chemical Analysis.* Measurement Science & Technology, 2001. **12**.
121. Qiao, N., *Investigation of carbamazepine-nicotinamide cocrystal solubility and dissolution by a UV imaging system.* De Montfort University, 2014.
122. Lacey, A.A., D.M. Price, and M. Reading, *Theory and Practice of Modulated Temperature Differential Scanning Calorimetry.* Hot Topics in Thermal Analysis & Calorimetry, 2006. **6**: p. 1-81.
123. Gaffney, J.S., N.A. Marley, and D.E. Jones, *Fourier Transform Infrared (FTIR) Spectroscopy*2012: John Wiley & Sons, Inc. 145–178.
124. Flower, D.R., et al., *High-throughput X-ray crystallography for drug discovery.* Current Opinion in Pharmacology, 2004. **4**(5): p. 490–496.
125. Bragg, L., *X-ray crystallography. Scientific American.* Acta Crystallographica, 1968. **54**(6-1): p. 772–778.
126. Gerber, C., et al., *Scanning tunneling microscope combined with a scanning electron microscope*1993: Springer Netherlands. 79-82.
127. Foschiera, J.L., T.M. Pizzolato, and E.V. Benvenutti, *FTIR thermal analysis on organofunctionalized silica gel.* Journal of the Brazilian Chemical Society, 2001. **12**.
128. Boetker, J.P., et al., *Insights into the early dissolution events of amlodipine using UV imaging and Raman spectroscopy.* Molecular pharmaceutics, 2011. **8**(4): p. 1372-1380.
129. Gordon, M.S., *Process considerations in reducing tablet friability and their effect on in vitro dissolution.* Drug development and industrial pharmacy, 1994. **20**(1): p. 11-29.
130. *Brithish Pharmacopeia. Volume V. Appendix I D. Buffer solutions*. Vol. V. 2010.
131. Daimay, L.V., ed. *Handbook of infrared and raman charactedristic frequencies of organic molecules.* 1991, Academic Press: Boston.
132. Qiao, N., et al., *In Situ Monitoring of Carbamazepine - Nicotinamide Cocrystal Intrinsic Dissolution Behaviour.* European Journal of Pharmaceutics and Biopharmaceutics, (0).
133. Bhatt, P.M., et al., *Saccharin as a salt former. Enhanced solubilities of saccharinates of active pharmaceutical ingredients.* Chemical Communications, 2005(8): p. 1073-1075.
134. Rahman, Z., Samy, R.,Sayeed, V.A.,and Khan, M.A., *Physicochemical and mechanical properties of carbamazepine cocrystals with saccharin.* Pharmaceutical Development &Technology, 2012. **17**(4): p. 457-465.
135. Y., H., *The infrared and Raman spectra of phthalimide,N-D-phthalimide and potassium phthalimide.* J Mol Struct, 1978. **48**: p. 33-42.
136. LI Runyan, C.H., MAO Huilin, GONG Junbo, *Study on preparation and analysis of carbamazepine-saccharin cocrystal.* Highlights of Sciencepaper Online, 2011. **4**(7): p. 667-672.
137. Hanai, K., et al., *A comparative vibrational and NMR study of cis-cinnamic acid polymorphs and trans-cinnamic acid.* Spectrochimica Acta Part A: Molecular and Biomolecular Spectroscopy, 2001. **57**(3): p. 513-519.
138. Jennifer M.M., M.P., Hopkinton,MA.,Michael J.Z.,Tampa,FL.,Tanise S.,Sunrise, FL.,Magali B.H.,Medford, MA., *PHARMACETUCAIL CO-CRYSTAL COMPOSITIONS AND RELATED METHODS OF*

USE, 2010, Transform Pharmaceuticals, Inc.,Lexington, MA(US);University of South Florida, Tampa,FL(US).

139. Basavoju, S., D. Bostrom, and S.P. Velaga, *Indomethacin-saccharin cocrystal: design, synthesis and preliminary pharmaceutical characterization.* Pharmaceutical Research, 2008. **25**(3): p. 530-541.
140. Liu, X., et al., *Improving the chemical stability of amorphous solid dispersion with cocrystal technique by hot melt extrusion.* Pharmaceutical Research, 2012. **29**(3): p. 806-817.
141. Lehto, P., et al., *Solvent-mediated solid phase transformations of carbamazepine: Effects of simulated intestinal fluid and fasted state simulated intestinal fluid.* Journal of Pharmaceutical Sciences, 2009. **98**(3): p. 985-996.
142. Gagnière, E., et al., *Formation of co-crystals: Kinetic and thermodynamic aspects.* Journal of Crystal Growth, 2009. **311**(9): p. 2689-2695.
143. Seefeldt, K., et al., *Crystallization pathways and kinetics of carbamazepine–nicotinamide cocrystals from the amorphous state by in situ thermomicroscopy, spectroscopy, and calorimetry studies.* Journal of Pharmaceutical Sciences, 2007. **96**(5): p. 1147-1158.
144. Porter Iii, W.W., S.C. Elie, and A.J. Matzger, *Polymorphism in carbamazepine cocrystals.* Crystal Growth and Design, 2008. **8**(1): p. 14-16.
145. K.Thamizhvanan, S.U., K.Vijayashanthi, *Evaluation of solubility of faltamide by using supramolecular technique.* International Journal of Pharmacy Practice & Drug Research, 2013: p. 6-19.
146. Moradiya, H.G., et al., *Continuous cocrystallisation of carbamazepine and trans-cinnamic acid via melt extrusion processing.* CrystEngComm, 2014. **16**(17): p. 3573-3583.
147. Liu, X., et al., *Improving the Chemical Stability of Amorphous Solid Dispersion with Cocrystal Technique by Hot Melt Extrusion.* Pharmaceutical Research. **29**(3): p. 806-817.
148. Li, M., N. Qiao, and K. Wang, *Influence of sodium lauryl sulphate and tween 80 on carbamazepine-nicotinamide cocrystal solubility and dissolution behaviour.* pharmaceutics, 2013. **5**(4): p. 508-524.
149. Katzhendler, I., R. Azoury, and M. Friedman, *Crystalline properties of carbamazepine in sustained release hydrophilic matrix tablets based on hydroxypropyl methylcellulose.* Journal of Controlled Release, 1998. **54**(1): p. 69-85.
150. Sehi04, S., et al., *Investigation of intrinsic dissolution behavior of different carbamazepine samples.* Int J Pharm, 2009. **386**(386): p. 77–90.
151. Tian, F., et al., *Visualizing the conversion of carbamazepine in aqueous suspension with and without the presence of excipients: a single crystal study using SEM and Raman microscopy.* European Journal of Pharmaceutics & Biopharmaceutics, 2006. **64**(3): p. 326–335.
152. Hino, T. and J.L. Ford, *Characterization of the hydroxypropylmethylcellulose-nicotinamide binary system.* International Journal of Pharmaceutics, 2001. **219**(1-2): p. 39-49.
153. Ueda, K., et al., *In situ molecular elucidation of drug supersaturation achieved by nano-sizing and amorphization of poorly water-soluble drug.* European Journal of Pharmaceutical Sciences, 2015: p. 79–89.
154. Tian, F., et al., *Influence of polymorphic form, morphology, and excipient interactions on the dissolution of carbamazepine compacts.* Journal of pharmaceutical sciences, 2007. **96**(3): p. 584–594.
155. 森部, 久. and 顕. 東, *Nanocrystal formulation of poorly water-soluble drug.* Drug delivery system : DDS : official journal of the Japan Society of Drug Delivery System, 2015. **30**(2): p. 92-99.
156. Lang, M., A.L. Grzesiak, and A.J. Matzger, *The Use of Polymer Heteronuclei for Crystalline Polymorph Selection.* Journal of the American Chemical Society, 2002. **124**(50): p. 14834-14835.
157. Li, M., et al., *Investigation of the Effect of Hydroxypropyl Methylcellulose on the Phase Transformation and Release Profiles of Carbamazepine-Nicotinamide Cocrystal.* Pharmaceutical Research, 2014: p. 1-14.
158. Qiao, N., et al., *In situ monitoring of carbamazepine–nicotinamide cocrystal intrinsic dissolution behaviour.* European Journal of Pharmaceutics and Biopharmaceutics, 2013. **83**(3): p. 415-426.

159. Remenar, J.F., et al., *Celecoxib:Nicotinamide Dissociation: Using Excipients To Capture the Cocrystal's Potential.* Molecular Pharmaceutics, 2007. **4**(3): p. 386-400.
160. Huang, N. and N. Rodríguez-Hornedo, *Engineering cocrystal solubility, stability, and pHmax by micellar solubilization.* Journal of Pharmaceutical Sciences, 2011. **100**(12): p. 5219-5234.
161. Li, M., N. Qiao, and K. Wang, *Influence of sodium lauryl sulfate and tween 80 on carbamazepine–nicotinamide cocrystal Solubility and dissolution behaviour.* pharmaceutics, 2013. **5**(4): p. 508-524.
162. Good, D.J. and N. Rodríguez-Hornedo, *Solubility Advantage of Pharmaceutical Cocrystals.* Crystal Growth & Design, 2009. **9**(5): p. 2252-2264.
163. Good, D.J. and N.r. Rodríguez-Hornedo, *Cocrystal Eutectic Constants and Prediction of Solubility Behavior.* Crystal Growth & Design, 2010. **10**(3): p. 1028-1032.
164. Li, M., et al., *Investigation of the Effect of Hydroxypropyl Methylcellulose on the Phase Transformation and Release Profiles of Carbamazepine-Nicotinamide Cocrystal.* Pharmaceutical Research, 2014. **31**(9): p. 2312-2325.
165. Qiu, S. and M. Li, *Effects of coformers on phase transformation and release profiles of carbamazepine cocrystals in hydroxypropyl methylcellulose based matrix tablets.* International Journal of Pharmaceutics, 2015. **479**(1): p. 118-128.
166. Brouwers, J., M.E. Brewster, and P. Augustijns, *Supersaturating drug delivery systems: The answer to solubility-limited oral bioavailability?* Journal of Pharmaceutical Sciences, 2009. **98**(8): p. 2549-2572.
167. Xu, S. and W.-G. Dai, *Drug precipitation inhibitors in supersaturable formulations.* International Journal of Pharmaceutics, 2013. **453**(1): p. 36-43.
168. Warren, D.B., et al., *Using polymeric precipitation inhibitors to improve the absorption of poorly water-soluble drugs: A mechanistic basis for utility.* Journal of drug targeting, 2010. **18**(10): p. 704-731.
169. Childs, S.L., P. Kandi, and S.R. Lingireddy, *Formulation of a Danazol Cocrystal with Controlled Supersaturation Plays an Essential Role in Improving Bioavailability.* Molecular Pharmaceutics, 2013. **10**(8): p. 3112-3127.
170. Bley, H., B. Fussnegger, and R. Bodmeier, *Characterization and stability of solid dispersions based on PEG/polymer blends.* International Journal of Pharmaceutics, 2010. **390**(2): p. 165-173.
171. Zerrouk, N., et al., *In vitro and in vivo evaluation of carbamazepine-PEG 6000 solid dispersions.* International Journal of Pharmaceutics, 2001. **225**(1–2): p. 49-62.
172. Kolter, K. and D. Flick, *Structure and dry binding activity of different polymers, including Kollidon® VA 64.* Drug development and industrial pharmacy, 2000. **26**(11): p. 1159-1165.
173. *Pharmaceutical Development Report Example QbD for MR Generic Drugs*, 2011.

APPENDICES

Predict solubility of CBZ cocrystals

Solubility of cocrystal is predicted by Equ.2.12.

$$S_{A_yB_z} = \sqrt[y+z]{[A]_{tr}^{y}[B]_{tr}^{z}\delta_{coformer}^{z}\delta_{drug}^{y}/y^{y}z^{z}} \quad \text{Equ.2.12}$$

Table S2.1 lists the transition concentration values ($[drug]_{tr}$ and $[coformer]_{tr}$) for cocrystal measured at the in variant point where two solid phases (drug and coformer) are in equilibrium with aqueous. All cocrystal C_{tr} values were confirmed by XRPD analysis of the solid phase, isolated from equilibrium with solution [9].

Table S2.1 Cocrystal Transition Concentration ($[drug]_{tr}$ and [coformer]tr), Component Solubilities [9]

Cocrystal	solvent	pH	$[coformer]_{tr}$ (mM)	$[drug]_{tr}$ (mM)	S_{drug} (mM)[a]	pKa	% nonionized[b]
CBZ-NIC	water	6.0	8.5×10^{-1}	5.8×10^{-3}	4.6×10^{-4}	3.5	100
CBZ-SAC	water	2.1	8.6×10^{-3}	6.8×10^{-4}	4.6×10^{-4}	1.6	24

[a] Solubility of hydrated forms are indicated for aqueous samples. [b] Calculated for the measured pH using referenced pKa values.

For 1:1 CBZ-NIC cocrystal:

$$S_{A_yB_z} = \sqrt[y+z]{[A]_{tr}^{y}[B]_{tr}^{z}\delta_{coformer}^{z}\delta_{drug}^{y}/y^{y}z^{z}}$$

$$= \sqrt[2]{[A]_{tr}B_{tr}\delta_{drug}} = \sqrt[2]{[CBZ]_{tr}[NIC]_{tr} \times 100\%}$$

$$= \sqrt[2]{8.5\times10^{-1}\times8.6\times10^{-3}\times100\%} = 7.02\times10^{-2}\text{(mM)}$$

Solubility ratio, $[drug]s_{cc}/s_{drug} = \frac{7.2\times10^{-2}}{4.6\times10^{-4}} = 152$ times

For 1:1 CBZ-SAC cocrystal:

$$S_{A_yB_z} = \sqrt[y+z]{[A]_{tr}^{y}[B]_{tr}^{z}\delta_{coformer}^{z}\delta_{drug}^{y}/y^{y}z^{z}}$$

$$= \sqrt[2]{[A]_{tr}B_{tr}\delta_{drug}} = \sqrt[2]{[CBZ]_{tr}[SAC] \times 24\%}$$

$$= \sqrt[2]{8.6 \times 10^{-3} \times 6.8 \times 10^{-4} \times 24\%} = 1.2 \times 10^{-3} \text{(mM)}$$

Solubility ratio, [drug] $S_{cc}/S_{drug} = \frac{1.2 \times 10^{-3}}{4.6 \times 10^{-4}} = 2.6$ times

For 1:1 CBZ-CIN cocrystal:

CIN coformer is presented as HA, a monoprotic acid. The equilibrium reactions for cocrystal dissociation and coformer ionization are given below:

$$CBZHA_{solid} \rightleftharpoons CBZ_{soln} + HA_{soln}$$

$$K_{sp} = [\text{CBZ}][\text{HA}] \qquad \text{Equ.S2.1}$$

$$\text{HA} \rightleftharpoons A^- + H^+$$

$$K_a = \frac{[H^+][A^-]}{[HA]} \qquad \text{Equ.S2.2}$$

K_{sp} is the solubility product of the cocrystal, and K_a is the acid ionization constant. Species without subscripts indicate solution phase. The sum of the ionized and non-ionized species, is given by:

$$[A]_T = [HA] + [A^-] \qquad \text{Equ.S2.3}$$

While total drug, which is non-ionizable, is given by:

$$[R]_T = [R] \qquad \text{Equ.S2.4}$$

By substituting for [HA] and $[A^-]$ from equations from Equations S.2.1 and S.2.2, respectively. Equation S.2.3 is rearranged as:

$$[A]_T = \frac{K_{sp}}{[R]_T}\left(1 + \frac{K_a}{[H^+]}\right) \qquad \text{Equ.S2.5}$$

For a 1:1 molar ratio binary cocrystal, the solubility is equal to the total concentration of either drug or coformer in solution,

$$S_{cocrystal} = \sqrt{K_{sp}\left(1 + \frac{K_a}{[H^+]}\right)} \qquad \text{Equ.S2.6}$$

Equation S2.6 predicts that cocrystal solubility will increase with increasing pH (decreasing $[H^+]$).

Table S.2.1 CQAs of Example Sustained release tablets [173]

Quality Attributes of the Drug Product		Target	Is it a CQA?	Justification
Physical Attributes	Appearance	Color and shape acceptable to the patient. No visual tablet defects observed.	No	Color, shape and appearance are not directly linked to safety and efficacy. Therefore, they are not critical. The target is set to ensure patient acceptability
	Odor	No unpleasant odor	No	In general, a noticeable odor is not directly linked to safety and efficacy, but odor can affect patient acceptability and lead to complaints. For this product, neither the drug substance nor the excipients have an unpleasant odor. No organic solvents will be used in the drug product manufacturing process.
	Friability	Not more than 1.0% w/w	No	A target of not more than 1.0% mean weight loss is set according to the compendial requirement and to minimize post-marketing complaints regarding tablet appearance. This target friability will not impact patient safety or efficacy.
Identification		Positive for drug substance	Yes	Though identification is critical for safety and efficacy, this CQA can be effectively controlled by the quality management system and will be monitored at drug product release. Formulation and process variables do not impact identity.
Assay		100.0% of label claim	Yes	Variability in assay will affect safety and efficacy; therefore, assay is critical.
Content Uniformity	Whole tablets	Conforms to USP. Uniformity of dosage units	Yes	Variability in content uniformity will affect safety and efficacy. Content uniformity of whole and split tablets is critical.
	Split tablets			
Drug release	Whole tablet	Similar drug release profile as reference drug.	Yes	The drug release profile is important for bioavailability, therefore, it is critical.

	CBZ-NIC cocrystal	CBZ III
Before dissolution test	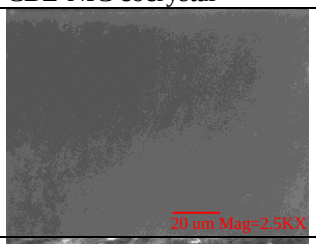	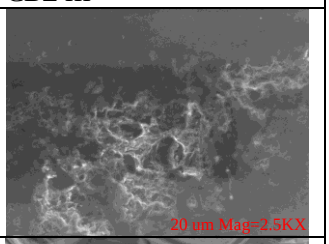
water	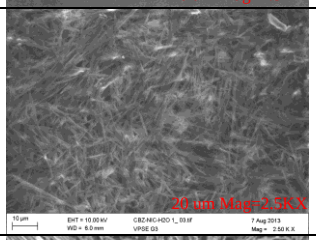	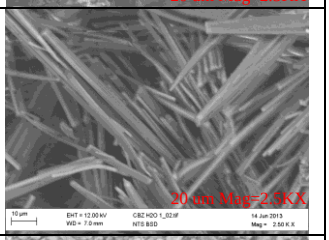
0.5 mg/ml HPMC	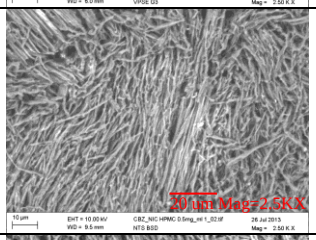	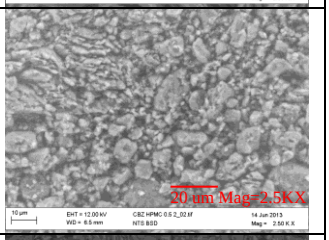
1 mg/ml HPMC	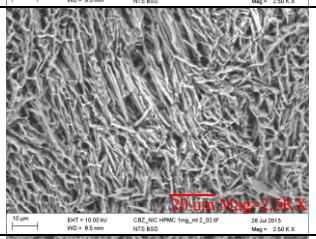	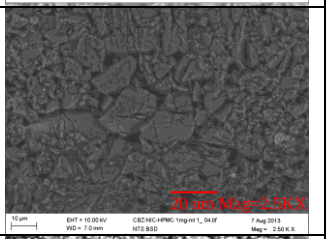
2 mg/ml HPMC	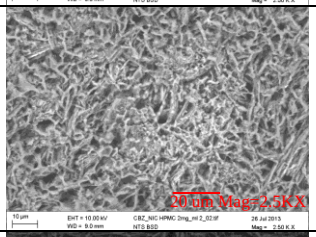	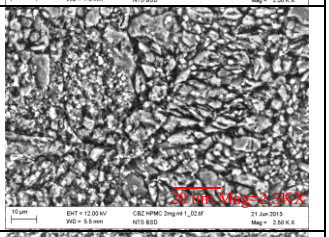
5 mg/ml HPMC	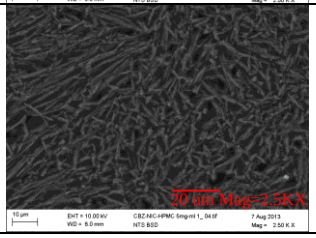	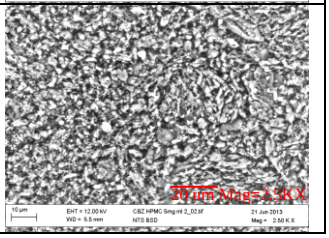

Fig.S5.1 SEM photographs of the sample compacts before and after dissolution tests at different HPMC concentration solutions

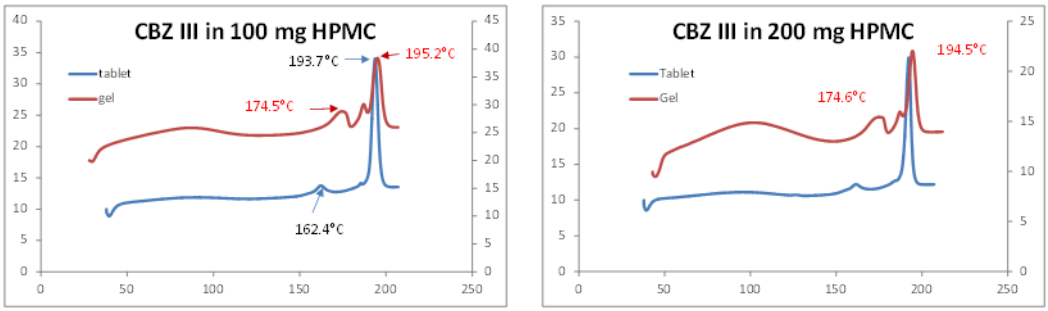

(a)

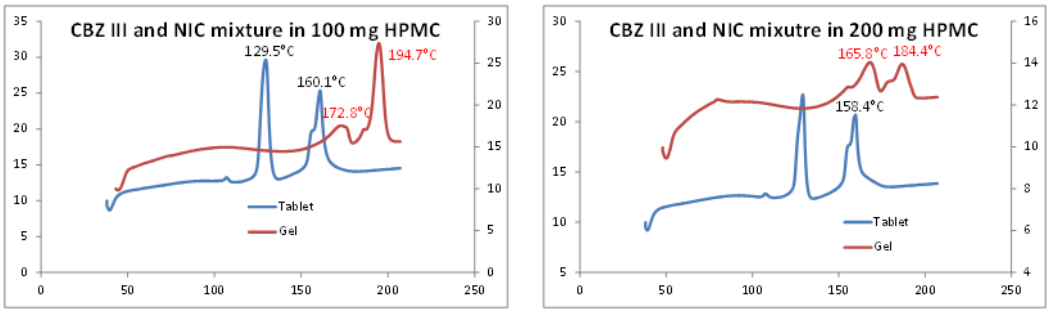

(b)

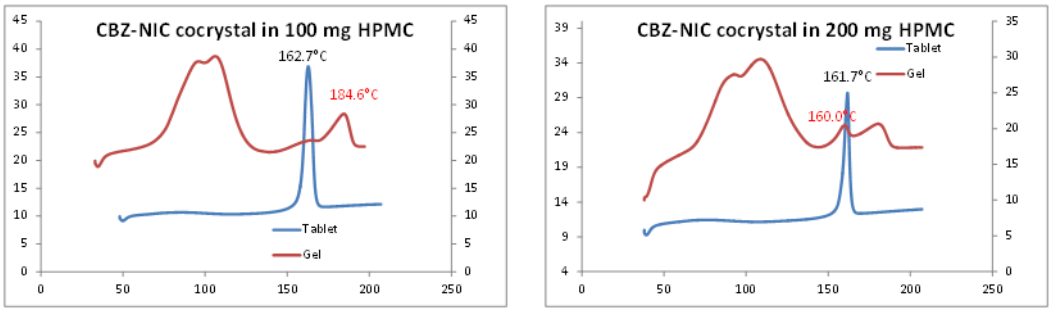

(c)

Fig.S5.2 DSC thermographs of gels of different formulations obtained after dissolution tests: (a) CBZ III formulations; (b) physical mixture formulations; (c) cocyrstal formulations

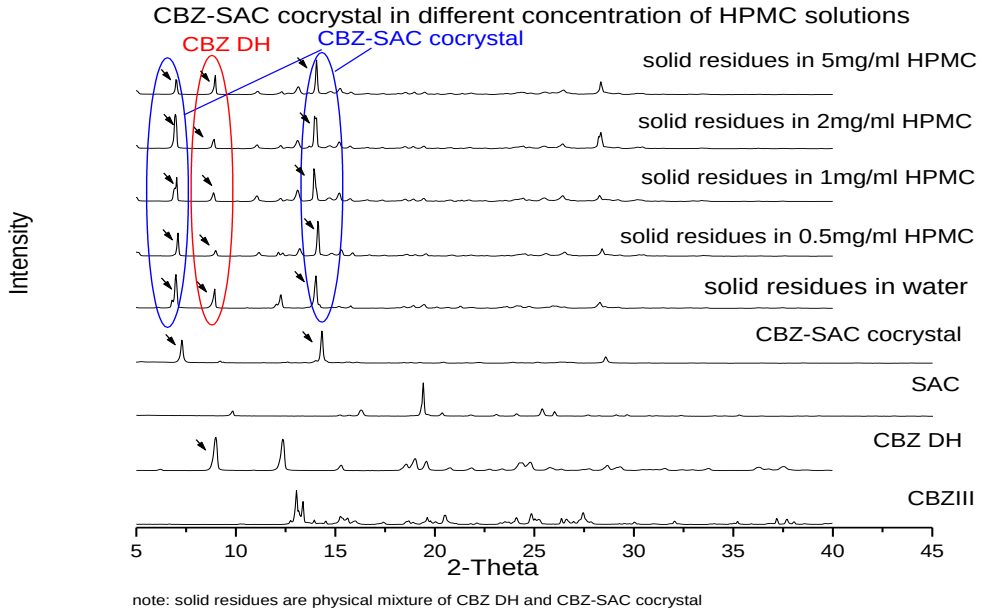

(a)

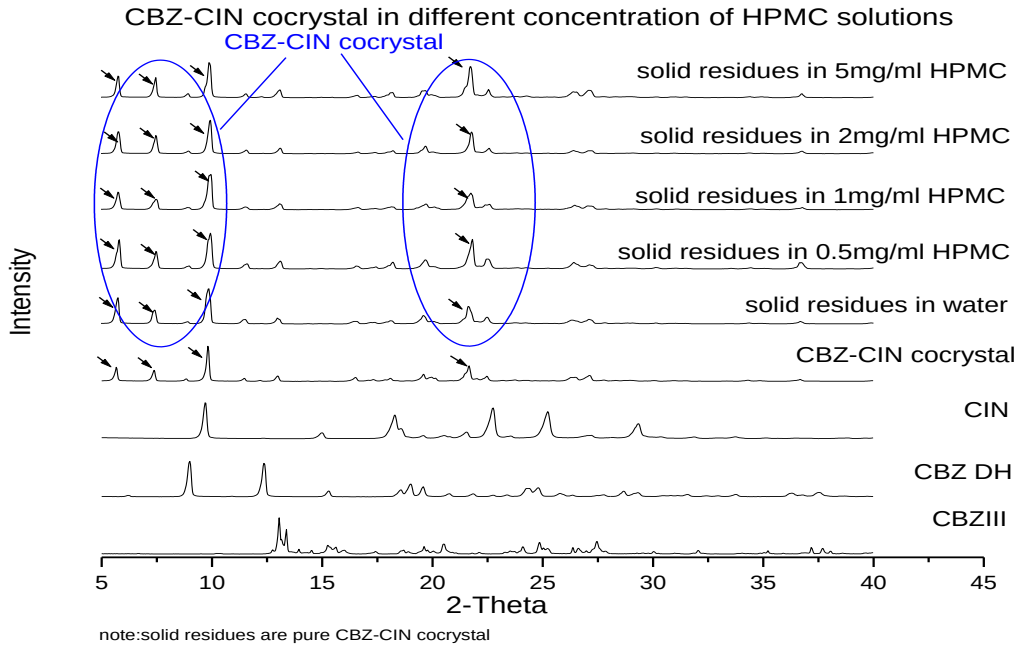

(b)

Fig.S6.1 XRPD patterns of solid residues of solubility tests: (a) CBZ-SAC cocrystal; (b) CBZ-CIN cocrystal

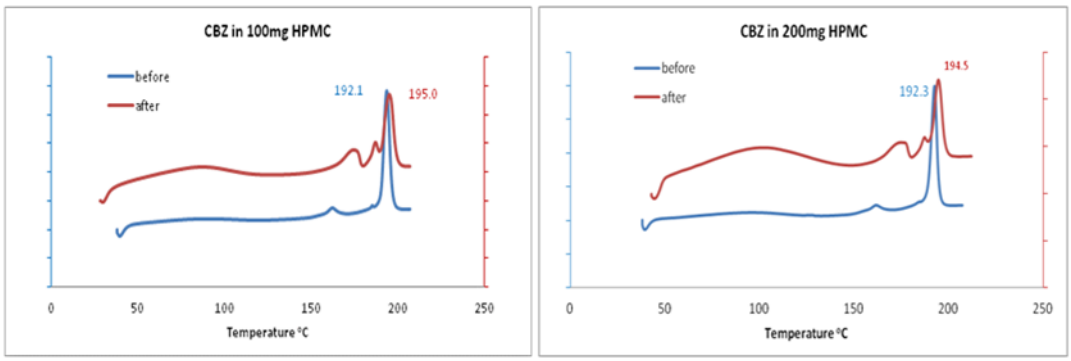
CBZ in 100mg HPMC
before
after
192.1
195.0
0
50
100
150
200
250
Temperature °C
CBZ in 200mg HPMC
before
after
192.3
194.5
0
50
100
150
200
250
Temperature °C

(a)

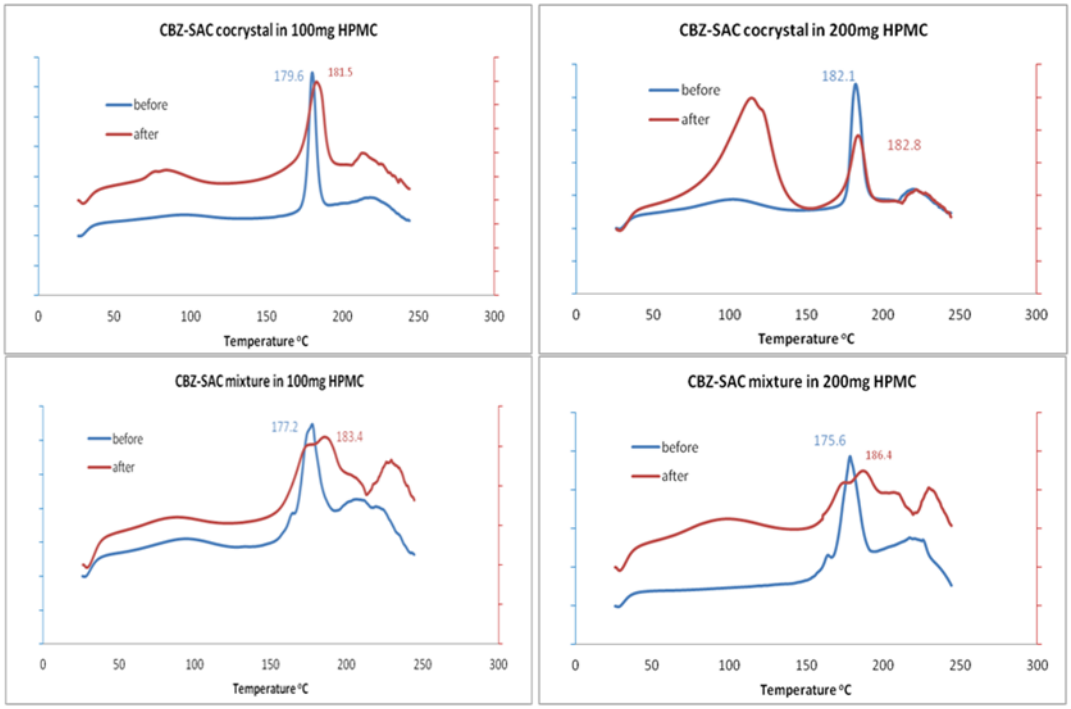
CBZ-SAC cocrystal in 100mg HPMC
before
after
179.6
181.5
0
50
100
150
200
250
300
Temperature °C
CBZ-SAC cocrystal in 200mg HPMC
before
after
182.1
182.8
0
50
100
150
200
250
300
Temperature °C
CBZ-SAC mixture in 100mg HPMC
before
after
177.2
183.4
0
50
100
150
200
250
300
Temperature °C
CBZ-SAC mixture in 200mg HPMC
before
after
175.6
186.4
0
50
100
150
200
250
300
Temperature °C

(b)

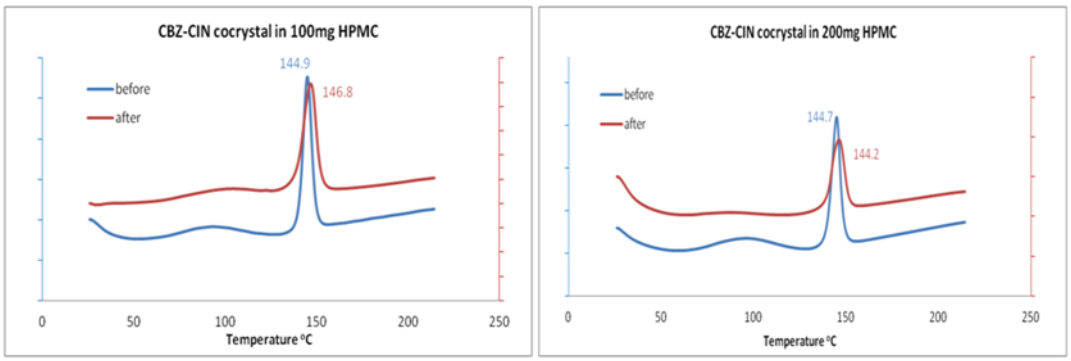
CBZ-CIN cocrystal in 100mg HPMC
before
after
144.9
146.8
0
50
100
150
200
250
Temperature °C
CBZ-CIN cocrystal in 200mg HPMC
before
after
144.7
144.2
0
50
100
150
200
250
Temperature °C

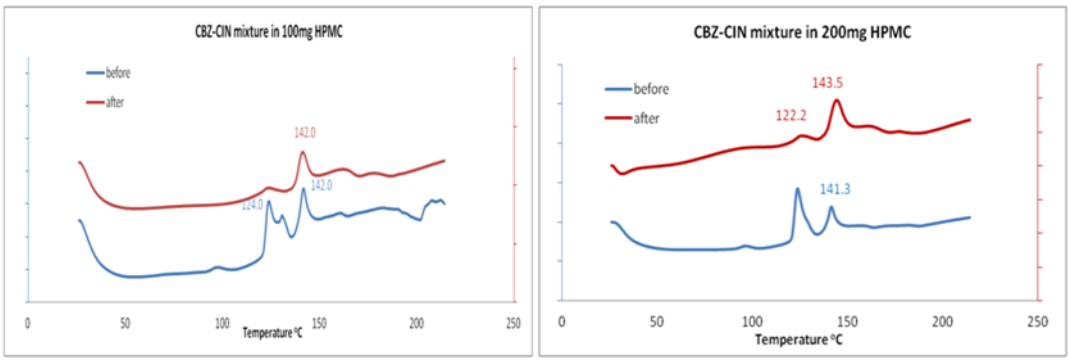

(c)

Fig.S6.2 DSC results of solid residues of different formulations after dissolution tests: (a) CBZ III formulations; (b) CBZ-SAC cocrystal and physical mixture formulations; (C) CBZ-CIN cocrystal and physical mixture formulations

Polymer (mg/ml)		CBZ III	CBZ-NIC cocrystal	CBZ III-NIC physical mixture	CBZ-SAC cocrystal	CBZ III-SAC physical mixture	CBZ-CIN cocrystal	CBZ III-CIN physical mixture
0.5	HPMCAS	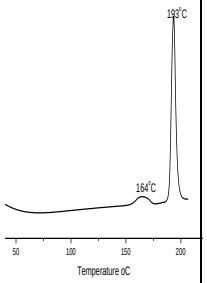	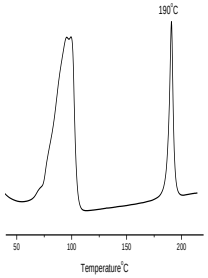	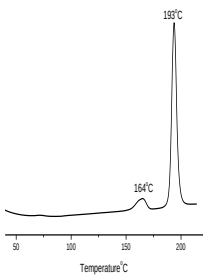	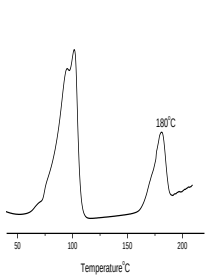	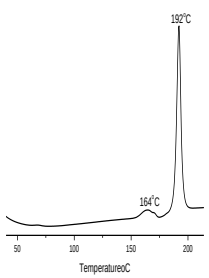	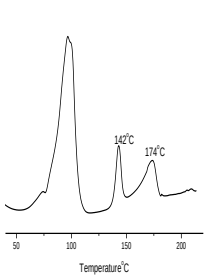	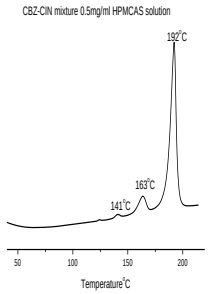
	PVP	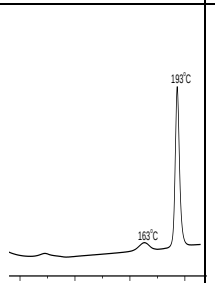	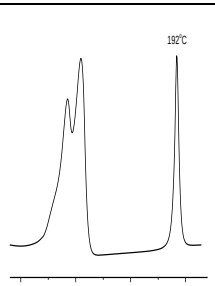	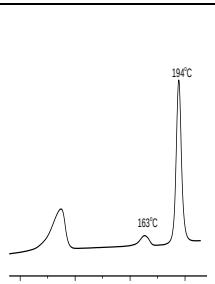	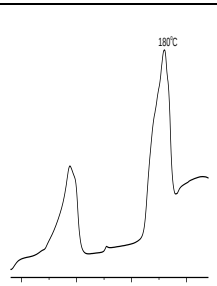	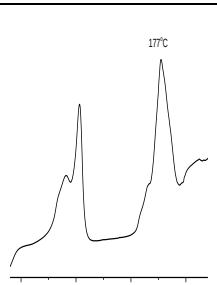	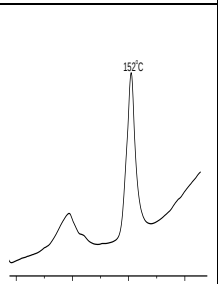	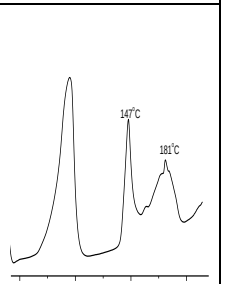
	PEG	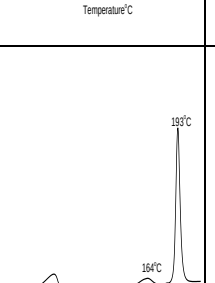	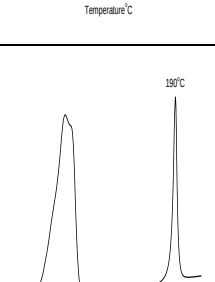	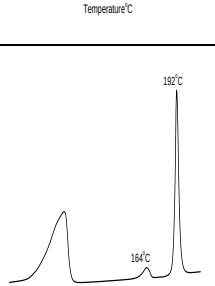	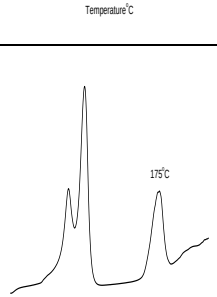	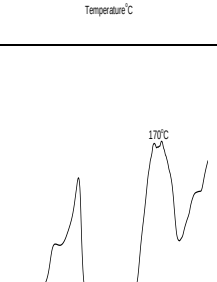	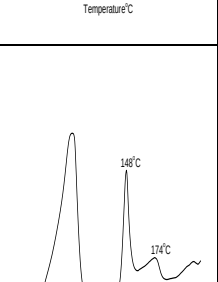	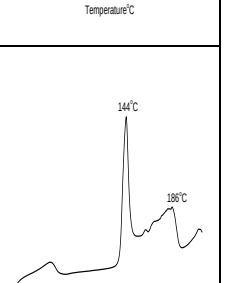

1.0	HPMCAS	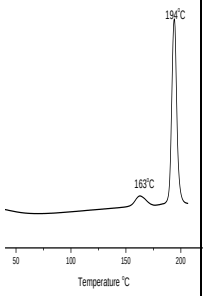	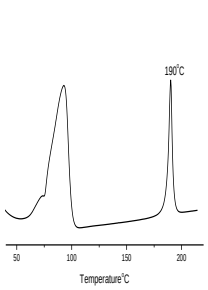	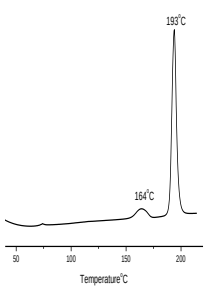	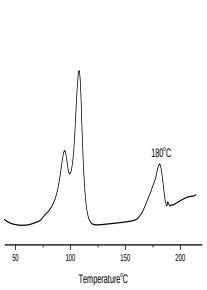	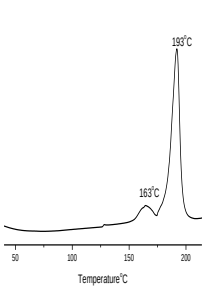	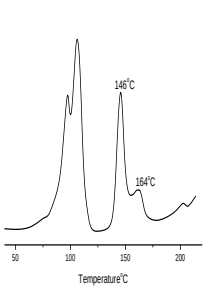	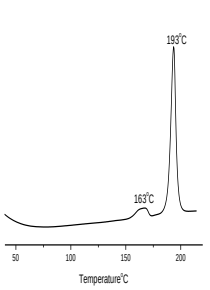
	PVP	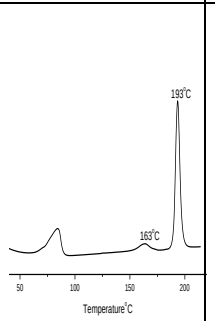	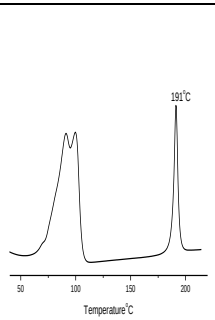	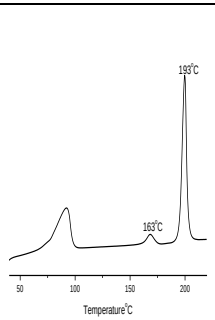	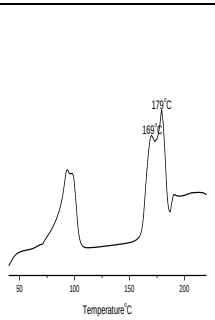	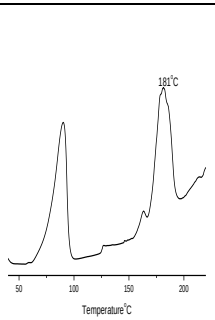	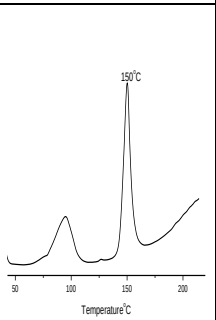	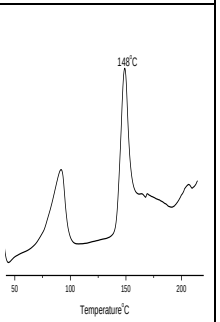
	PEG	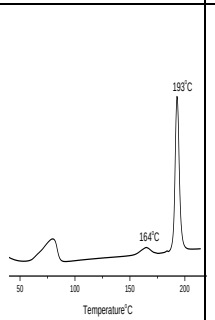	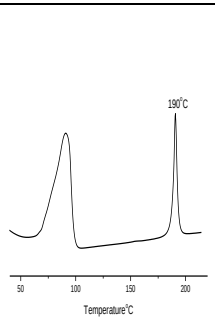	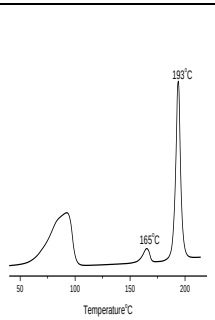	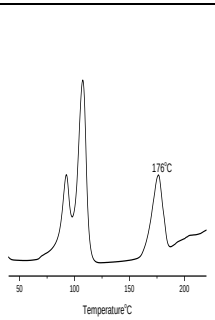	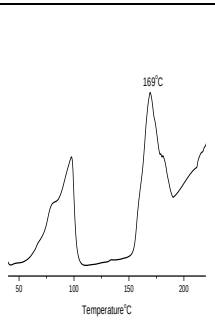	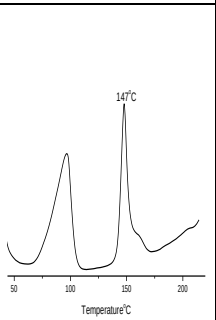	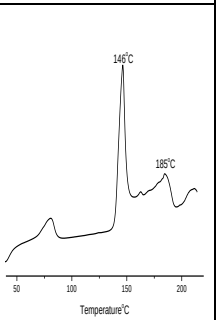

5.0	HPMCAS	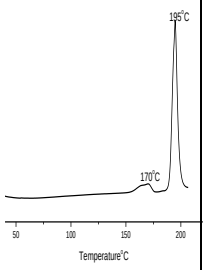	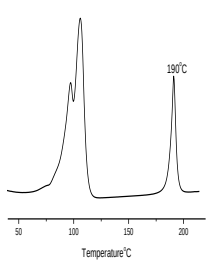	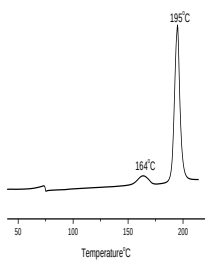	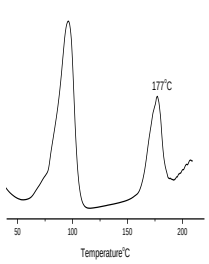	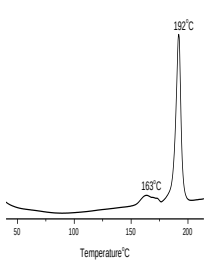	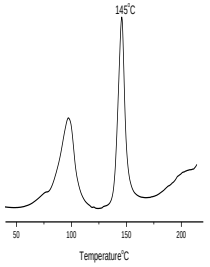	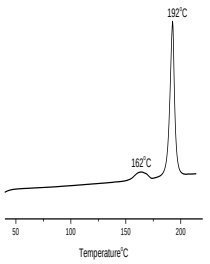
	PVP	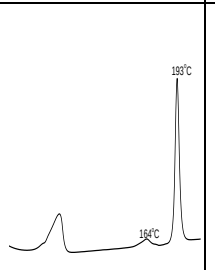	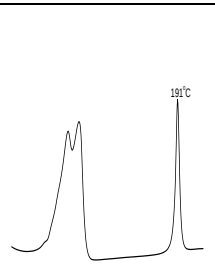	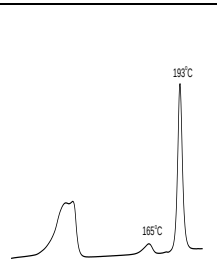	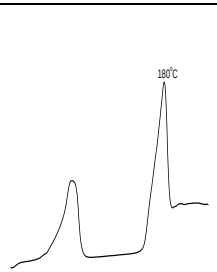	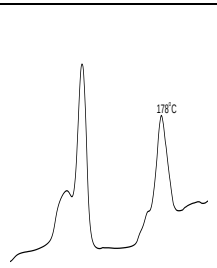	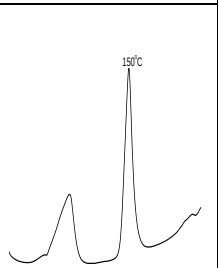	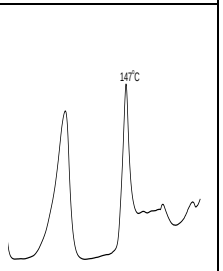
	PEG	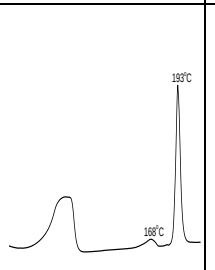	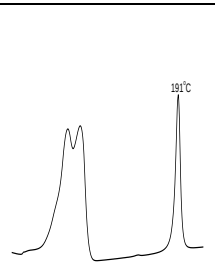	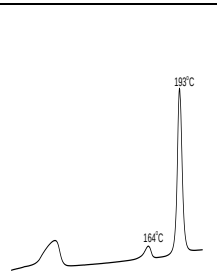	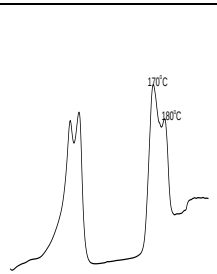	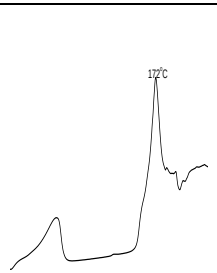	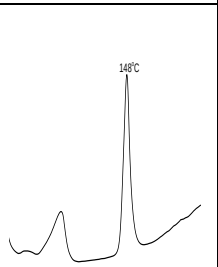	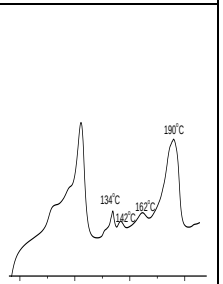

Fig.S7.1 DSC thermographs of solid residues retrieved from solubility studies in the presence of different concentrations of a polymer in pH 6.8 PBS

Polymer (mg/ml)		CBZ III	CBZ-NIC cocrystal	CBZ-NIC mixture	CBZ-SAC cocrystal	CBZ-SAC mixture	CBZ-CIN cocrystal	CBZ-CIN mixture
0.5	HPMCAS	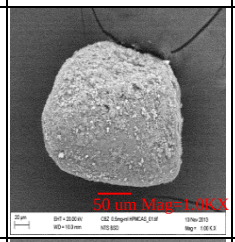	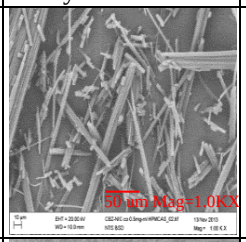	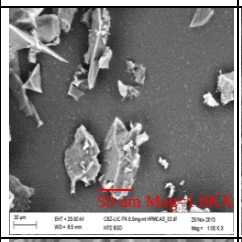	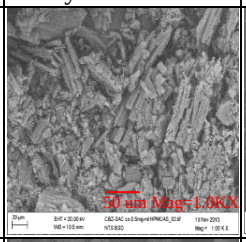	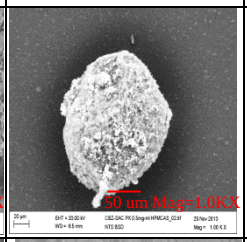	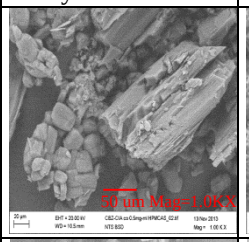	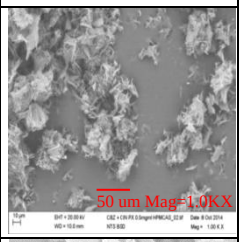
	PVP	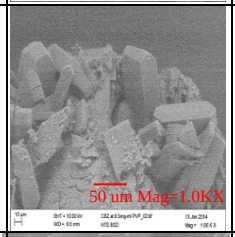	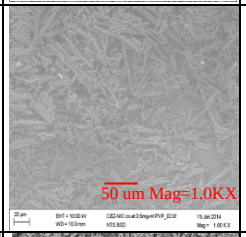	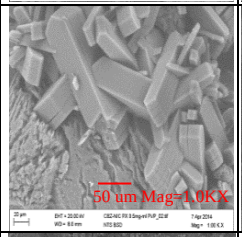	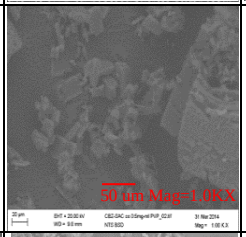	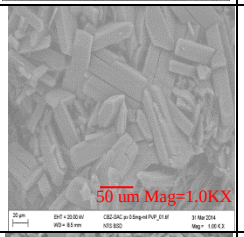	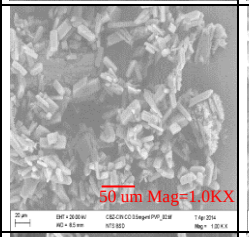	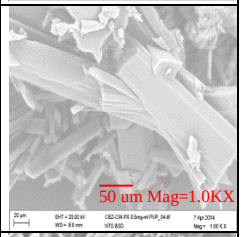
	PEG	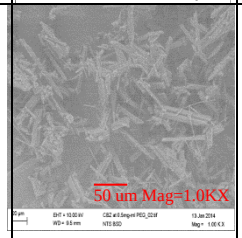	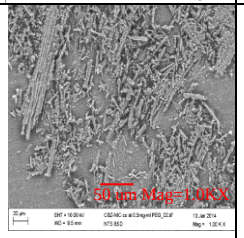	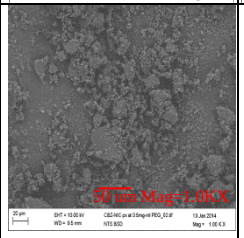	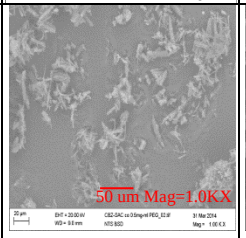	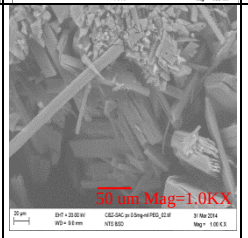	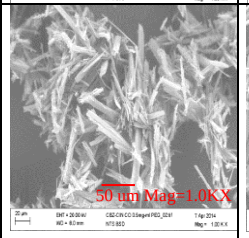	
1.0	HPMCAS	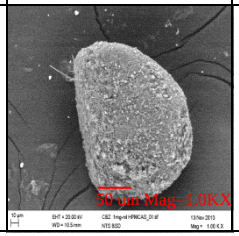	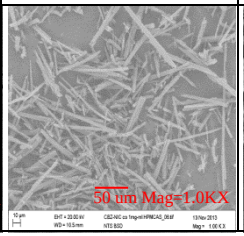	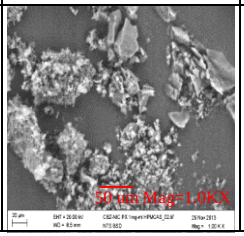	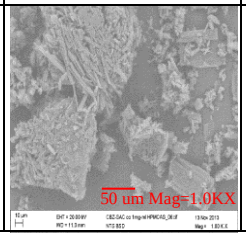	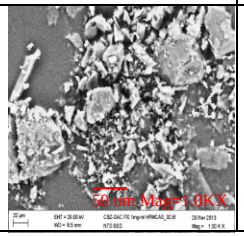	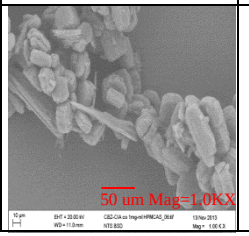	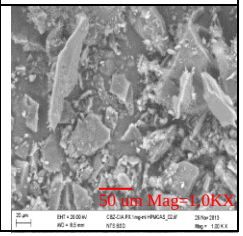

	PVP	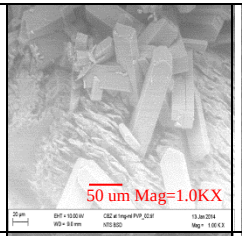	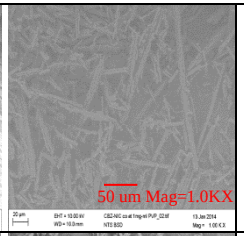	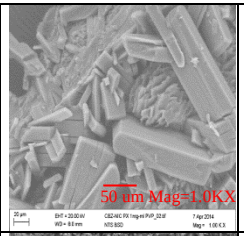	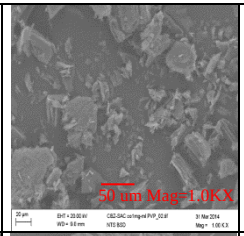	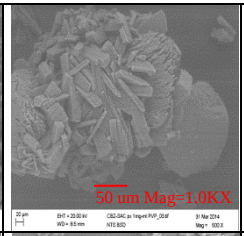	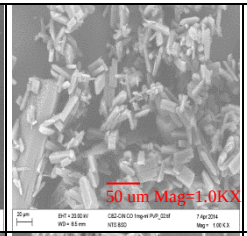	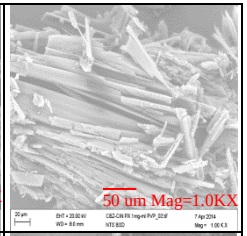
	PEG	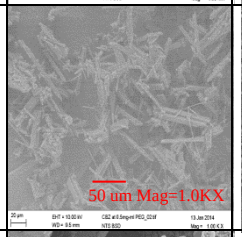	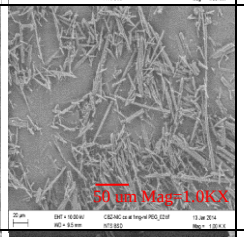	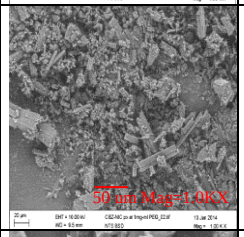	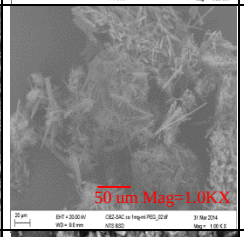	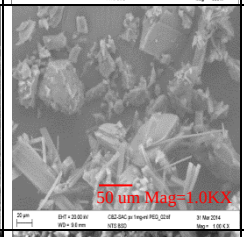	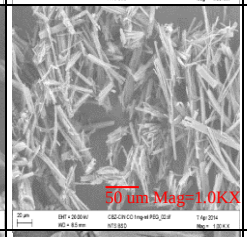	
5.0	HPMCAS	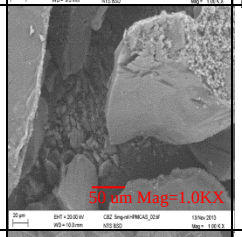	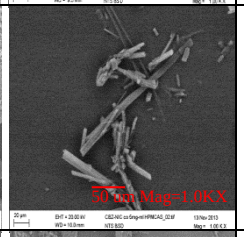	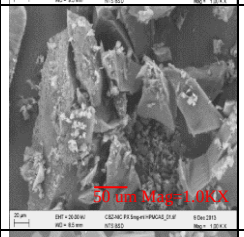	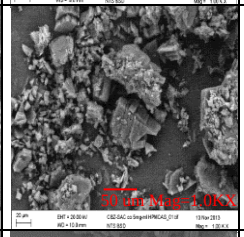	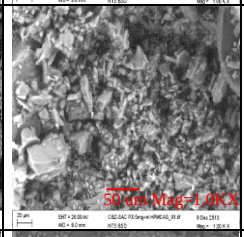		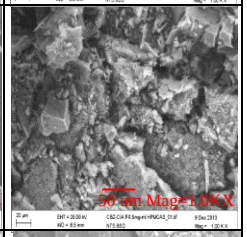
	PVP	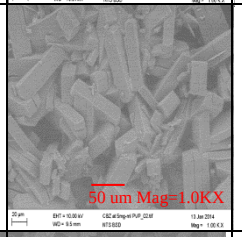	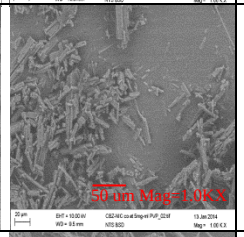	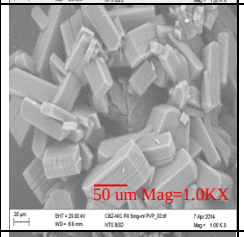	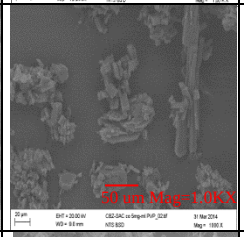	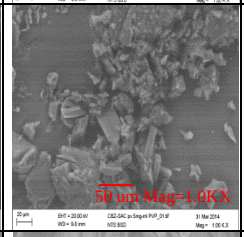	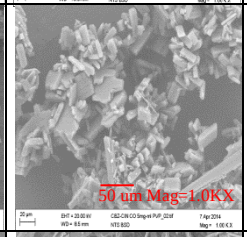	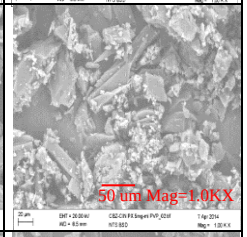
	PEG	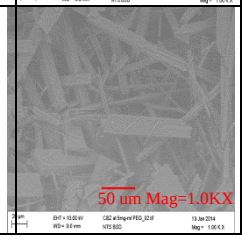	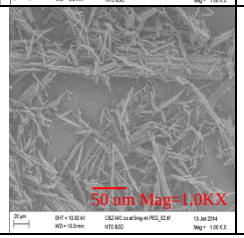	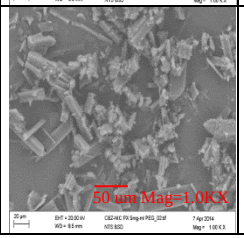	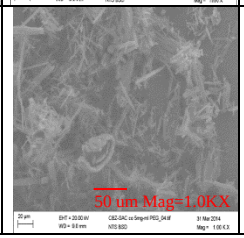	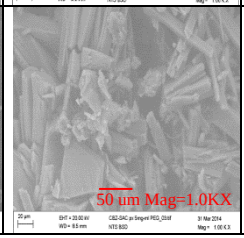	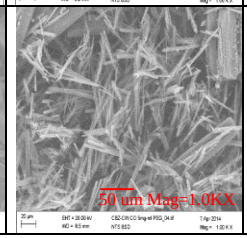	

Fig.S7.2 SEM photographs of the solid residues retrieved from solubility studies in the presence of different concentrations of a polymer in pH 6.8 PBS

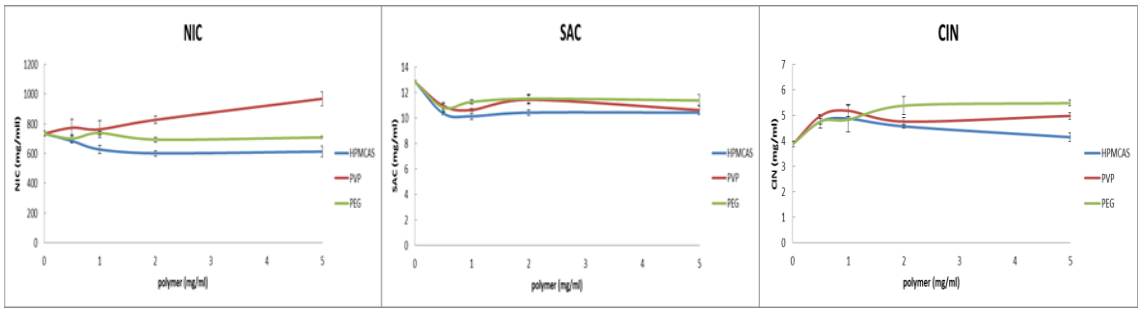

(a)

	CBZ concentrations of CBZ III, CBZ-NIC cocrystal and physical mixture of CBZ III-NIC	CBZ concentrations of CBZ III, CBZ-SAC cocrystal and physical mixture of CBZ III-SAC	CBZ concentrations of CBZ III, CBZ-CIN cocrystal and physical mixture of CBZ III-CIN
HPMCAS	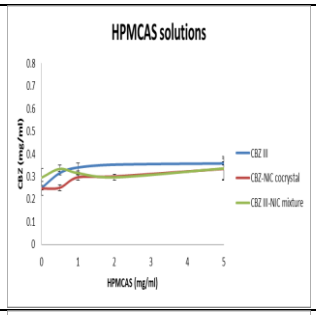	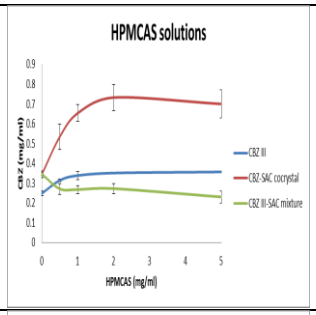	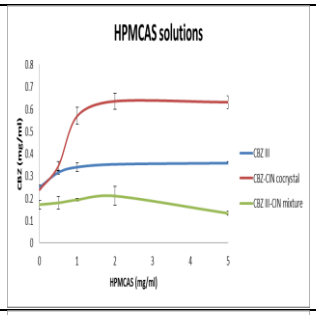
PVP	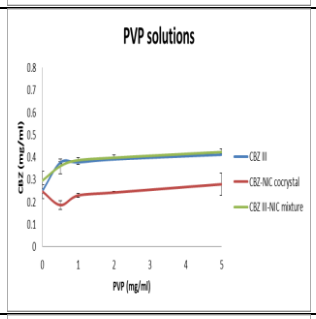	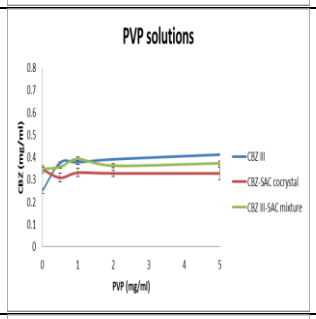	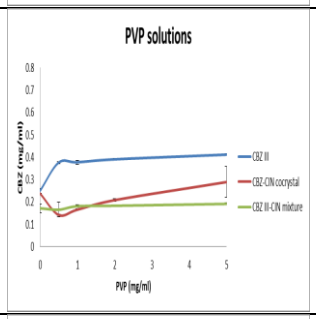
PEG	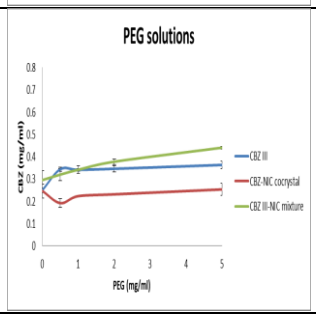	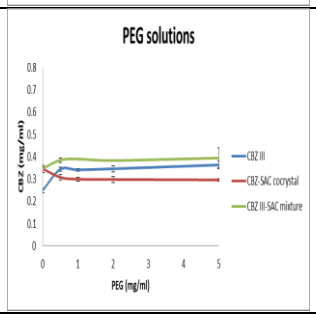	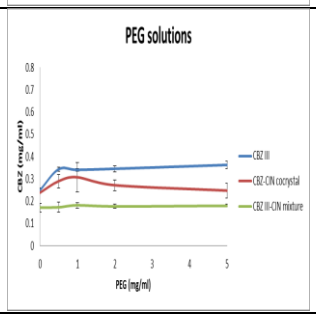

(b)

Fig.S7.3 Coformer concentrations and comparison of CBZ concentrations of CBZ III, CBZ cocrystals and physical mixtures in the absence and presence of the different concentrations of pre-dissolved polymers in pH 6.8 PBS at equilibrium after 24 hours: (a) coformer concentration; (b) comparisons of CBZ concentrations of CBZ III, CBZ cocrystals and physical mixtures

	CBZ III	CBZ-NIC cocrystal	CBZ-NIC mixture	CBZ-SAC cocrystal	CBZ-SAC mixture	CBZ-CIN cocrystal	CBZ-CIN mixture
100mg HPMCAS	×	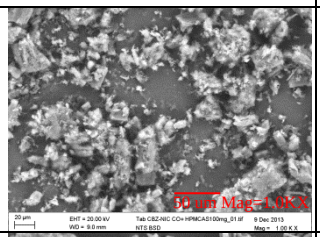	×	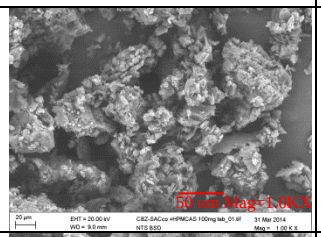	×	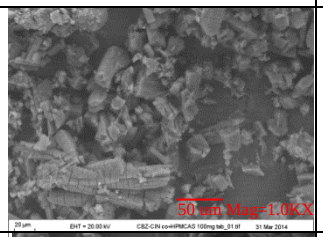	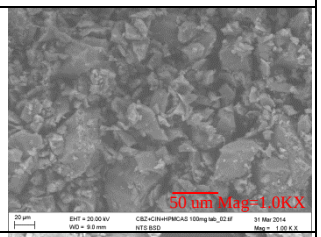
200mg HPMCAS	×	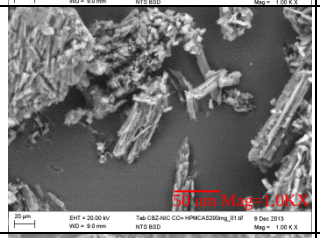	×	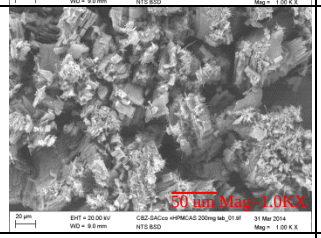	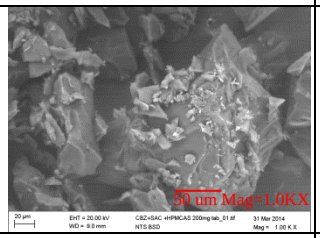	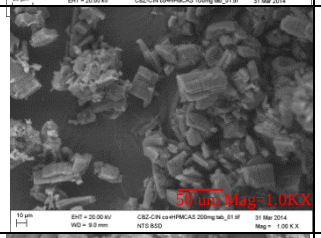	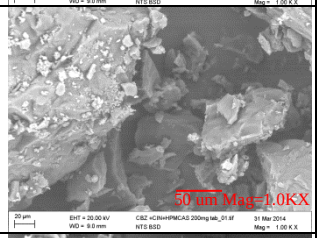
100mg PVP	×	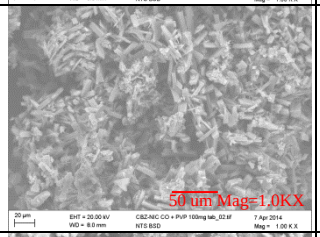	×	×	×	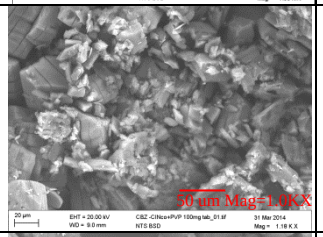	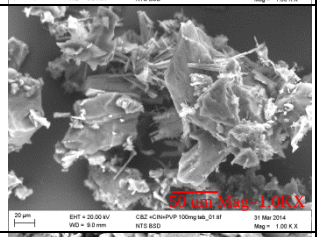
200mg PVP	×	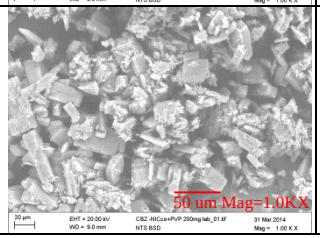	×	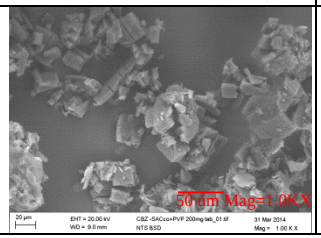	×	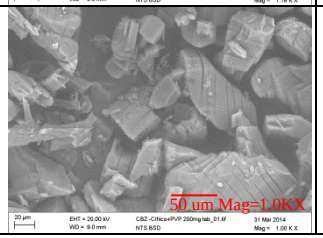	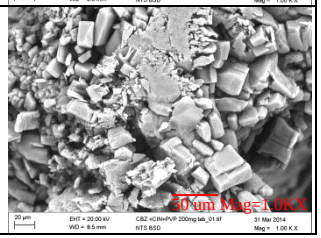

100mg PEG	×	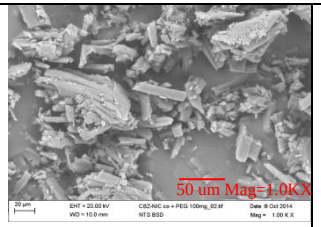	×	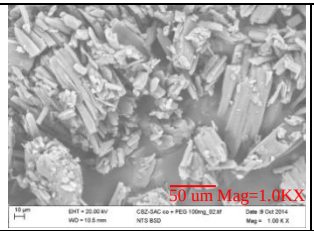	×		×
200mg PEG	×	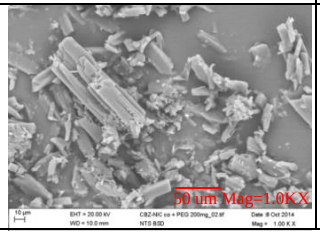	×	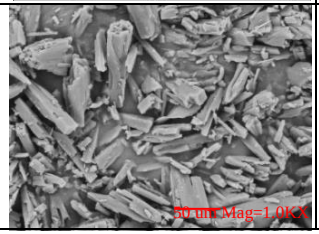	×	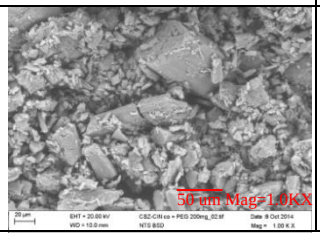	×

Fig.S7.4 SEM photographs of solid residues of different formulation after dissolution tests (×, it indicated no solid left)

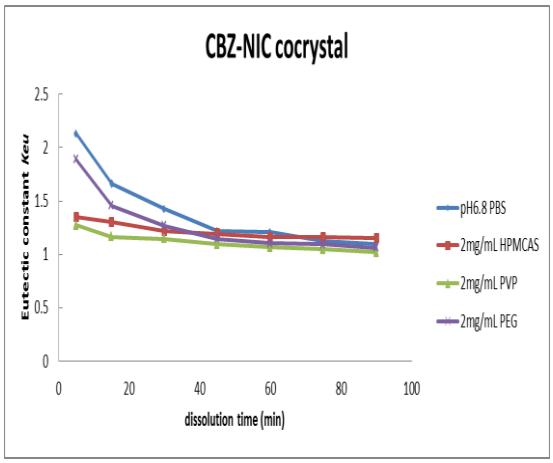

(a)

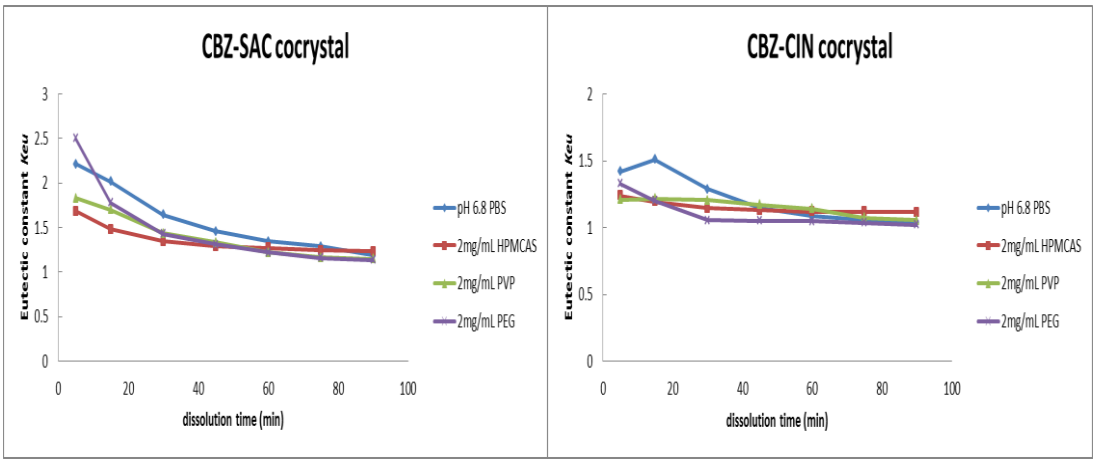

(b) (c)

Fig.S7.5 Eutectic constant K_{eu} of CBZ cocrystals in the absence and presence of a 2 mg/ml polymer in pH 6.8 PBS during powder dissolution tests: (a) CBZ-NIC cocrystal; (b) CBZ-SAC cocrystal; (c) CBZ-CIN cocrystal

PUBLICATIONS

Journal publications

[1] **Shi Qiu** and Mingzhong Li. "Effects of Coformers on Phase Transformation and Release Profiles of Carbamazepine Cocrystals in Hydroxypropyl Methylcellulose Based Matrix Tablets" International Journal of Pharmaceutics 497(2015), pp.118-128

[2] **Shi Qiu**, Ke Wang and Mingzhong Li "In Vitro Dissolution Studies of Immediate-Release and Extended-Release Formulations Using Flow-Through Cell Apparatus 4" Dissolution Technologies, May 2014

[3] Mingzhong Li, **Shi Qiu**, Yan Lu, Ke Wang, Xiaojun Lai, Mohammad Rehan "Investigation of the Effect of Hydroxypropyl Methylcellulose on the Phase Transformation and Release Profiles of Carbamazepine-Nicotinamide Cocrystal" Pharmaceutical Research. Published online: 04 March 2014

[4] **Shi Qiu**, Ke Wang, Xiaojun Lai and Mingzhng Li "Role of polymers in solution and tablet based carbamazepine cocrystal formulations" –submitted to International Journal of Pharmaceutics

Conference publications

[1] **Shi Qiu**, Mingzhong Li. In Vitro Dissolution Studies of Immediate-Release and Extended-ReleaseFormulations Using Flow-Through Cell Apparatus 4.Proceeding 2012 APS Pharmsci Conference, Nottingham, UK, 12th-14th September 2012

[2] **Shi Qiu**, Mingzhong Li. Investigation of the Effect of Hydroxypropyl Methylcellulose on the Phase Transformation and Release Profiles of Carbamazepine-Nicotinamide Cocrystal. Proceeding 2014 BACG 45th Annual Conference of the British Association for Crystal Growth, Leeds, UK 13th -15th July 2014

Oral Presentation

Shi Qiu, Investigation of the Effect of Hydroxypropyl Methylcellulose on the Phase Transformation and Release Profiles of Carbamazepine-Nicotinamide Cocrystal.Proceeding 2014 BACG 45th Annual Conference of the British Association for Crystal Growth, Leeds, UK 14th July 2014